Arming ColoAd1 with Tumor Necrosis Factor α and Lymphotoxin α

Jorien Anne Koelen

Keble College

University of Oxford

A thesis submitted for the degree of Doctor of Philosophy

to the Department of Oncology, University of Oxford

Michaelmas term 2015

Supervisors: Professor Leonard Seymour and Dr. Kerry Fisher

Arming ColoAd1 with tumor necrosis factor α and lymphotoxin α

Jorien Anne Koelen, Keble College, University of Oxford

A thesis submitted for the degree of Doctor of Philosophy
to the Department of Oncology, University of Oxford, Michaelmas Term, 2015

Abstract

Colon and rectum cancers (CRCs) are the third most prevalent cause of cancer-related mortality. Advanced metastatic CRC has a very poor prognosis; indicating the need for improved therapy. Tumour necrosis factor (TNF) can induce an immune response against tumours and cause cell death of the tumour-associated vasculature. However, dose-limiting toxicity occurs with systemic TNF treatment. In order to assess the effects of expressing TNF and lymphotoxin α (LTA) locally in the tumour microenvironment, a syngeneic CT26 CRC model expressing soluble (sm), full length (fm) or membrane-bound (mbm) murine TNF or LTA under a doxycyclin-dependent promoter. Moreover, an oncolytic adenovirus (ColoAd1) was modified to express fm or mbm TNF or LTA under its major late promoter (MLP). ColoAd1 is a novel chimeric species B adenovirus based on serotypes Ad11p and Ad3 and is currently in clinical phase 2 trials.

- In the CT26 model, expression of mbm TNF decreases tumour growth and increases survival compared to control mice not receiving doxycyclin. Expression of sm or fm TNF had no effect on tumour growth or survival. Increased immune infiltration, especially myeloid cells ($CD45^+$ $CD11b^+$) was seen in mice bearing tumours expressing sm, fm and mbm TNF.
- ColoAd1 can express functional TNF constructs without a substantial impact on virus replication or yield *in vitro*.
- Arming ColoAd1 with TNF did not increase efficacy or innate immune infiltration compared to parental ColoAd1, *in vivo*. Administration of ColoAd1, ColoAd1 fm TNF and ColoAd1 mbm TNF increases immune cell infiltration compared to PBS, especially dendritic ($CD45^+$ $CD11b^+$ $F4/80^-$ $CD11c^+$), monocytic ($CD45^+$ $CD11b^+$ $Ly6C^{high}$ $Ly6G^-$) and granulocytic ($CD45^+$ $CD11b^+$ $Ly6C^{low}$ $Ly6G^+$) cell populations were enriched in virus treated tumours. Expression of TNF from ColoAd1 was well tolerated and systemic toxicity was not observed, *in vivo*.
- A statitistically significant derecrease in ColoAd1 mbm TNF genome copies and non-statistically significant decrease in ColoAd1 fm TNF genome copies were found in tumours compared to ColoAd1. This may indicate increased viral clearance or decreased replication of these armed viruses. The decrease in virus progeny in tumours may have been a major hurdle for increasing the efficacy of ColoAd1 TNF.

Synergy between adenoviruses and radiation has been observed for species C virus but little is known about the effects of species B virus on the DNA damage response.

- *In vitro*, induction of γH2AX and phospho-ATM was seen upon ColoAd1 infection of DLD cells and compared to Ad5, less Rad50 and Mre11 degradation occurs in ColoAd1 or Ad11p infected cells. Like all other species of Ad studied, ligase IV is degraded during ColoAd1 infection.
- Combination of ColoAd1 with radiation therapy, *in vivo*, led to an increase in viral genome copies in the tumour lysate, 10 days post radiation. However, no synergistic effects of combining virus with radiation was observed. Additionally, contrary to other Ad5 viruses armed with TNF, no evidence for synergy between mTNF expressing ColoAd1 and radiation was found.

In conclusion, ColoAd1 can deliver therapeutic proteins to the tumour microenvironment and could potentially be a very useful approach to treat refractive cancers. However, the limitations of relevant pre-clinical models will need to be over-come or new phase 0 mechanistic trial designs will be required to move the technology to reach full potential.

Declaration of Authentication

All the work presented in this thesis was performed by me and in no way forms part of any other thesis in this or any other university. Contributions made by others have been acknowledged in this thesis. The work was performed under the supervision of Dr. Kerry Fisher and Professor Len Seymour, both Department of Oncology, Division of Medical Sciences, University of Oxford.

Acknowledgements

I would like to thank my supervisors, Professor Leonard Seymour and Dr Kerry Fisher. I wish to thank Professor Seymour for giving me this opportunity and his scientific guidance and supervision throughout this project. I am also grateful to Dr Fisher for his scientific insights and discussions. I wish to thank Professor Nicola Sibson, for her scientific advice and help with some of the in vivo experiments included in this this. I am thankful for the technical support and scientific advice that I have received from past and present members of the Seymour laboratory.

I am grateful to PsiOxus Therapeutics for their help with ColoAd1 cloning. In particular, I would like to thank Dr Alice Brown and Prithvi Kodialbail for their help. I wish to thank Dr Stavros Melemenidis for his help in some of the in vivo experiments. I am also very grateful to Dr Selvakumar Anabalagan and Katarzyna Leszczynska, who helped have me with the in vitro radiation studies.

I am very grateful to the Marie Curie Advance initial training network, for providing my salary and training opportunities throughout this DPhil. Also, I would like to thank the Marie Curie ITN members for the interesting and fun times around Europe. I am also thankful to the Dr Hendrik Muller's Vaderlandsch Fonds for their financial aid.

Most of all, I would like to thank my parents for their continuous love and support.

Table of Contents

List of Abbreviations

/	per
3’	3 prime end of DNA
5’	5 prime end of DNA
°C	degrees Celsius
µ	micro
Ad	adenovirus
ADCC	antibody-dependent cell-mediated cytotoxicity
APC	antigen presenting cells
ATM	ataxia telangiectasia mutated
ATR	ataxia-telangiectasia and Rad3-related
bp	base pair
BSA	bovine serum albumin
c	centi
CAR	Coxsackievirus and adenovirus receptor
CCL	CC chemokine ligand
CD	cluster of differentiation
cDNA	copy DNA
CMV	cytomegalovirus
CRC	colorectal cancer
CXCL	C X C motif ligand
DC	dendritic cell
DMBA	7,12-Dimehtylbez(a)anthracene
DMEM	Dulbecco’s modified Eagle’s medium
DMSO	dimethyl sulphoxide
DNA	deoxyribonucleic acid
Dox	doxycycline
ds	double stranded
DSB	double-strand break
DSG-2	desmoglein 2
ECM	extracellular matrix
EGFR	epidermal growth factor receptor
ELISA	enzyme linked immunosorbent assay
FCS	fetal calf serum
fh TNF	full length human TNF
fm TNF	full length murine TNF
Fwd	forward
g	gram
g	gravitational force
GM-CSF	granulocyte-macrophage colony stimulating-factor
Gr-1	granulocyte-differentiation antigen-1
HEPES	4-(2-hydroxyethyl)-1-piperazineethanosulphonic acid
HER2	human epidermal growth factor receptor 2
HEV	high endothelial venule
HRP	horseradish peroxidase
HSP	heat shock protein
HSV	herpes simplex virus

hLTA	human lymphotoxin α
hTNF	human tumor necrosis factor
IL	interleukin
ILP	isolated limb perfusion
IFN	interferon
i.t.	intratumoural
i.v.	intravenous
k	kilo
kDa	kilo Dalton
KIR	killer inhibitory receptors
KO	knock out
KRAS	Kirsten rat sarcoma viral oncogene homolog
l	litre
LTA	lymphotoxin alpha
Luc	luciferase
Ly6C	lymphocyte antigen 6C
Ly6G	lymphocyte antigen 6G
m	metre
m	milli
mb TNF	membrane-bound TNF
mbm TNF	membrane-bound murine TNF
MCA	mehtylcolanthrene
MDSC	myeloid derived suppressor cell
MHC	major histocompatibility complex
min	minute(s)
MLP	major late promoter
mLTA	murine lymphotoxin α
MMP	matrix metalloprotease
mRNA	messenger RNA
Mre11	meiotic recombination 11 homolog A
MTOC	microtubule organizing center
mTNF	murine tumor necrosis factor
MTS	(3-(4,5-dimethylthiazol-2-yl)-5-(3-carboxymethoxyphenyl)-2-(4 sulfophenyl)-2H-tetrazolium)
n	nano
n	number
ni	no insert
NF-κB	nuclear factor kappa B
NK	natural killer
orf	open reading frame
PEG	polyethylene glycol
PCR	polymerase chain reaction
QPCR	quantitative polymerase chain reaction
Rev	reverse
RGD	arginylglycylaspartic acid
RLU	relative light units
ROS	reactive oxygen species
RPMI	Roswell Park Memorial Institute
SD	standard deviation

SEM	standard error of the mean
sm TNF	soluble murine TNF
SNP	single nucleotide polymorphism
sTNF	soluble TNF
TACE	tumor necrosis factor alpha converting enzyme
tetR	tetracycline repressor protein
TGF-β	transforming growth factor beta
TNF	tumor necrosis factor
TNFR	tumor necrosis factor receptor
TRAIL	TNF-related apoptosis inducing ligand
Tregs	regulatory T cells
vp	virus particle
wt	wild type
x	multiplied by

Chapter 1: Introduction

Cancer remains a leading cause of death in the developed world, despite being the focus of intense research and drug development (*1*). The disease is hallmarked by mutated cells that are self-sufficient in growth signalling, resist apoptosis and anti-proliferative growth signalling, acquire replicative immortality, induce angiogenesis and invade and metastasize to other tissues (*2*). Additionally, tumour cells must avoid immune destruction and tumours can induce tumour-promoting inflammation, see figure 1.1 (*3*). These critical carcinogenic properties can be acquired through loss-of-function mutations, epigenetic silencing and tumor suppressor gene deletions in combination with gain-of-function mutations, amplifications and overexpression of oncogenes (*4*).

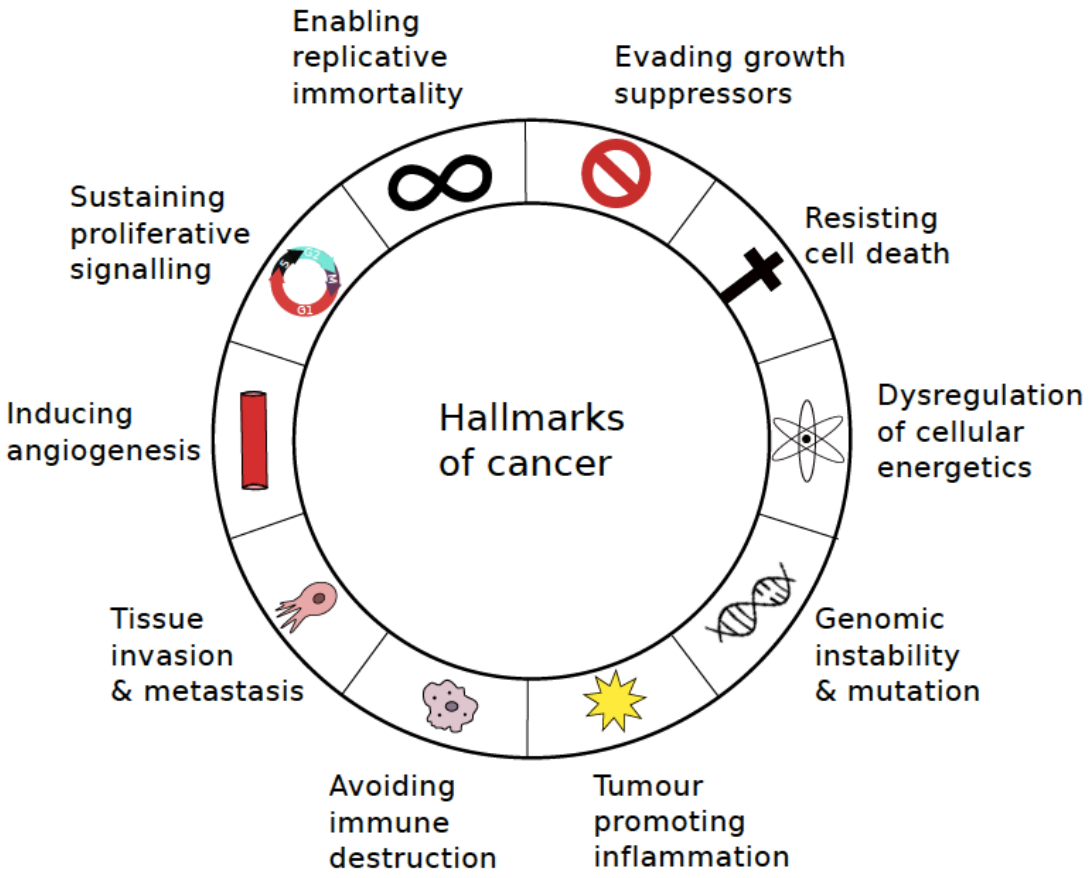

Figure 1.1: The hallmarks of cancer. Figure adapted from Hanahan et al (*3*).

1.1 Colorectal cancer

Colon and rectum cancers (CRCs) are the third most prevalent cause of cancer related death worldwide (*1*). The incidence is low in people under 50 years of age, but increase as people age and the median age at diagnosis is 69 (*5*). Moreover, the incidence is high in Europe, North America and Oceania, whereas incidences are lower in south and central Asia, Africa and South America (*6*). Several risk factors have been identified to date, including old age, male sex, family history, inflammatory bowel disease, smoking, diabetes, obesity, and excessive alcohol consumption (*7*). Additionally, there is some evidence that high consumption of red and processed meat contributes to the development of CRC, whereas consumption of fish, fruit and vegetables and a diet high in fiber may slightly reduce the risk of CRC (*7*), however this remains contentious.

Most CRCs arise from large benign polyps. Approximately half of the polyps over 2 cm undergo malignant transformation, whereas malignant transformation is rare in polyps under 5 mm (*8-10*). The development from polyps to CRCs can take many years. Frequent events in the development of malignant CRCs are mutations in the APC gene, activating mutations in KRAS and inactivation of p53 (*11-15*). Depending on tumour size, depth of invasion, involvement of lymph nodes (LNs), and the presence of distant metastasis, CRC is staged (stage I to IV). Survival correlates with the stage of disease; stage I is the least advanced disease and has the best prognosis (*16*). The 5-year survival rate for patients with stage IV colon or rectal cancer is below 10% (*17*), thus clearly indicating the need for improved therapy options for these patients.

1.1.1 Current treatment options

For CRCs, surgical resection of the tumour and resection of regional LNs is the preferred treatment. Resection of LNs reduces local tumour recurrence. Approximately 10-20% of the CRC patients are first diagnosed with metastatic disease (stage IV). For patients with unresectabe metastatic CRC, chemotherapy regimes, including fluoropyrimidines, oxaliplatin or irinotecan, are used. Patients with advanced metastatic disease on these regimens have a median survival of only 2 years (*18*). This low median survival clearly indicates the need for improved therapy options for patients with advanced disease. One of the new therapeutic approaches for advanced CRC currently being developed is oncolytic virus therapy.

The aim of this thesis is to develop a novel chimeric Adenovirus, ColoAd1, armed with tumor necrosis factor α (TNF) and lymphotoxin α (LTA). By arming this virus with pro-inflammatory cytokines the aim is to overcome the immunosuppressive tumour environment and improve the efficacy of oncolytic virus therapy.

1.2 Oncolytic viruses

Viruses are RNA or DNA containing particles that enter cells and exploit the cellular machinery for replication and expression of their genetic material. These properties make viruses a good tool for gene therapy or oncolytic virus therapy. Oncolytic virus therapy uses replication-competent viruses that infect and selectively replicate in tumour cells, leading to lytic death of transformed cells. Several viruses appear to have a natural selectivity for infection of and

replication in tumour cells (*19*). For successful infection, viruses need to interfere with the cell-cycle control and DNA damage sensing mechanisms of cells. The resistance to apoptosis, the loss of interferon signalling and the loss of cell cycle checkpoints make tumour cells more susceptible to virus therapy than non-transformed cells (*20, 21*). Additionally, as tumours develop, they acquire mutations that allow them to avoid immune detection and destruction, which are important mechanisms for limiting viral infections in healthy tissue (*22*). Numerous viruses have been used for oncolytic virus therapy including, including measles virus, vaccinia, vesicular stomatitis virus, reovirus, myxoma virus, Newcastle disease virus, herpes simplex virus and adenovirus, reviewed by Parato et al. (*21*). One of the major benefits of oncolytic virus therapy is that the concentration of therapeutic virus can be amplified within the tumour, upon successful infection, see figure 1.2.

Deletion of viral genes targeting cell cycle and apoptosis, replacement of viral promoters with tissue or tumour specific promoters, insertion of microRNA target sequences, or targeting to antigens that are overexpressed on tumour cells are common strategies to enhance tumour specificity of oncolytic viruses (*21, 23*). Additionally, the combination of virotherapy with other therapeutic modalities is currently investigated.

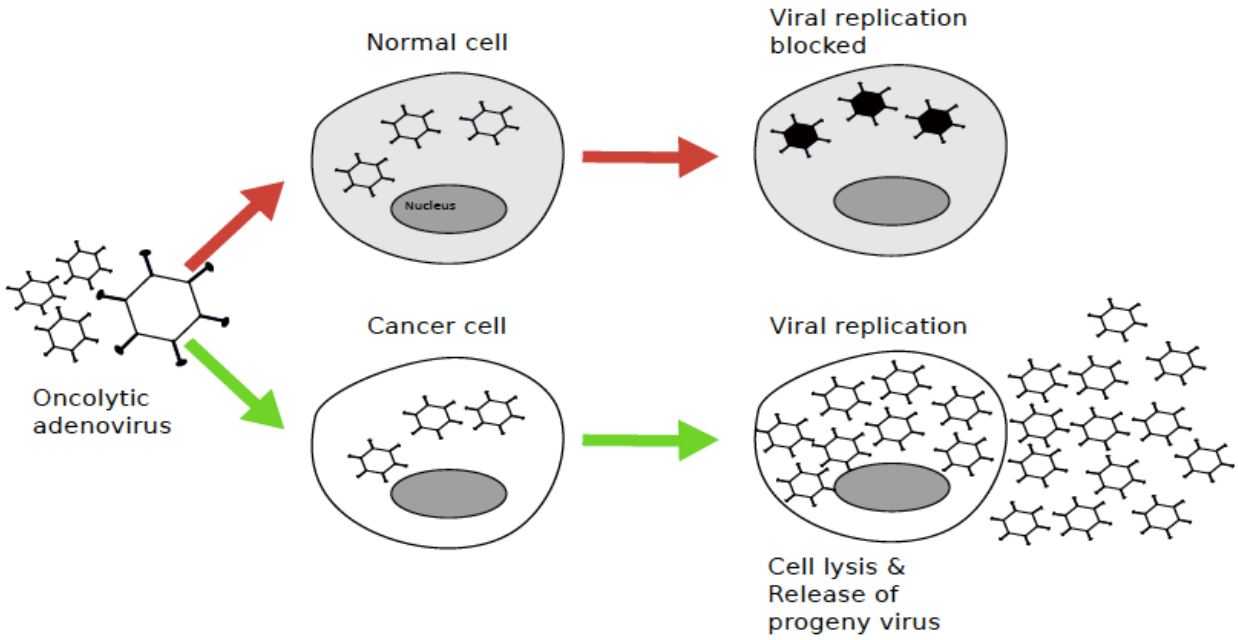

Figure 1.2: Schematic overview of rationale behind oncolytic adenovirus therapy. Mutations in the viral genome inhibit replication in non-transformed cells, whereas cancer cells are permissive to viral replication and will be lysed upon viral progeny release. Figure adapted from Choi et al (24).

1.2.1 Arming oncolytic viruses

In addition to modifications to that increase tumour-specificity, viruses can also be "armed" to express and secrete proteins from tumour cells to further enhance anti-tumour effects with minimal systemic toxicity. Several armed oncolytic viruses are currently in clinical trials. T-Vec, an oncolytic herpes virus encoding granulocyte macrophage colony-stimulating factor (GM-CSF) recently met its primary endpoint in in Phase III trial for melanoma (*25, 26*). In 2015, an FDA committee has recommended approval for treatment of advanced melanoma. GM-CSF is a powerful recruiter and activator of dendritic cells (DCs) and the efficacy of T-Vec is thought to rely partially on systemic anti-tumour immune stimulation (*27*). T-Vec is an important proof-of-concept for arming oncolytic viruses to enhance anti-tumour immunity and have increased interest in the development of other oncolytic viruses encoding immune modulatory proteins.

Please see table 1.1 for an overview of oncolytic viruses armed with immune stimulatory molecules currently in clinical trials. Two possible candidates for arming oncolytic viruses are tumor necrosis factor α (TNF) and lymphotoxin α (LTA) and these are the subject of this thesis. Both proteins are potent immune activators, however systemic toxicity has limited their clinical use by i.v. delivery. The rationale for using these cytokines is discussed in more detail in section 1.5.

Virus	**Therapeutic transgene**	**Clinical trial**	**Reference**
Herpes Simplex Virus I	GM-CSF	Phase III, advanced melanoma	(*25, 26*)
Adenovirus (Ad5/Ad3-E2F-Δ24)	GM-CSF	Phase I, refractory solid tumours	(*28*)
Adenovirus (Ad5)	GM-CSF	Phase I, invasive bladder cancer	(*29*)
Vaccinia Virus	GM-CSF	Phase II, hepatocellular carcinoma	(*30*)
Vesicular Stomatitits Virus	IFNβ	Phase I, hepatocellular carcinoma	Trial no. NCT01628640
Adenovirus (Ad2)	HSP70	Phase I, advanced solid tumours	(*31*)

Table 1.1: An overview of engineered viruses armed with immune stimulatory transgenes currently in clinical trials.

1.3 Adenoviruses

Adenovirus have a long history of applied research and are the basis of several experimental vaccines, gene therapies and oncolytic approaches (*32*). They have several properties that lend themselves to clinic use including relative ease of manufacture, good safety profile, stability of capsid and genome (high fidelity polymerase). The well understood genetics low mutation rate and ability to use promoters (unlike RNA viruses) make them a useful therapeutic platform.

Adenoviruses are found in a wide range of vertebrates, including fish, birds and mammals. So far, 52 human serotypes (Ad1-Ad52) have been identified, classified into seven species (A-G) (*33*). Traditionally, adenoviruses were classified based on hemagglutination and serology but this has now been replaced with by classification based on genome homology. Ad5 and Ad2 (both species C) are the best characterized and most studies on adenovirus biology have used these serotypes. Ad5 is also the virus most commonly used for oncolytic virus therapy to date. Perhaps as a result of the pre-existing antibody levels in humans, clinical results with oncolytic Ad5 have been disappointing.

Ad virion structure

Ads are double-stranded DNA (30-38 kbp) non-enveloped viruses with an icosahedral capsid. The virion capsid is composed of 240 hexon trimers, 12 penton-base pentamers and 12 fiber trimers (*34*). Furthermore, the capsid contains several minor capsid proteins, including protein IIIa, VI, VIII and IX, see figure 1.3. The minor capsid proteins help stabilize the major capsid proteins.

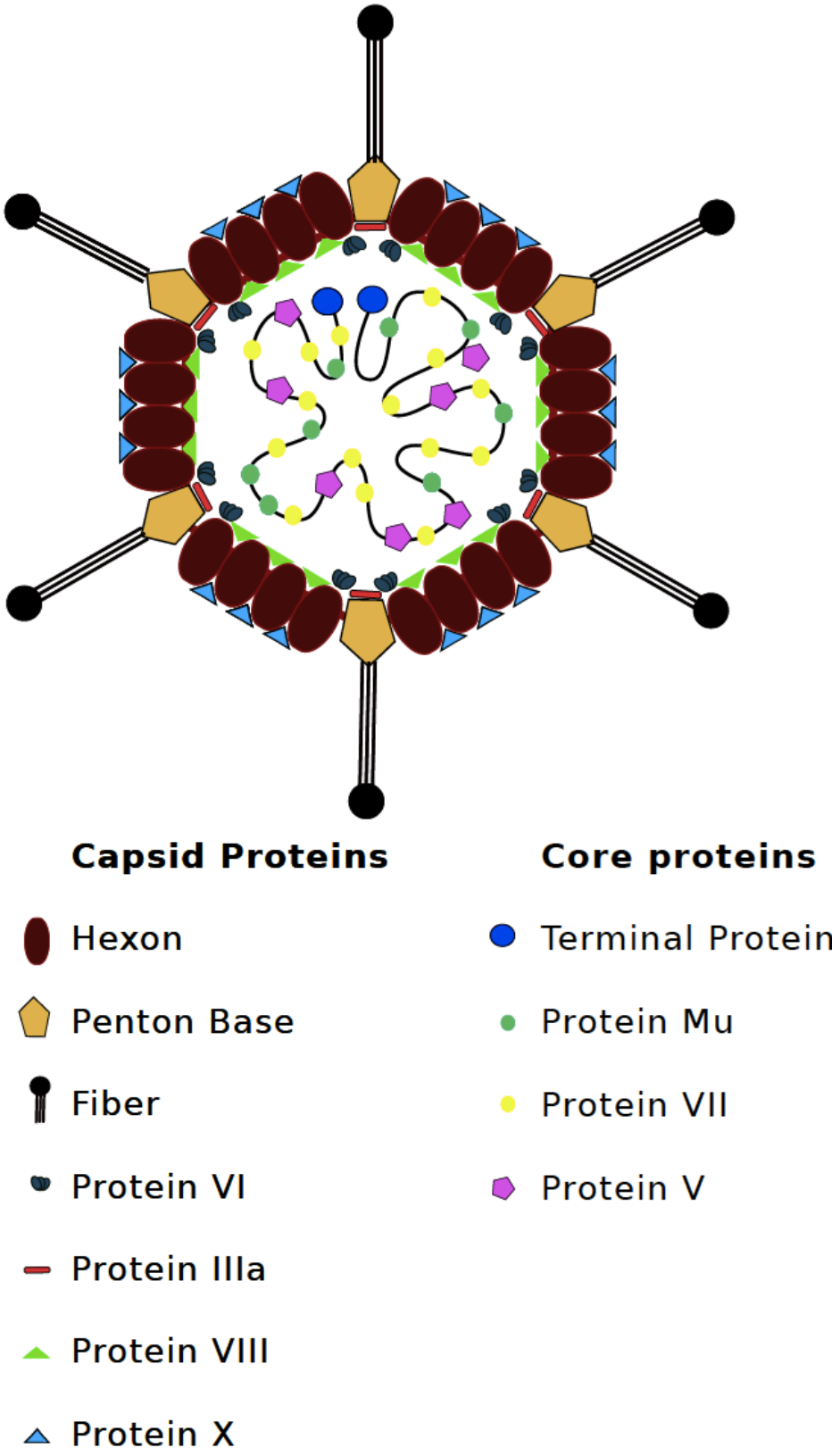

Figure 1.3: Schematic view of adenovirus particle structure (*35*). Schematic cross-section view showing the eleven structural proteins of the human adenovirus virion, based on cryo-electron microscopy and crystallography studies. The hexon, penton and fiber proteins form an icosahedral capsid. Figure redrawn from Nemerow et al (*35*).

Adenovirus life cycle

The adenovirus life cycle can be divided into several stages, including cellular attachment and entry, endosomal escape and nuclear trafficking, replication and cell lysis and release.

Cellular attachment and entry

The earliest interaction between cells and virions is the binding of the fiber knob to cellular surface receptors. In species A, C, D, E and F the fiber knob binds to the Coxsackie and adenovirus receptor (CAR) (*36*). For species B adenoviruses, CD46 and desmoglein-2 (DSG-2) have been reported as cellular entry receptors (*37, 38*).

Virion attachment via fiber is followed by a lower affinity binding of cellular integrins $\alpha_V\beta_3$ and $\alpha_V\beta_5$ to the RGD loop domains of the penton bases (*39*). This interaction triggers the clathrin-mediated endocytosis of the virion in most Ad species. However, in Ad3 and Ad35 (both species B viruses) uptake via clathrin-independent macropinocytosis has been reported (*40, 41*).

Endosomal escape and nuclear uptake

After cellular uptake, adenoviruses rapidly escape the endosome. Escape from the endosome requires an acidic pH. Failure to escape the endosomes leads to maturation of the early endosomes into late endosomes and fusion of these intracellular vesicles with the lysosome. This leads to degradation of the virion and its DNA (*42*). Escape from the lysosome has been reported as a slower process for species B adenoviruses compared to species C (*43*).

Upon escape into the cytosol, the partially dismantled capsid interacts with the dynein to get transported to the nucleus via the microtubule (*44*). Next, interaction with the nuclear pore complex is necessary for the complete disassembly of the capsid and release of the viral DNA (*45*).

Gene expression, translation and replication

The adenovirus genome contains 5 early genes (E1A, E1B, E2, E3 and E4), 4 intermediate genes (IX, Iva2, L4 intermediate and E2 late) and one late transcription unit under the control of the major late promoter (MLP) (*32, 46*).

Once in the nucleus, the E1A gene is the first to be expressed, followed by E1B. Briefly, E1A proteins activate transcription and push the cell towards the S-phase, whereas E1B proteins inhibit the cellular apoptosis. E2 encodes proteins that are required for replication; E3 encodes proteins involved in inhibition of host immune responses and E4 proteins have numerous functions, including regulation of transcription and translation (*32, 46*).

The MLP controls the expression of the late genome regions (L1- L5); these regions encode structural proteins that are required for packaging progeny virus. The late viral mRNAs are preferentially translated over host cell mRNAs due to ribosome shunting (*47*). Eventually, progeny virus is assembled and is released upon lytic death of the host cell.

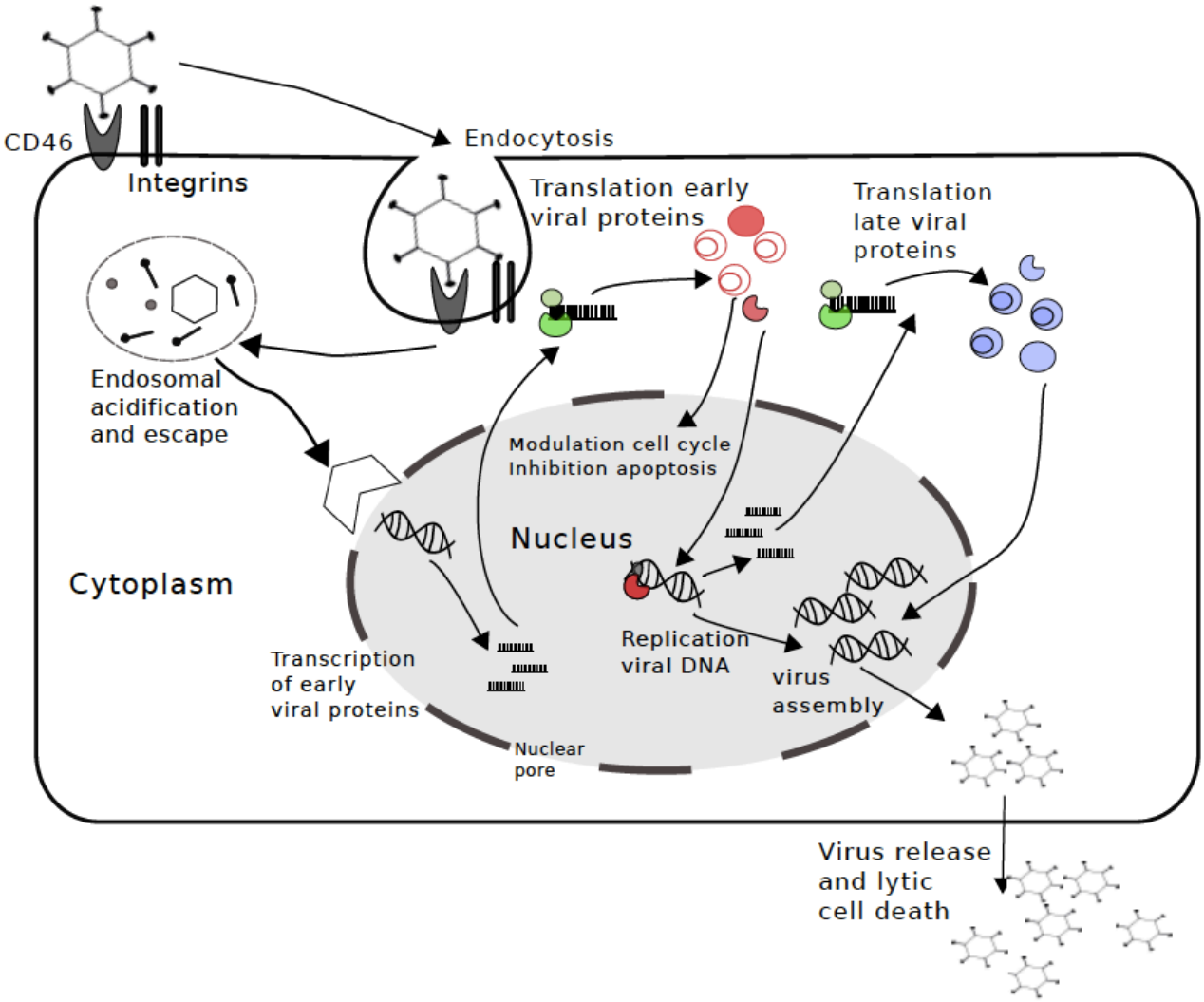

Figure 1.4: schematic overview of the adenovirus life cycle. Virus infection starts upon binding of the virus to cellular receptors, followed by internalization via endocytosis or macropinocytosis. The virus is dismantled in the endosomes and subsequently escapes the endosome. The partially dismantled is trafficked along the microtubule towards the microtubule organizing center, via dynein motors. Attachment to the nuclear pore complex and further dismantling of the capsid allows the viral DNA to enter the nucleus. Early viral genes are expressed and later in transfection, the structural late proteins are expressed from the major late promoter (MLP). These structural proteins enter the nucleus, where the progeny virus is packaged. Finally, the particles are released from the cell upon cell lysis. Figure adapted from Lenaerts et al (*48*).

1.3.1 Ads and the immune system

Adenoviruses encode at least eight proteins that help infected cells evade the host's immune response (*49*). So far, most functions of E3 proteins have been determined using Ad5. The E3 region codes for proteins that protect Ad-infected

cells from MHC-restricted cytotoxic T lymphocytes, block cytotoxic effects of proapoptotic cytokines and block immune-mediated inflammation. E3-gp19K is integral membrane protein and it is mostly located in the ER. E3-gp19K is very abundant among the early synthesized viral proteins (*49*). E3-gp19K prevents MHC class I molecules from transporting to the cell surface by interfering with class I terminal glycosylation (*50-54*). Additionally, E3-gp19K interferes with peptide loading onto MHC class I molecules (*54*). Several adenovirus proteins act on the TNF pathway. The E1A region makes cells susceptible to cytotoxicity by TNF (*55*). Conversely, the 14.7K protein protects infected cells from lysis by TNFα (*56*). The 14.7K protein inhibits internalization of the TNFR1 and formation of the death inducing signalling complex (DISC) (*57*). The 10.4K and 14.5K E4 proteins also inhibit lysis by TNF in some, but not all, murine cell lines (*58*). In human cells, the E1B-19K protein can protect fibroblasts and several cancer cell lines from lysis by TNF, whereas this protein cannot protect lysis by TNF in murine cells when infected with mutant Ad5 viruses that lack the E3 region (*59*). Thus in humans, several proteins can interfere with lysis by TNF and is not solely dependent on the E3-14.7K protein. The 10.4/14.5K complex, also called receptor internalization and degradation (RID) complex, induces a loss of Fas expression on the cell surface and blocks Fas-induced cell death of infected cells (*60*). The E3 encoded 6.7K protein can interact with the 10.4/14.5K complex and downregulates the TRAIL receptor (TRAIL-R) 1 and TRAIL-R2 (*61*).

1.3.2 ColoAd1

A downside of rationally-designed oncolytic viruses is that changes made with the intention to achieve one improvement, for example selectivity, can have undesirable effects such as lower potency (*21*). Bioselection on the other hand allows for the genome to find the best solution to the problem (or selection criteria) being asked. Selection is a process that works well for viruses and using this approach to identify viruses that specialize in cancer cells can provide interesting therapeutic candidates as well as telling us a little bit about how cancer cells behave. A process in which genetic mutations rendering favorable phenotypes are selected can be used to overcome the attenuation in cancer cells.

A chimeric Ad11p/Ad3 virus (see figure 1.5), named ColoAd1 (also known as Enadenotucireve), was identified with this approach. Specifically, a chimeric library of adenoviruses was produced by growing a range of adenovirus serotypes at high MOI, to promote recombination. The recombinants, with increased potency on cancer cell lines were selected, by repeated passage. ColoAd1 has increased potency compared to the parental viruses or Ad5 on tumour cells and reduced toxicity on non-transformed cells, thus increasing its therapeutic window, *in vitro* (*62*). ColoAd1 is currently in phase I/II clinical trials (NCT02028442), using i.v. delivery for metastatic carcinomas.

Analysis of the virus genome shows deletions in the E3 region and in the E4 open reading frame (orf)4. Additionally, the E2B region is a chimeric region with some substitutions of Ad11p sequences with Ad3 sequences. The E2B region encodes pre-terminal protein and DNA polymerase.

E3 proteins are non-essential for replication, but E3 is a virulence factor involved in interference with host immunity (discussed in more detail later). *In vitro*, or possibly in immune suppressed tumours, functional immune cells may not be a strong selection pressure. Losing this genomic region may help to increase potency, while also providing space for arming. The E4orf4 deletion is interesting, E4orf4 activates mammalian target of rapamycin (mTOR) and is thought to be involved in dysregulating cellular nutrient pathways to allow more resources to be directed towards synthesis of viral DNA and macromolecules. Most cancer cells have already dysregulated cellular energetic pathways, so the E4or4 gene may be redundant in cancer. Thus, the loss of E4orf4 may contribute to increased specificity of ColoAd1 in cancer cells. Indeed work on E4orf4 has shown that its loss does attenuate adenoviruses in normal cells (*63*), while being surplus in tumour cells.

Using a species B virus as oncolytic virus therapy may have several advantages over using a species C virus such as Ad5 and Ad2. Compared to Ad5 and Ad2, the prevalence of pre-existing immunity against Ad11 is very low, making it a good candidate for oncolytic adenoviral therapy (*64*). Additionally, Ad11 has been shown to have similar anticancer activity to Ad5 in mice carcinoma models. A decrease in liver toxicity with Ad11 was seen in this model (*65*).

The mutations in ColoAd1 compared to the parental Ad11p virus are listed in table 1.2.

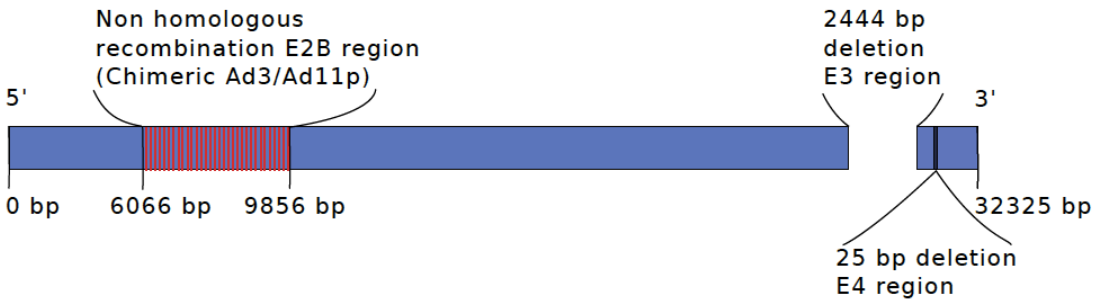

Figure 1.5: Schematic overview of the ColoAd1 genome. Blue indicates identical sequence to Ad11p. Frequent substitutions of Ad11p with Ad3 sequences are found in the E2B region. Additionally, there are deletions in the E3 and E4 regions. Figure redrawn from Kuhn et al (62).

Gene	Alteration
E2B	Ad3 substitutions
E3 10.3	Deletion
E3 15.2	Deletion
E3 18.5K	Fused with 15.3 K
E3 15.3K	Fused with 18.5K
E4orf4	Partial deletion

Table 1.2: Differences in ColoAd1 proteins compared to parental Ad11p virus.

1.4 The tumour microenvironment system

Besides the intrinsic properties of transformed cells (*66*), the tumour microenvironment and immune system also play important roles in disease development. Solid epithelial cancers, known as carcinomas, are complex tissues composed of numerous cell types, including the transformed cancer cells, and several non-transformed cell types such as fibroblasts, epithelial cells and innate and adaptive immune cells (*67*). These different cells have complex interactions with other cells in the tumour mass. Importantly, the tumour associated non-transformed cells can actively enhance cancer progression (*3*).

1.4.1 Tumour-infiltrating immune cells

A dual role for immune cells is seen in cancer, as both antitumoural and tumour-promoting properties are seen in various immune cells. Epidemiological studies show that individuals suffering from chronic inflammatory disease have an increased risk of developing cancer (*68*). Chronic inflammation can result in excessive tissue remodelling, oxidative stress which can lead to DNA damage, which increases the risk of cancer (*67*). An increase in CRC has also been reported for patients that received solid organ transplants and subsequent immunosuppressive therapy to avoid host versus graft disease (*69, 70*), indicating that the immune system may be important in reducing the development of cancer. The immune system also plays an important role in controlling the growth of established tumours, as the presence of tumour infiltrating lymphocytes has been correlated with a better prognosis for patients (*71-75*). Increased cancer susceptibility is also seen in immune compromised animal models. RAG2 KO mice, deficient in both T and B cells, developed more lung and colon adenocarcinomas when challenged with methylcholanthrene (MCA) than wt mice (*76*). Moreover, mice lacking both STAT1 and RAG2, thus also having impaired IFN-γ signalling, were even more sensitive to MCA. The tumours that developed in RAG2 KO mice were more immunogenic and rejected at higher frequency compared to tumours from wt controls when inoculated into immune competent mice. These findings led to the development of the cancer immunoediting hypothesis, in which the immune system not only reduces tumour formation, but also shapes tumour immunogenicity (*77*). According to this hypothesis, for cancers to develop, three sequential phases occur, namely elimination, equilibrium and finally immune escape. During the first phase,

mutated cells express altered antigens or stress ligands or dying cells release danger signals. Innate and adaptive immune cells can recognize these signals and destroy tumours, the elimination phase. Tumours surviving this elimination phase may get to an equilibrium in which the immune system prevents tumours from growing. Immunoediting of tumours occurs during this phase, as more immunogenic cells are destroyed, whereas less immunogenic cells avoid destruction. Finally, an escape phase occurs, where tumours develop active strategies to circumvent the immune system and tumours can grown on to present as clinical disease (*77*).

1.4.1.1 T cells

High numbers of T lymphocytes has been correlated to a good prognosis in many different types of cancer, including melanoma, ovarian cancer, esophageal cancer and colorectal cancer (*71-75*). High $CD8^+$ T cell infiltration into CRCs has been correlated with decreased recurrence (*78*) and better survival (*74*). However, few patients have high levels of $CD8^+$ infiltration, thus attracting more cytotoxic T cells may be beneficial for the majority of cancer patients. $CD8^+$ T cells recognize infected cells through the presentation of foreign peptide antigens presented on the cell surface by MHC class I molecules. Peptides derived from proteosomally-degraded proteins in the cytoplasm get transported to the endoplasmic reticulum (ER) via the transporter associated with antigen processing (TAP). TAP mediates loading of peptides to MHC class I molecules and the loaded MHC class I molecules get transported to the cell surface (*79*). Foreign antigens on the MHC class I molecule interacts with T cell receptors and causes $CD8^+$ cells to release perforin, granzymes or interaction with Fas and TRAIL receptors on the target cell.

High levels of mRNA encoding genes typically associated with $CD4^+$ T-helper 1 cells also correlated to lower metastasis in CRC patients (*75*). Furthermore, expression of Th1 associated molecules correlates with prolonged disease-free survival in CRC patients (*80*). In this study, no correlation between prognosis and Th2 responses were seen. Finally, a high infiltration of memory T cells ($CD3^+CD45RO^+$ cells) in primary colorectal cancer is associated with an absence of early signs of metastasis (*81*).

Tregs

Regulatory T cells (Tregs) are important in maintaining peripheral immune tolerance. However, in cancer they are an important factor in immunosuppression and immune escape. In patients, infiltration of Tregs into tumours is associated with a poor prognosis (*82*). Tregs are able to recognize tumour-associated antigens and dampen T cell responses against them (*83*). Additionally, Tregs secrete immunosuppressive cytokines such as TGFβ and IL-10 and immunosuppressive metabolites such as adenosine (*84*). Tregs also induce cytolysis of effector T cells by granzyme A or B and inhibition of the maturation and activation of DCs (*84*).

1.4.1.2 Natural Killer cells

NK cells play an important role in anti-tumour immune responses, in both human and murine models (*85-88*). Approximately 5-15% of human peripheral blood lymphocytes are NK cells. These cells are also found in the spleen, lymph nodes, bone marrow and certain organs (*87*). NK cells have both activating receptors and killer inhibitory receptors (KIRs). Activating receptors can bind to ligands overexpressed on tumours. Additionally, KIRs bind to MHCI molecules

and downregulation of MHCI molecules by tumours can lead to NK cell activation. NK cells can also act through antibody-dependent cell-mediated cytotoxicity (ADCC) or by secretion of cytokines, such as IFNγ. In humans, NK cells are defined as $CD3^-$ $CD56^+$. Functional differences between NK cells expressing different levels of $CD56^+$ are found; cells expressing high levels are thought to have potent immunoregulatory properties, whereas NK cells expressing lower levels of CD56 are more cytotoxic (*89*).

Infiltration of high numbers of NK cells has been associated with a better prognosis in CRC patients (*90*) Downregulation of MHCI molecules is a frequent event in CRCs, making this tumour type a good target for NK cells (*91*). Interestingly, CRC stem cells express higher amounts of NKp30 and NKp44 ligands, which bind to activating receptors on NK cells, making these cells more sensitive to NK-mediated death (*92*).

NK cells markers used in this thesis are $CD45^+$ $CD49b^+$ or $CD45^+$ $NK1.1^+$ for flow-cytometry experiments in mice.

1.4.1.3 Macrophages

Macrophages are terminally differentiated myeloid cells derived from monocytes (*93*). Macrophages are very plastic cells that can have an M1 or M2 phenotype (*94, 95*). It should be noted that these are likely extremes on the spectrum and many macrophages exhibit both M1 and M2-like characteristics.

Bacterial substances, such as LPS and the Th1 cytokine IFNγ induce polarization towards an M1 phenotype, whereas the Th2 cytokine IL-4 induces M2 polarization (*96*). M1 macrophages are “classically activated” macrophages and these macrophages release pro-inflammatory and microbicidal and tumoricidal cytokines such as IL-6, IL-12, IL-23 and TNFα. Cytokines secreted by M1

macrophages promote the activity of NK cells, Th1 cells and cytotoxic T cells. M2 macrophages are more phagocytic, have a high expression of mannose and galactose receptors, and express high levels of IL-10 and IL-1 decoy receptor (*94, 95, 97*). These M2 macrophages are thought to be involved in matrix deposition, tissue repair and immunoregulation. IL-10 pushes T helper cells towards a Th2 phenotype and enhances Treg activity (*93*). Additionally, M1 and M2 macrophages secrete distinct patterns of chemokines, with M1 secreting more CXCL9 and CXCL10, which attract Th1 T cells and cytotoxic T cells, whereas M2s secrete higher levels of CCL17, CCL22 and CCL24. These chemokines attract Tregs, Th2 T cells, eosinophils and basophils (*98*).

Infiltration of macrophages into the tumour microenvironment is seen in all solid tumours (*99*). In most types of cancer, extensive infiltration of macrophages has been linked to poor patient outcomes. Tumour associated macrophages (TAMs) exhibit several tumour promoting actions, including the promotion of angiogenesis, tumour cell invasion and metastasis in breast cancer models and the induction of chemotherapy resistance by $CD68^+$ macrophages in myeloma patients (*100-102*). In CRCs, however, peritumoural $CD68^+$ macrophages have been linked to good prognosis (*103-105*).

For this thesis, macrophages markers used in flow-cytometry analysis are $CD45^+$ $CD11b^+$ $F4/80^+$.

1.4.1.4 Dendritic cells

Dendritic cells (DCs) are terminally differentiated cells, often from a myeloid origin. Their primary function is to process and present antigens. Two subsets of DCs exist, the conventional DC (cDC) and the plasmacytoid DC (pDC). These subsets differ in function, morphology and markers. Most DCs differentiate along

the myeloid-lineage pathway, but DCs can also stem from common lymphoid progenitor (CLP) cells. Finally, monocytes can also differentiate into cDCs (*93, 106*). DCs are activated by numerous stimuli, such as viruses, bacteria and tissue damage. Upon an encounter with these stimuli, DCs mature and gain full activation. DCs play an important role in developing an antitumour response, as these cells are the most potent antigen presenting cells (APCs). Presentation of tumour antigens by DCs can induce tumour specific T-cell responses. However, abnormal myeloid differentiation and DC activation leads to defects in the antitumour immune response (*106*). CD80 and CD86 are important co-stimulatory molecules expressed by activated DCs. Expression of these co-stimulatory molecules was seen in less than 10% of DCs infiltrating colon carcinomas in a rat model (*107*). Moreover, DCs infiltrating these tumours could induce T-cell anergy. TNF, CD40 and GM-CSF are known inducers of CD80 and CD86 expression in DCs (*106*).

For this thesis, the markers used for flow-cytometry analysis of cDCs are $CD45^{+}$ $CD11b^{+}$ $CD11c^{+}$ $F4/80^{-}$ (*93*).

1.4.1.5 Myeloid derived suppressor cells

Myeloid derived suppressor cells (MDSCs) are a very heterogeneous group of cells, containing precursor macrophages, immature myeloid cells, dendritic cells and granulocytes. MDSCs have been defined as $CD11b^{+}$ $Gr\text{-}1^{+}$ cells. Gr-1 comprises both Ly6C and Ly6G antigens. Based on levels of Ly6C and Ly6G antigens, the MDSC have been subdivided into $Ly6C^{low}$ $Ly6G^{+}$, granulocytic cells and $Ly6C^{high}$ $Ly6g^{-}$ monocytic cells in mice (*108*). In CRC patients, increased MDSCs in the peripheral blood is correlated to nodal metastasis and MDSC infiltration in the tumour is correlated to distant metastasis and tumour stage

(*109*). A correlation between increased MDSCs in the blood and tumour stage in CRC patients was also seen by Zhang et al (*110*). MDSCs promote tumour development by inhibiting immune responses and promoting angiogenesis and metastasis. MDSCs can specifically inhibit T cell responses and secrete immune suppressive cytokines such as TGF-β and IL-10 (*111*).

Granulocytic cells

Neutrophils are the most common granulocytic cells in the body. Like macrophages, neutrophils can have both tumour-stimulating and anti-tumour responses. In CRC patients, a high ratio of neutrophils to lymphocytes in the peripheral blood is a marker for poor prognosis (*112*). One of the main pro-cancer activities of granulocytic cells is through the promotion of angiogenesis and secretion of matrix degrading proteins (*113, 114*). Neutrophils have also been reported to provide support to pre-metastatic niches and subsequent development of metastatic tumours in the lung (*115*). Depletion of granulocytic cells has been correlated with reduced tumour growth in UV-induced syngeneic tumours (*114*). Additionally, in mice, $CD11b^+$ $Ly6G^+$ cells have immunosuppressive effects on antigen-specific $CD8^+$ T cell proliferation, through a ROS-mediated pathway (*108*).

However, neutrophils can also display anticancer effects in some models. Depletion of neutrophils increases mammary adenocarcinoma growth *in vivo* (*116*). Through ROS, metastasis in breast tumours can also be inhibited by neutrophils (*117*). Through the release of nitrogen peroxide, nitric oxide and inhibition of glutamine uptake by tumours, neutrophils can decrease tumour growth (*116, 118, 119*). The effects of neutrophils on tumour development are

likely influenced by the tumour microenvironment. For example, when TGF-β signalling is blocked, neutrophils become cytotoxic and secrete more pro-inflammatory cytokines and activate $CD8^+$ T cell responses (*120*).

Granulocytic cells markers used in this thesis are $CD45^+$ $CD11b^+$ $Ly6C^{low}$ $Ly6G^+$ (*93*).

Monocytic MDSCs

Monocytes enter the circulation expressing high levels of Ly6C and the Ly6C levels decrease progressively as monocytes mature (*121*). The normal differentiation of myeloid cells is blocked in cancer, causing an increase in immature monocytic MDSCs. On a functional level, monocytic MDSCs have higher levels of iNOS, whereas granulocytic MDSCs have higher levels of ROS (*108, 121*). *In vitro*, monocytic MDSCs derived from tumour-bearing mice can be induced to differentiate into DCs and macrophages (*108*). Monocytic MDSCs have been linked to Treg infiltration in tumours, in mice (*122*).

Monocytic MDSCs have been defined as $CD45^+$ $CD11b^+$ $Ly6C^{high}$ $Ly6G^-$ for flow cytometry analysis experiments performed in this thesis (*93*).

1.4.1.6 NK T cells and γδ T cells

NK T cells have characteristics that are both like NK cells and T cells. NK T cells recognize glycolipid antigens presented by CD1d, an MHCI-like molecule. Activated NK T cells secrete pro-inflammatory cytokines and cytotoxic molecules such as perforin, TRAIL and Fas-L. In CRC patients, increased NK T cell infiltration correlates with a better prognosis (*123*). γδ T cells have strong cytotoxic effects against CRC cells (*124*). γδ T cells recognize antigens in a non

MHCI-restricted way and can recognize metabolites made by cancer cells or heat shock proteins.

1.5 TNF Superfamily of Ligands and Receptors

Most members of tumor necrosis factor (TNF) ligand superfamily and TNF receptor (TNFR) superfamily are expressed by immune cells (*125*). There are more than 20 separate ligand-receptor interactions in the TNF superfamily and this signalling network is involved in cell proliferation, survival, differentiation and apoptosis of target cells in the bone, ectodermal and lymphoid organs (*126*).

1.5.1 TNF receptor signalling

TNF and LTA are located in a tightly linked locus within the major histocompatibility complex on chromosome 6 in humans and chromosome 17 in mice (*126*). Both TNF and LTA can signal through TNF Receptor (TNFR) 1 and 2. TNFR1 is expressed on almost all cell types, except erythrocytes (*127*), whereas TNFR2 is mainly expressed on immune and endothelial cells (*128*). Signalling through the TNFR2 leads to activation of multiple pathways, including NF-κB, JNK, p38, ERK, MAPK and PI3K (*129*). Contrary to the TNFR2, the TNFR1 has a death domain (DD) and can induce apoptosis and/or necroptosis. The TNFR2 is thought to be able to mediate cell death indirectly by enhancing the effects of the TNFR1 (*130*).

Like many members of the TNF ligand superfamily, TNF assembles into homotrimers. TNF is expressed initially expressed as a 26 kDa type II membrane-bound protein (mbTNF) and can be converted into a soluble 17 kDa protein (sTNF) by ADAM17/TACE (*131*). The TNFR1 can be activated by both

sTNF and mbTNF, wereas mbTNF is superior to sTNF in activating the TNFR2 (*132*). The stalk region, an extracellular region close to the transmembrain domain, of the TNFR2 inhibits receptor enrichment and clustering upon binding of sTNF but not mbTNF, thereby signalling only upon mbTNF binding (*133*). Moreover, substitution of this region in the TNFR2 to the stalk region of TNFR1 could induced signalling through the TNFR2 by sTNF (*133*).

TNF simultaneously activates both pro-apoptotic and anti-apoptotic pathways. The apoptotic signalling pathway does not require de novo protein synthesis, whereas pro-survival signalling depends on NF-κB activation and subsequent expression of pro-survival genes (*134*). Binding of the ligand causes the TNFR1 to form homotrimers, subsequently complex I is formed, consisting of TNFR1, TNFR-associated death domain (TRADD), TRAF2 and RIP. This complex mediates the activation of NF-κB, through the MEKK3, IKK and IκB cascade. NF-κB is activated through the ubiquitin-dependent degradation IκBα, which keeps the transcription factor in the cytosol (*128*). NF- κB is a group of 5 closely related transcription factors, Rel, RelA, RelB, NF-κB1 and NF-κB2, that regulate the expression of numerous anti-apoptotic proteins, including A20, cellular inhibitor of apoptosis (cIAP)1 , cIAP2, Bcl-xL, XIAP and IEX-1L (*135*).

Alternatively, apoptotic signalling occurs via the formation of complex II, consisting of RIP, TRADD, FADD and caspase 8 (*136*). Caspase 8 can be autocleaved, which starts a cascade of caspase 3, and caspase 7 activation, leading to DNA fragmentation and apoptosis. Caspase-8 can also activate BCL-2 interacting domain (Bid). Activated Bid causes the loss of the mitochondrial membrane potential and release of cytochrome c. This leads to mitochondrial mediated, intrinsic, apoptosis (*135*). Finally, TNF can cause cell death through a

programmed necrosis (necroptosis) pathway. RIP kinase activity, activation of Nox1 NADPH oxidase, and the formation of reactive oxygen species (ROS) mediate the necrotic cell death (*137-139*).

The balance between pro-apoptotic and anti-apoptotic signalling determines the cellular reaction to TNF (*128*). Downstream signalling of TNR1 and TNFR2 is depicted in figure 1.6.

Several mechanisms exist to regulate the TNF signalling and avoid prolonged TNF signalling. Upon binding of the ligand to the TNFR, the complex is rapidly internalized and degraded in the lysosomes (*140-142*). However, recycling of the TNF receptors to the cell surface has also been reported (*143*). Besides internalization, receptor shedding also occurs. Receptor shedding modulates responses to TNF. In humans, mutations affecting receptor shedding is associated with recurrent fevers and inflammatory disease. In mice, receptor shedding has been shown to protect against endotoxic shock and autoimmune disease (*144*).

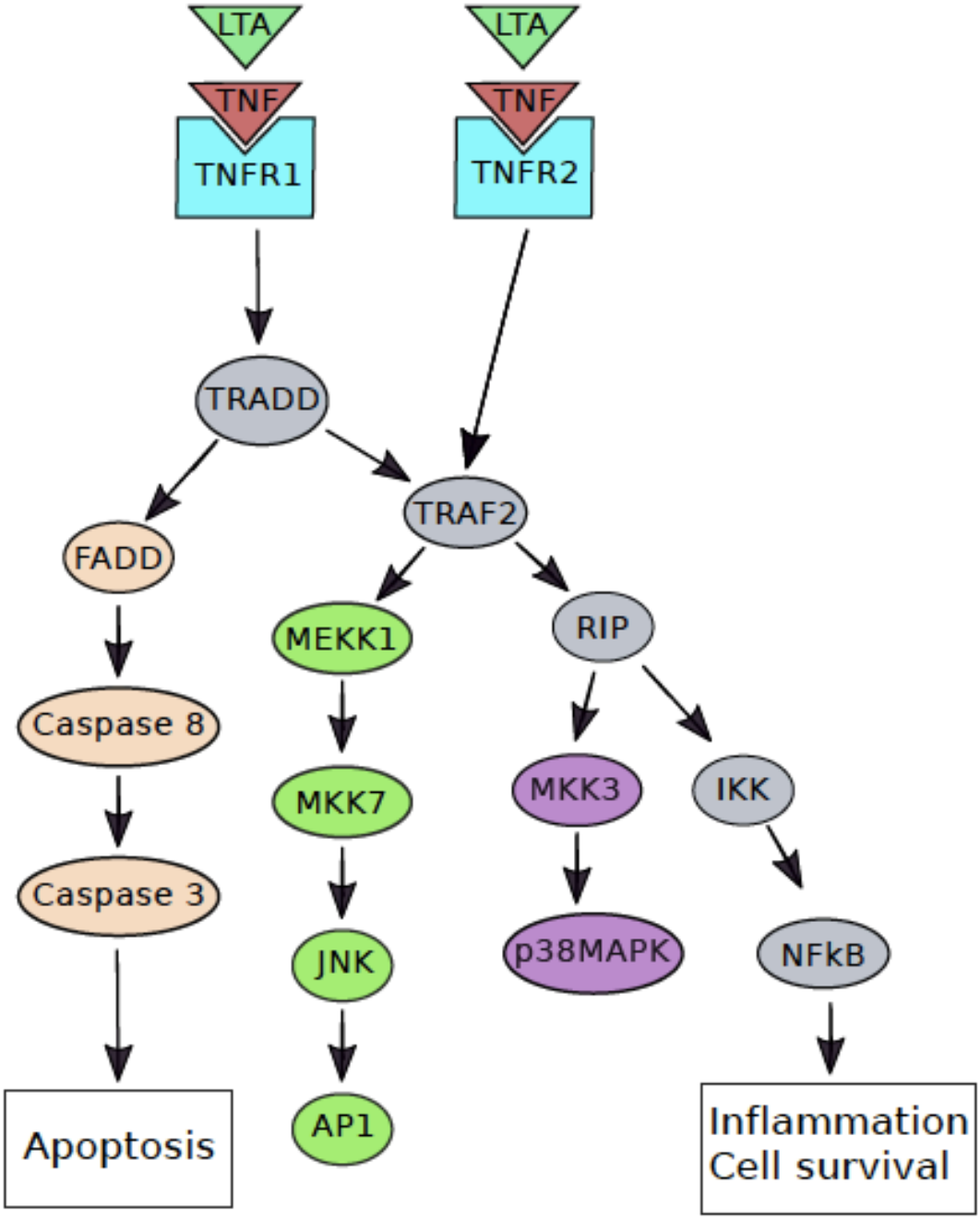

Figure 1.6: Signalling pathways downstream of TNFR1 and TNFR2. Binding of TNF or LTA to the TNFR can cause activation of caspases and subsequent cell death. Alternatively, activation of NF-κB can enhance cell survival and activate transcription of inflammatory genes . Figure adapted from Aggarwal et al (128).

1.5.2 LTA

LTA also constitutes an interesting molecule for therapeutic expression within tumours, because it mediates several of the functions of TNF and is reported also to cause increased lymphocyte influx into the tumour interstitium.

In 1968, LTA was first described as a lymphocyte derived anti-cancer protein (*145*). LTA does not have a transmembrane domain and homotrimers (LTA_3) are always secreted. Activated T, B and NK cells can secrete LTA_3 (*146*) LTA can also bind to LT-β and form heterotrimers. These heterotrimers can be membrane bound and signal mainly through the LT-β receptor. LTA_3 can bind Herpes Virus Entry Mediator (HVEM) as well as the TNFR1 and TNFR2.

Studies on LTA have reported weaker TNFR1-induced cell death, NF-κB activation, induction of cell surface markers and cytokine production compared to TNF. However, this is still controversial (*147*).

LTA KO mice do not have lymph nodes or Peyer's patches. Additionally, the spleen has abnormal architecture (*148*). Moreover, LTA KO mice show increased melanoma growth and metastasis and reduced NK cell infiltration in tumours (*149*). Additionally, antagonists of LTA or TNF inhibit NK cell-mediated killing of tumour cells (*150*). An antibody-LTA fusion protein targeting tumours, increases survival and reduces tumour growth in a syngeneic mouse melanoma model (*151*). An increase in high endothelial venules (HEVs) and increased T cell infiltration and priming was seen in mice treated with this fusion protein. Using a mononclonal agonistic antibody against LTβR inhibits the growth of CRCs in a syngeneic mouse model (*152*). Using this approach, increased lymphocyte infiltration and tumour necrosis were seen. Blocking LTβR signalling with a

neutralizing antibody reduced the anticancer effects of cytotoxic T cells, *in vitro* and (*153*).

Like many pro-inflammatory cytokines, LTA has also been found to contribute to pro-tumorigenic inflammatory processes. Single nucleotide polymorphisms (SNPs) in the LTA gene or promoter have been linked to increased incidence of cancer in humans (*154*). In a murine fibrosarcoma model, activation of the LTβR could also increase tumour growth, by inducing angiogenesis (*155*). Prolonged LTβR signalling has also been implicated in the development of hepatitis-induced hepatocellular carcinoma (*156*). Finally, B-cell produced LTA-LTβ heterodimers can activate LTβR on prostate cancer cells and activate NF-κB and increase tumour growth in a castration resistant mouse model (*157*).

Infiltration of especially $CD8^+$ cells into CRCs is associated with favorable clinical outcomes (*75, 78*). High endothelial venules (HEVs) are specialized venules containing cuboid endothelial cells that allow large numbers of lymphocytes to extravasate from the blood. HEVs are mainly restricted to secondary lymphoid organs but also occur at sites of chronic inflammation and tumours (*158*). In breast cancer, HEV density correlates with T- and B-lymphocyte infiltration and favorable clinical outcomes (*158*). Interestingly, the misexpression of LTA can induce the development of HEVs in mice (*159*).

1.5.3 TNF and cancer biology and treatment

Initially, TNF was seen as potent anticancer agents causing tumour necrosis (*160*). However dose-limiting systemic toxicity has limited its clinical use (*161*). More recently, TNF has also been linked to tumour progression and development.

Pro-tumour effects of TNF

Chronic inflammation is known to increase the risk of cancer. Pro-inflammatory cytokines may contribute to an inflammatory environment that promoter carcinogenesis. In chronic lymphocytic leukemia patients, increased levels of serum TNF are seen and high TNF levels correlate to a poor prognosis (*162*). Elevated levels of circulating TNF has also been correlated to increased CRC prevalence (*163*). Elevated TNF levels are also seen neoplastic tissue and positively correlated to tumour stage (*162, 164, 165*).

SNPs in the TNF promoter region have also been associated with cancer susceptibility. A SNP in the -308 position (-308G/A) has been linked to increased risk of numerous cancers, including CRC, non-Hodgkin's lymphoma, hepatocellular carcinoma, cervical cancer and non-small cell lung cancer and non-Hodgkin's lymphoma (*166-170*). A SNP at the -283A site lowers the risk of several cancers, including CRC, lung, renal, gastric and uterine cervical cancer (*170, 171*). Thus, several clinical observations link TNF to carcinogenesis and disease development. Numerous preclinical have also linked TNF to tumour progression. TNF KO mice are less susceptible to developing skin tumours compared to wild type mice when challenged with 7,12-dimethylbenz[a]-anthracene (DMBA) or 12-0-tetradeconyl-phorbol-13-acetate (TPA). Once tumours were established, similar rates in tumour progression were seen in wt and KO mice, suggesting that TNF mainly promoted tumorigenesis in the early stages in this model (*172*). TNFR1 KO mice are susceptible to colonic carcinogens (*173*) and showed fewer liver metastases in a colon adenocarcinoma model (*174*).

Long-term exposure to TNF makes cells more susceptible to malignant transformation upon exposure to MCA (*175*). Inhibition of TNF production by stromal cells also reduces the development of liver tumours by reducing NF-κB activity (*176*). TNF may also promote carcinogenesis by stimulating damaged cells to survive, via activation of NF-κB, TNF released by macrophages increased the survival of asbestos-damaged mesothelial cells and rendered the damaged cells more susceptible to malignant transformation (*177*). The upregulation of ROS by TNF can also contribute to carcinogenesis, as TNF-induced ROS can cause DNA damage and genetic instability (*178, 179*). Finally, TNF can stimulate tumour invasiveness and metastasis, through upregulation of matrix metalloproteases (MMPs) (*180, 181*). MMPs are proteolytic enzymes that are involved in many aspects of cancer biology, including cell growth, angiogenesis, differentiation, remodelling of the extracellular matrix and invasion and metastasis. Upregulation and increased activation of MMPs are found in most human cancers and MMP expression. In preclinical models, benign cancer cells can undergo malignant transformation upon MMP upregulation and cellular malignant behaviour can be reduced upon blocking MMP expression or activity (*182*).

In the majority of cancers, MMPs are not upregulated through gene amplification or activating mutations, but through increased expression by transcription factors, such as NF-κB and β-catenin (*180, 182*).

For example, TNF causes increased transcription of MMP9 in cancer cells mediated by NF-κB (*180, 182*).

However, tumour cells are not the only source of MMPs and stroma cells also contribute to MMP expression. Tumour cells may induce MMP expression by

stroma cells through immunomodulatory proteins, growth factors and emmperin (*182*) .

Anticancer effects of TNF

TNF appears to have multiple modes of action against tumours. At the cellular level, TNFR1 signalling can trigger activation of caspases and subsequent apoptosis or necrosis (*183, 184*). However, TNF sensitivity varies widely between cancer cell lines (*184*).

An increased susceptibility of TNF KO mice to developing sarcomas upon MCA exposure has been reported (*185*). A supportive role of TNF in immunesurveillance or immunoediting was suggested as a possible mechanism. Furthermore, in an *in vivo* model mixing tumour cells expressing antigens together with cells not expressing antigens, expression of TNF by $CD8^+$ cells was necessary to eradicate the non-antigen expressing cells (*186*). T cell-deficient mice have smaller anti-tumour responses upon TNF treatment than wt mice and mice cured of Meth A sarcomas by TNF show T cell mediated anticancer immunity (*187, 188*). In a rat model, blocking TNF signalling with polyclonal αTNF antibodies increased tumour growth, by dampening DC activation and subsequent T cell activation (*189*). Antagonists of LTA or TNF also inhibit NK cell-mediated killing of tumour cells (*150*). At high local concentrations, TNF can mediate the destruction of tumour vessels and induce anti-tumour immunity, *in vivo* (*68*). Additionally, synergy with radiation and chemotherapy has been found in preclinical and clinical studies. A more in depth discussion about TNF and radiation synergy can be found in the chapter 5.

In conclusion, TNF has seemingly contradictory roles in cancer biology. Like many other cytokines, the effects of TNF may be context-dependent. Endogenous expression of TNF and chronic exposure to low levels of TNF may contribute to a tumour-promoting microenvironment. However, at high doses, TNF can be tumoricidal.

1.5.3.1 Soluble and membrane-bound TNF

The majority of research on TNF as cancer therapy has used recombinant soluble TNF. However, several studies indicate differences between soluble and membrane bound TNF, as is also shown for other ligands of the TNF superfamily. The expression of mb TNF on $CD4^+$ cells has been identified as a co-stimulatory signal in the interaction between T and B cells (*190*). Additionally, mb TNF expressed on $CD4^+$ lymphocytes can activate macrophages and cytokine release in response to an intracellular parasite, whereas s TNF does not enable macrophage activation (*191*). Expression of mb TNF is crucial in inducing Tregs, whereas secreted TNF seems less important for Treg activation (*192*). Expression of mb TNF on lymphocytes or monoctyes can induce cytotoxicity in tumour cells resistant to soluble TNF (*193*). Thus, mb TNF mediates important non-redundant biological functions.

Soluble and membrane-bound TNF in cancer biology

A recent study found that sm TNF increased tumor growth, whereas mbm TNF (Δ1-9 K11E) inhibited growth and myeloid infiltration in mouse lung carcinoma tumours in C57Bl/6 mice (*194*). Additionally, tumours expressing sm TNF were found full of myeloid cells, but tumours expressing mbm TNF had a low

percentage of myeloid cells. The expression of mbm TNF was shown to induce ROS and cell death via the induction of ROS of tumour-associated myeloid cells.

A study comparing fm TNF and mbm TNF (Δ1-9 K11E) expressed from a E1 deleted, partial E3 deleted Ad5 vector found greatly reduced mouse mortality using the Ad5-mbm TNF compared to Ad5-fm TNF at high doses. Moreover, whilst showing less systemic toxicity, mice treated with Ad5-mbm TNF showed similar partial and complete regression rates as Ad5-fm TNF treated mice (*195*).

Opposite effects of sm TNA and mbm TNF in a different tumour model have also been found. Expression of mbm TNF (Δ1-12 TNF) on 4T1, murine mammary carcinoma cells, has been shown to increase tumour growth BALB/c mice by Hu et al, whereas sm TNF reduced tumour growth compared to control cells. Furthermore, an increase in $CD11b^+$ $Gr\text{-}1^+$ cells was seen in tumours expressing mbm TNF, as well as increased production of TGF-β and IL-10. Finally, in mice bearing tumours expressing sm TNF, an increase in $CD4^+$ and $CD8^+$ lymphocytes was seen, whereas a decrease was seen in lymphocyte infiltration in 4T1 mbm TNF tumours. *In vitro*, the expression of mbm TNF showed an induction of MDSC activity, which inhibited T cell proliferation, and increase in the arginase, iNOS and NO levels (*196*).

Several studies have used murine tumour cells expressing human TNF in syngeneic tumour models. In a murine hepatic carcinoma model, expression of human soluble TNF, wt and mb TNF all reduced tumour growth, compared to control cell lines in BALB/c mice. Expression of s TNF by tumour cells promoted $CD4^+$ and $CD8^+$ lymphocyte infiltration, whereas expression of mbm TNF increased Fas expression and reduced metastasis (*197*). In a mouse sarcoma model, constitutive full length TNF expression led to an increase in tumour

regression, possibly through $CD4^+$ and $CD8^+$ T cell mediated mechanisms (*198*). Karp et al. found that expression of soluble human TNF by murine fibrosarcoma cells reduced tumour growth, expression of human mb TNF did not affect tumour growth (*199*). It should be noted that signalling through the TNFR2 is species specific and human TNF cannot activate TNFR2 signalling.

1.5.3.2 TNF and the tumour-associated vasculature

Achieving adequate drug delivery to solid tumours is a major hurdle in cancer therapy. In order to achieve a good anticancer effect, drugs need to penetrate the tumour and reach all cells in sufficient concentration. Thus, tumour-associated vasculature is an important factor in the sensitivity of tumours to therapy (*200*).

There are several histological and functional differences between tumour associated vasulature and vasculature of normal tissue that reduce drug delivery to tumour sites. Blood vessels within solid tumours are more disorganized and more dilated, excessively branched and have more arteriolar-venous shunts compared to normal blood vessels. Additionally, irregular blood flow occurs at tumour sites and the growing mass of tumour cells can compress blood vessels and lymphatic vessels (*201*).

The collaps of lymphatic vessels reduces fluid drainage from the tumour sites and increases the interstitial fluid pressure (IFP), which can decrease drug delivery (*201*). The abnormal tumour associated vasculature causes hypoxia and the occurrence of nutrient gradients and chemotherapeutic gradients within solid tumours. This can influence the responsiveness of cancer cells to chemo and radiation therapy (*200, 201*).

The tumour-associated vasculature is highly sensitive to TNF (*183, 184*). TNF has multiple modes of action against the tumour-associated vasculature. At tumour

sites, the tight junctions of epithelial cells are disrupted by TNF through a RhoA/Rho kinase pathway, leading to increased vascular permeability (*202*). Also, the formation of hemorrahagic necrosis within tumours upon TNF injection also aids drug delivery (*203*). High IFP is thought to decrease drug delivery to tumours and reduced IFP has been observed upon i.v. TNF aministration in melanoma xenograft models (*204*). Finally, induction of thrombotic events in tumour-associated vasculature and necrosis within tumours has been observed in mice upon treatment with a adenoviral vector expressing TNF (*205, 206*).

Due to the effects TNF has on the vasculature, increased drug delivery into tumours when administering this cytokine has been found in numerous studies. In a murine subcutaneous xenograft CRC model, both i.t. and i.v. injection of human TNF increased vascular permeability. Using i.t. injections, up to 10 increase of extravasation of radioactive labeled IgG was observed in the tumours, 1 h after treatment, whereas i.v. injection of TNF increased the tumour vascular permeability approximaterly 3 fold (*207*). Similarly, increased levels of anti-CEA antibody were seen in tumours treated with TNF (both administered i.v.). Similarly, increased uptake of gandolinium, or radiolabelled trastuzumab was seen at brain metastasis sites upon TNF or LTA injection in a murine mammary carcinoma model (*183*).

The combination of TNF with doxorubicin or melphalan, in an isolated limb perfusion (ILP) model in rats, causes an increase of chemotherapeutic drug in the sarcoma tissue (*208, 209*). Moreover, synergistic effects were seen on tumour growth by combining TNF with chemotherapy in these studies. Drug accumulation at tumour sites is also observed when liposomal doxorubicin is administered in combination with TNF in a murine melanoma model (*210, 211*).

ILP using a combination of TNF and chemotherapy is also used clinically for sarcomas and melanoma.

Seki et al. showed that i.v. injection of TNF 30 min before i.v. administration of a non-replicating Ad5 vector expressing luciferase (AdLuc) could increase AdLuc accumulation at the tumour site 3-fold (*202*).

Together these results suggest that TNF may be helpful in increasing vascular permeability and drug delivery of a wide range of drugs including chemotherapeutic compounds, antibodies, liposomal chemotherapeutics and viral vectors into tumours.

1.5.3.3 Clinical use of TNF

Based on promising studies of TNF in mice, clinical studies were started using human recombinant TNF. Phase I studies estimated the maximum tolerable dose in humans as 150-300 μg/m^2 per day for bolus administration (*212-214*). Based on the phase I studies, several phase II studies were performed. In these phase II studies, objective tumour responses were seen in some patients (*215-220*). However, dose limiting toxicities, such as hypotension, fatigue and nausea, were observed. Additionally, fevers, chills, rigors, anorexia, vomiting and headaches were common side effects in patients. Furthermore, the phase I clinical studies indicated a short plasma half-life for human recombinant TNF, at less than half an hour (*221-223*).

Due to the systemic toxicity, the clinical use of TNF is restricted to isolated limb perfusion for soft tissue sarcoma and melanoma in combination with melphalan (*224-227*).

1.5.3.4 Strategies used to achieve high local doses of TNF

Since the failure of systemic TNF therapy, several attempts to achieve better intratumoural delivery of TNF have been made. Methods used include encapsulation of TNF in liposomes, linking TNF to homing peptides and antibodies and expressing TNF locally from viral vectors.

Encapsulation of TNF in PEGylated liposomes reduces systemic toxicity, upon i.v. administration. Synergy between radiation therapy and TNF liposomes was observed (*228, 229*). Interestingly, an increase in lymphocyte activation and NK cell number was seen in the blood and spleen of mice treated with TNF liposomes combined with radiation therapy (*229*). Additionally, the combination of liposomal TNF and radiation increased macrophage, neutrophil and NK cell infiltration into tumours (*228*). A study by ten Hagen et al. showed that doses up to 200 μg/kg of liposomal TNF were safe in mice. Synergy between liposomal TNF and liposomal doxorubicin was observed in a murine sarcoma model (*230*).

TNF has also been linked to antibodies binding tumour antigens and proteins overexpressed in tumours, such as EGFR, HER2, fibronectin and gp240 antigen or a bispecific antibody that binds TNF and CEA (*231-235*). Linkage of TNF to antibodies decreased its systemic toxicity and leads to accumulation of the complex within the tumours and reduced tumour growth. Synergy with radiation and immune activation are seen with this approach (*233, 234*).

TNF has also been targeted to the tumour-associated vasculature using NGR or RGD peptides linked to TNF. NGR-TNF and RGD-TNF increase the efficacy of numerous chemotherapeutic agents by increasing drug delivery (*236-239*).

Based on the synergy between TNF and ionizing radiation, a E1, E4, partial E3-deleted replication-deficient Ad5 vector encoding TNF under a radiation

inducible early growth response (Egr-1) promoter, called TNFerade, was made. Combination of TNFerade with standard of care proved safe, yet ultimately ineffective in prolonging life in a phase III study for advanced pancreatic cancer (*240*). Using another non- replicating Ad5 vector, membrane bound TNF was found to have a better safety profile than a vector expressing full length TNF (*197*). A herpes simplex virus (HSV) has also been armed with full length TNF (*241*). A comparison of CMV-driven TNF or TNF under the US11 promoter, a late promoter of HSV, showed increased safety and improved anti-cancer efficacy using US11.

In March 2015, Hirvinen et al. published a replicating Ad5 vector expressing human TNF. An increased delay in tumour growth and synergy with radiation was found using the Ad5-TNF virus compared to Ad5 control. Additionally, in a syngeneic model, an increase in cytotoxic T cells and B cells was found in the tumours (*242*).

1.6 Aims of the thesis

The overall aim of this thesis is to study the feasibility of expressing a highly potent cytokine (TNF or LTA) by oncolytic viruses. In order to achieve this there are 4 component objectives:

A) Develop a Dox-inducible transplantable tumour model to study the effects of expressing TNF and LTA inside established tumours. This inducible model will allow study of the immune effects of acute expression of murine TNF (mTNF) and LTA in syngeneic mouse models with both innate and adaptive immune systems, acting as a surrogate for transgene expression for oncolytic adenoviruses in order to guide the choice of which agent to express within 'armed' ColoAd1.

B) Use this model to compare the immune and therapeutic effects of soluble murine (sm) TNF, full length murine (fm) TNF and membrane bound murine (mbm) TNF on tumour growth, immune status and angiogenesis.

C) Arm ColoAd1 with murine TNF and murine LTA and study the effects on tumour growth, immune infiltrate and tumour-associated vasculature in human xenograft tumour models.

D) Evaluate possible synergy between species of ColoAd1 armed with TNF and radiation therapy.

Chapter 2: Materials and methods

2.1 Cell culture

2.1.1 Cell culture

All cells were grown in a humidity-controlled incubator with 5% CO_2, at 37°C. Once cells reached 80-95% confluency, cells were split using sterile techniques in a class II laminar-flow cabinet. Briefly, the supernatant was removed, cells were washed with PBS and incubated in trypsin-EDTA until cells detached from the flask. After cells had detached, media, containing serum, was added to the cells and cells were split into a new flask containing DMEM or RPMI containing 10% fetal calf serum (FCS) and 1% penicillin/streptomycin.

Cell line	Description	Growth medium	Obtained from
293A	Human embryonic kidney cells	DMEM, 10% FCS	Gift from PsiOxus Therapeutics LtD.
293T	Human embryonic kidney cells	DMEM, 10% FCS	Gift from the Jenner institute (University of Oxford)
RAW264.7	Murine macrophage cell line (Abelson murine leukemia virus transformed)	RPMI-1640, 10% FCS	Gift from Prof. Ruth Muschel lab (University of Oxford)
CT26	Murine colon carcinoma cell line	RPMI-1640, 10% FCS	ATCC
CT26 tetR	CT26 cell line transduced with tetR protein	RPMI-1640, 10% FCS	Gift from Dr. Aliaa Alamoudi, University of Oxford
DLD-1	Human Dukes' type C colorectal adenocarcinoma	RPMI-1640, 10% FCS	Gift from Prof. Gillies McKenna Lab (University of Oxford)

A549	Human lung epithelial carcinoma	DMEM, 10% FCS	ECACC
HT29	Human colorectal adenocarcinoma	DMEM, 10% FCS	ATCC
HCT 116	Human adenocarcinoma	McCoy's 5A, 10% FCS	Gift from PsiOxus Therapeutics LtD.

Table 2.1: Details of cell lines used in this thesis.

2.1.2 Storage of Cell lines

Cells were cultured and trypsinized as described in cell culture. Cells were spun down for 5 minutes at 350 g. The pellet of cells was resuspended in freezing solution containing 10% sterile dimethyl sulphoxide (DMSO) and 90% FCS. 1 mL aliquots were made in cryovials, and stored at -80°C in a Mr. Frosty container (Nalgene; Thermo Scientific, UK) over night. For long time storage, cells were transferred to liquid nitrogen tanks. Before use, cells were thawed in the water bath at 37°C. 10 mL culture media was added to thawed cells and cells were spun for 5 min at 350 g. Supernatant was removed, and the cell pellet was resuspended in culture media and transferred to flask. Supernatant was removed and fresh culture medium was added the day after thawing the cells.

2.1.3 Cell counting

Adherent cells were washed with PBS and incubated in trypsin-EDTA. Fresh culture medium was added and cells were gently mixed. Cells were loaded in a haemocytometer (Marienfield) and counted under a light microscope (Eclipse TS100, Nikon).

2.1.4 Cell plating

Unless stated otherwise, cells were counted and diluted to the needed concentration in appropriate culturing media containing 10% FCS. Cells were seeded in plates appropriate for the assay for 16h and kept in the incubator until further treatment or analysis.

2.2 Cell viability assays

2.2.1 MTS cell viability assays

Cell viability was measured using the CellTiter 96 Aqueous One Solution Cell Proliferation Assay (Promega, UK) according to manufacturer's manual. This MTS assay is a colourimetric method that uses metabolic activity as a measure for cell viability. MTS [3-(4,5-dimethylthiazol-2-yl)5-(3-carboxymethoxyphenyl)-2-(4-sulphophenyl)-2H-tetrazolium] is reduced into a formazon product by metabolically active cells, see figure 2.1. All MTS assays were performed in 96 well plates. 20 µL MTS reagent was added to 100 µL culture media without phenol red. Plates were incubated for 1-4 hours before the amount of formazan product was measured by absorption at 490 nm wavelength using a Wallac 1420 Victor^2 multi-label counter (PerkinElmer Life and Analytical Sciences, UK).

Wells not containing cells served as a control and the values obtained from these wells were subtracted from readings of wells containing treated cells. Cell viability was normalized to non-treated control cells.

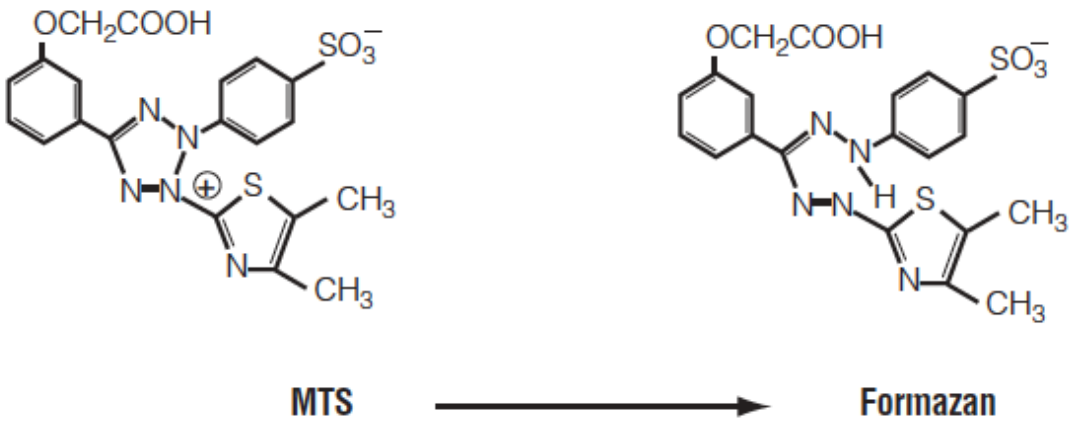

Figure 2.1: Conversion of the MTS reagent by viable cells. MTS tetrazolium salt an is reduced into the formazan product by metabolically active cells (*243*).

2.2.2 Resazurin assay

Resazurin is a weakly fluorescent dye that is reduced to resorufin by metabolically active cells. Cells were plated and treated in clear 96 well plates. The supernatants were removed and 100 µl resazurin (0.05 mg/ml) was added and incubated for 1-2h.

Fluoresence of resorufin is read at 590 nm, using a Wallac Victor^2 multi-label counter (PerkinElmer Life and Analytical sciences).

Wells not containing cells used as a negative control. Values obtained from these wells were subtracted from the values of obtained from cells. Cell viability was normalized to non-treated control cells.

2.2.3 XCelligence

DLD cells (5 x 10^3 cells/well) were seeded overnight 16-well plates microplates containing a micro-electronic biosensor (Roche Diagnostics, Germany). Microelectrodes at the bottom of the plates measured attachment, spreading and

proliferation of the cells, using the XCelligence RTCA DP machine (Roche Diagnostics, Germany).

2.3 Cellular Assays and Methods

2.3.1 L929 cell cytotoxicity assay

$1x10^4$ L929 cells/well were seeded overnight. Cells were treated with serial dilutions of human or murine recombinant TNF or LTA or supernatant derived from cells expressing TNF. TNF or LTA in the supernatants produced by cells were quantified using a sandwich ELISA. Both the standard curve and experimental samples contained 8 μg/mL actinomycin D. Cell viability was measured after 24h incubation, using an MTS assay.

2.3.2 Virus infection

Cells were seeded overnight in appropriate media containing 10% FCS. After 16h, the supernatant was removed and medium containing virus (quantified by PicoGreen® assay) and 2% FCS were added to the cells, unless stated otherwise. VP/cell was calculated based on the amount of cells seeded. If cells were used for QPCR analysis, the supernatant containing virus was removed and cells were washed with PBS, before adding fresh medium containing 2% FCS.

2.3.3 Comet assay

1x 10^5 DLD cells were seeded overnight in 6 well plates. Cells were infected with 100 vp/cell Ad5, Ad11p or ColoAd1 for 24h. Next, cells were irradiated using a Cs137 source dose rate 1.938 Gy/min; GSRD1, Gamma-Service Medical GmbH). Cells were trypsinized and diluted in of PBS. The cells embedded into 1 % low-melting agarose solution kept at 37 °C (Life Technologies) and added to slides. The agarose was allowed to solidify on the slides and transferred to ice cold lysis buffer (2.5 M NaOH, 100 mM EDTA, 10 mM Tris base; pH =10.5) and incubated for 1h. Slides were removed from lysis buffer and washed with electophoresis buffer (300 nM NaOH, 1mM EDTA; 1% DMSO; pH>13) twice. Slides were put into an electrophoresis tank and incubated in electrophoresis buffer for 30 min at RT. Slides were subjected to electrophoresis at 25 V and 300 mA for 25 min.
Next slides were was 3 times 10 min with neutralization buffer (500 mM Tris-HCl; pH=8.0). Slides were washed in deionized water (pH set to 8.0 using KOH solution), air dried overnight.
Slides were rehydrated in deionized water (pH=8.0) at RT. Next DNA was stained with SYBR gold (1:10000 in dH_2O; Stratagene, La Jolla, CA, USA) for 30 min at RT. Slides were washed in dH_2O and allowed to air dry overnight. Comet slides were imaged by microscopy on a Leica confocal system (Leica Microsystems, Heidelberg, Germany)

2.3 General cloning and DNA purification methods

2.3.1 Bacterial transformation by heat shock

For amplification of plasmid DNA, heat shock competent XL10 Gold Ultracompetend E. coli bacteria (Agilent technologies, UK) were used. The bacteria were stored at -80 °C and thawed on ice for 10 minutes. Up to 10 µl ligation product or 10 ng of plasmid DNA was added to the bacteria and incubated on ice for 20 min. Bacteria were heat shocked at 42 °C for 30 sec. Subsequently, the bacteria were incubated on ice for 2 more minutes. Antibiotic free LB or SOC media was added to the cells and the cells were incubated at 37 °C for 1 hour. Bacteria were plated on LB plates containing either ampicillin or kanamycin and incubated at 37 °C over night.

2.3.2 DNA ligation

The vector concentration used for ligations was 100 ng. Molar ratios of insert:vector of 1:1, 2:1 and 3:1 were set up in 10 µl reactions, containing 1 µl of T4 ligase (NEB) and 1 µl T4 ligase buffer (NEB). Water was added up to 10 µl. Control ligations missing the insert were also set up. Reactions were incubated at RT for 1h. After this incubation, E. coli bacteria were transformed with the ligation solution.

2.3.3 Plasmid amplification and DNA purification

Colonies of transformed E. coli bacteria were picked and grown in 5 ml fresh LB media containing ampicillin or kanamycin at 37 °C over night in a shaker incubator. When small quantities of DNA were needed, the DNA was isolated and

purified from the bacterial culture using a Qiaprep spin miniprep kit (Qiagen). Alternatively, when large quantities of DNA were needed, 1 ml of overnight culture was used to inoculate 200 ml of fresh LB media containing antibiotics. DNA was isolated and purified from this larger volume using a EndoFree plasmid Maxiprep kit (Qiagen, UK).

2.3.4 DNA digests

Plasmid DNA was digested using the appropriate endonuclease enzymes (NEB) and buffers (NEB). For visualization purposes, 0.5 µg of DNA was digested, whereas 7 µg was digested when DNA fragments were needed for subsequent DNA cloning. DNA digests were typically set up in 20 µl reactions and incubated at 37 °C in a thermocycling machine for 3h. Subsequently, the endonuclease enzymes were inactivated by heat inactivation at 65 °C for 5 min and kept at 4 °C until further processing.

2.3.5 Gel electrophoresis of DNA fragments

Visualization and separation of DNA fragments was achieved by agarose gel electrophoresis. 1% agarose (Sigma-Aldrich) was added to 1x TAE buffer. The solution was heated in a microwave until the agarose was dissolved. The solution was allowed to cool down before ethidium bromide (5 µg/ml) was added and the gel was poured into electrophoresis boxes. Once the gel was solidified, TAE buffer was added to the electrophoresis tanks and DNA samples and DNA ladders were loaded onto the gel. The gels were run at 10 V/cm for 60 min and DNA was visualized using a UV transluminometer (Alpha Imager, Alpha Innotec, USA).

If needed, DNA bands were excised and the DNA was purified using a QIAquick Gel extraction kit (Qiagen, UK), according to manufacturer's manual.

2.3.6 DNA quantitation

DNA concentrations are calculated using the absorbance at 260 nm, as measured by a UV/vis DU730 spectrophotometer (Beckman Coulter). All DNA samples were blanked using the buffer the buffer in which they were dissolved.

2.3.6 DNA sequencing

When DNA visualization following gel electrophoresis showed DNA bands at the expected size of the insert, plasmids were sent off to Source Bioscience for sequencing to confirm the correct insertion and sequence of the constructs made.

2.4 Generation of lentiviruses and stably transduced cell lines

2.4.1 Puromycin and G418 selection

Cell viability after puromycin (CT26 and HT29) and G418 (HT29) treatment was titrated, to determine the optimal antibiotic concentration for selection. 10 000 CT26 and HT29 cells were plated in clear 96 well plates and incubated o/n. After 16h, A range of 2-fold serial dilutions of puromycin (Clontech) or G418 (Clontech) was added to the cells. Cell viability was assessed after 4 days for puromycin and 8 days for G418, using a resazurin assay. The lowest concentration of antibiotic causing complete cell death was chosen (12.5 μg/ml

puromycin for CT26 cells; 1 µg/ml puromycin and 2000 µg/ml G418 for HT29 cells), see figure below.

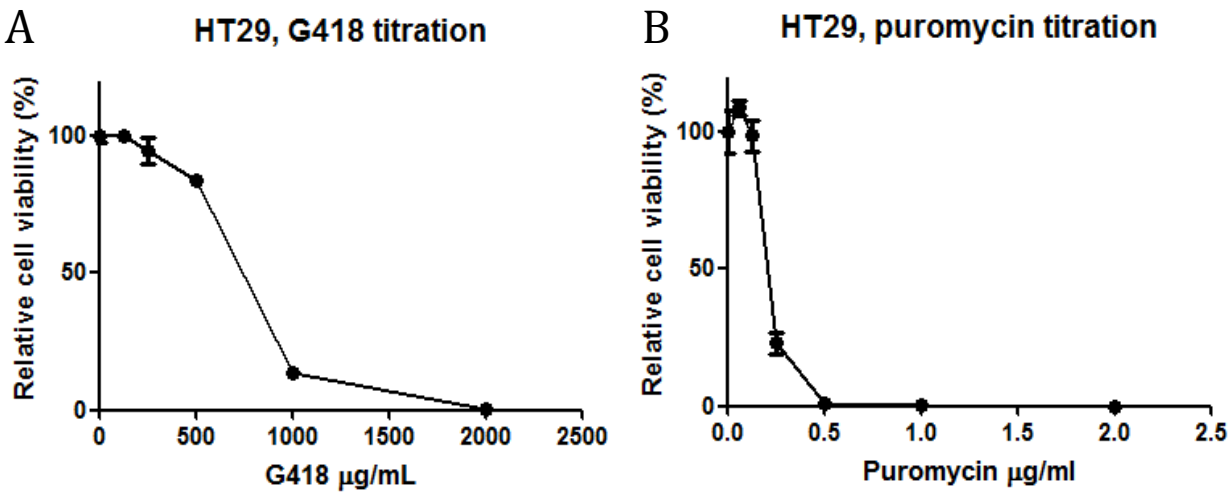

Figure 2.2: Titration of G418 and puromycin on HT29 cell viability. 10,000 cells per well were plated and treated with different concentrations of G418 (A) or puromycin (B). After 4 days (B) or 8 days (A) of incubation, a resazurin assay was done to determine cell viability. N=3, mean and SD are shown.

2.4.2 Lentivirus packaging

Lentiviral vectors were generated by cotransfection of packaging plasmids with the pTight- TNF, LTA or empty vector plasmid. Packaging of lentivirus was done according to manufacturer's manual. Briefly, $5x10^6$ 293T cells were plated in 100 mm tissue culture dishes over night. The cells were transfected once cells reached approximately 80% confluency. 36 µl Lenti-X HTX packaging mix and 7 µg Lenti-X pTight TNF or LTA plasmid was added to a total volume of 600 µl of Xfect reaction buffer. In a second tube, 7.5 µl transfection polymer was added to 592.5 µl Xfect reaction buffer. Both tubes were vortexed and the polymer solution was added to the DNA solution, vortexed and incubated for 10 min. The transfection mixture was added to the cells and incubated for 4h. The medium

was replaced with 10 mL of fresh DMEM medium and supernatant, containing lentivirus vector, was collected 48h after transfection. The supernatant was sterile filtered through a 45 μM filter and aliquoted and stored at -80 °C until further use.

2.4.3 Lentiviral transductions and cell line generation

For lentiviral transduction, $2x10^5$ cells were plated in 6 well plates o/n. Serial dilutions of lentiviral vectors were added to 1.35 ml media containing 4 μg/ml final concentration polybrene (Sigma-Aldrich). 1 ml of virus solution was added to each well and cells were centrifuged for 90 min at 1200 g, at 32 °C. Cells were incubated at 37 °C o/n and the media was subsequently replaced by media containing antibiotics.

HT29 cells were infected pLVX-Tet-On vector and transduced colonies subsequently selected using G418. CT26 tetR cells were a gift from Dr. Aliaa Alamoudi. HT29 tetR cells and CT26 tetR cells were infected with pLVX-Tight-Puro vector and selected using puromycin resistance. A cloning cylinder (Sigma-Aldrich) was used to isolate separate colonies of antibiotic resistant cells, using sterile techniques and transferred to a 96 well plate. The cells were grown in progressively larger flasks and kept in under antibiotic selection for at least 2 weeks.

2.4.4 Cloning TNF and LTA into pLVX-Tight-Puro

DNA sequences encoding full length human (fh) TNF, soluble human (sh) TNF with insulin-secretory peptide, human LTA, full length mouse (fm) TNF and mouse (m) LTA were synthesized by Life Technologies. Using endonuclease

enzymes (BamHI and MluI), the DNA sequences were digested and separated from the backbone using electrophoresis. The DNA sequences were excised from the gel and cleaned up and subsequently ligated into the pLVX-Tight-Puro plasmid.

Generating an sm TNF construct

Through PCR reactions, a soluble mouse TNF with insulin-secretory peptide was created. 10 ng of the Life Technologies full length mouse TNF plasmid was used as a template and 300 nM forward Fwd 1 primer (Rev) 1 primer (see table 2.2) using a PCR mastermix (Invitrogen). The PRC was run for 40 cycles, with 30 sec denaturing at 95°C and annealing and extension for 90 sec at 72°C. The PCR product was run on a 1% agarose gel and extracted using a Qiagen kit according to manufacturer's manual. Subsequently, 10 ng DNA from the previous PCR was used using the Fwd 2 primer and the Rev 2 primer, see table 2.2. Using electrophoresis, the PCR product was visualized and isolated. The DNA sequence was digested with XbaI and MluI and ligated into the pLVX-Tight-Puro vector plasmid.

Fwd 1 primer	CTGGCGCTGCTGGCGCTGTGGGGCCCGGATCCGGCGGCGGCGCTC AGATCTCTTCTCAAAATT
Rev 1 primer	GGGAAAAGCGCCTCCCCTACCCGGTAGAATTCACGCGTTCACAGA GCAATGACTC
Fwd 2 primer	CTCTAGAGCCGCCATGGCGCTGTGGATGCGCCTGCTGCCGCTGCT GGCGCTGCTGGCG
Rev 2 primer	GGGAAAAGCGCCTCCCCTACCCGGTAGAATTCACGCGTTCACAGA GCAATGACTCC

Table 2.2: primers used to generate sm TNF

Generating an mbm TNF construct

Mbm TNF (Δ1-9 K11E) was made using insertional mutagenesis PCR, using 10 ng of the Life Technologies fm TNF plasmid as a template and 500 nM Fwd primer: (5' phosphorylated GACGAGCCTGTAGCCCACGTCGTAGCAA) and 500 nM Rev primer (TGTGAGGGTCTGGGCCATAGAAC) using a 2x Phusion Master Mix (NEB Phusion High Fidelity) The PRC was run for 40 cycles, with 30 sec denaturing at 94°C and annealing and extension for 90 sec at 72°C. The PCR product was run on a 1% agarose gel and purified using a gel extraction kit. Subsequently, the DNA was ligated together by setting up a ligase reaction on ice using T4 ligase. This ligation reaction was incubated at 16 °C o/n. The ligation reaction was used to transform bacteria. Minipreps of the plasmid were digested using BamHI and MluI and run on a 1% agarose gel. Mbm TNF DNA was subsequently ligated into the pTight puro vector.

2.5 Generating ColoAd1 expressing TNF

2.5.1 Cloning TNF and LTA into ColoAd1

ColoAd1 SA fh TNF, ColoAd1 SA fm TNF, ColoAD1 SA sm TNF and ColoAd1 S mLTA were made using protocols optimized by PsiOxus Ltd. A schematic overview of the cloning strategy used can be seen in figure 2.4.

First, pLVX-Tight-Puro encoding fh TNF, fm TNF, sm TNF and mLTA were used as DNA template for a PCR using Phusion mastermix (NEB). The PCR protocol can be seen in table 2.3 and the primer sequences used can be found in table 2.3. The PCR reaction was set up to add a SgfI restriction site and a splice acceptor (SA; CAGG) site and kozak sequence (CCGCC) before the TNF or LTA sequence and a NheI restriction at the end of the sequence.

Cycles	Step number	Stage	Temp (^{o}C)	Time (Secs)
1	Step 1	Initial Denaturation	98	60
10	Step 2	Denaturation	98	20
	Step 3	Annealing	58	30
	Step 4	Extension	72	60
20	Step 5	Denaturation	98	20
	Step 6	Annealing	65	30
	Step 7	Extension	72	60
1	Step 8	Final Extension	72	300
	Step 9	Hold	4	Hold

Table 2.3: PCR conditions for ColoAd1 TNF and LTA cloning

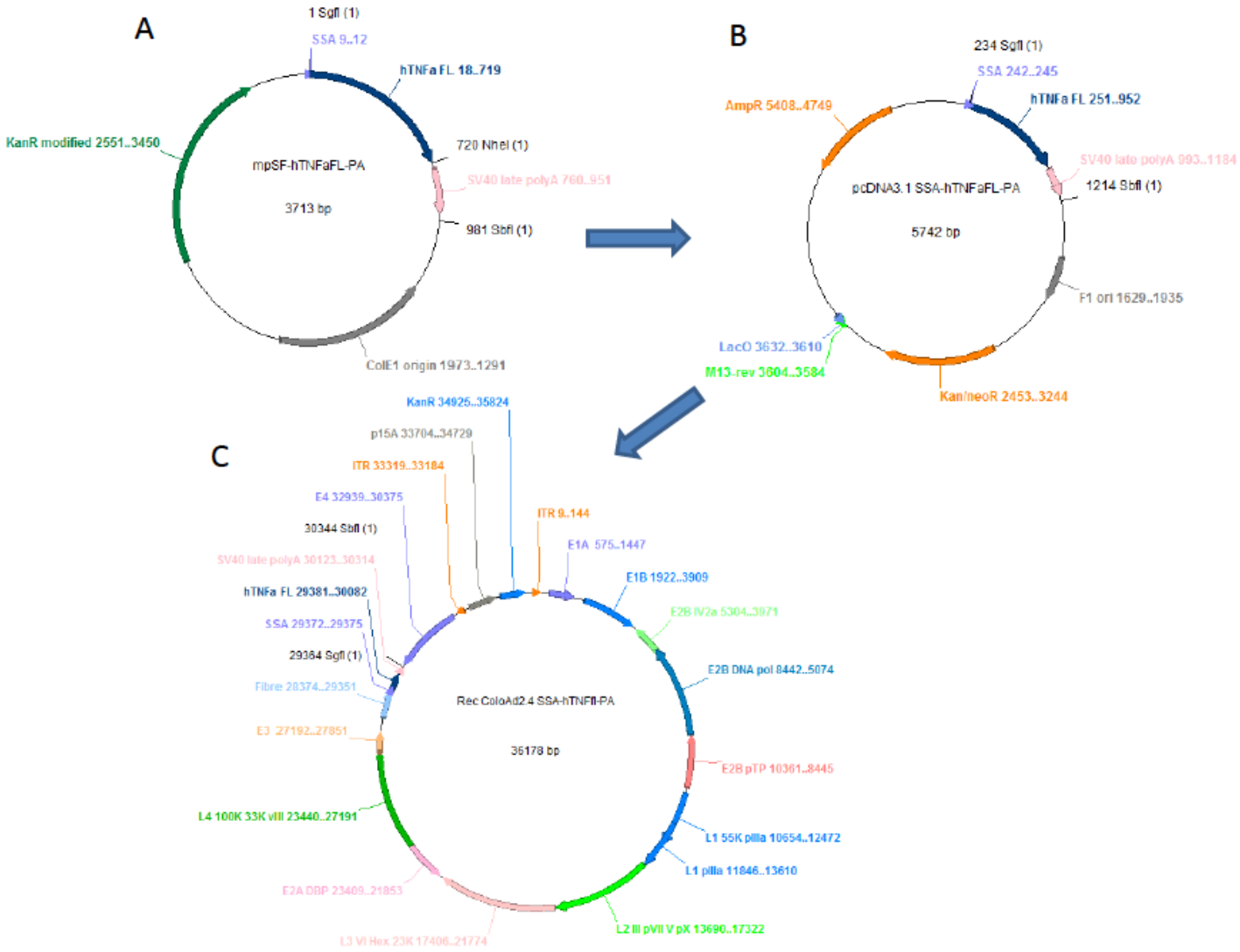

Figure 2.4: Schematic overview of ColoAd1 cloning. The insert (hTNF) was incorporated into a mpSF plasmid (A), after adding a splice acceptor site (SA) and SgfI and NheI restriction sites, through PCR. The SA-hTNF construct with a polyA tail was incorporated into a pcDNA3.1 plasmid (B). Subsequently, the SA-TNF (or LTA)-polyA construct was cloned into a ColoAd1 2.4 vector (C).

Primer Construct	Sequence
Fh TNF Forward	TATGCGATCGCCAGGCCGCCATGAGCACTGAAA
Fh TF Reverse	TAGTAGCTAGCTCACAGGGCAATGATCCCAAAG
Fm TNF Forward	TATGCGATCGCCAGGCCGCCATGAGCACAGAAA
Fm TF Reverse	TCTACGTGCTAGCTCACAGAGCAATGACTCCAAAGT
Sm TNF Forward	TATGCGATCGCCAGGCCGCCATGGCGCTGTGGA
Sm TNF Reverse	ATCCGACGCAGCTAGCTCACAGAGCAATGACTCCAAAGTAGAC
mLTA Forward	TATGCGATCGCCAGGCCGCCATGACACTGCTC
mLTA Reverse	AGCTCAGCTAGCCTACAGTGCAAAGGCTCCAAAGAA

Table 2.3: PCR primers used include a SgfI, SA and NheI site.

Upon completion of the PCR reaction, 1 µl of the reaction was ran on a agarose gel to confirm proper amplification of the constructs, see figure 2.5.

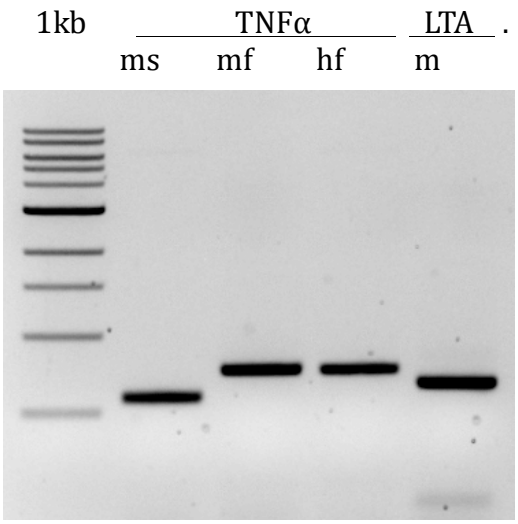

Figure 2.5: diagnostic gel showing the PCR products for ColoAd1 cloning

PCR products and the mpSF Vector were digested with SgfI (AsiSI) and NheI-HF, gel purified and the insert and mpSF vector were ligated. The ligation reaction was used to transform bacteria. Colonies of bacteria were grown on agar plates containing kanamycin. Colonies were picked and miniprepped.

The mpSF construct and the pcDNA3.1 constructed were digested with SgfI and SbfI. A ligation between the insert obtained from the mpSF construct and the pcDNA3.1 backbone was set up. Again, bacteria were transformed and colonies were picked and miniprepped. Finally, the insert was cut out of the pcDNA3.1 plasmid using SgfI and SbfI. A ColoAd2.4 plasmid vector was also cut with SgfI and SbfI. Both digests were cleaned up using a DNA column. Next, the SA TNF or LTA – polyA constructs were inserted into the ColoAd2.4 vector using a ligase reaction. Bacteria were transformed and colonies were picked miniprepped. The

minipreps were sent off for sequencing, and upon correct sequencing a maxiprep was performed.

2.5.2 Gibson assembly mbm TNF

A PCR was set up to add an NcoI, SA site (CAGG) and Kozak site (CCGCC) in front of the mbm TNF construct and a XhoI site at the end. The PCR (Phusion Master Mix; NEB Phusion High Fidelity) was set up using the pLVX-pTight-puro mbm TNF plasmid as a template and details of the primers can be found in table 2.4. The PRC was run for 40 cycles, with 30 sec denaturing at 94°C and annealing and extension for 90 sec at 60°C. The PRC was run for 40 cycles, with 30 sec denaturing at 94°C and annealing and extension for 90 sec at 72°C.

Fwd primer	AAACCATGGCAGGCCGCCATGAGCACAGA
Rev primer	TTTTCTCGAGTCACAGAGCAATGACTCCAAAGTAG

Table 2.4: Primers used for mbmTNF cloning

Both the PCR product and the mpSF vector (see figure 2.4 A) was digested with NcoI and XhoI. Both digests were up using a DNA column. A ligation reaction was set up to clone the mbm TNF insert into the mpSF plasmid (figure XA) using L4 ligase. The mpSF plasmid served to add a poly A tail at the end of the construct. Next a PCR was done to create an overhang with the ColoAd2.4 vector and to add a SbfI restriction site in front of the SA site. Also an overhang with the ColoAd1 vector and SbfI site after the polyA tail were added. For details of the primers used, see figure 2.5.

Fwd primer	CAAATAAAGTTTGCGATCGCTACCCTGCAGGCAGGCCGCCatgagcac
Rev primer	GATTTTCAAATAAACAAGTTCCTGCAGGATAGCTGACGACTACCAC

Table 2.5: Primers used for Gibson assembly.

The ColoAd2.4 vector was digested with SbfI and a Gibson assembly reaction was set up according to manufacturer's manual (NEB). Briefly, 100 ng of digested ColoAd2.4 vector was added to 3-fold excess of mbm TNF insert (mol:mol ratio). 10 µl of Gibson assembly master mix was added and the mixture was diluted to 20 µl in deionized water. In a thermocycler, the mixture was incubated for 15 min at 50 °C. Subsequently, cells were transformed with 5 µl of the Gibson assembly product as described in section 2.3.1. Colonies were plated an picked and miniprepped. Upon correct sequencing, a maxiprep of the ColoAd1 SA mbm vector was performed.

2.5.3 Linearizing the ColoAd1 vector plasmids and phenol:chloroform purification

7 µg ColoAd1 vector DNA was digested with AscI for 2 hours at 37 °C, to linearize the vector. 50 µl H_2O was added to the digest, to bring the total volume up to a 100 µl. 100 µl of phenol:chloroform: isoamyl alcohol (Sigma Aldrich) was added to the digest and vortex until the mixture looks cloudy. The mixture was centrifuged at 13,000 rpm for 5 min and the top aqueous layer was transferred to a new tube. Again, 100 µl of phenol:chloroform: isoamyl alcohol was added, vortexed and spun at 13,000 rpm for 5 min. The top aqueous layer was transferred to a new tube and 450 µl 95% ethanol and 15 µl 3M sodium acetate was added to the aqueous mixture and stored at -20 °C until further use.

2.5.4 Rescue of the virus

$1.2x10^6$ 293 A cells were plated into a T25 flask and incubated over night. The linearized vector was spun at 13,000 rpm for 10 minutes to pellet the DNA. Supernatant was removed after the spin and the pellet was allowed to air-dry. The pellet was then resuspended in 30 µl H_2O. To assure that DNA had not been lost during the purification step, the DNA concentration was assessed by a nanodrop. 500 µl Optimem was added to the viral DNA. Next, 20 µl lipofectamine 2000 was added and incubated at RT for 20 minutes. The media was removed from the T25 flask and 1 mL of DMEM 2% FCS was added. The transfection mix was then added dropwise to the flask and incubated for 1 h at 37 °C. After this incubation, 4 mL of 2% FCS DMEM was added to the cells and cells were incubated until significant CPE developed. Once CPE developed, both cells and supernatant were transferred to a 15 mL falcon tube. Rapid freeze thawing by alternating liquid nitrogen/water bath at 37 °C for 3 cycles was done to release the virus from the cells. The tube was then spun for 10 minutes at 2000 rpm, to get rid of cellular debris, and supernatant was transferred to a new tube and stored in the -80°C until needed.

2.5.5 Propagation of the virus

For propagation of the virus, 2 hyperflasks per virus were seeded with 293 A cells in 10% FCS DMEM. Cells were incubated until approximately 90% confluent. The media was removed and 300 µl of the rescued virus, or when titer of virus stock was known 1 $x10^{10}$ vp, was added to 2% FCS DMEM. The virus was added to the cells and incubated until significant CPE developed. Once CPE developed, cells were tapped off from the hyperflask and supernatant and cells

were spun for 10 min at 2000 rpm. Supernatant was removed and hyperflasks were washed with PBS and spun for another 10 minutes at 2000 rpm in the same tube containing the cellular pellet. Supernatant was removed and the pellet was resuspended in 10 mL 2% FCS-DMEM per hyperflask and stored at -80 °C until needed.

2.5.6 Virus purification

To release the virus from the cells into the supernatant, 3 freeze thaw cycles were used, alternating the tube from liquid nitrogen to the water bath at 37 °C. Tubes were spun at 2000 rpm for 10 minutes and the supernatant was transferred to new tubes. Add 1/100th volume of N-butanol (Sigma-Aldrich) to the supernatant and incubate on ice for 60 minutes. After incubation the mixture was spun for 10 minutes at 2000 rpm and the supernatant was transferred to a new tube.

Caesium chloride gradients of 3 mL ρ = 1.35 (32.0 g CsCl, 6.8 mL 0.5 M Tris (pH=7.9) in 61.2 mL H_2O) on top of 2 mL ρ= 1.45 (20.5 g CsCl, 2.9 mL 0.5 M Tris (pH=7.9) in 25 mL H_2O) were made in ultracentrifuge tubes (Beckman Coulter). Supernatant was placed on to of the gradients. Tubes were spun for 16h at 25000 K using the High Speed Ultracentrifuge (Beckman) with the SW40 rotor (Beckman) and corresponding swing out buckets (Beckman).

The lower, slightly blue, virus band was removed from the tubes with a sterile 21G needle (BD Bioscience) attached to a 5 mL syringe (BD Bioscience) and transferred into a dialysis cassette (10,000 MW cut off, Thermo Fisher Scientific) and dialyzed overnight at 4 °C in dialysis buffer 1. After dialysis virus was transferred to a new tube and incubate with 6 µl benzonase (Sigma-Aldrich) per

mL of virus solution for 30 minutes to remove any DNA not packaged into the virus. The virus was then spun on the same CsCl gradient for 2h at 25000K, using the same centrifuge and rotor as before (both Beckman). Again, the lower, slightly bluish viral band was removed from the tubes using a 21G needle. The virus was then dialyzed in a slide-a-lyzer dialysis cassette (Thermo Scientific) overnight at 4 °C in dialysis buffer 2. After this dialysis, virus was recovered from the dialysis cassette using a 21G needle. The virus was stock was sterile filtered and aliquoted and stored at -80 °C until further use.

Reagent	**Concentration Dialysis buffer 1**	**Concentration Dialysis buffer 2**
HEPES (pH=8)	50 mM	50 mM
PBS	1 x	1 x
$MgCl_2$ (hexahydrate)	0.2 g/L	0.1 g/L
$CaCl_2$	0.1 g/L	0.1 g/L
Glycerol	10% (v/v)	10% (v/v)

Table 2.6: dialysis buffer 1 and 2.

2.5.7 PicoGreen® assay

PicoGreen® is a fluorescent cynanine dye that binds to double-stranded DNA, resulting in increased fluorescence (*244*). Based on the fluorescence of the standard curve with known quantities of bacteriophage λ DNA, the amount of adenoviral DNA can be calculated. Subsequently, the number of viral particles (vp) can be calculated, assuming that 1 µg/ml of DNA equals $2.7x10^{10}$ vp/ml (*245*). The Quant-iT™ PicoGreen® kit (Life Technologies) was used with a modified protocol for analysis of viral DNA. Briefly, virus was diluted in Tris-EDTA (TE) buffer, containing 0.05% SDS) and heated in the water bath at 56 °C

for 30 minutes. A logarithmic standard curve of λ-DNA (0.5 µg/ml to 0.0078 µg/ml) was made in TE-0.05% SDS. 50 µl of the standard curve or the sample was dispensed, in triplicates, in wells of a black 96-half well microplate. Next, 50 µl of PicoGreen® reagent (diluted 1:200 in TE) was added to each well. Plates were incubated for 2 min at RT and fluorescence was measured in a Wallac 1420 Victor^2 multilabel counter (PerkinElmer), at excitation 485 nm and emission 484 nm.

2.6 Protein assays

2.6.1 Protein assays

A Bradford protein assay was used to determine protein concentrations. A known concentration (2 µg/µl) of BSA (NEB) were diluted to make a seven point standard curve using 2-fold serial dilutions in the same buffer as the samples tested. 5 µl of the standard curve or sample were added to each well of a clear 96 well plate and incubated with 250 µl of Advanced Protein Assay Reagent. Both standard curve and samples were tested as triplicates and samples were diluted to fall within the linear range of the standard curve. Absorbance was measured at 595 nm using a Wallac 1420 Victor^2 multilabel counter (Perkin Elmer).

2.6.2 Luciferase assays

The luciferase assay system (Promega) was used to quantify luciferase activity in homogenized tumour lysate or cell culture lysates. For tissue culture lysates, cells were washed with PBS and lysed using 100 µl lysis solution (Promega). Cells were frozen at -80 °C and thawed to further complete lysis. The lysate was

warmed to RT and resuspended. 25 µl of sample was added to luminometer tubes and placed in the luminometer (Lumat LB 9507, Berthold Technologies, UK), where 25 µl D-luciferin was injected into the samples. Using ATP and Mg as co-factors, the firefly luciferase protein converts D-luciferin into oxyluciferin, releasing light in the process. After 2 sec incubation, relative luminescence units (RLU) was measured for 10 sec.

2.6.3 SDS page and Western Blot

Sample preparation

Supernatant was removed from the cells. The cells were washed in PBS and trypsinized. Appropriate medium was added to neutralize trypsin and cells were spun at 300 g for 5 min and washed with PBS. Subsequently cells were lysed in 50 µl lysis buffer (Promega) or TNN buffer supplemented with 1x protease inhibitor (Thermo Scientific) and 1x phosphatase inhibitor and stored at -80°C. Protein concentrations were determined using a protein assay (see above) and equal amounts of protein (30-50 µg) per sample was used. Equal amounts of β mercaptoethanol-containing sample buffer was added to each sample and diluted to equal volumes in H_2O. The samples were incubated at 95 °C for 10 min to denature the proteins.

Running gel

Precast 4-10% or 10% Tris-HCl gels (BioRad) were used with the Mini-PROTEAN III electrophoresis system. All wells were washed with running buffer and acclimatized for 30 min before loading with the samples. Samples were separated run at 130 V for 90 minutes.

Transfer to nitrocellulose.

Nitrocellulose membrane (BioRad) was pre-incubated in 100% methanol for 10 min. Filter paper and fiber pads were soaked in transfer buffer. Fiber pads and filter paper were place on the transfer cassette. The gel was placed on top of the filter pad and the membrane was added on top of the gel. On top of the membrane another layer of filter paper, followed by fiber pads was added. The cassette was closed and placed into a mini-gel Western transfer tank (BioRad). The gel was placed at the negative electrode. The transfer was performed at 300 mA, for 90 min at 4 °C.

Staining and developing of the membrane

Upon completion of the transfer, the membrane was transferred to ponceau reagent (Thermo Scientific) to confirm proper transfer of the protein from the gel to the membrane. The membrane was washed 3 times 5 min with PBS-T or TBS-T when staining for phosphorylated protein. Next, the membrane was blocked in 5% skimmed milk or BSA in PBS-T or TBS-T, for at least 45 min at RT. The membrane was incubated with primary antibody overnight at 4 °C, see table x. After removal of the primary antibody, the membrane was washed 3 times 10 min with PBS-T or TBS-T. Next, the membrane was incubated with appropriate HRP-conjugated secondary antibody, at RT for 1 h. The antibody was removed and the membrane was washed 3 times 5 min with PBS-T or TBS-T. The membrane was developed with Super Signal West Dura Extended Duration Substrate (Thermo Scientific) and chemiluminesce was detected by exposure on

X-ray film (SuperRX, Fujifilm). The X-ray films were developed and fixed in an automatic developer (CP1000, Afga).

Antibody	Concentration	Company
IκBα	1:2000	Cell Signalling
tetR	1:1000	Clontech
p53	1:1000	Santa Cruz
Phospho p53 (Ser15)	1:1000	Cell Signalling
Phospho ATM	1:2000	Millipore
γH2AX	1:5000	Milipore
Mre11	1:1000	Abcam
DNA ligase IV	1:1000	Abcam
Rad50	1:1000	Cell Signalling
β-actin	1:5000	Sigma-Aldrich
GAPDH	1:5000	Cell Signalling
Anti-rabbit IgG-HRP	1:10000	DAKO
Anti-mouse IgG-HRP	1:10000	DAKO

Table 2.7: Details of antibodies used for Western blotting.

2.6.4 Sandwich ELISA assays

Antibody sets compatible for a sandwich-ELISA for human TNF, human LTA and murine TNF were purchased from R&D Systems and used according to manufacturers manual.

For mLTA, plates were coated with 5 µg/ml polyclonal rabbit α mLTA antibody (Novus Biologicals, NBP1-19765) and 1µg/ml polyclonal biotinylated goat α mLTA detection antibody (R&D systems, BAF749) was used.

Briefly, 100 µl capture antibody in PBS was added to ELISA plates (Nunc) and incubated o/n. Plates were washed 3x in PBS-Tween 20 and incubated in PBS-1% BSA. Subsequently 100 µl sample or standard curve, was added and incubated for 2h at RT. Samples were removed and plates were washed 3x in PBS-T. Next, 100 µl detection antibody was incubated for 2h. Plates were washed 3x in PBS-T and incubated in 1:200 avidin-HRP in PBS-BSA for 20 minutes. Plates were washed 3x in PBS-T and 50 µl 1-step Ultra TMB-ELISA reagent (Thermo

Scientific) was added to develop the ELISAs. Reactions were stopped by adding 50 µl stop solution (Alpha Diagnostic, USA). All incubations in this protocol were done at RT. Absorbance was measured at 450 nm using the VICTOR and 560 nm for a background reading. Absorbance was calculated by subtracting the 560 nm reading from the 450 nm.

All samples were tested in triplicates and concentrations were calculated in Microsoft Excel. All samples were diluted to fall within the linear range of the standard curve.

For tumour lysates from the animal experiments, a protein assay was done to normalize transgene expression per µg protein.

2.6.6 Flow-cytometry analysis of membrane associated TNF

Cells were washed with PBS and scrapped off the plates using a cell scraper. Cells were spun at 350 g for 5 min, the supernatant was removed and washed with PBS three times. Cells were counted and resuspended to $1x10^6$ cells/100 µl in PBS. Cells were incubated with an PE-labelled anti-TNF antibody (1:100 dilution, BD bioscience) or PE-labelled isotype control (1:100 dilution BD bioscience) for 1 h at 4 °C. Again, cells were spun at 350 g for 5 min, the supernatant was removed and washed with PBS three times. Flow cytometry analysis was done using a FACS Calibur (BD bioscience) and analysed using Flow-Jo analysis software (Tree Star Inc, USA).

2.6.7 Immunocytochemistry

Cells were seeded overnight ($1x10^4$ cells/well in a 96 well plates). Cells were infected with 100 vp/cell adenovirus. Radiation was done using a Caesium 137 source (dose rate 1.938 Gy/min; GSRD1, Gamma-Service Medical GmbH).

After incubation, cells were washed with 100 µl PBS and subsequently fixed for 10 min in 4% PFA. Cells were washed 2 times in PBS and stored at 4 °C until further processing. Blocking was done using 100 µl PBS, 0.1 Triton X, 1% BSA for 1h at RT. Cells were incubated with 50 µl primary antibody diluted in PBS, 0.1 Triton X, 1% BSA overnight at 4 °C. Next, cells were washed 3 times with 200 µl PBS. Cells were incubated with 1:1200 dilution of secondary antibody and 1 µg/ml DAPI diluted in PBS, 0.1 Triton X, 1% BSA for 1 h at RT. Next, cells were washed 3 times with 200 µl PBS.

Antibody	**Concentration**	**Company**
53BP1	1:500	Novus Biologicals
γH2AX	1:500	Millipore
Phospho ATM (1981)	1:100	Millipore

Table 2.8: Details of primary antibodies used for IHC.

53BP1 foci were counted in the nuclei of cells automatically using In Cell 1000 Cellular Imaging and Analysis System (G E Healthcare).

2.7 RNA and DNA quantitation assays

2.7.1 DNA extraction

DNA was extractions from samples obtained from *in vitro* experiments were extracted using a genomic DNA extraction kit (Fisher-Scientific), according to manufacturer's manual. Samples obtained from *in vivo* experiments were extracted using a genomic DNA extraction kit (Sigma-Aldrich), according to manufacturer's manual.

2.7.2 Standard curve preparation QPCR

Standard curves were treated the same as all test samples. Serial 10-fold dilutions of known viral content were made in lysis buffer. The viral dilutions were spiked into the lysate of uninfected cells. Typical standard curve concentrations ranged from 10^{10} vp to 10^{4} vp. DNA from the standard curves were extracted using the same method and reagents as the experimental samples. All samples were compared to standard curves generated from the same viral stock.

2.7.3 QPCR

Ad5 (see table 2.9), Ad11p and ColoAd1 (see table 2.10) genome copies were quantified using the Taqman® system. Primers (0.2 μM) and FAM and TAMRA labelled probe (0.1 μM) were added to 2 x Hi-Rox master mix (PCR Biosystems) and diluted up to 20 μl per well. Next, 5 μl of standard curve or sample was added to each well of a 96 well PCR plate (Applied Biosystems). The QPCR

reactions were performed using a StepOnePlus Real-Time PCR system (Applied Bioscience). The amplification cycle started at 50 °C for 2 min and a denaturation step at 95°C for 10 min. Next, 40 cycles of denaturation at 95 °C for 15 sec and annealing and extension at 60 °C for 1 min were performed. Data was analysed using StepOnePlus v2.1 software (Applied Bioscience) and compared the standard curve.

Probe	6FAM-TCCAATATCTGGAACAGTTCAAAGTGCTCATCT-TAMRA
Forward Primer	TGGCTGTTAAAGGCAGTTTGG
Reverse Primer	GCACTCCATTTTCGTCAAATCTT

Table 2.9: Primers and Probes used to quantify Ad5

Probe	6FAM-CCGGACTCAGGTACTCCGAAGCATCCT-TAMRA
Forward Primer	TACATGCACATCGCCGGA
Reverse Primer	CGGGCGAACTGCACCA

Table 10: Primers and Probes used to quantify ColoAd1 and Ad11p

2.7.4 mLTA mRNA quantification

CT26 cells (5x 10^5 cells/cells) were seeded overnight. Subsequently, cells were treated with 2.5 µg/ml Dox for 12h. RNA was extracted 12h after start of Dox treatment using an RNA extraction kit according to manufacterer's manual (Qiagen). The collected RNA was converted to cDNA using a kit according to manufacturer's manual (Applied Biosciences). The amount of mLTA mRNA expression was measured by QPCR. A mastermix containing primers and probes for murine LTA and murine GAPDH (Life Technologies) were used for the QPCR, according to manufacturer's manual.

2.8 Animal Experiments

2.8.1 Housing and regulations

All animal experiments were performed in accordance with the regulations of the United Kingdom Home Office. For all studies female BALB/c mice (6-8 weeks old, BMS) or female BALB/c nude mice (6-8 weeks, Charles River) were used, unless stated otherwise.

Mice were housed in temperature and humidity-controlled conditions with a 12-hour light-dark cycle, at the Biomedical Services, John Radcliffe Hospital, Headington, UK or the Radiobiology Research Institute (RRI), Churchill Hospital, Headington, UK. Mice were given free access to sterile tap water and formulated diets. A maximum of 6 mice per cage were housed in environmentally enriched and individually ventilated cages. Experiments were carried out under the Home Office Project License number PPL30/2819 under protocol 2, or PPL 30/3187, under protocol 2.

2.8.2 General anesthesia

For all procedures, except weighing mice and measuring tumour sizes, mice were anesthetized by inhalation of oxygen and isoflurane (2-5%).

2.8.3 Tumour implantation

Mice were anaesthetized and injected subcutaneously with 1 x 10^6 cells/50 µl (syngeneic models using CT26 cells) or 5 x 10^6 cells/50 µl (xenograft models using HCT116, HT29 or DLD cells). Injections (50 µl) were done using a 27 gauge (G) needle and 300 µl syringe.

2.8.4 Measuring tumour growth

The length (l), width (w) and depth (d) of tumours were measured every 2-3 days, using a caliper. The tumour sizes were calculated using the formula for calculating ellipsoid volumes: $1^1/_3 \times \pi ((0.5 \times w)(0.5 \times l)(0.5 \times d))$.

2.8.5 Administering Doxycycline

Dox was administered in the drinking water (2 mg/mL) in the presence of 5% sucrose. Control group received 5% sucrose drinking water. Control mice were given 5% sucrose to the water as well. The drinking water was changed every two days due to instability of the Dox.

2.8.6 *In vivo* bioluminescence imaging

Mice bearing CT26 FLuc tumours were imaged before the start of Dox treatment and after two days of Dox treatment to confirm inducibility of the pTight system *in vivo*. Mice were anaesthetized using isoflurane and injected with 200 µL D-luciferin (15.8 mg/mL in PBS; Promega, UK) intraperitoneal, 4 minutes prior to imaging using an IVIS 100 system (Xenogen, USA). Luciferase activity was analysed with Living Image Software (Xenogen, USA).

2.8.7 I.T. injections of PBS or virus

Mice were anesthetized during injections by inhalation of oxygen and isofluorane (2-5%) through a face mask. All viruses were diluted to $5x10^9$ vp/20 µl in PBS. Tumours were injected with 20 µl virus solution or PBS. Upon injection, the needle was left inside the tumour for approximately 90 sec, to avoid back flow of virus solution or PBS.

2.8.8 In vivo irradiation

Mice were anesthetized during irradiation by inhalation of oxygen and isoflurane (2-5%) through a face mask. A dose of 15 Gy was delivered to the tumours using 300 kV X-rays (Gulmay 320 kV irradiator; 2 Gy/min). The set up allowed irradiation of the tumours and left leg only.

2.8. Evans blue extravasation

Mice were injected with a dose of 10 mg/kg of Evans blue dissolved in 100 µl PBS, intravenously. Six hours after the injections, mice were euthanized and the tumours were harvested at stored at -80 °C until further processing. The Evans blue quantification method used was based a study done by Matsumara et al. (*246*). Briefly, tumours were weighted and immersed in 1.5 mL of formamide for 48h at 60 °C. The tubes were spun and the supernatant was used for analysis. The concentration of Evan Blue in formamide was determined spectrophotometrically at 620 nm and referred back to a standard curve of known concentrations of Evans blue dissolved in formamide, see figure 2.6. Evans blue extravasation was calculated as µg/g of tumour tissue.

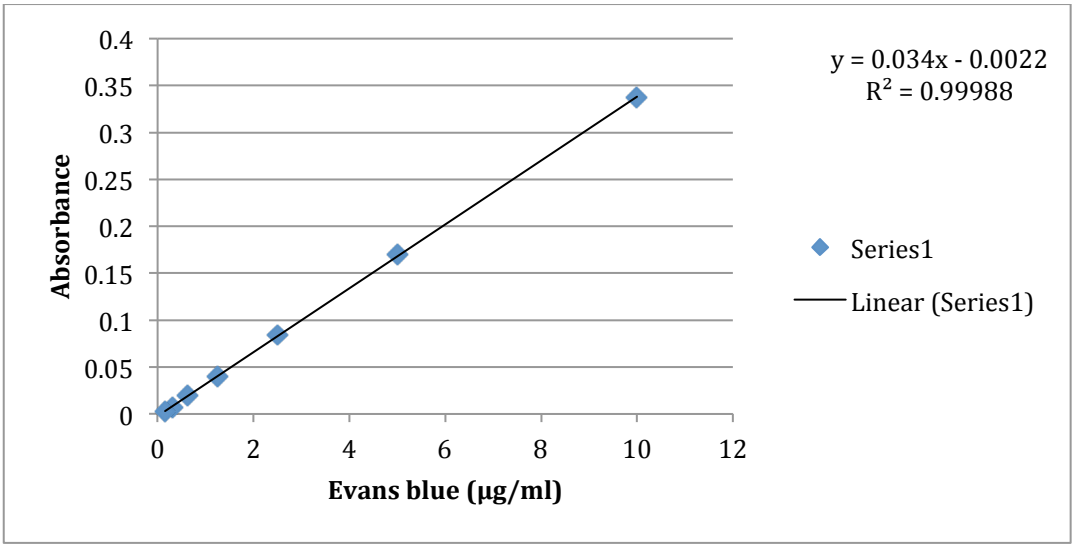

Figure 2.6: Standard curve for Evans blue. Evans blue was dissolved in formamide and absorbance at 620 nm was measured by spectrophotometer.

2.8.9 Tumour homogenization

Snap-frozen tumour tissue was thawed on ice. Subsequently, T-Per Tissue Protein Extraction Reagent (Fisher Scientific) was added. Tissues were homogenized using a tissue homogenizer (Ultra Turrax, IKA, USA) and spun at 2000 g for 5 minutes. Supernatants were stored at -80°C until further processing.

2.8.10 Flow cytometry of tumours

Tumours

The tumour were mechanically dissociated using scalpels and incubated in RPMI containing 0.05 mg/mL Collagenase IV (Worthington Biochemical, UK) and DNase I (Sigma-Aldrich) for 120 min at 37°C on a shaker. Next, dissociated tumour tissue was resuspended in RPMI and filtered through a 70 µM cell strainer (BD; Plastipak). Cells were washed once in PBS. Next, cells were spun down and incubated in 5 mL red blood cell lysis buffer (Sigma-Aldrich) for 5 min

to remove erythrocytes. 30 mL PBS was added and cells were spun again. Red blood cell lysis was repeated, if necessary.

Cells were washed twice in PBS. Cells were counted using a haemacytometer. A Zombie NIR™ or Zombie Green™ live/dead staining (Biolegend; for CT26 tumours) or Aqua live/dead staining (Thermo Fisher Scientific; DLD tumours) was performed for 20 min at RT. Live/dead reagent was used at 1 µl reagent per $5x10^6$ cells, diluted in PBS. Cells were washed in three times in PBS and resuspended to $1x10^6$ cells/100 µl MACS buffer. Cells were incubated with 1:100 Fc-block (BD bioscience) at 4°C for 10 min. Subsequently, cells were incubated with fluorescently labeled antibody for 1 h at 4 °C. Antibody concentrations were based on titration experiments. Cells were washed twice with MACS buffer and fixed in PFA for 20 min. Cells were washed twice with MACS buffer and stored at 4°C, until further analysis.

Spleens

Spleens were mechanically dissociated with a plunger from a 5 mL syringe (BD) and resuspended in serum free RPMI and filtered through a 70 µM cell strainer. Next, cells were spun down and incubated in 5 mL red blood cell lysis buffer (Sigma-Aldrich) for 5 min to remove erythrocytes. 30 mL PBS was added and cells were spun again. Red blood cell lysis was repeated, if necessary. Splenocytes were washed in PBS 3x. Cells were counted using a haemacytometer and resuspended to $1x10^6$ cells/100 µl PBS. Splenocytes were stained using 1:100 dilution of antibody, see table 2.11.

For the flow-cytometry experiments on CT26 inducible tumours and spleens, all samples were run on a FACSCalibur (BD). Flow-cytometry analysis of DLD xenograft tumours and spleens, samples were analysed using a CyAn ADP analyzer (Beckman Coulter). Data was analysed using FlowJo 8.8.6 for Macintosh. All gates were set based upon the isotype control staining of tumour samples or spleen samples. The percentage of cells stained minus the percentage of cells stained with corresponding isotype was calculated.

Antibody	**Clone**	**Concentration CT26 tumours**	**Concentration DLD tumours**	**Company**
CD45 PE	30-F11	1:100	1:100	BD bioscience
CD11b Alexa488	M1/70	1:500	1:500	BD bioscience
CD4 Alex488	RM4-5	1:500	-	BD bioscience
CD8 Alexa488	53-6.7	1:100	-	BD bioscience
CD49b FITC	DX5	1:100	-	BD bioscience
NK1.1-APC	PK136	-	1:100	BD bioscience
Ly6C PE	AL-21	1:5000	-	BD bioscience
Ly6C-PerCp-Cy5.5	AL-21	-	1:1000	BD bioscience
Ly6G PE	18A	1:500	-	BD bioscience
Ly6G- APC	18A	-	1:500	BD bioscience
Gr-1 Alexa488	RB6-8C5	1:500	-	BD bioscience
F4/80 APC	BM8	1:500	1:500	Biolegend
CD11c- Pe-Cy5	N418	-	1:500	Biolegend
Isotype Alexa488	A95-1	1:100	1:500	BD Bioscience
Isotype – PeCy5	HTK888		1:500	Biolegend
Isotype – APC	RTK2758	1:500	1:500	Biolegend
Isotype PE	A95-1	1:100	1:100	BD Bioscience

Table 2.11: Details of antibodies used for flow-cytometry.

2.9 Data processing and statistical analysis

Data was processed using GraphPad Prism 5 for Windows (GraphPad Software, USA) or Office Excel 2010 (Microsoft Corporation, USA). All statistical analysis was performed in GraphPad 5 for Windows prism or SPSS (version 23; IBM). The identity of the statistical test will be indicated at each individual figure throughout this thesis.

Chapter 3: inducible cell lines to observe cytokine functions within tumours

3.1 Introduction

The over-arching aim of this thesis is to develop an oncolytic adenovirus (ColoAd1) encoding TNF, for expression within permissive tumour masses and secretion into the tumour microenvironment. However there are few useful preclinical models to explore the consequences of TNF expression from oncolytic adenoviruses, as murine cells are not permissive to replication of human adenovirus. Hence animal studies on ColoAd1 require the use of human tumour xenograft models. The immune-incompetent murine hosts used to support xenografts cannot be used for study of the adaptive immune response, and studies are restricted to the innate immune response. Accordingly, in this chapter, an immune competent animal model expressing different forms of TNF locally within established tumours was developed, as a surrogate approach to help define the biology and therapeutic potential of expressing TNF locally within tumour deposits from an oncolytic virus.

As described in Chapter 1, TNF is a powerful pro-inflammatory cytokine. It has a complex role in tumour biology and is associated with both tumour promoting properties and anti-cancer effects. Numerous studies have looked at the biological and therapeutic consequences of administering TNF to tumour bearing mice, both by intravenous delivery and also by local injection. A drawback of systemic TNF treatment is the systemic toxicity observed with TNF. Furthermore, many studies have used human TNF in mice. Perhaps partially due to the species specific nature of the TNFR2, these studies have under estimated

the toxicity of TNF. In the 1980s, severe toxicity was seen in clinical trials using intravenous delivery of recombinant human TNF to cancer patients. Subsequent studies have found that the lethal doses (LD50) is approximately 50 times higher for human TNF than murine TNF in mice.

No previous studies have evaluated the effects expressing TNF locally in established tumours using an inducible system. Such a system could be expected to mediate a more uniform level of the cytokine throughout the tumour, by avoiding delivery artifacts and might also exploit more juxtacrine effects by being present at relatively high levels between adjacent cells. Moreover, contrary to the use of constitutive promoters, using an inducible promoter will allow the study of effects in tumours that have not developed under the selective strain of TNF expression.

A recent study based on similar principles compared the effects of expressing sm TNF and mbm TNF under the constitutive CMV promoter in a mouse lung carcinoma and melanoma model (*194*). A limitation of this model is the lack of temporal control over TNF expression, with expression being permanently 'on'. The aim of this chapter is to develop a model expressing murine TNF under a Dox inducible promoter within murine tumour cells, to add temporal control over local TNF expression. In this way it should be feasible to establish and grow tumours in mice, without TNF expression, and then to induce TNF expression by adding DOX when required, to evaluate the biological and therapeutic consequences of its expression. This could provide a good model for the consequences of encoding secreted TNF within an oncolytic virus. Apart from informing on the therapeutic effects of TNF generally, the data obtained with this

model should provide a tool to select the best form of TNF with which to arm an oncolytic adenovirus.

Murine (CT26) and human (HT29) colorectal cells (CRCs) were engineered to express murine (CT26) or both murine and human (HT29) TNF and LTA using a lentiviral transduction system.

3.1.1 The Doxycycline inducible model

Tetracycline (Tet) inducible systems are the most commonly used inducible gene expression tool (*247*). The Tet system is well tolerated by mammalian cells, and cellular metabolic functions seem largely unaffected by the system. Doxycycline (Dox) is a broad-spectrum antibiotic of the tetracycline group, which has a long half-life in the body. Dox-inducible expression cassettes have been encoded into multiple viral vectors, including lentiviruses and other retroviruses, adenoviruses and adeno-associated viruses (AAVs). In this chapter, the lentivirus based Lenti-X Tet-on system will be used for inducible regulation of TNF and LTA.

The Tet-on system has several advantages, when compared to other inducible systems. Unlike the Cre-recombinase system, the Dox-inducible system will allow for temporary induction of gene expression. Additionally, the expression levels are somewhat controllable by adjusting the amount of tetracycline used (*247, 248*). Moreover, tetracyclines are widely used antibiotics, thus its clinical use is well characterized and doses required for preclinical and clinical tests are known to be safe and these antibiotics have a wide therapeutic window. These drugs have a good bioavailability and are rapidly metabolized, allowing great

temporal control (*247, 248*). However, a potential disadvantage may be immunogenicity, as the system has been derived from bacteria (*247*).

3.1.1.1 The Lenti-X tet ON system

The spatial and temporal control of TNF expression using this system will allow us to study the role of TNF and LTA within established tumours that were allowed to develop under normal physiological conditions. Furthermore, temporal control of TNF and LTA will be important, as these proteins may have different effects during the different stages of tumour development and disease progression. Additionally, the system will allow tight regulation within the tumours, so it may allow any systemic toxicities seen when these proteins are delivered into the circulation to be circumvented.

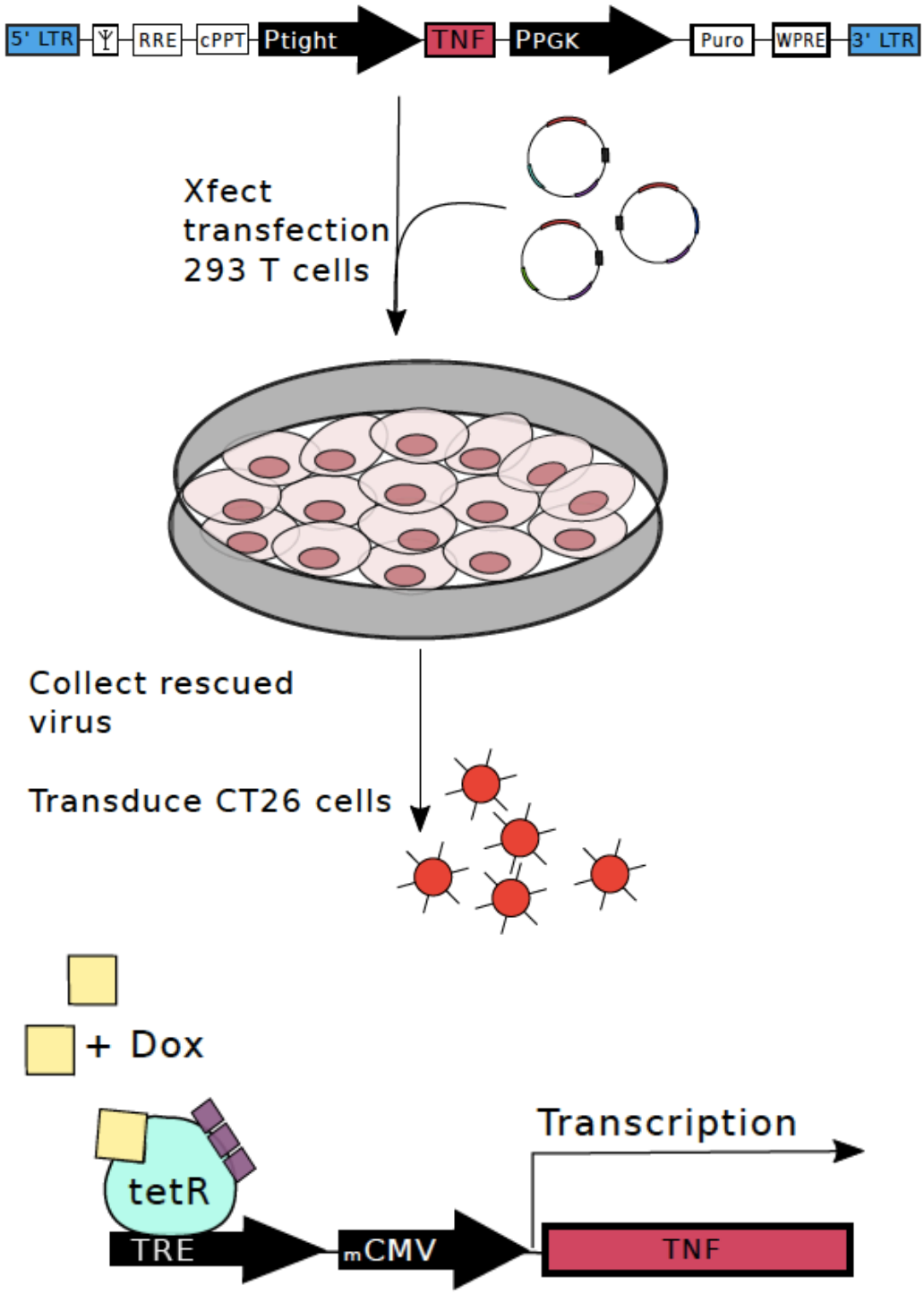

Figure 3.1: Schematic view of the Tet-On pTight system. The gene of interest (GOI; either TNF or LTA) was inserted into the multiple cloning site (MCS) under the control of a doxycycline (Dox) dependent promoter in the pLVX-Tight-Puro plasmid. The plasmid was packaged into a lentiviral vector in 293T cells. In pLVX-Tet-On transduced cells, tetR protein is constitutively expressed and adding Dox to cells transduced with both pLVX-Tet-On and pLVX-Tight-Puro vector leads to activation of the tetR protein and transcription of the gene of interest of the pLVX-Tight-Puro vector (*249*).

3.2 Chapter objectives and hypotheses

1) Establish and characterize syngeneic murine CRC cell lines expressing soluble murine (sm), full length murine (fm) and membrane bound murine (mbm) TNF and LTA under a doxycycline inducible promoter.
2) Induction of the different forms of mTNF and mLTA within established tumours leads to differences in innate and adaptive immune cell infiltration into the tumours.
3) The expression different forms of mTNF and mLTA within the tumour microenvironment has different effects tumour growth.
4) Local expression of mTNF and mLTA can avoid the side effects seen with systemic treatment.

3.3 Results

3.3.1 Cloning and generating cell lines expressing TNF and LTA

The first step in developing the Tet-on system to express TNF and LTA within tumours was to create CT26 and HT29 cells stably transduced with both the tetR-encoding vector and the pTight lentiviral vector. Human cell lines were generated to be able to study the effects of expressing TNF in a human xenograft model without introducing a virus to the tumour microenvironment. CT26 tetR cells and the lentiviral pLVX-Tet-on vector encoding the tetR protein were a gift from Dr. Aliaa Alamoudi.

HT29 cells were transduced with the pLVX-Tet-on vector as described in the materials and methods. Subsequently, the HT29 cells were selected using G418. The concentration of G418 used for selection was based a titration performed on HT29 cells, using a resazurin assay as a measure for cell viability.

G418-resistant colonies were selected using a cloning cylinder and grown until ready for further testing and cryopreservation. Once cell lines were established, the presence of the tetR protein in the CT26 tetR and HT29 tetR cell lines was confirmed using a western blot, see figure 3.2. Cell lysates from the parental CT26 and HT29 cell line was used as a negative control.

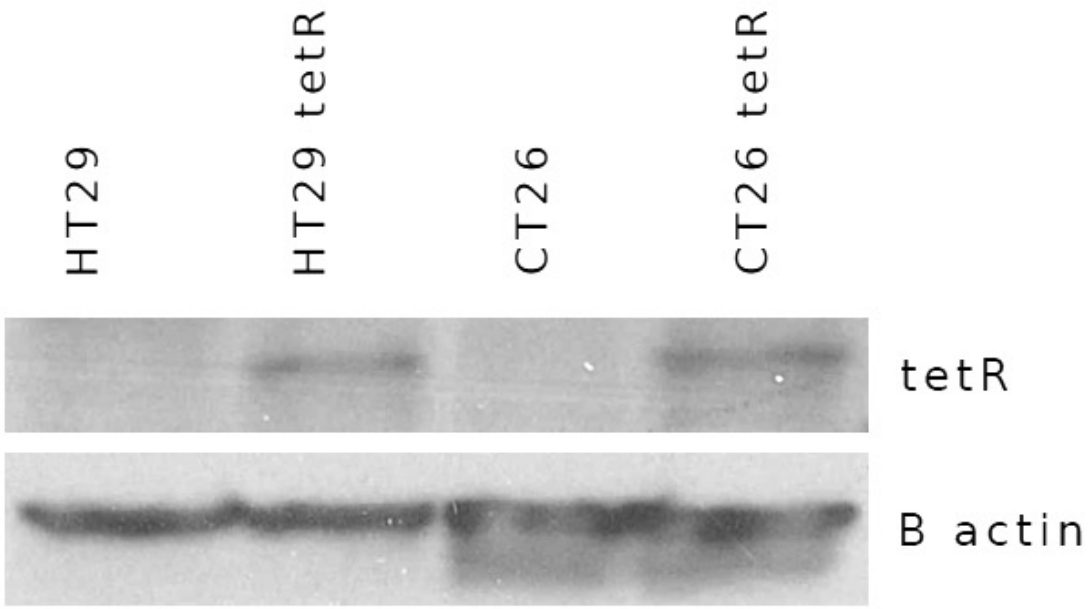

Figure 3.2: Detection of tetR protein expression. A western blot analysis on the cell lysate of CT26, CT26 tetR, HT29 and HT29 tetR cell lines for the tetR protein. TetR protein was detected at 30 kDa in the CT26 tetR and HT29 tetR cell line, whereas no bands were detected at this size in the parental CT26 and HT29 cell lines. β-actin was used as a loading control.

As seen in figure 3.2, using an anti-tetR antibody, a positive band was seen at the correct molecular weight (30 kDa) in the transduced cell lines but not in the controls. Thus, CT26 and HT29 cells were successfully transduced with the pLVX-Tet-On lentiviral vector in CT26 and HT29 cells and tetR protein was expressed in these cells.

Construction of pLVX Tight puro TNF plasmids

cDNA sequences encoding full length human and mouse TNF, soluble human TNF (DNA encoding the 17kDa TNF protein with an insulin secretion tag), murine and human LTA were ordered from GeneArt (Life Technologies). These constructs were cloned into the pLVX Tight-puro plasmid using endonuclease enzymes. Soluble mouse TNF (TNF- with an insulin secretion tag), and membrane-bound mouse TNF (Δ1-9 K11E) cDNA constructs were made using PCR insertional

mutagenesis. Subsequently, these constructs were cloned into the pLVX Tight-puro plasmids using endonuclease enzymes. For a more detailed cloning strategy, see materials and methods.

Lentiviral packaging and colony selection

After cloning into the pLVX Tight-puro plasmids all constructs were and lentiviral packaging of the plasmids was performed in 293T cells. CT26 and HT29 cells were titrated for puromycin resistance. Next, these cell lines were transduced with pLVX-Tight-Puro lentiviral vectors encoding TNF or LTA under a Dox-dependent promoter at different multiplicities of infection (MOI). Cells were selected for puromycin resistance and single colonies were picked using a cloning cylinder. When multiple colonies were saved, the colony expressing the highest amount of transgene, as measured by ELISA in the presence of Dox, was used for subsequent studies.

3.3.1.1 Measurement of transgene expression

The colonies of transduced cells were treated with Dox for 48h and the amount of transgene was measured using an ELISA, see table 3.1 and 3.2. Transgene expression from these cell lines was found to be highly stable and unchanged after numerous passages or freezing and waking cells up (data not shown). Samples were assayed in triplicates. The average amount of TNF or LTA (in ng ± standard deviation) in the supernatant at 24 h and 48 h is shown below.

Cell line	Transgene in the supernatant at 24h (in ng/ 2 x 10^5 cells)	Transgene in the supernatant at 48h (in ng/ 2 x 10^5 cells)
HT29 tetR	N.D.	N.D.
HT29 hLTA	3.04 (±0.5)	9.62 (±0.77)
HT29 sh TNF	9.02 (±0.76)	33.23 (±0.74)
HT29 fh TNF		43.65 (± 1.23)
HT29 fm TNF	0.83 (±0.04)	1.52 (± 0.12)
HT29 mLTA	N.D.	N.D.

Table 3.1: Quantification of in vitro transgene expression from transduced HT29 cells in response to Dox. Transduced HT29 cells (2 x 10^5/well) were seeded and incubated overnight. The cells were subsequently treated with 2.5 µg/ml Dox for 24 or 48 h. The supernatant was collected and transgene expression was measured by sandwich ELISA and is expressed as ng produced per 2 x 10^5 HT29 cells. Experiment performed in triplicates. Mean and SD are shown, n=3. N.D. = not detectable

Cell line	Transgene in the super-natant at 48h (in ng)
CT26 ni	0
CT26 sm TNF	40.02 (±1.87)
CT26 fm TNF	6.7 (±0.51)
CT26 mbm TNF	4.3 (±0.23)
CT26 mLTA	N.D.

Table 3.2: Quantification of in vitro transgene expression from transduced CT26 cells in response to Dox. Transduced CT26 cells (5 x 10^5/well) were seeded and incubated overnight. The cells were subsequently treated with 2.5 µg/ml Dox for 48 h. The supernatant was collected and transgene expression was measured by sandwich ELISA and is expressed as ng produced per 5 x 10^5 CT26 cells. Experiment performed in triplicates. Mean and SD are shown, n=3. N.D.= not detectable

To test whether mTNF was membrane associated in the transduced CT26 cells, a flow-cytometry experiment was set up. Cells were treated with 2.5 µg/ml Dox for 24 h. The cells were scraped of the plate and stained with a TNF antibody without permeabilization of the cells. Cells were gated on a Forward/Side scatter plot. As, expected, CT26 mbm TNF showed brighter intensity stained compared to full length TNF, see figure 3.3 below.

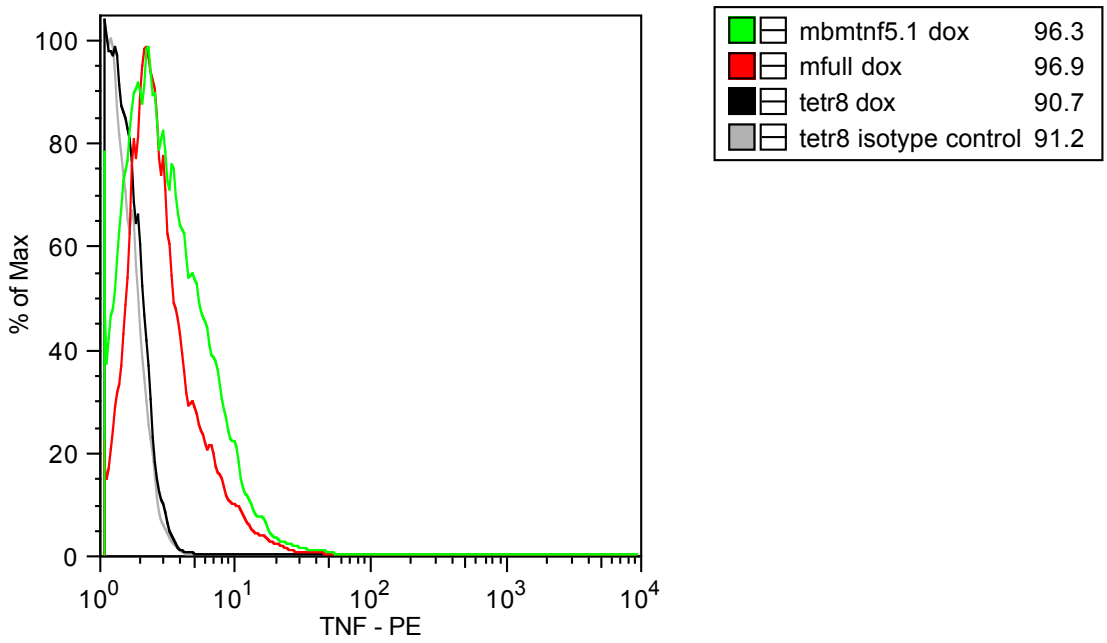

Figure 3.3: TNF expression on the cell membrane of CT26 fm TNF and CT26 mbm TNF cells. Cells (1 x 10^6/well) were seeded over night and subsequently treated with 2.5 µg/ml Dox for 24h. Cells were scraped off the plates and washed and stained for TNF without permeabilization. Membrane-associated TNF was assessed by flow-cytometry.

Murine LTA protein was not detected using a sandwich ELISA in any transduced HT29 or CT26 cells or even in cells transiently transfected with the pLVX-Tight-Puro mLTA plasmid. Additionally, the supernatant or cell lysate of mLTA-transduced cells did not induce cell death in L929 cells, whereas treatment of L929 cells with murine recombinant LTA did induce cell death (data not shown). Together, these results indicate that the absence of LTA in the ELISA assays is not indicative of a detection problem, but confirms an absence of mLTA produced. In the absence of detectable mLTA protein, it was unclear whether there was a problem with transcription of the gene sequence, or with translation of the mRNA. Accordingly, a reverse transcriptase PCR was set up to look for mLTA mRNA expression.

CT26 mLTA cells were treated with Dox (or untreated control) for 12h. RNA was extracted from the cells and a cDNA library was made using a reverse

transcriptase kit. Subsequently, a QPCR was performed to detect mLTA and GAPDH mRNA. Murine mLTA mRNA levels were normalized to the GAPDH control and compared with CT26 mLTA cells that were not treated with Dox. As can be seen in figure 3.4, an approximately 18-fold induction of mLTA mRNA was seen upon Dox treatment in CT26 mLTA cells. The induction of mRNA suggests the lack of mLTA protein might be due to post-transcriptional downregulation or protein instability.

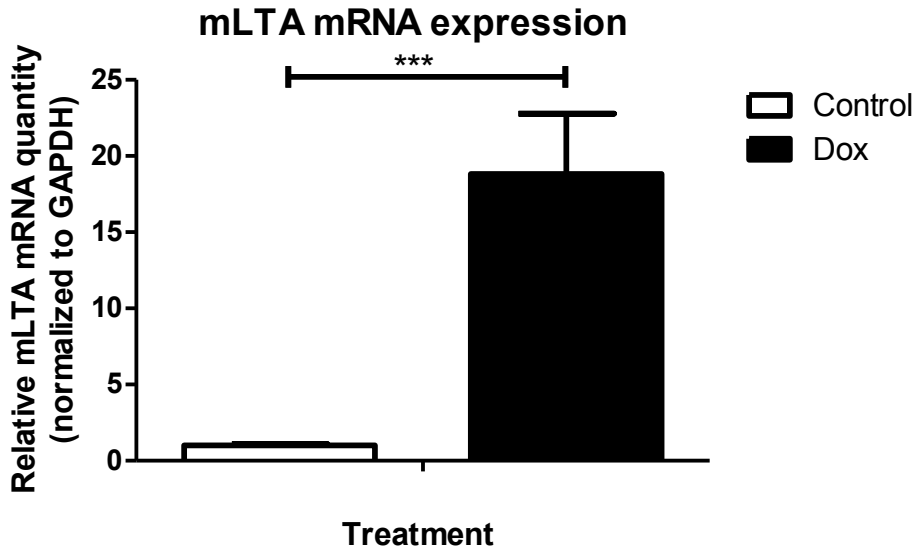

Figure 3.4: mLTA mRNA expression in CT26 mLTA cells treated with Dox. CT26 mLTA ($5x10^5$ cells/well) were seeded overnight. Subsequently, the cells were treated with 2.5 µg/ml Dox or control for 12 h. The cells were harvested and RNA was isolated from these cells. Using a reverse transcriptase reaction, a cDNA library was made and QPCR analysis to quantify mLTA expression. Values obtained for mLTA were normalized to GAPDH. A statistically significant increase in mLTA mRNA was seen in CT26 mLTA cells upon Dox treatment. A students t-test was done to assess statistical significance. ***=$p<0.0001$. Mean and SD shown, n=3.

3.3.1.2 Bioactivity of the transgene

ELISA is a good technique to quantify the total amount of TNF or LTA produced, but it will not discriminate functional protein from non-functional protein. To determine the biological activity of the TNF and LTA produced a functional study

was performed. The L929 cytotoxicity assay is well-known and standard biosensitivity assay for TNF (*250*). In this assay, the TNF-sensitive murine L929 cell line is further sensitized to TNF by treating the cells with the RNA polymerase inhibitor actinomycin D. Inhibition of transcription inhibits the production of pro-survival genes by NF-κB activation by TNF and leads to cell death in L929 cells.

Using this assay, similar cytotoxicity from TNF and LTA expressed by HT29 cells and the corresponding recombinant proteins was seen, see figure 3.5.

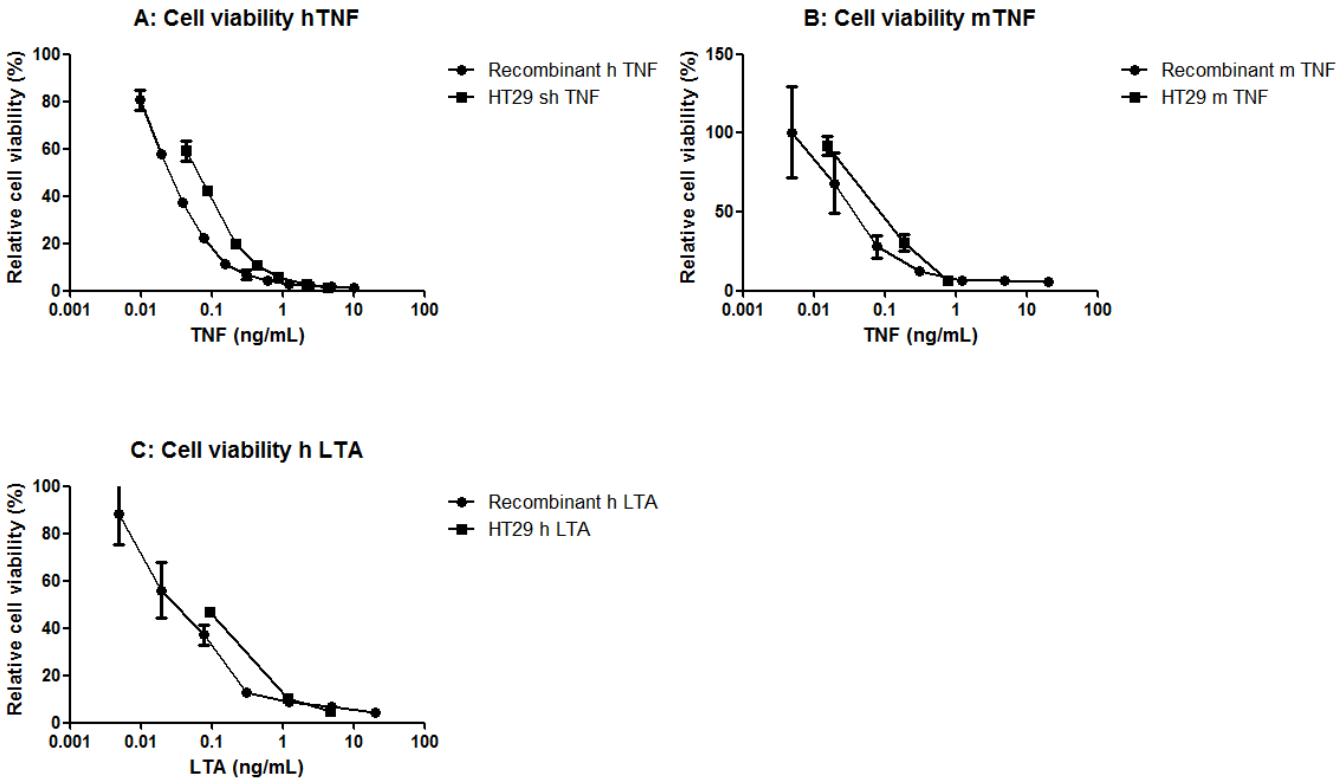

Figure 3.5: Bioactivity of transgenes produced by transduced HT29 cells. HT29 fh TNF (A), HT29 fm TNF (B) or HT29 h LTA (C) cells ($2x10^5$) were seeded overnight and subsequently treated with 2.5 µg/ml Dox for 24 h. The supernatant was collected and cellular debris was spun down. The supernatant was subsequently added to L929 cells ($1x10^4$/well) in the presence of Actinomycin D. Additionally, serial dilutions of recombinant hTNF (A), mTNF (B) or hLTA (C) in the presence of Actinomycin were added as a control to other L929 cells. L929 cells were incubated with TNF or LTA for 24h before measuring cell viability using an MTS assay. TNF (both human and murine) and hLTA produced by HT29 cells induced cytotoxicity of L929 cells. Mean and SD shown, n=3.

TNF is a well-known activator of NF-κB. To see whether expression of fm TNF in CT26 activates NF-κB, a western blot for IκBα on Dox treated and control CT-26-tetR-fmTNF cells was performed on samples collected 8, 24 and 48h after Dox treatment. IκBα is a NF-κB inhibitory protein, which keeps NF-κB in the cytosol. Upon IκBα degradation, NF-κB can migrate to the nucleus and initiate transcription.

Within 8h after adding 2.5 μg/ml Dox, and thus inducing the expression of TNF from CT26 cells after (Dox 8h), a decrease in IκBα was seen compared to non-Dox treated cells (- 8h). This decrease in IκBα was still visible 24h after Dox treatment of CT26 fm TNF cells (Dox 24h) compared to non-Dox treated controls (- 24h), see figure 3.6.

The degradation of IκB upon TNF expression by CT26 cells indicates the activation of NF-κB. Treatment of CT26 cells with 20 ng/mL TNF served as a positive control, see figure 3.6. Treatment of CT26 tetR cells with Dox did not induce degradation of IκBα (data not shown), suggesting that the effects are dependent on TNF expression and not Dox treatment in CT26 cells.

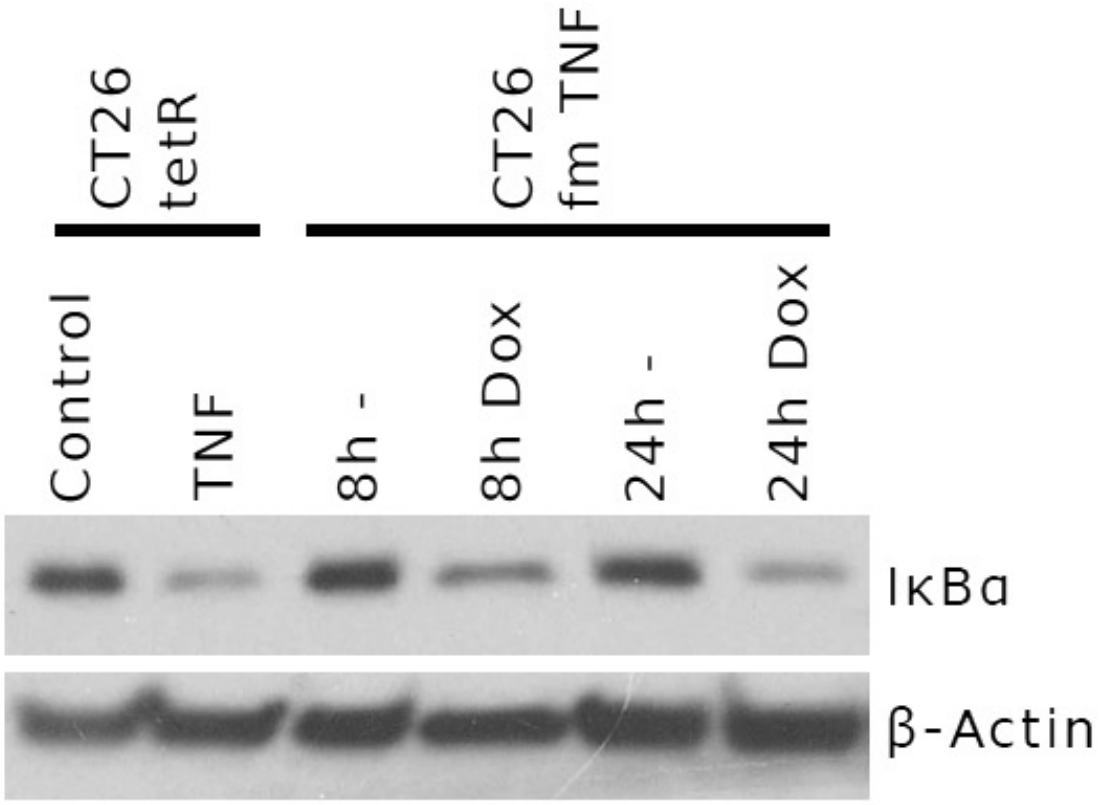

Figure 3.6: IκBα degradation in CT26 fm TNF cells treated with Dox. CT26 fm TNF or CT26 tetR cells ($5x10^5$ cells/well were seeded over night. Subsequently, cells were treated with 2.5 µg/ml Dox or control (-) for 8h or 24h. Additionally, as positive control, CT26 tetR cells were treated with recombinant mTNF (20 ng/ml) for 30 min. A western blot analysis on the cell lysate for IκBα was performed. B-actin was used as a loading control. A decrease in IκB was seen in CT26 tetR cells treated TNF and in CT26 fm TNF cells treated with Dox and thus expressing TNF.

3.3.1.3 In vitro Proliferation of myeloid cells

Transgene expressing cells were treated with Dox for 24, 48 or 72 h. Cell viability was assessed using an MTS assay. Using a two-way ANOVA, a significant increase in cell viability of CT26 tetR, CT26 sm TNF, CT26 fm TNF and CT26 mbm TNF (all $p<0.0001$) and cells upon Dox treatment was found, see figure 3.7. The increased proliferation in CT26 tetR cells seen in Dox treated cells indicates that the increased proliferation seen in Dox treated CT26 cells are due to an intrinsic effect of Dox on this cell line and is not due to TNF expression.

Contrary to CT26 tetR cells, treatment with 2.5 µg/ml of Dox did not alter HT29 tetR cell viability, see figure 3.8. Moreover, induction of TNF expression by Dox did not induce cell toxicity on HT29 cells, as cell viability of HT29 sh TNF or HT29 fh TNF cells was unchanged in Dox treated cells and cells not treated with Dox.

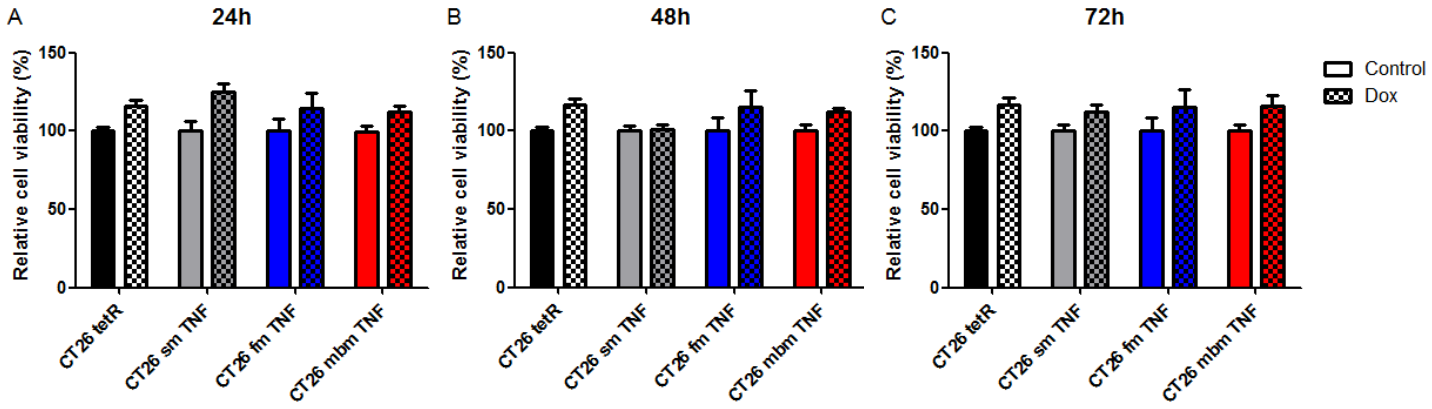

Figure 3.7: Effects of Dox on CT26 cell viability. CT26 tetR (black), CT26 sm TNF (grey), CT26 fm TNF (blue) or CT26 mbm TNF (red) (1 x 10^4/well) were seeded overnight. Cells were treated with 2.5 µg/ml Dox 24 (A), 48 (B) or 72 (C) h. Cell viability was measured using an MTS assay. Comparisons were made between Dox treatment (checked bars) or control (plain coloured bars) for each cell line. Increased cell viability was seen in Dox treated cells. Mean and SEM are shown, n=12.

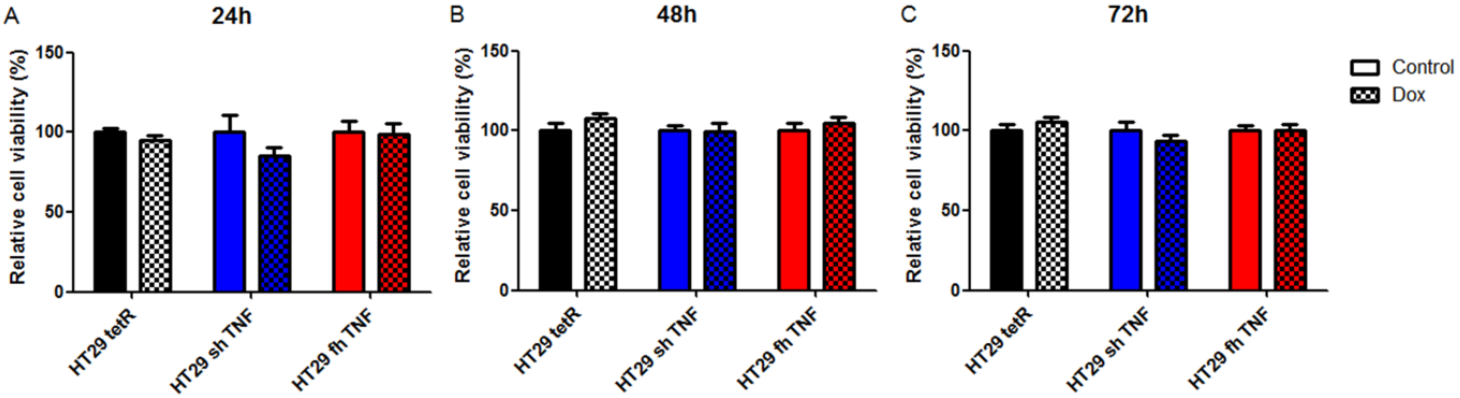

Figure 3.8: Effects of Dox on HT29 cell viability. HT29 tetR (in black), HT29 sh TNF (in blue) and HT29 fh TNF (in red) cells were seeded (1x10^4 cells/well) overnight. Cells were treated with 2.5 µg/ml Dox 24 (A), 48 (B) or 72 (C) h. Comparisons were made between Dox treatment (checked bars) or control

(plain coloured bars) for each cell line. A 1-way ANOVA was used to analyse data. No statistically significant differences in cell viability were found. Mean and SEM shown, n=12.

3.3.2 In vivo studies

3.3.2.1 Pilot study: expression of mTNA and mLTA from CT26 cells in vivo

Inducibility of TNF expression from CT26 cells was seen, *in vitro.* The next step was to conduct a pilot study to assess whether the pTight system was also inducible *in vivo*. Additionally, to determine and visualize the inducibility of the pLVX-Tight-Puro system and the kinetics of expression *in vivo*, an inducible cell line expressing firefly luciferase (Fluc) was included in the *in vivo* pilot study. CT26 fm TNF (n=4), CT26 mLTA (n=4) or CT26 firefly luciferase (CT26 Fluc; n=4) (1 x 10^6) cells were implanted subcutaneously on the flanks of BALB/c mice.

At day 13 post tumour implantation, mice were randomly divided into the Dox group, or the control group. In mice bearing CT26 Fluc tumours, luciferase activity was measured immediately before the start of Dox treatment and after two days of Dox treatment, see figure 3.9.

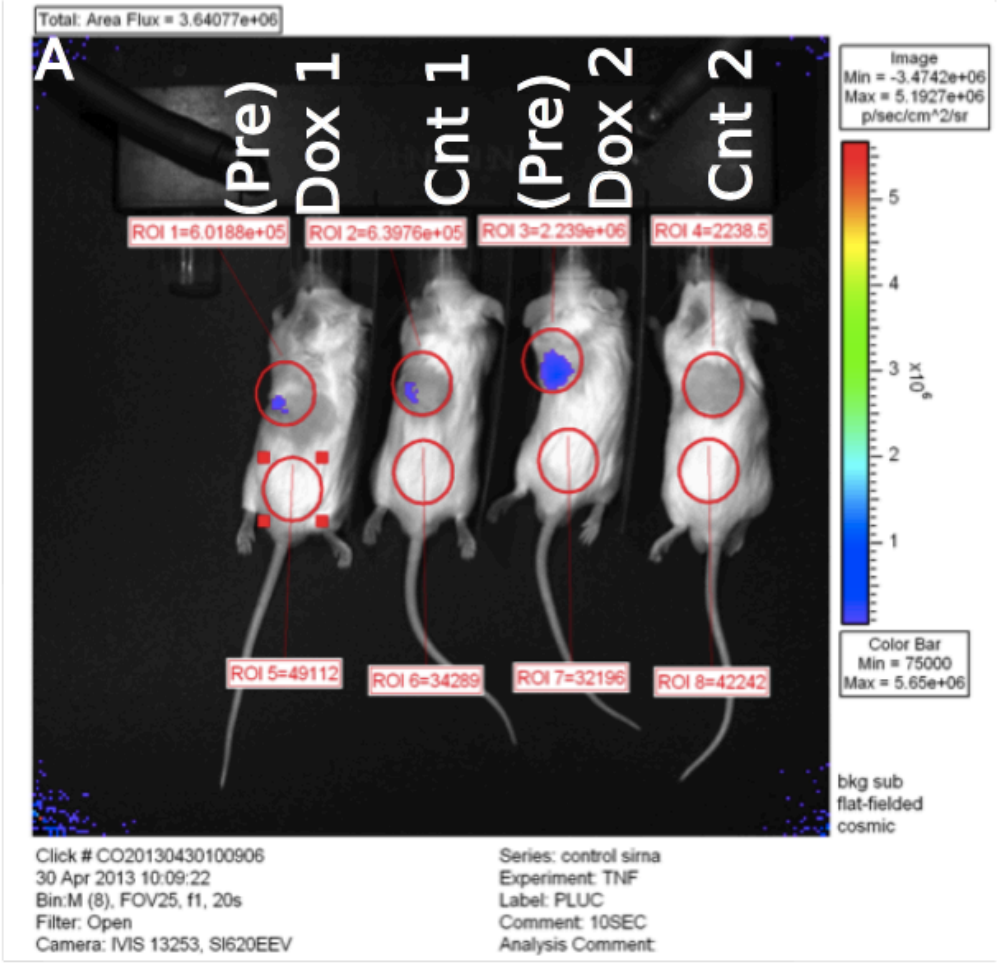

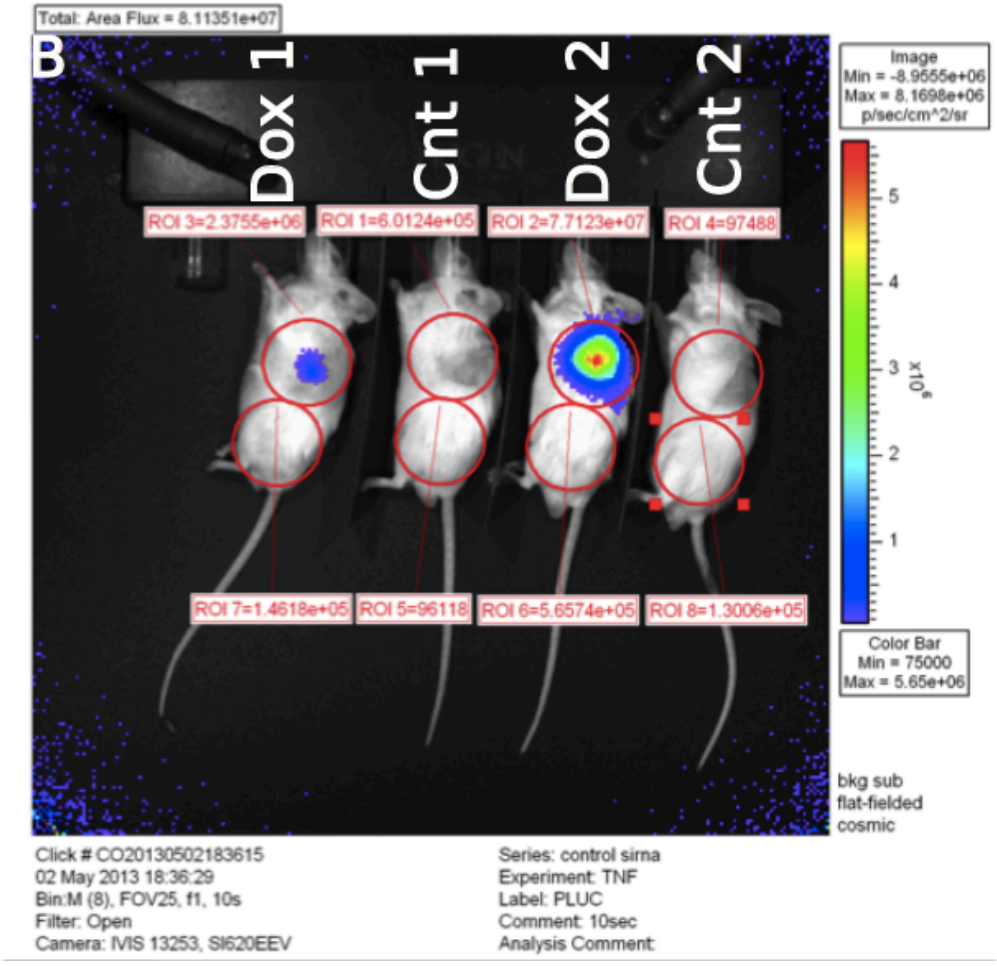

Figure 3.9: Induction of luciferase activity in CT26 Fluc cells vivo by Dox, *in vivo*. Mice were implanted with subcutaneous CT26 Fluc cells. On day 13 post implantation, the mice were either given 2 mg/ml Dox in the drinking water (Dox) or control. Luciferase expression was measured using an IVIS100 camera in animals right before treatment with Dox (A; day 13; (Pre) Dox 1 and 2) and two days post-Dox measurement (B; Dox 1 and 2) or kept as controls (Cnt 1 and 2).
Cnt= control

Mouse	Pre Dox (ROI tumour – ROI background)	Post Dox (ROI tumour – ROI background)	Fold induction (post Dox/ pre Dox)
L Dox	5.5×10^5	2.2×10^6	4.0
R Control	6.0×10^5	5.1×10^5	0.8
LR Dox	2.2×20^6	7.7×10^7	34.69

Table 3.3: Quantification of Fluc activity in vivo. The ROIs, as measured in figure 3.9, of mice pre and post Dox treatment of tumour bearing mice are expressed. An increase in Fluc activity was seen in the mouse treated with Dox.

A downside of the pLVX-Tight puro vector system is that despite optimization of the Tet On system, leakiness of the promoter still occurs in the absence of Dox (*251*). In an effort to reduce background transgene levels, cell line clones with low levels of transgene expression and high inducibility, as assessed by ELISA, were selected for further studies. Yet, Fluc activity was seen prior to Dox adminsitration as well as in the control mouse, indicating leakiness of the Dox-inducible system *in vivo*. Additionally, leakiness of TNF expression also occurred (also discussed later in this chapter). In the mice treated with Dox, an increase in Fluc signal was seen after two days, whereas this was not seen in the control mouse bearing an CT26 Fluc tumour Dox, thus confirming the inducibility of the pTight system *in vivo*.

Tumour growth

All tumour-bearing mice were kept on Dox treatment or control until day 26 after tumour implantation or humane endpoints were reached. Tumour growth of mice on Dox and control are depicted below. Due to the limited group size, tumour growth of individual mice is depicted in figure 3.10.

On CT26 fm TNF bearing tumour regressed after two days of Dox treatment. Additionally, minimal tumour growth was seen in the other Dox treated CT26 fm TNF mouse. Due to the small group sizes, it is unclear whether TNF expression influenced tumour growth, or random variation in tumour sizes was observed.

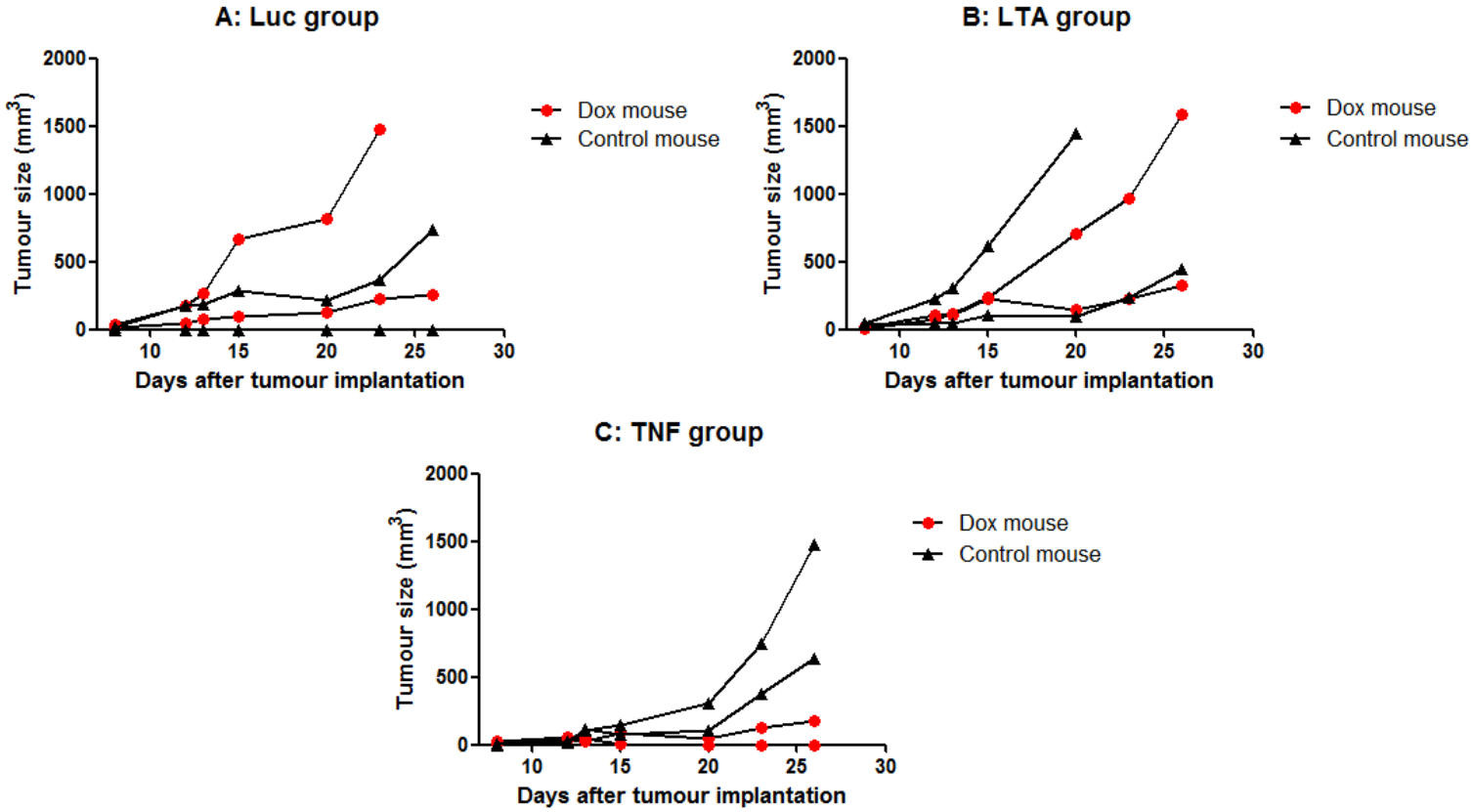

Figure 3.10: Tumour growth of individual mice bearing CT26 FLuc, CT26 mLTA or CT26 fm TNF tumours. Mice were received subcutaneous injections with 1x 10^6 CT26 Fluc (A), CT26 mLTA (B) or CT26 fm TNF (C) cells on day 0. Dox treatment started 13 days after tumour implantation. At day 26 post implantation, mice were euthanized and tumours were harvested L, R, LR, NC and LL are the ear markings used to identify each mouse.

Characterization of the TNF expression in vivo

At day 26 post tumour implantation, animals were killed, tumours were dissected and snap frozen on dry ice. The tumours were homogenized and an ELISA for TNF and LTA was performed as well as a luciferase assay. TNF

expression and luciferase activity were measured and normalized by protein content.

Leakiness in luciferase expression in control mice was seen. Additionally, in mice bearing CT26 fm TNF tumours that did not receive Dox, low levels of TNF were detected in the tumour lysates, whereas TNF levels were not detectable in the lysates of mice bearing CT26 Luc or CT26 mLTA tumours.

Mouse	TNF concentration (ng/g protein)
CT26 fm TNF Dox (LR)	34
CT26 fm TNF Control (L)	3.97
CT26 fm TNF Control (R)	1.74

Table 3.4: Quantification of TNF expression in the tumour lysate of the pilot study mice. Concentrations TNF (ng) in the tumour lysate were determined using a sandwich ELISA and normalized to protein content of tumour lysate. TNF was detectable in the lysate of the control mice, and higher TNF levels were detected in the CT26 fm TNF mouse treated with Dox.

Mouse	Luciferase activity (RLU/µg protein)
L Dox	1237.55
LR Dox	544.37
R Control	99.55

Table 3.5: Firefly luciferase activity (RLU) in the tumour lysate of individual mice. Tumours were harvested and homogenized. A Fluc assay was performed and the luciferase activity was normalized to protein contents.

Using an ELISA, mLTA protein was not detectable in the tumour lysates of the CT26 mLTA Dox or control mice. Due to the absence of mLTA expression both *in vitro* and *in vivo*, this cell line was not taken further for further testing.

In the initial pilot *in vivo* study, CT26 Fluc cells were used to monitor and image the Dox-mediated induction of transgene expression, using bioluminsence imaging *in vivo*. This cell line contains a lentivirus and Dox-inducible cassette, but

expresses no exogenous TNF, hence might be suitable as a control cell line to monitor tumour growth. However Fluc is an exogenous protein to mice, and adaptive immune responses against Fluc protein produced by CT26 cells in BALB/c mice have been reported (*252*). Therefore in the following studies, preference was given to less immunogenic control cell line. A CT26 tetR cell line transduced with a pLVX-Tight-Puro vector without an insert under the CMV promoter was made, known as the CT26 no insert (ni) cell line.

3.3.2.2 Comparison of soluble, full length and membrane bound TNF on tumour growth

To assess the effects of the different forms of TNF, 1 x 10^6 CT26 ni, CT26 sm TNF, CT26 fm TNF or CT26 mbm TNF cells were implanted s.c. on the flanks of mice (n=15 for each group). Tumour growth was measured every 2 days and mice were divided into Dox or Control groups when tumours reached approximately 100 mm^3 in size. Drinking water including Dox was changed every 2 days due to instability of Dox in water (*253*). All mice were kept until the tumour volume reached 1200 mm^3 or another humane endpoint (such as ulceration, etc.) was reached. Graphs depicting tumour growth and survival time are shown in figures 3.11 and 3.12.

Once mice had to be euthanized, tumours were excised and snap frozen on dry ice.

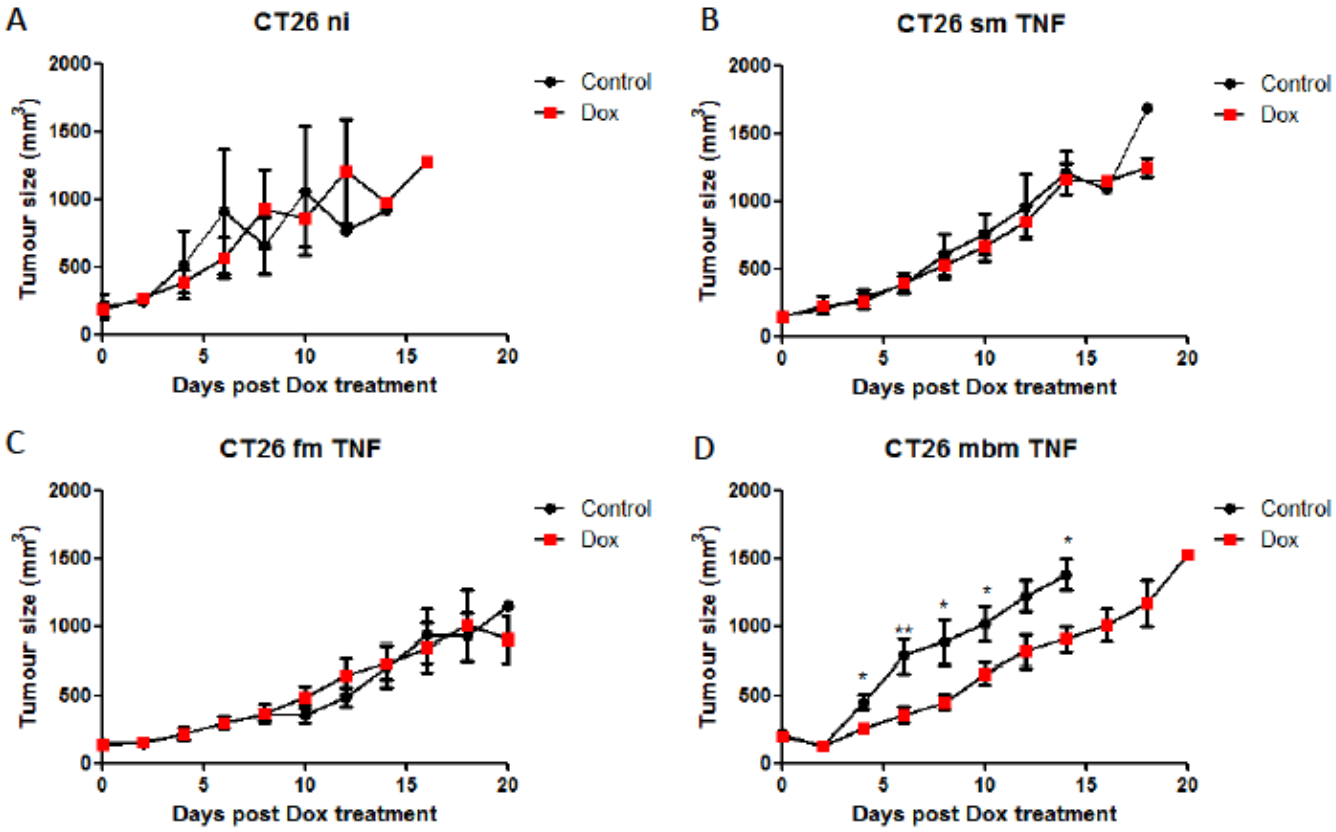

Figure 3.11: The effects of expressing mTNF in established CT26 tumour on tumour growth. $1x10^6$ CT2 ni (A; control n=3; Dox n=4), CT26 sm TNF (B; control n=5; Dox n=6), CT26 fm TNF (C; control n=4; Dox=n=5) or CT26 mbm TNF (D; control n=7; Dox n=8) cells were implanted subcutaneously in mice. Once tumours reached approximately 100 mm^3 the mice were randomly assigned to the control group (5% sucrose added to the drinking water) or the Dox group (2 mg/mL of Dox into the drinking water and 5% sucrose). Tumour growth was measured every 2 days and. Mean and SEM are shown. An unpaired student t test at each time point was performed to test for significance. *=$p<0.05$, **=$p<0.01$.

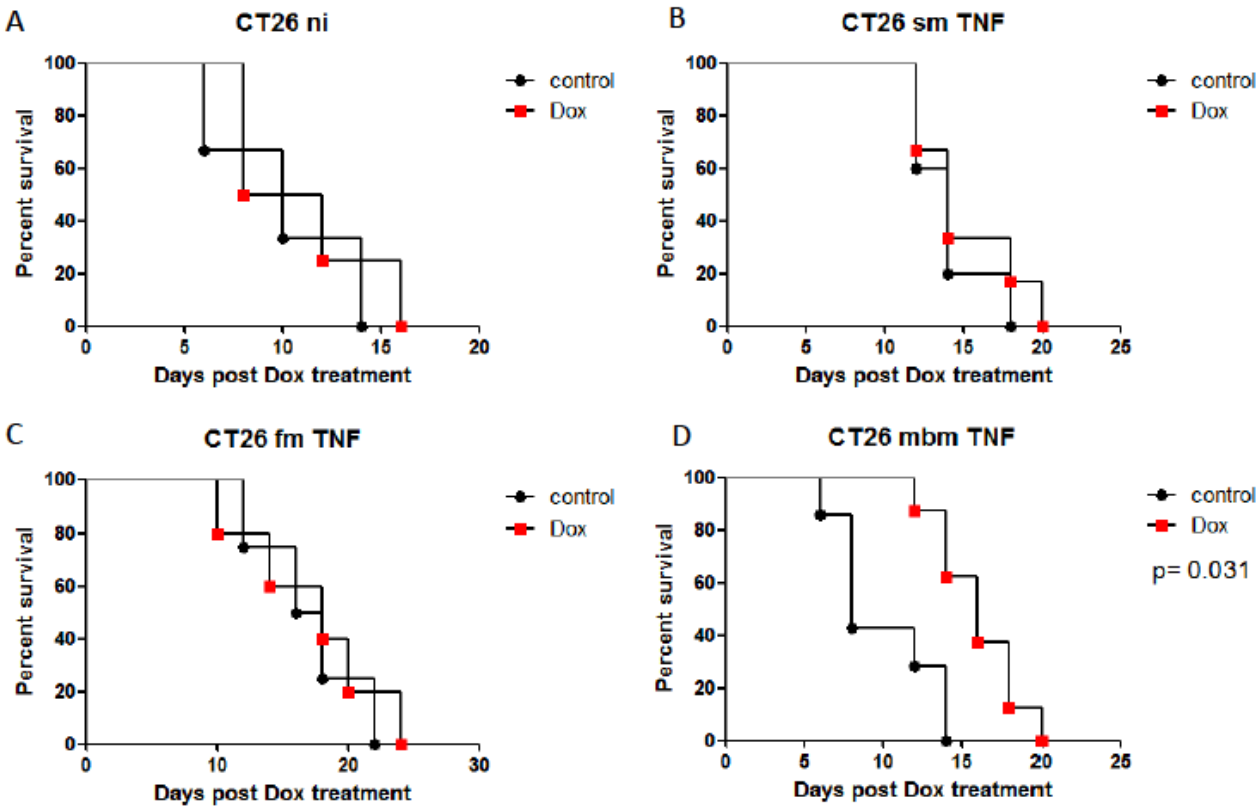

Figure 3.12: The effects of expressing mTNF in established CT26 tumours on animal survival. $1x10^6$ CT26 ni (A; control n=3; Dox n=4), CT26 sm TNF (B; control n=5; Dox n=6), CT26 fm TNF (C; control n=4; Dox=n=5) or CT26 mbm TNF (D; control n=7; Dox n=8) cells were implanted subcutaneously in mice. Once tumours reached approximately 100 mm^3 the mice were randomly assigned to the control group (5% sucrose added to the drinking water) or the Dox group (2 mg/mL of Dox into the drinking water and 5% sucrose). A Log-rank (Mantel Cox) test was used to analyse the survival data. A statistically significant increase in survival was seen in CT26 mbm TNF mice on Dox, compared to the control mice (p=0.031).

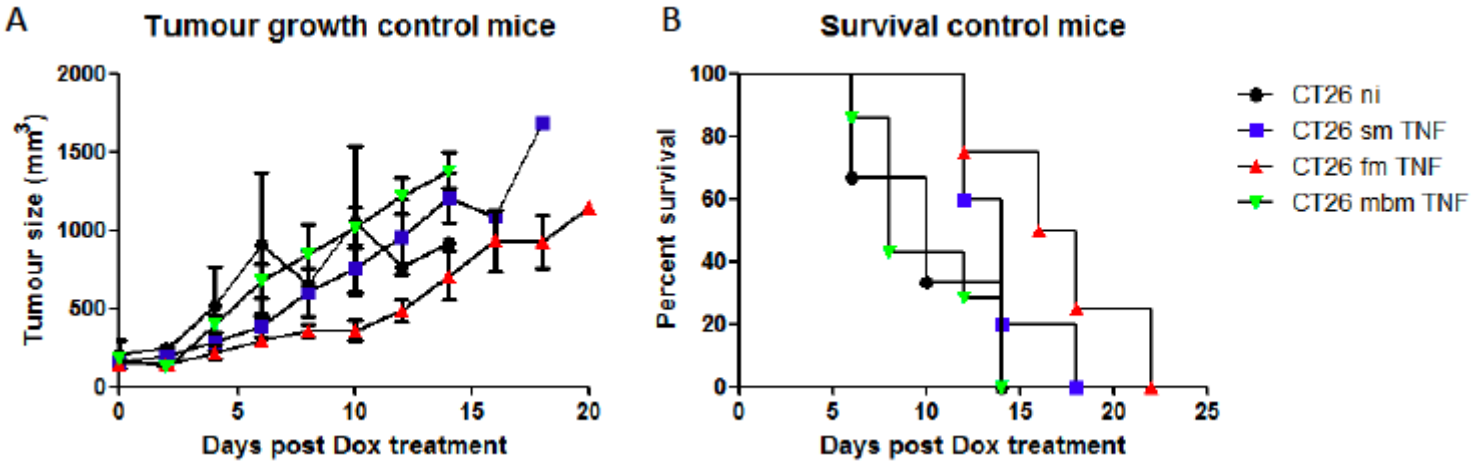

Figure 3.13: Comparison of tumour growth and survival of CT26 ni, CT26 sm, CT26 fm and CT26 mbm TNF in control mice. A: Mice injected with $1x10^6$ CT26 ni (control; n=3), CT26 sm TNF (control n=5), CT26 fm TNF (control n=4) or CT26 mbm TNF cells (control n=7). Once tumours reached approximately 100 mm^3 mice randomly allocated to the control group and were given 5% sucrose in the drinking water. The mice were euthanized once tumours reached 1200 mm^3 or other humane endpoints, such as tumour ulceration. Tumour growth was compared using a 1 way ANOVA, followed by a Bonferroni Multiple comparison post test. No statistically significant differences were found between the different cell lines.
B: Comparison of survival between the control mice bearing CT26 ni, CT26 sm, CT26 fm or CT26 mbm TNF tumour. Survival depended on reaching humane endpoints. A Log-rank (Mantel Cox) test was used to compare survival between the different groups. No statistically significant differences were found between the different cell lines.

In vitro, an increase in cell viability is seen when CT26 cells are treated with 2.5 µg/ml of Dox, see figure 3.7. *In vivo*, Dox treatment did not seem to have an effect on tumour growth, as CT26 ni Dox and control mice have very similar growth curves. Induction of mbm TNF expression (Dox group) reduces tumour growth and increase survival compared to the control. However, the growth rate of the CT26 mbm TNF appears to be higher than the CT26 fm TNF and CT26 sm TNF cell lines, *in vivo*, although the difference was not statistically significant (p= 0.18).

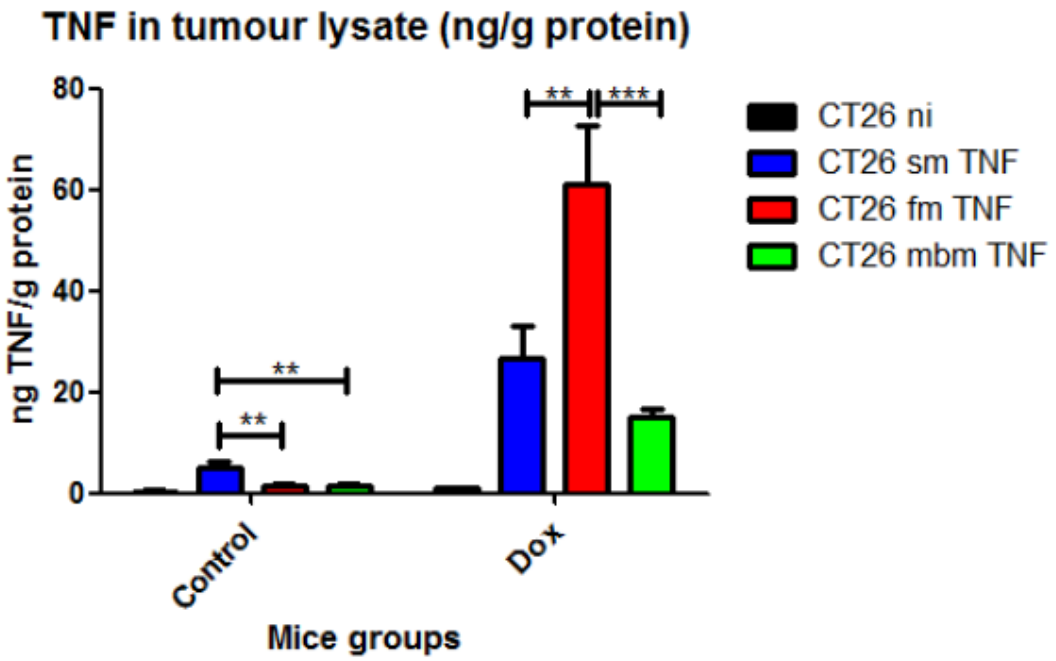

Figure 3.14: Long-term TNF expression in CT26 tumours. Tumours were harvested when mice were euthanized. The tumours were homogenized and TNF levels were measured by sandwich ELISA. The TNF levels were normalized to protein concentration, using a Bradford assay. A statistically significant increase in TNF levels was seen in CT26 sm TNF, fm TNF and mbm TNF bearing mice treated with Dox their respective control mice or CT26 ni Dox mice. Moreover, the TNF levels of CT26 sm TNF and fm TNF mice on Dox were significantly higher than in CT26 mbm TNF Dox mice. The levels of TNF within tumours of CT26 sm TNF control mice were significantly higher than in control mice bearing CT26 fm TNF or CT26 mbm TNF tumours. *=$p<0.05$, **$p<0.01$.

At the time of euthanasia, levels of TNF in CT26 sm TNF and CT26 fm TNF Dox mice were significantly higher than the levels in CT26 mbm TNF Dox mice. No statistically significant differences were found between CT26 sm TNF and CT26 fm TNF. For all three TNF cell lines, a statistically significant increase in TNF expression between Dox and control was seen. Between control cell lines, TNF levels of CT26 sm TNF tumours were significantly higher than the other controls.

3.3.2.3 Comparison of the effects of acute expression of soluble, full length and membrane bound mTNF on immune infiltration in established CT26 tumours

TNF is known to activate immune cells and induce the expression of other cytokines and chemokines. TNF is capable of inducing anticancer immune responses (*198*)

Local TNF expression has been reported to increase $CD4^+$ and $CD8^+$ lymphocyte infiltration and both increases and decreases of myeloid cell populations have been attributed to local TNF expression (*194, 196*). Previous studies have used constitutively active promoters, rather than inducible promoters. To look at the effects of inducing TNF expression on the immune infiltrates in established tumours, flow-cytometry, measuring different immune populations was set up.

Staining for $CD45^+$ (general immune cell infiltrates), $CD45^+$ $CD11b^+$ (myeloid cells), $CD45^+$ $CD8^+$ (cytotoxic T cells), $CD45^+$ $CD4^+$ (T helper cells), $CD45^+$ $Gr\text{-}1^+$ (MDSCs), $CD45^+$ $CD49b^+$ (NK cells), $CD11b^+$ $Ly6G^+$ (granulocytic MDSCs), CD11b+ $Ly6C^{high}$ (monocytic MDSCs), and $F4/80^+$ (macrophages) was optimized on control mice. All antibodies were titrated alongside their respective isotype control antibodies and concentrations providing the highest signal to noise ratio were picked, see materials and methods. Live/dead staining was included, so non-specific binding of antibodies to dead cells could be excluded from the data analysis.

Flow-cytometry optimization

To optimize the flow-cytometry staining, tumours were digested and single cell suspension were obtained. Serial dilutions of each antibody in MACS buffer were made and used to stain 1 x 10^6 tumour cells, suspended in 100 µl MACS buffer.

For example, in figure 3.15, cells were stained with 1:100 (A), 1:500 (B) or 1:1000 (C) dilution of CD11b-Alexa488 (on the X-axis). Based on these results 1:500 dilution was used for further studies.

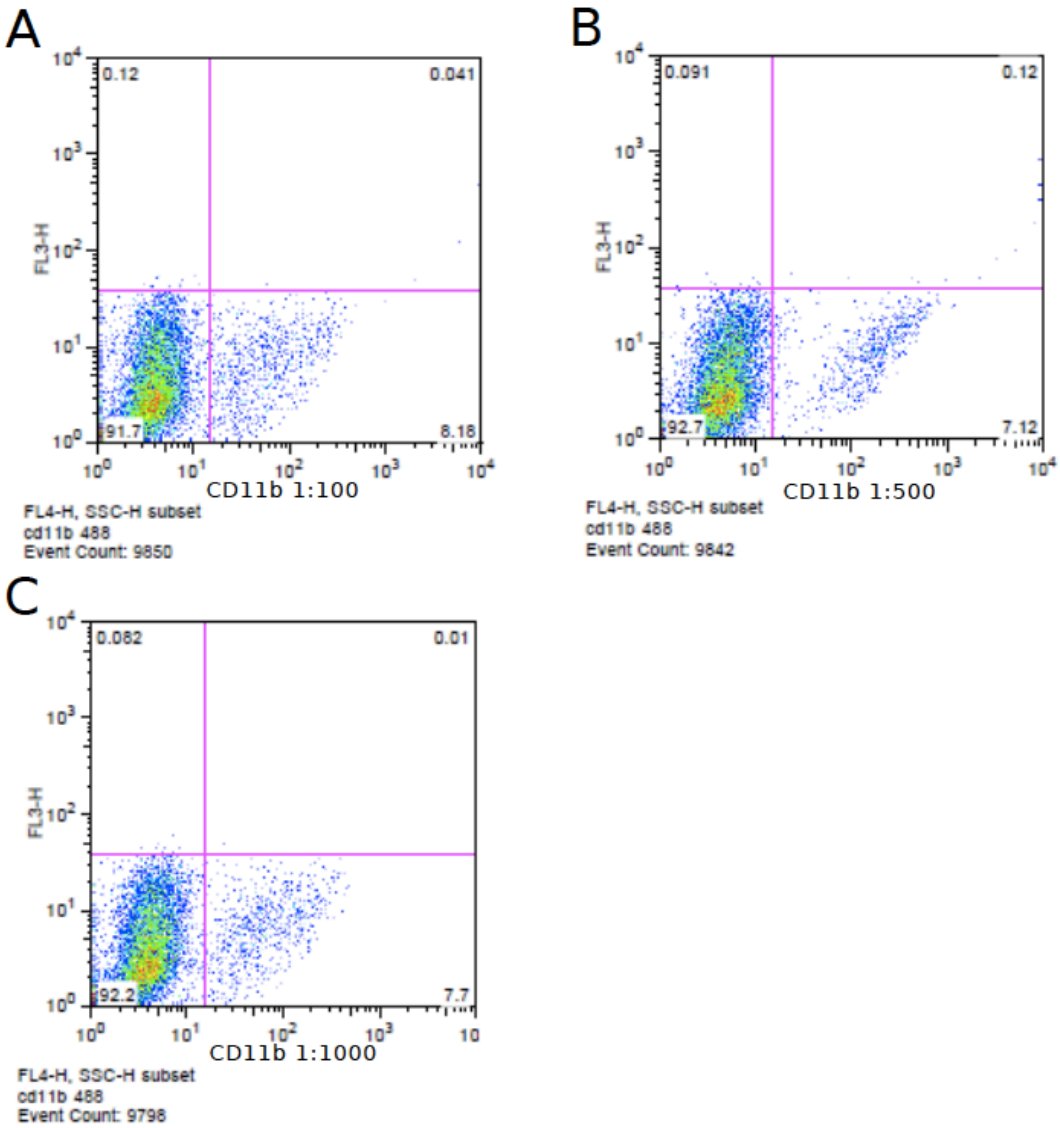

Figure 3.15: Titration of flow-cytometry antibodies for murine tumours. CT26 tumours were harvested and processed to a single cell suspesion. A live/dead staining was performed and cells were counted for further staining. A solution of 1 x 10^6 tumour cells/ 100 µl were stained with 1:100 (A), 1:500 (B) or 1:1000 (C) dilution of CD11b-Alexa488 (FL-1).

Flow-cytometry experiment

To assess the effects of expressing sm, fm or mbm TNF in established tumours, CT26 cells were implanted subcutaneously in BALB/c mice. When tumours

reached approximately 100 mm^3, mice were divided randomly into Dox or control group. The Dox was changed every two days and tumour size and mice weight were measured every two days. Seven days after the start of the treatment, mice were euthanized and the tumours and spleens were harvested for flow cytometry. A small part of the tumours was snap frozen on dry ice, for further protein analysis.

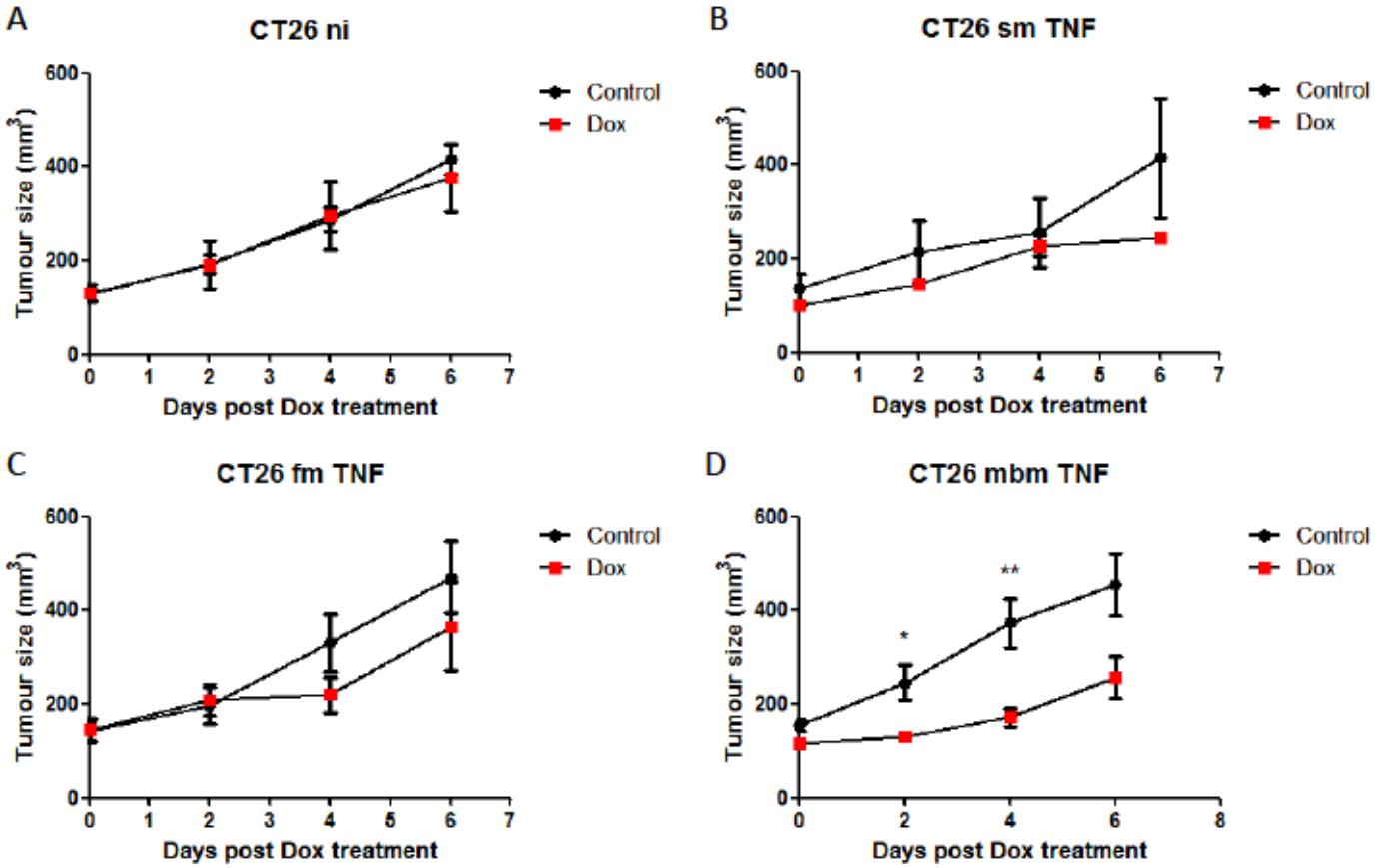

Figure 3.16: Tumour growth of CT26 tumours. Mice were injected with $1x10^6$ CT26 ni (A; control n=4, Dox n=3), CT26 sm TNF (B; Dox and control n=3), CT26 fm TNF (C: control and Dox n=4), and CT26 mbm TNF (D: control n=3, Dox n=4) cell. Once tumours reached approximately 100 mm^3 mice were randomly divided into Dox or control groups. A statistically significant reduction in tumour growth was seen in CT26 mbm TNF mice on Dox, compared to control. Mean and SEM are shown. *=$p<0.05$, **$p<0.01$.

Similar to the previous tumour growth experiment, the CT26 mbm TNF Dox mice showed a reduction in tumour growth compared to the control mice. For all other cell lines, no differences in tumour growth between Dox and control were found.

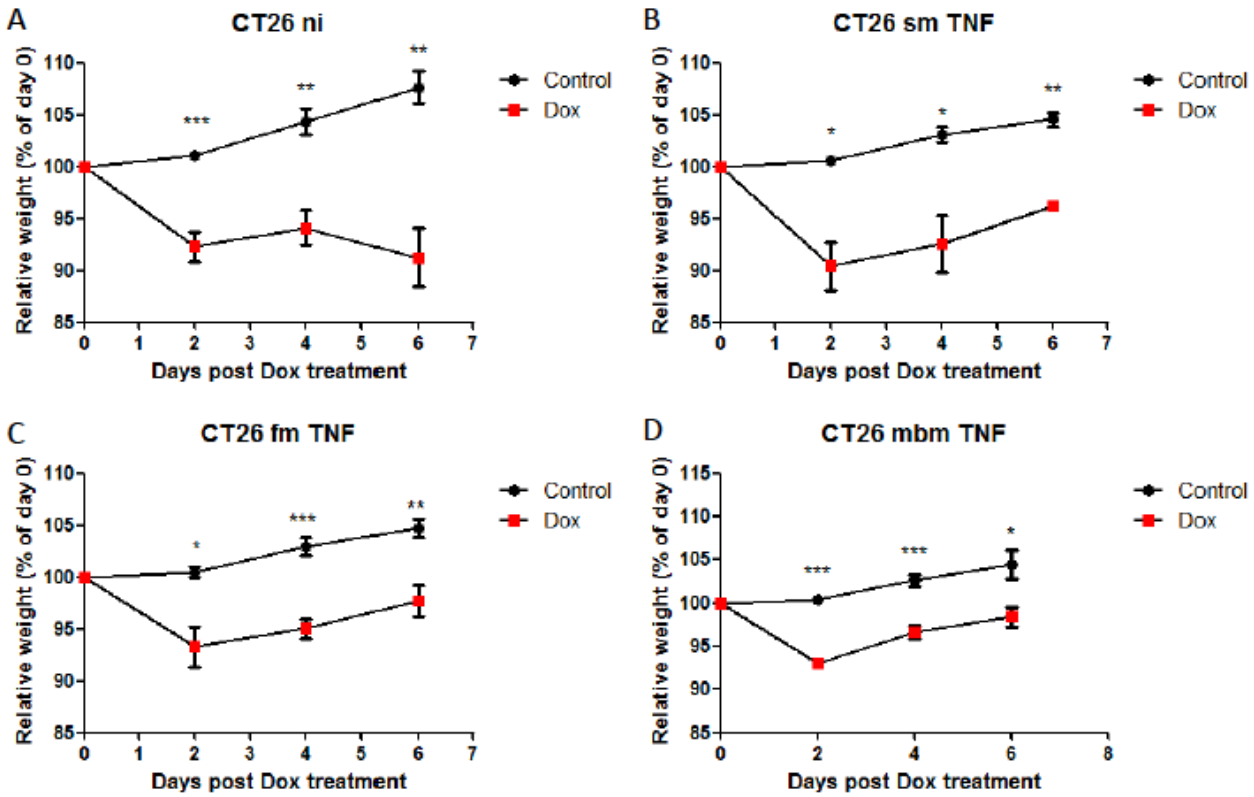

Figure 3.16: Weight loss in mice treated with Dox. The body weights of mice bearing CT26 ni (A; control n=4, Dox n=3), CT26 sm TNF (B; Dox and control n=3), CT26 fm TNF (C; control and Dox n=4) or CT26 mbm TNF (D; control n=3, Dox n=4) tumours was measured every 2 days. The body weight was normalized and expressed as a percentage of the last measurement before mice were started on Dox or control (day 0). An unpaired student T-test was done on all time points to compare the weight of the mice in the Dox group versus the weight in the control group. Mice in all Dox groups lost a significant amount of weight compared to the control groups. Mean and SEM are shown. *=p<0.05, **=p<0.01, ***p<0.001.

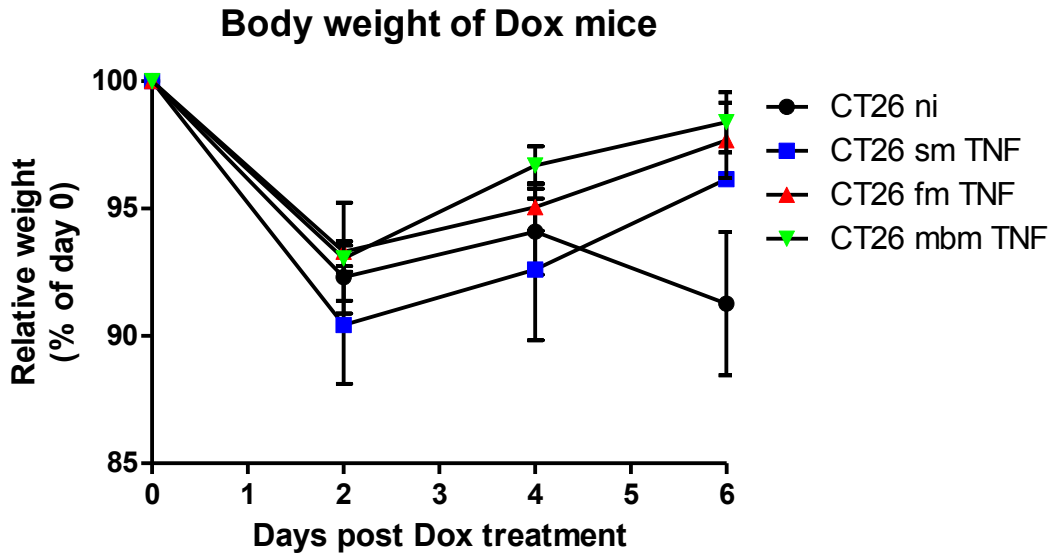

Figure 3.17: Comparison of body weight of Dox mice bearing TNF expressing tumours. A comparison of the body weight of Dox mice bearing CT26 ni (n=3), CT26 sm TNF (n=3), CT26 fm TNF (n=4) or CT26 mbm TNF (n=4) tumours. Body weights were normalized to the last measurement before starting Dox treatment (day 0). A one way ANOVA was used to assess differences in body weight at each time point. No statistically significant differences in weight were found between mice bearing TNF expressing tumours or controls. Mean and SEM are shown.

As seen in figure 13.16 and 13.17, mice on started Dox lost weight, as early as 2 days after the start of Dox treatment. Most mice recovered some weight after the initial drop in body weight, however despite gaining back weight post day 2 of treatment, the average body weight of Dox mice remained significantly lower than the weight of control mice, see figure 3.16. Despite efforts to mask the bitter taste of Dox by adding 5% sucrose to the drinking water, a reduction in the consumption of water by mice was noticed between Dox and control groups, especially at the start of Dox treatment. The reduction in body weight is likely the result of reduced hydration and calorific intake, as both the control and Dox drinking water was spiked with 5% sucrose.

Interestingly, no difference in weight loss was observed between Dox-treated mice expressing TNF compared to the CT26 ni Dox group at any time. This is

compatible with a lack of systemic toxicity when TNF is expressed locally within tumours.

A small part of the tumours were snap frozen on dry ice and used to analyse the TNF expression at day 7 post Dox treatment.

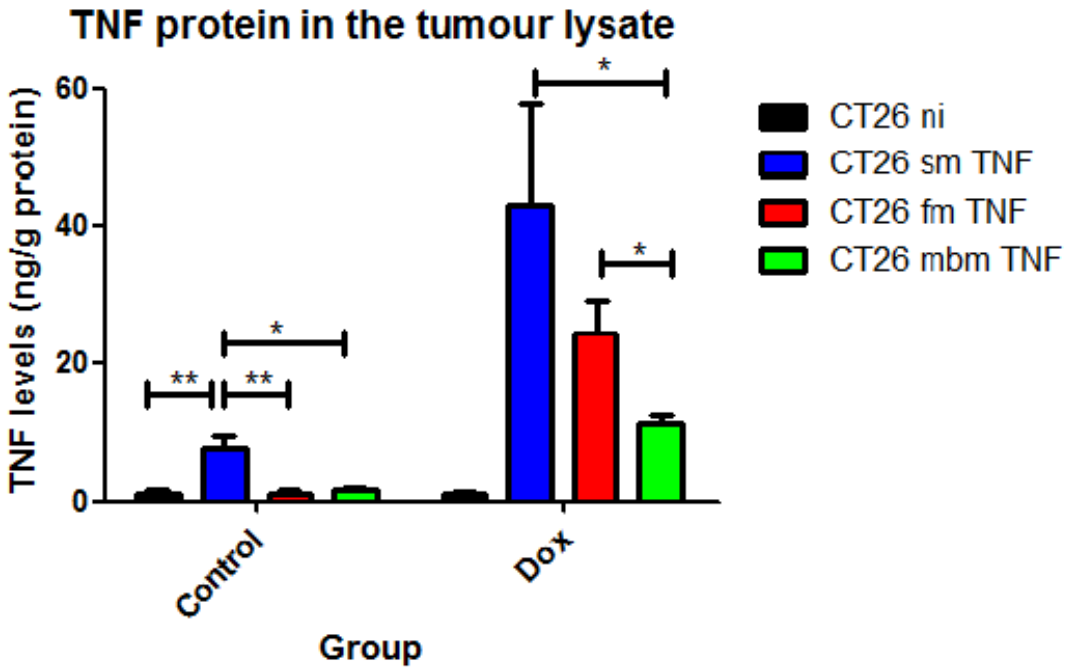

Figure 3.18: TNF expression in CT26 tumours at day seven of Dox treatment. Tumours were harvested at day 7 after the start of Dox or control treatment. The tumours were homogenized and TNF levels were measured by sandwich ELISA and normalized to protein concentrations. A two way ANOVA, followed by Student's T test was done to compare the TNF levels between the different cell lines. The highest TNF levels were seen in CT26 sm TNF Dox tumours. Average and SEM are depicted. *= $p<0.05$, **=$p<0.01$.

Consistent with TNF levels seen in lysates of the tumour growth study, CT26 sm and CT26 fm TNF both have significantly higher levels of TNF than CT26 mbm TNF Dox mice ($p<0.05$). Again, CT26 sm control mice had more TNF detectable in the tumour lysate compared to other control mice.

In the tumour lysates of mice in the tumour growth study, TNF levels were significantly higher in the tumour lysates CT26 fm TNF Dox mice compared to CT26 sm TNF. When tumours were taken out after 7 days of Dox treatment, CT26 sm TNF seem to have higher levels of TNF than CT26 fm TNF Dox mice, although this difference is not statistically significant (p=0.22). Comparing TNF expression from CT26 fm TNF cells, a statistically significant increase in TNF was seen at the time of euthanasia in the tumour growth study (Mean ± SEM: 60.88 ng/g protein ±11.77) versus the levels found after 7 days of Dox treatment (24.38 ± 4.9) (p=0.0286). No differences in CT26 sm TNF (43.08±14.59 at day 7 versus 26.75 ± 6.5 in the tumour growth study; p=0.27) or CT26 mbm TNF levels were found (11.15 ± 1.36 at day 7 versus 14.64± 3.05 at the time of euthanasia in the previous study; p=0.372).

To see whether the induction of TNF expression influenced the receptor levels within the tumours, a sandwich ELISA was done for receptor levels. Using this approach, no differences in TNF receptor levels were found, see figure below.

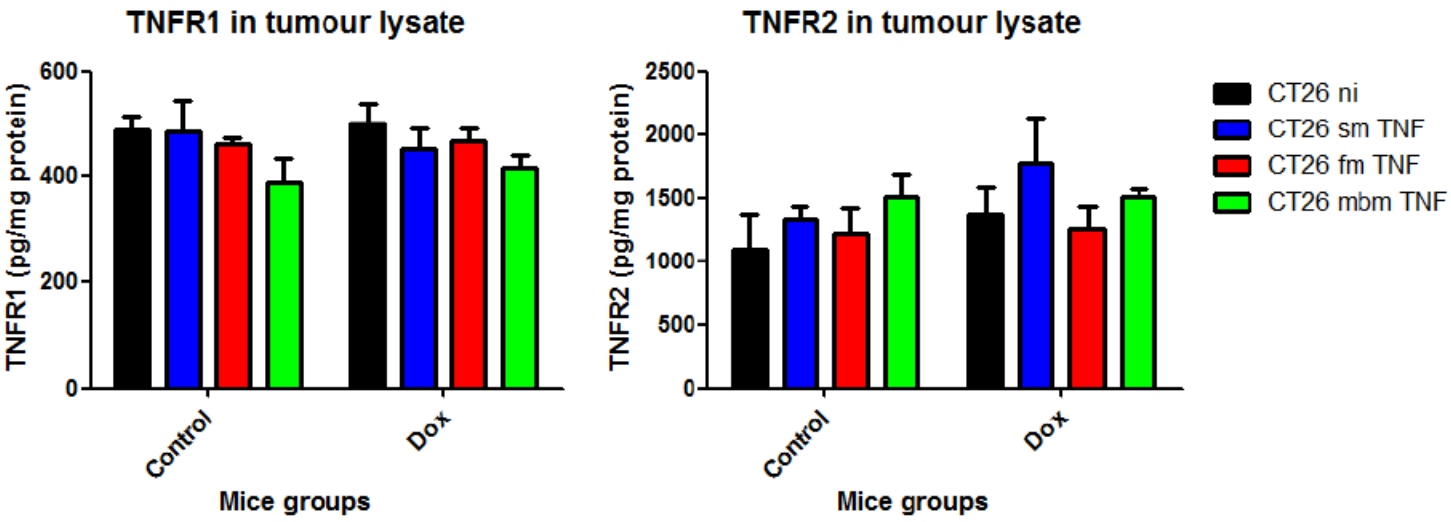

Figure 3.19: TNFR levels in CT26 tumours at day seven of Dox treatment. TNFR1 and TNFR2 protein expression in tumour lysate was measured using a sandwich ELISA. A 2way ANOVA was performed to assess statistical significance. No statistically significant changes in TNF receptor 1 or 2 levels were detected.

Flow-cytometry

Immediately after mice were euthanized, the majority of the tumour tissue was transferred to tubes with RPMI media. Additionally, spleens were harvested and transferred into separate tubes with, also RPMI media. Both tumours and spleens were kept on ice and processed as soon as possible. Tumours were dissociated mechanically and subsequently enzymatically. Spleens were dissociated mechanically. For the flow-cytometry protocol see section 2.8.10.

Total immune cell ($CD45^+$), myeloid cell ($CD45^+$ $CD11b^+$), cytotoxic T cell ($CD45^+$ $CD8^+$) and T helper cells ($CD45^+$ $CD4^+$), total MDSCs ($CD45^+$ $Gr\text{-}1^+$), granulocytic MDSCs ($CD11b^+$ $Ly6G^+$), monocytic MDSCs ($CD11b^+$ $Ly6C^{high}$), and NK cells ($CD45^+$ $CD49b^+$) infiltration was analysed into tumours were analysed, see figure 3.20 and 3.21. Additionally, splenocytes were stained as a measure for any systemic effects on the immune system due to local TNF expression (figures 3.23 and 3.24).

A

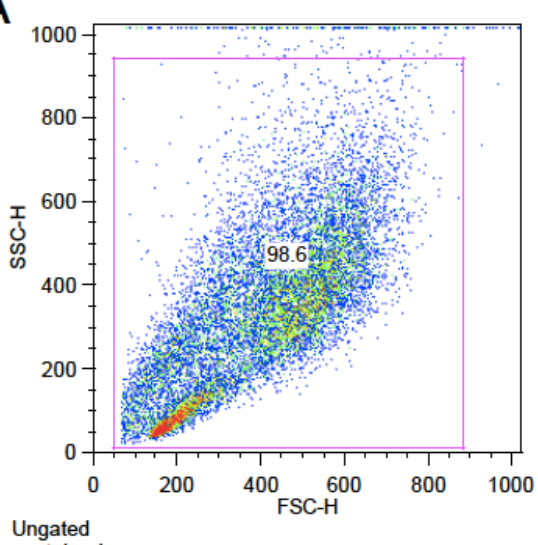

Ungated
unstained
Event Count: 14870

B

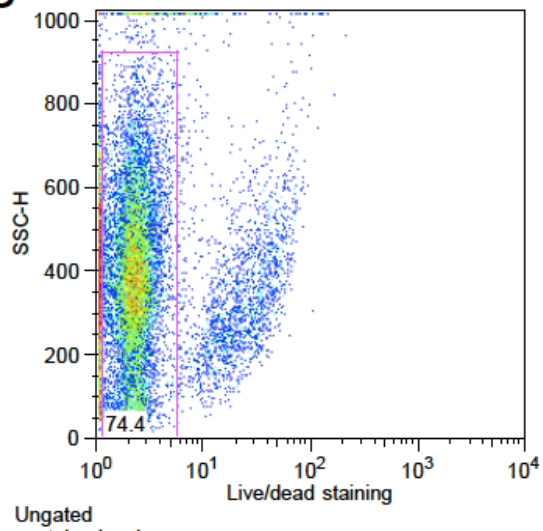

Ungated
unstained red
Event Count: 15644

C

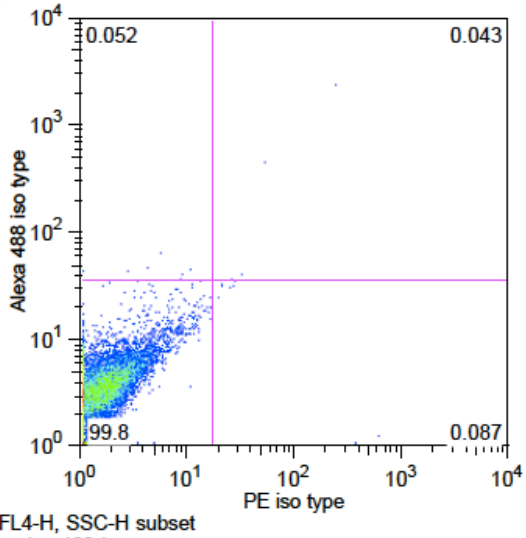

FL4-H, SSC-H subset
pe iso 488 iso
Event Count: 11531

D

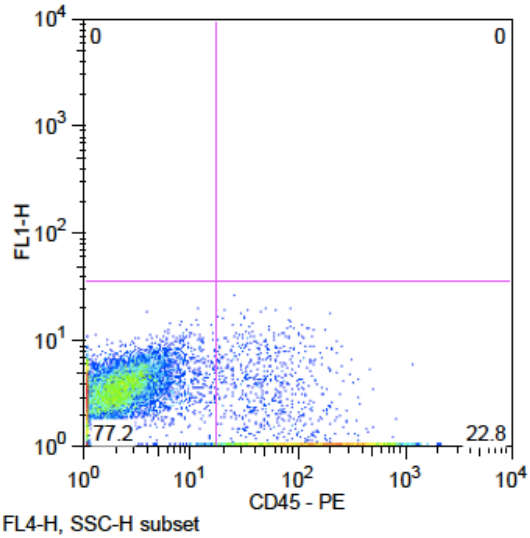

FL4-H, SSC-H subset
cd45
Event Count: 11629

E

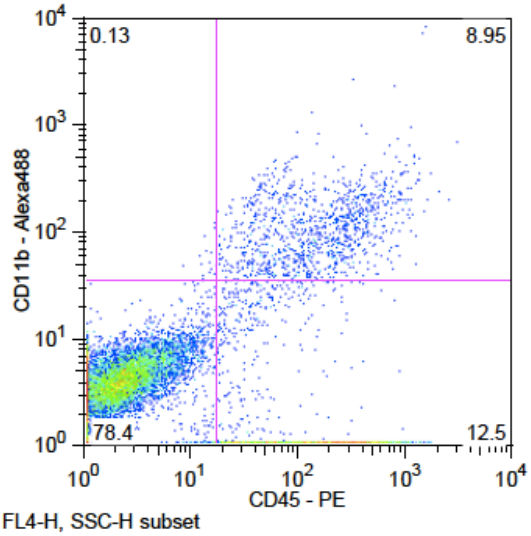

FL4-H, SSC-H subset
cd45 cd11b
Event Count: 11572

F

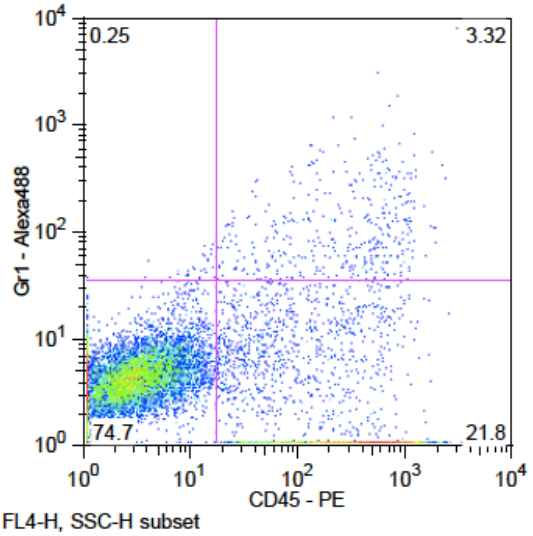

FL4-H, SSC-H subset
cd45 gr1
Event Count: 11655

G

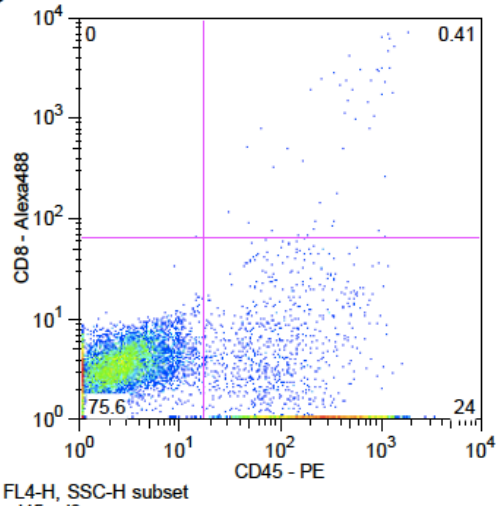

FL4-H, SSC-H subset
cd45 cd8
Event Count: 11607

H

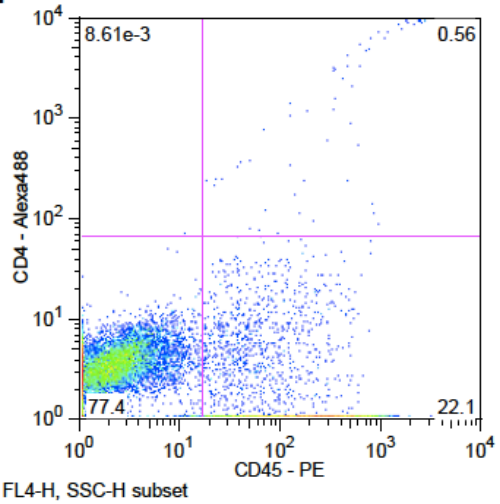

FL4-H, SSC-H subset
cd45 cd4
Event Count: 11610

I

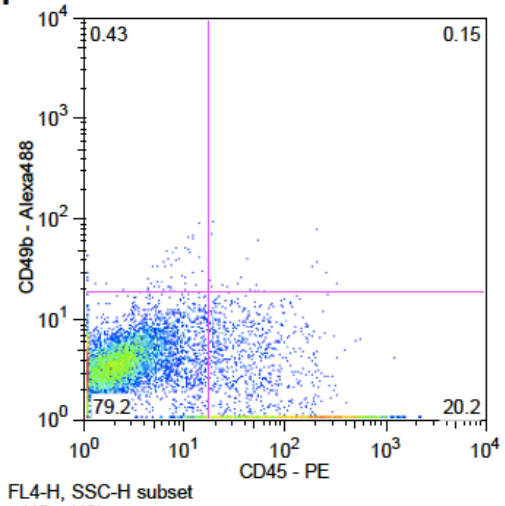

FL4-H, SSC-H subset
cd45 cd49b
Event Count: 11724

J

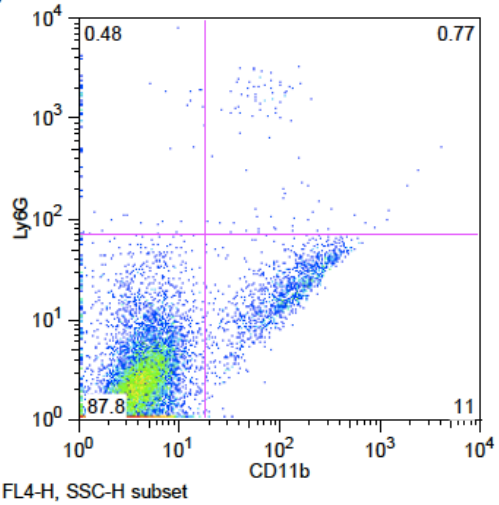

FL4-H, SSC-H subset
cd11b ly6g
Event Count: 11788

K

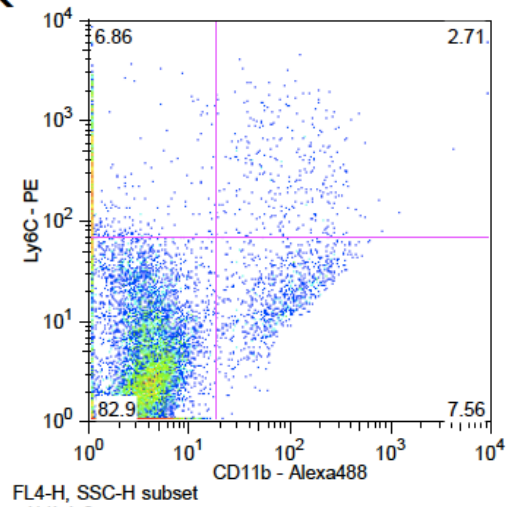

FL4-H, SSC-H subset
cd11b ly6c
Event Count: 11733

L

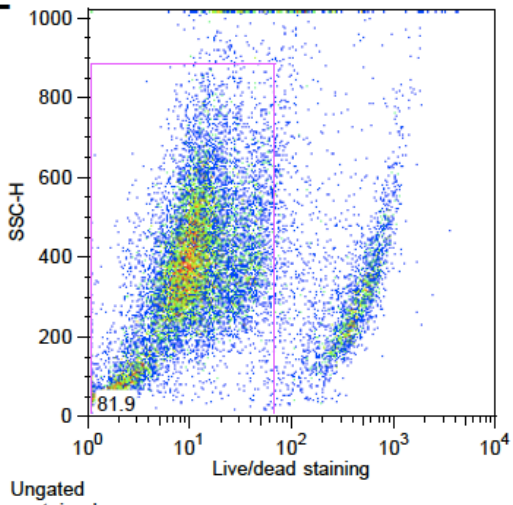

Ungated
unstained
Event Count: 15610

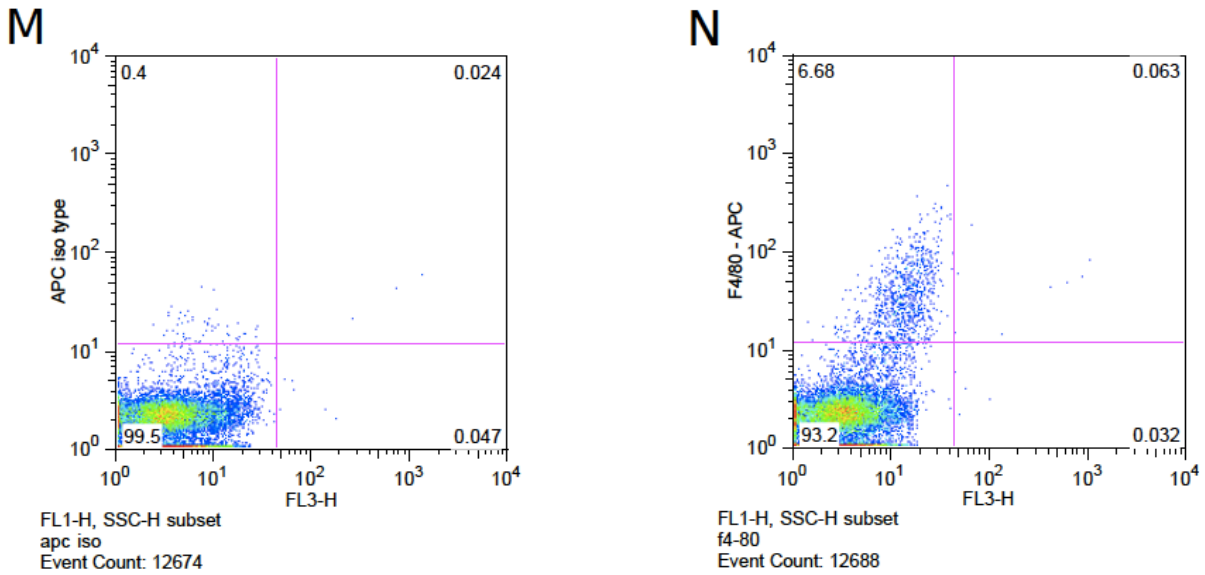

Figure 3.20: Flow cytometry analysis of immune infiltrates in CT26 tumours expressing mTNF. 1x10^6 CT26 cells were implanted s.c. Once tumours were approximately 100 mm^3 mice were treated with 2 mg/ml Dox in the drinking water, or control for 7 days. At day 7, tumours were harvested and stained. Tumours were stained with Zombie NIR™ (near infra red) (A-K) or Zombie Green™ (L-M). A: gating of single cells on the Forward/Side scatter plot. B: Gating of live cells. C: Alexa488-isotype control on the Y-axis, PE isotype control on the X-axis. D: CD45 on the X-axis. E: CD45 on the X-axis, $CD11b^+$ on the Y-axis; F: CD45 on the X-axis, Gr-1 on the Y-axis. G: CD45 on the X-axis, CD8 on the Y-axis. H: CD45 on the X-axis, CD4 on the Y-axis; I: CD45 on the X-axis, CD49b on the Y-axis. J: CD11b on the X-axis, Ly6G on the Y-axis. K: CD11b on the X-axis, LY6C on the Y-axis. L: Live dead staining green. M: APC isotype control on the Y-axis. N: F4/80 on the Y-axis.

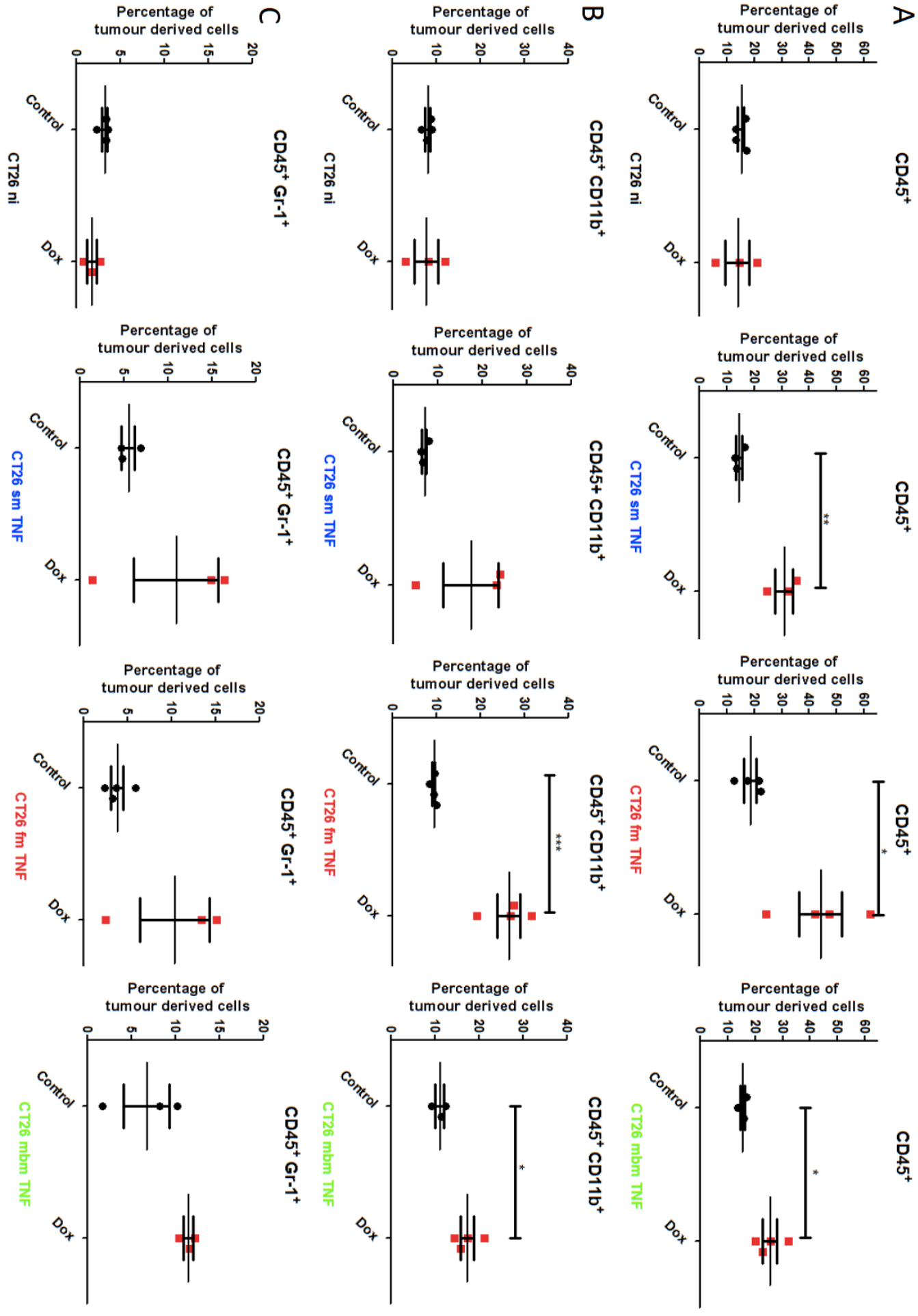
A
B
C
CD45+
CD45+ CD11b+
CD45+ Gr-1+
Percentage of tumour derived cells
Control
Dox
CT26 ni
CT26 sm TNF
CT26 fm TNF
CT26 mbm TNF
*
**
***

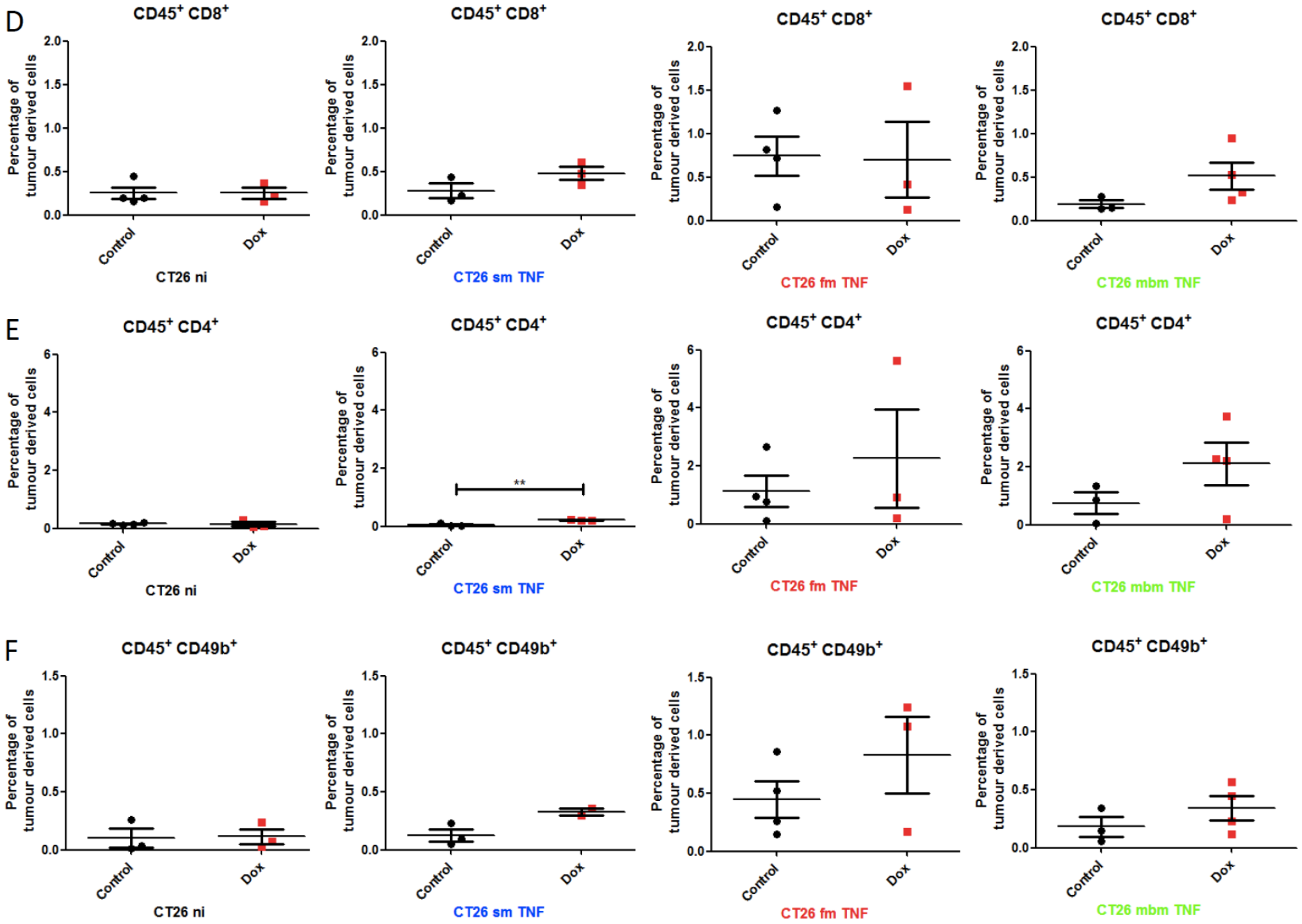
D
CD45+ CD8+
Percentage of tumour derived cells
Control
Dox
CT26 ni
CT26 sm TNF
CT26 fm TNF
CT26 mbm TNF
E
CD45+ CD4+
**
F
CD45+ CD49b+

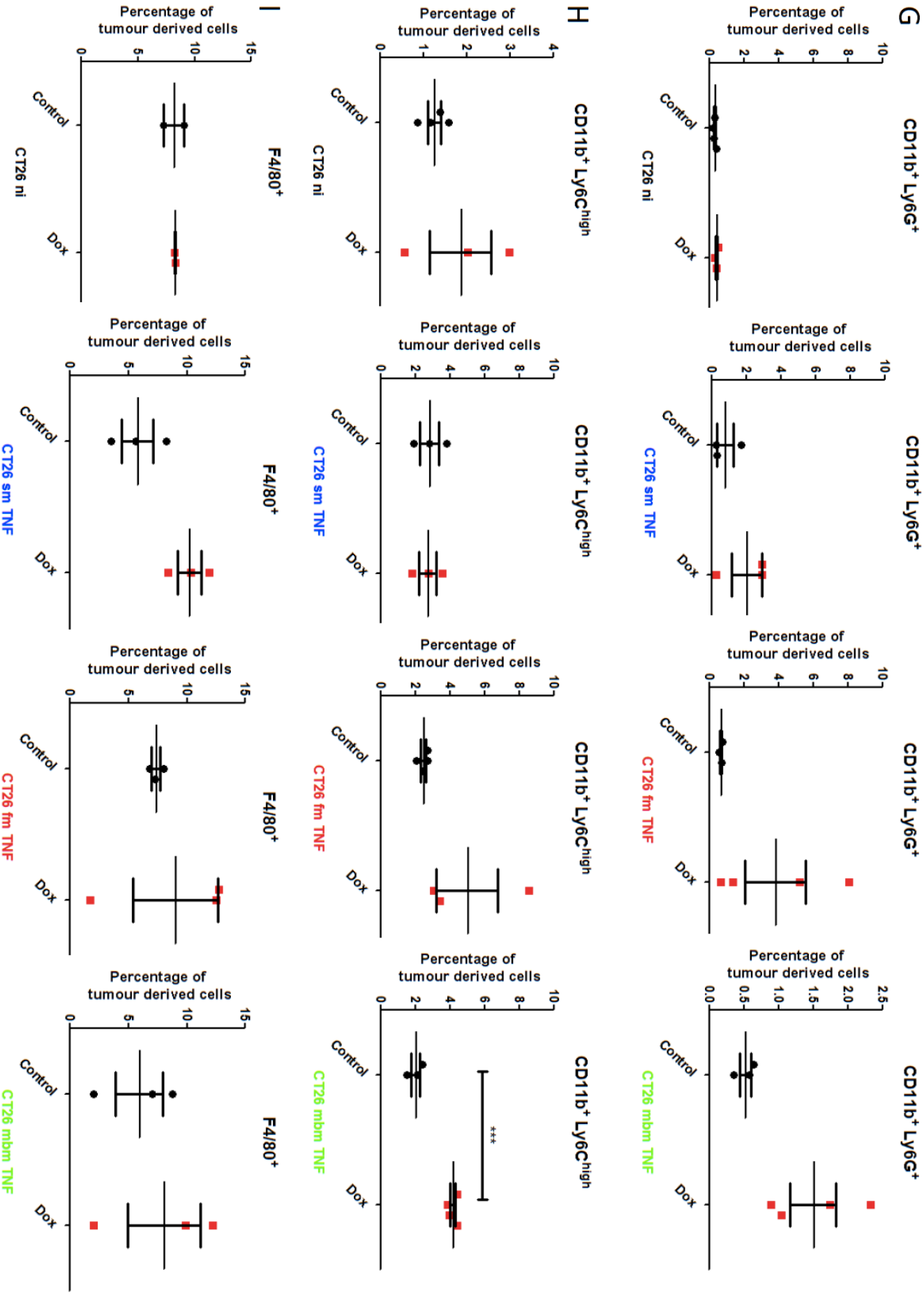
G
H
I
CD11b+ Ly6G+
CD11b+ Ly6Chigh
F4/80+
Percentage of tumour derived cells
Control
Dox
CT26 ni
CT26 sm TNF
CT26 fm TNF
CT26 mbm TNF
***

Figure 3.21: Quantification of immune infiltrates in CT26 tumours expressing mTNF. $1x10^6$ CT26 ni (A; control n=4, Dox n=3), CT26 sm TNF (B; Dox and control n=3), CT26 fm TNF (C; control and Dox n=4) or CT26 mbm TNF (D; control n=3, Dox n=4) cells were implanted subcutaneously on the flanks of female BALB/c mice. Once tumours were approximately 100 mm^3, the mice were randomly divided into a control and Dox group and treated for 7 days. At day 7, tumours were harvested and homogenized. Staining for A: CD45. B: $CD45^+$ $CD11b^+$. C: $CD45^+$ $CD11b^+$. D: $CD45^+$ $CD8^+$. E: $CD45^+$ $CD4^+$. F: $CD45^+$ $CD49b^+$. G: $CD11b^+$ $LY6G^+$. H: $CD11b^+$ $LY6C^{high}$. I: F/480+ was performed and analysed using flow-cytometry. A statistically significant increase in immune infiltrates (A; $CD45^+$) was seen in CT26 sm TNF, fm TNF and mbm TNF tumours treated with Dox compared to their respective controls. In CT26 fm TNF and CT26 mbm TNF tumours treated with Dox, an increase in $CD11b^+$ infiltration was seen compared to control (see B). Additionally, a statistically significant increase in $CD45^+$ $Ly6C^{high}$ infiltration was seen in CT26 mbm TNF tumours treated with Dox compared to control. A borderline not significant increase in $CD11b^+$ $Ly6G^+$ (G; p=0.057) was observed in CT26 mbm TNF mice when treated with Dox compared to control. Mean and SEM are shown. *=P<0.05, **=p<0.01, ***=p<0.001.

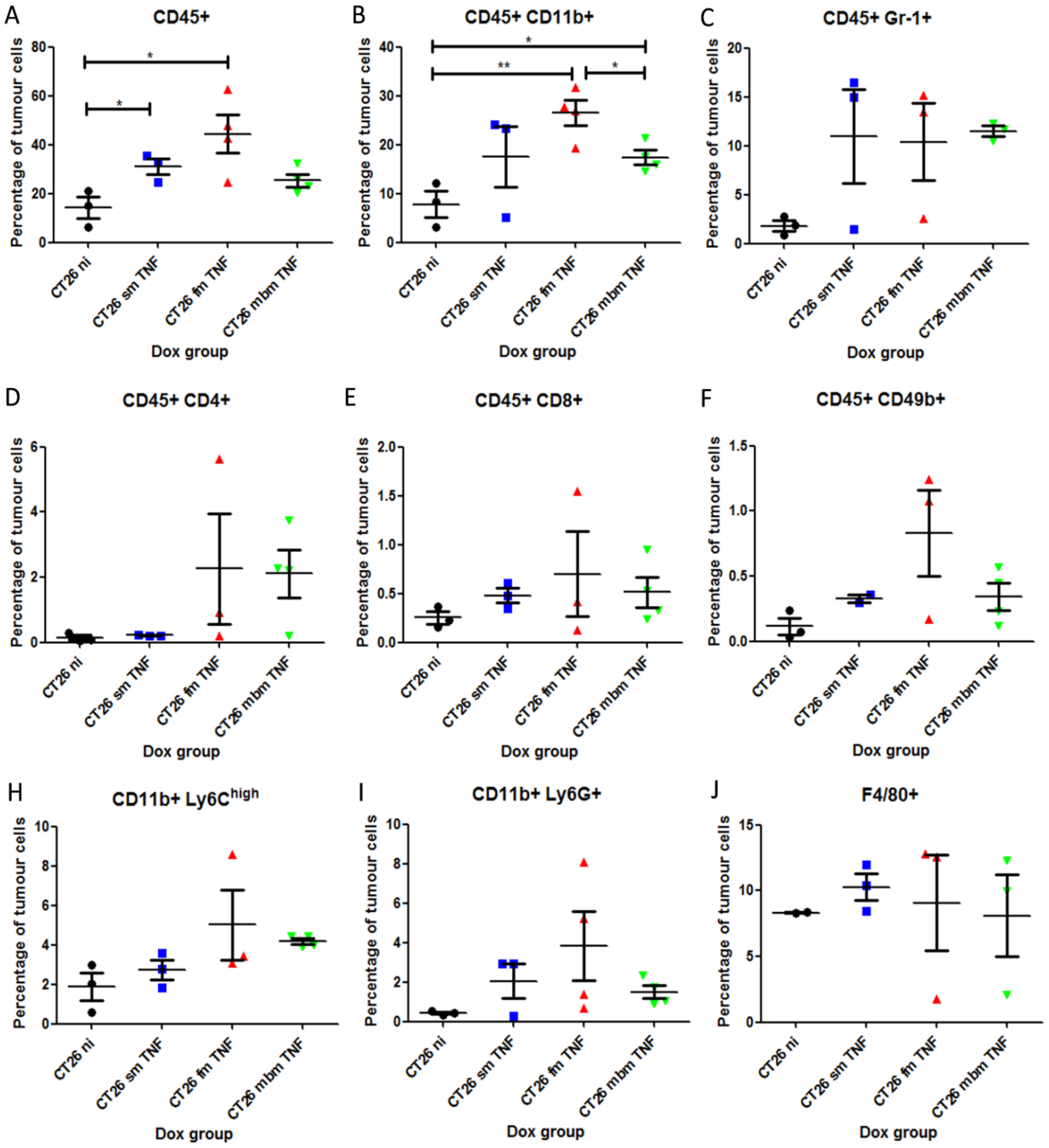

Figure 3.22: Comparison of immune cell infiltrates between CT26 ni, CT26 sm TNF, CT26 fm TNF and CT26 mbm TNF Dox groups. Infiltration of CD45$^+$ (A), CD45$^+$ CD11b$^+$ (B), CD45$^+$ Gr-1$^+$ (C), CD45$^+$ CD4$^+$ (D), CD45$^+$ CD8$^+$ (E), CD45$^+$ CD49b$^+$ (F), CD11b$^+$ Ly6C^{high} (H), CD11b$^+$ Ly6G$^+$ (I) or F4/80$^+$ (J) cells were analysed and compared between the different Dox groups. A one way ANOVA was performed to test for statistical significance. Unpaired student T-tests were done to assess differences between the Dox groups, when the ANOVA indicated statistical significance. A statistically significant increase in immune infiltration was seen in Dox treated CT26 sm TNF and CT26 fm TNF tumours compared to CT26 ni (A). Moreover, increased myeloid infiltration (CD45$^+$ CD11b$^+$) was seen in tumours expressing fm or mbm TNF compared to CT26 ni control. Mean and SEM are shown. *=$p<0.05$, **$p<0.01$.

The induction of TNF within the tumour increases immune infiltration, as a statistically significant increase in $CD45^+$ was seen in mice bearing sm TNF, fm TNF and mbm TNF tumours treated with Dox compared to control mice with the same tumour cell line. Additionally, CT26 sm and CT26 fm TNF Dox mice have a significantly higher percentage $CD45^+$ cells compared to CT26 ni Dox. A borderline not significant increase ($p=0.06$) was seen in CT26 mbm TNF Dox mice versus CT26 ni Dox mice. Increased myeloid infiltration was also seen in tumours expressing TNF. An increase in myeloid cells, as measured by $CD45^+$ $CD11b^+$ cells was seen in Dox mice bearing CT26 fm TNF and CT26 mbm TNF tumours, compared to control. The majority of infiltrating immune cells was $CD11b^+$ in CT26 ni (mean percentage ± SEM: 54.14 ± 2.09), CT26 sm TNF (53.16 ± 16.21), CT26 fm TNF (62.78±5.86) and CT26 mbm TNF (69.54 ± 6.363) Dox tumours, as well as in control tumours.

A trend towards higher infiltration was also seen in tumours expressing sm TNF, although this difference was not statistically significant ($p=0.22$).

A statistically significant increase in $CD11b^+$ $LY6C^{high}$ cells was seen in mice treated with Dox compared to control in mice bearing CT26 mbm TNF tumours.

A trend towards higher infiltration of $CD45^+$ $Gr\text{-}1^+$, $CD11b^+$ $Ly6C^{high}$ and $CD11b^+$ $Ly6G^+$ was seen in mice expressing TNF compared to the CT26 ni Dox group, although these differences were not statistically significant ($p=0.17$, $p=0.14$ and $p=0.225$, respectively).

No statistically significant differences were found in lymphocyte infiltration, however some mice expressing fm TNF and mbm TNF seem to have more infiltration of $CD4^+$ and $CD8^+$ cells. Due to the small group sizes used in this flow-

cytometry experiment, the experiment may not have been sufficiently powered to rule out effects of TNF on lymphocyte infiltration.

Unfortunately, due to the limited amount of channels available on the FACS Calibur machine and bleed over from the live/dead staining into the next channel, it was not possible to combine markers for activation status with cell markers in this experiment.

Splenocyte composition

The immune cell status of the spleen was assessed as a measure for systemic effects immune effects by local expression within the tumour microenvironment. No statistically significant differences in the composition of splenocytes were found in mice on Dox versus control mice, as can be seen in figure 3.23.

A

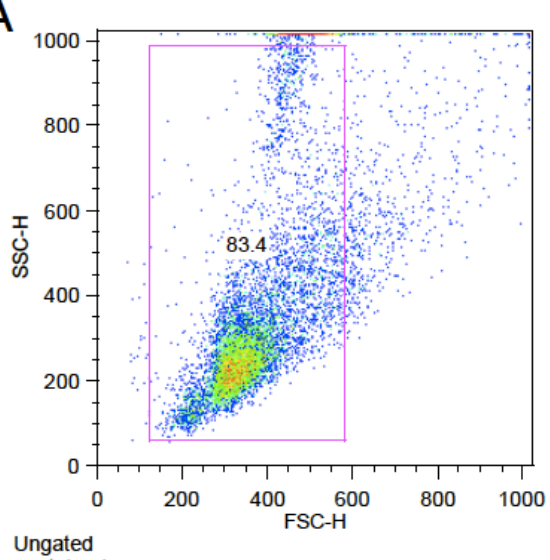

Ungated
unstained
Event Count: 10000

B

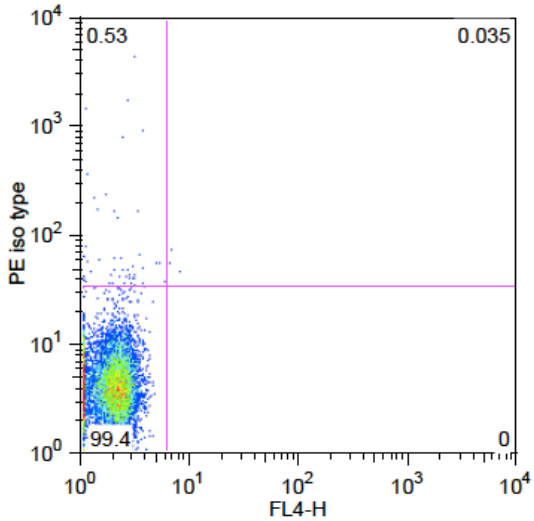

FSC-H, SSC-H subset
pe iso
Event Count: 8625

C

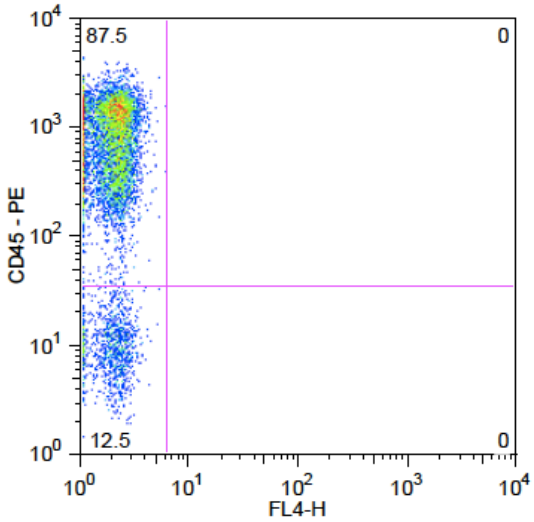

FSC-H, SSC-H subset
cd45
Event Count: 8247

D

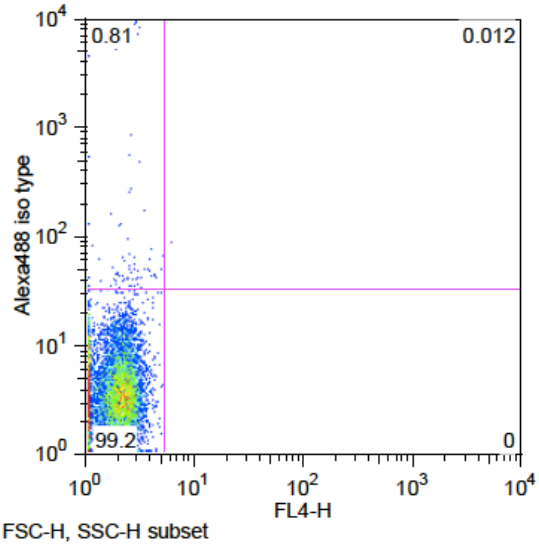

FSC-H, SSC-H subset
488 iso
Event Count: 8363

E

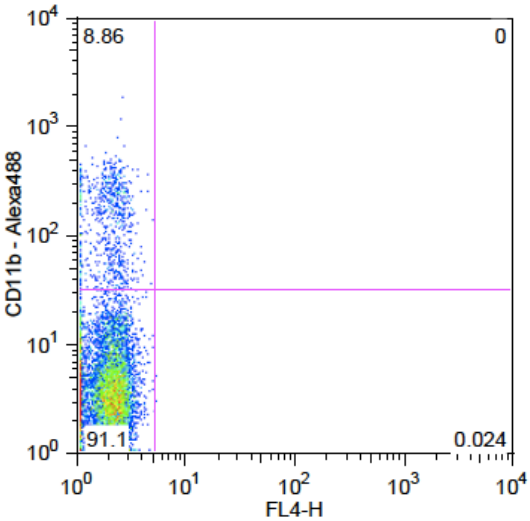

FSC-H, SSC-H subset
cd11b
Event Count: 8282

F

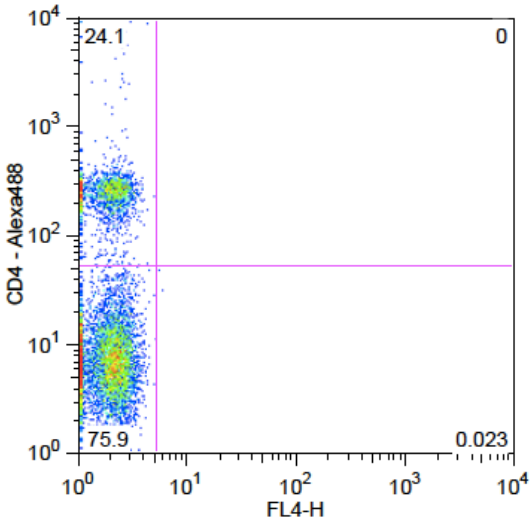

FSC-H, SSC-H subset
cd4
Event Count: 8554

G

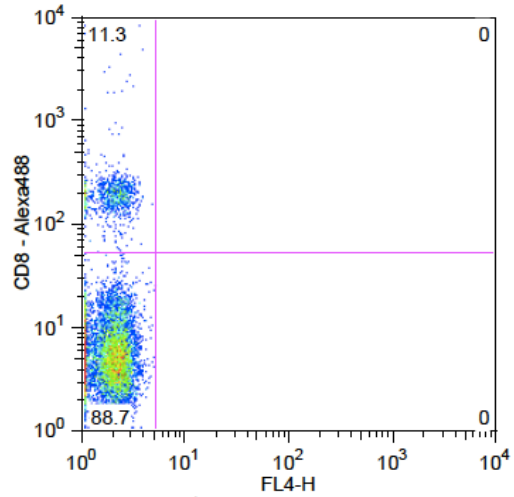

FSC-H, SSC-H subset
cd8
Event Count: 8557

H

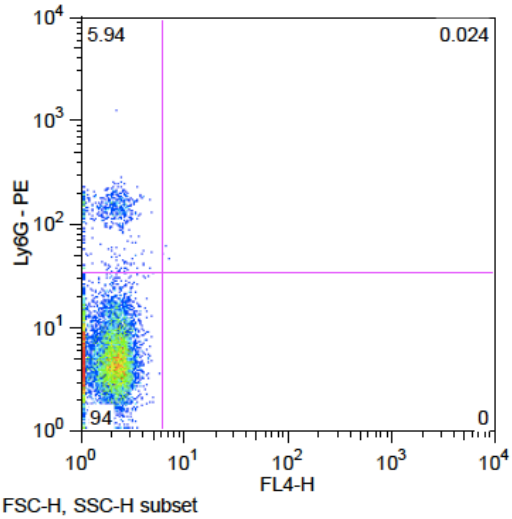

FSC-H, SSC-H subset
ly6g
Event Count: 8429

I

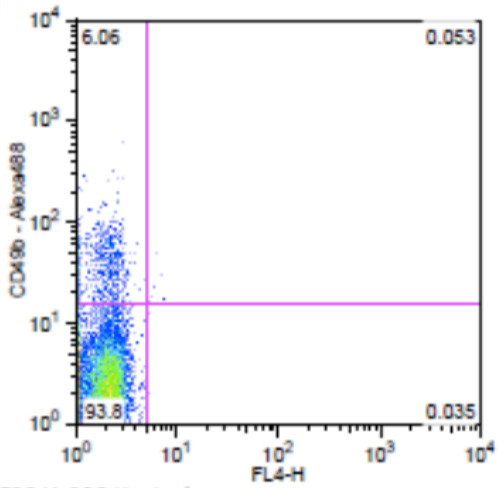

FSC-H, SSC-H subset
cd49b 488
Event Count: 11362

J

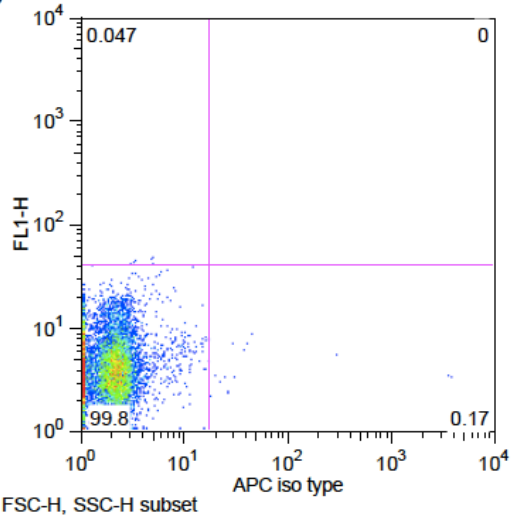

FSC-H, SSC-H subset
apc iso
Event Count: 8455

K

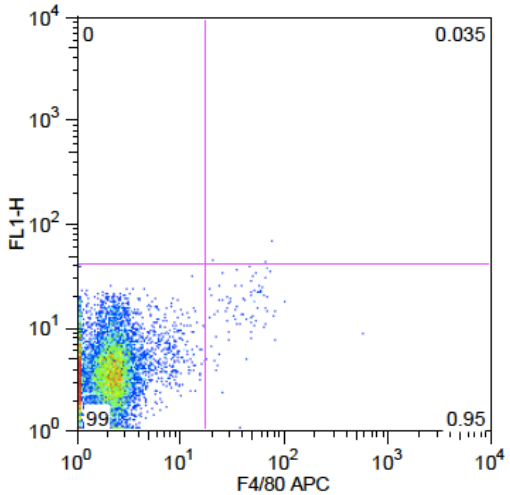

FSC-H, SSC-H subset
f4-80
Event Count: 8464

Figure 3.23: flow-cytometry analysis of splenocytes of BALB/c mice bearing CT26 tumours. Mice were implanted with $1x10^6$ CT26 ni (A; control n=4, Dox n=3), CT26 sm TNF (B; Dox and control n=3), CT26 fm TNF (C; control and Dox n=4) or CT26 mbm TNF (D; control n=3, Dox n=4) cells. Tumours were allowed to grow until approximately 100 mm^3. Subsequently, the mice were randomly assigned and treated with Dox or control for 7 days. Spleens were harvested and dissociated. Staining and flow-cytometry analysis was performed on the splenocytes. A: gating on the forward (X-axis) and side scatter (Y-axis) plot. B: PE-isotype control on the Y-axis. C: CD45-PE staining on the Y-axis. D: Alexa488 isotype control on the Y-axis. E: CD11b- Alexa488 staining on the Y-axis. F: CD4-Alexa488 staining on the Y-axis. G: CD8-Alexa488 staining on the Y-axis. H: Ly6G-PE staining on the Y-axis. I: CD49b-Alexa488 staining on the Y-axis. J: APC-isotype control on the X-axis. K: F4/80-APC staining on the X-axis.

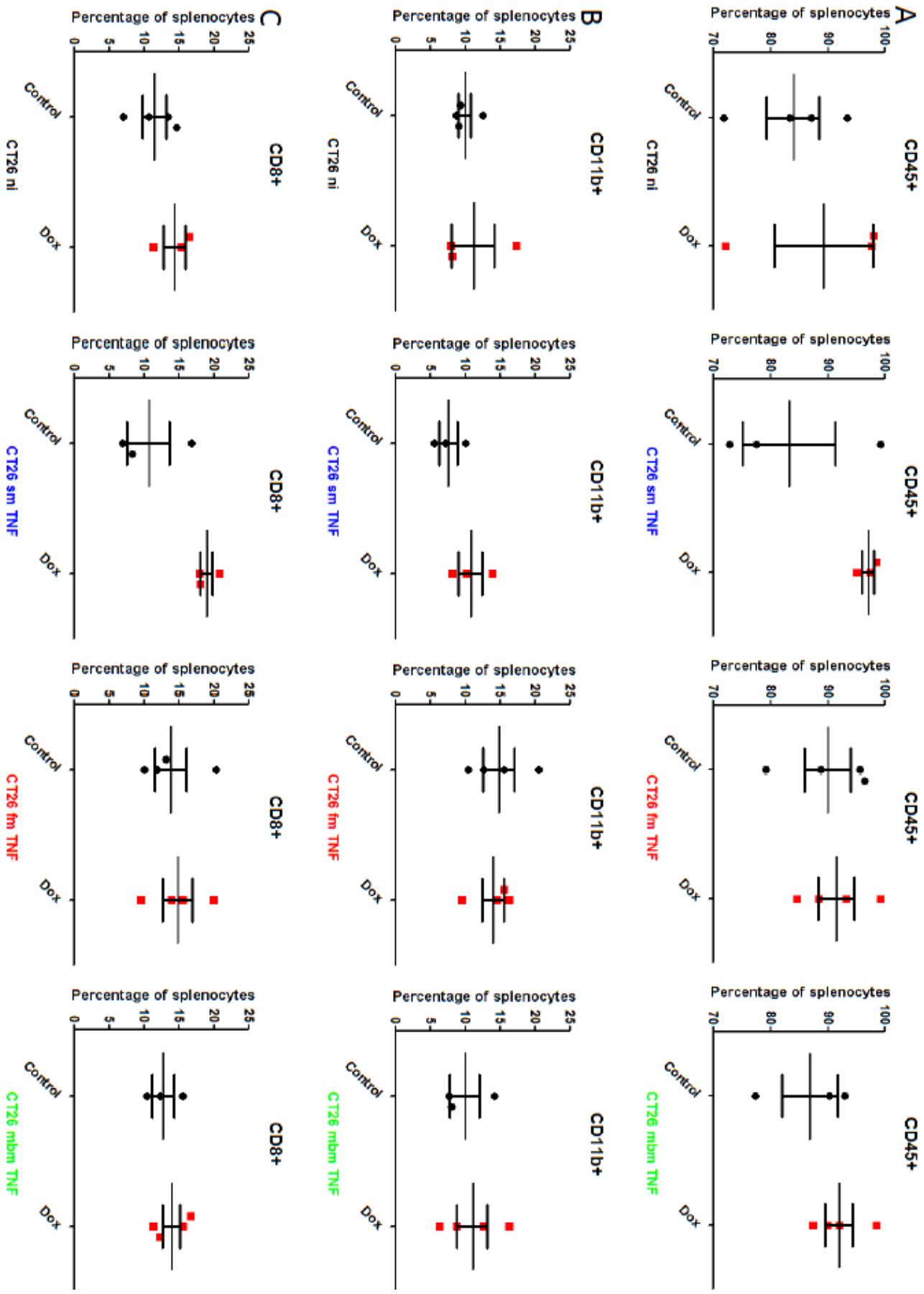
A
B
C
CD45+
CD11b+
CD8+
Percentage of splenocytes
Control
Dox
CT26 ni
CT26 sm TNF
CT26 fm TNF
CT26 mbm TNF

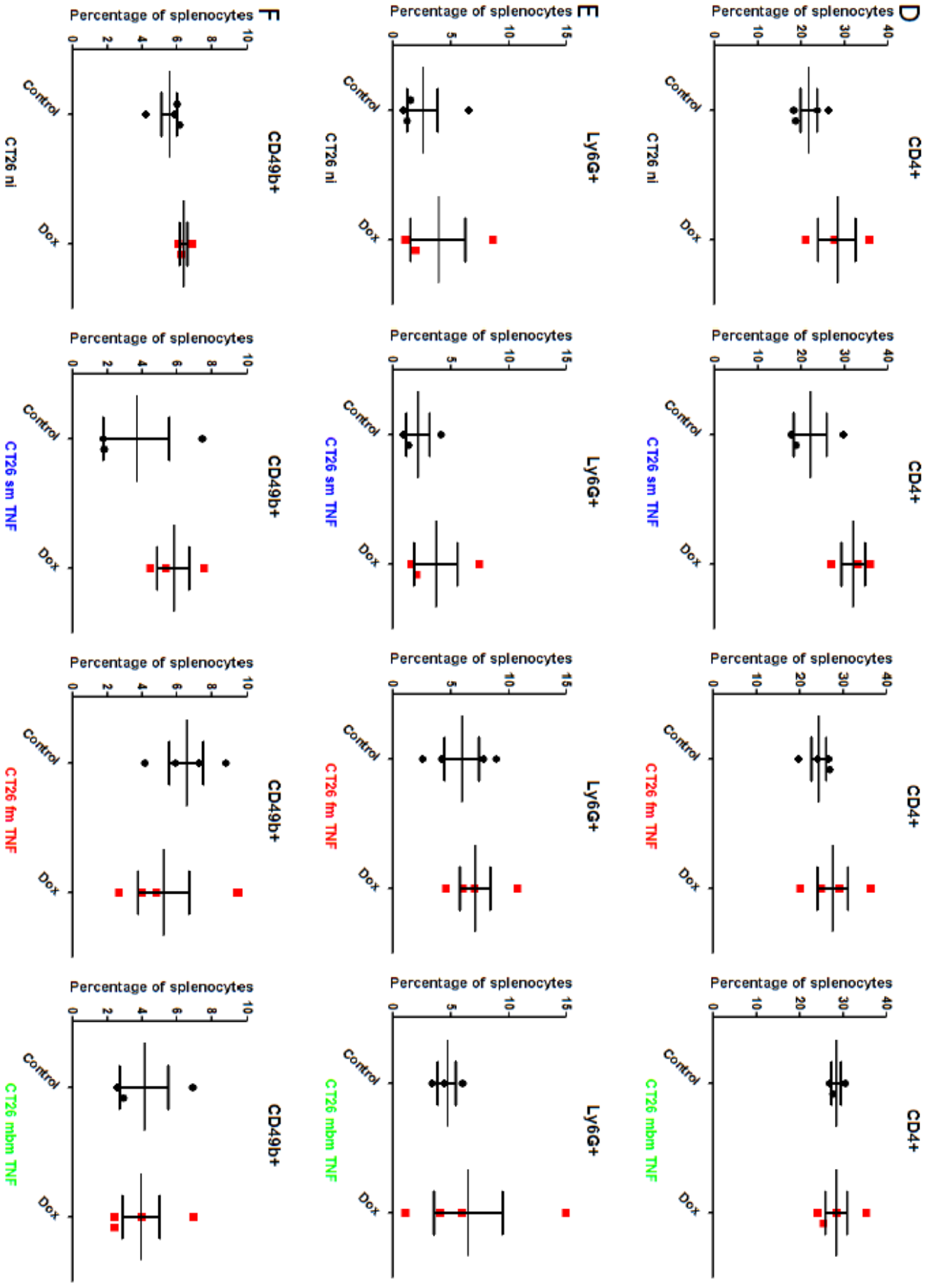
D
E
F
CD4+
Ly6G+
CD49b+
Percentage of splenocytes
Control
Dox
CT26 ni
CT26 sm TNF
CT26 fm TNF
CT26 mbm TNF

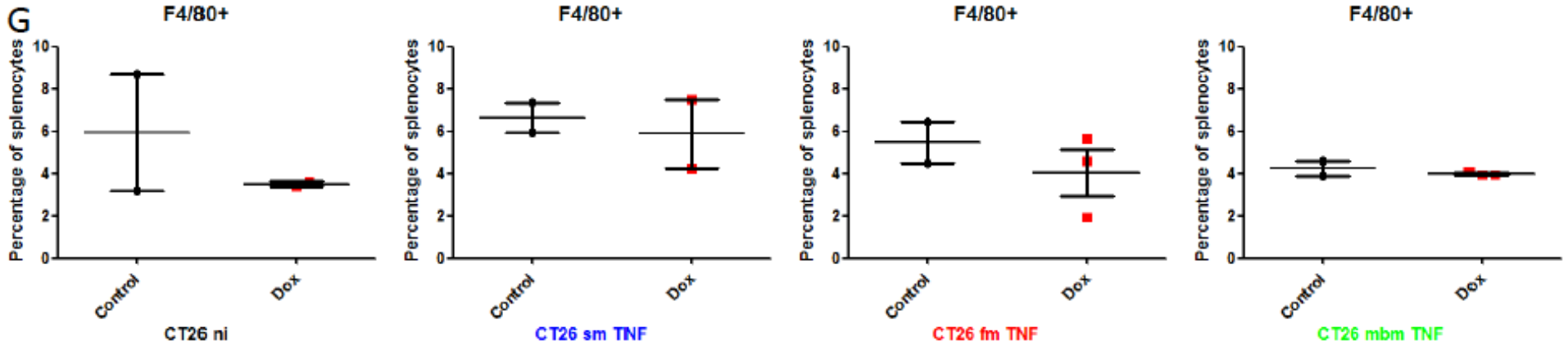

Figure 3.24: Quantification of the flow-cytometry staining of splenocytes Mice were implanted with $1x10^6$ CT26 ni (A; control n=4, Dox n=3), CT26 sm TNF (B; Dox and control n=3), CT26 fm TNF (C; control and Dox n=4) or CT26 mbm TNF (D; control n=3, Dox n=4) cells. Tumours were allowed to grow until approximately 100 mm^3. Subsequently, the mice were randomly assigned and treated with Dox or control for 7 days. Spleens were harvested and dissociated. The spleens were stained for A: CD45; B: CD11b; C: CD8; D: CD4; E: Ly6G; F: CD49b; G: F/480. Unpaired students T-tests were performed to compare control versus Dox mice. Mean and SEM are shown.

3.3.3 Mbm TNF and myeloid cells, in vitro

Expression of mbm TNF on tumour cells has been reported to decrease the cell viability of both the myeloid RAW 264.7 cell line and freshly isolated myeloid cells (*194*). However, in the flow-cytometry experiment on dissociated tumours, an increase in $CD11b^+$ cells was seen in tumours expressing sm, fm and mbm TNF. To test whether CT26 TNF cells altered myeloid cells, a similar assay was set up. Raw 264.7 or L9292 cells were coincubated with PFA fixed CT26 ni, CT26 sm TNF, CT26 fm TNF or CT26 mbm TNF cells treated with Dox for 24h or control, immediately prior to fixing. Cells were incubated in a target (RAW264.7 or L929) cell: Effector ratio (CT26 cells) of 1:10. Cell viability of the RAW 264.7 and L929 cells was measured using an MTS assay, 24 h after the start of the co-incubation. Cell viability was normalized to cells co-incubation with CT26 ni cells.

Absence of metabolic activity of fixed CT26 cells was confirmed in separate wells (data not shown).

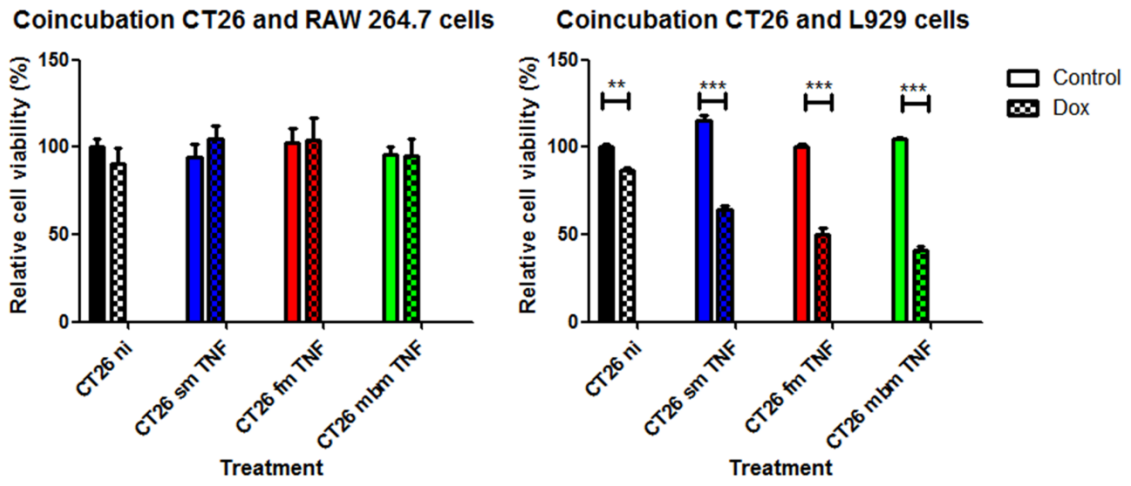

Figure 3.25: Cell viability of RAW 264.7 and L929 cells coincubated with fixed CT26 cells expressing TNF. CT26 ni (black), CT26 sm TNF (blue), CT26 fm TNF (red) or CT26 mbm TNF (green) cells treated with 2.5 µg/ml Dox (checkered bars) or control (even colored bars) for 24h. Cells were subsequently fixed in PFA (effector) and coincubated with RAW 264.7 or L929 cells (target), at an effector target ratio of 10:1 for 24h. Subsequently, the cell viability of target cells was determined using an MTS assay. Mean and SD shown, n=3.

Contrary to Ardestani et al. and consistent with the *in vivo* flow-cytometry, CT26 cells expressing TNF, did not reduce the cell viability of the myeloid RAW 264.7 cell line. Remarkably, L929 cell viability is decreased when coincubated with CT26 sm TNF cells, despite TNF being undetectable on the cell surface as measured by FACS. Possibly, the L929 assay is more sensitive and reacts to TNF levels undetectable by flow-cytometry analysis. Alternatively, the L929 toxicity may be due to TNF levels not associated with the cell membrane.

3.4 Discussion

TNF has shown to have powerful anticancer activities, but its clinical use is limited due to systemic toxicity. The aim of this chapter was to examine the effects of inducing acute TNF and LTA expression within established tumours, to help inform the choice of arming agents for oncolytic ColoAd1.To study the effects of TNF on the tumour and tumour microenvironment, murine soluble TNF, full length TNF, and membrane bound TNF and LTA were expressed from CT26 cells under the control of a Dox inducible promoter. Most studies to date have used recombinant soluble TNF to study the role of this protein in cancer biology and therapy. Very few studies have used sm, fm and/or mbm TNF expressed from cancer cell lines using constitively active promoters (*194, 196*). Using these promoters, the effect of TNF expression on tumour development is studied. The advantage of using the inducible cell lines is that it can assess the effects of TNF expression in a model more closely resembling the clinical situation: the induction of TNF expression within established tumours that have developed without expressing high levels of TNF.

The inducibility of the pLVX-Tight puro vector used in this chapter was confirmed both *in vitro* and *in vivo* using an ELISA and bioluminescence to quantify Fluc and TNF expression. Using Fluc, leakiness of the pLVX-Tight promoter was shown. TNF levels in the CT26 sm TNF control mice were higher compared to CT26 fm TNF and mbm TNF control mice. Possibly, this is caused by higher leakage of the pTight promoter in these cells. However, TNF itself is regulated by NF-κB, thus a low background level of leakage might also increase in NF-κB activity and thus endogenous TNF expression (*254*).

Unfortunately, mLTA could not be expressed from CT26 cells, possibly due to post-transcriptional regulation. *In vitro*, expression of different forms of murine or human TNF did not lead to significant toxicity on either HT29 or CT26 cells. Lack of cytotoxicity of TNF on HT29 and CT26 cells in concurrent with literature indicating that most tumour cells are resistant to direct killing by TNF (*255*). A statistically significant reduction in tumour growth and increase in survival was seen in mice bearing CT26 mbm TNF tumours treated with Dox compared to control. Levels of TNF in the tumour lysate of CT26 mbm TNF Dox mice were significantly lower at day 7 and at the time of euthanasia in the tumour growth experiment compared to CT26 sm TNF and CT26 fm TNF. Previous studies comparing soluble, full length and membrane-bound TNF have also found a lower expression of mb TNF, *in vitro* and *in vivo* (*195, 196*). Thus, the reduced tumour growth seen upon expression of mbm TNF, but not sm or fm TNF, cannot be attributed to higher levels of TNF within the tumour. Membrane-bound TNF is the main activator of TNFR2 signalling and the TNFR2 is mainly expressed on immune cells and endothelial cells (*128, 132*), suggesting that the effects of mbm TNF may be mediated through immune cells or by the tumour-associated vasculature. It should be noted that control CT26 mbm TNF mice had the fastest growing tumours and shortest survival time compared to the CT26 fm TNF or CT26 sm TNF control mice, although this difference was not statistically significant ($p= 0.18$). Differences in tumour growth of control mice may be related to the low levels of TNF expression due to leakage of the pTight promoter. Alternatively, it may be related to variation in intrinsic growth rates between the cell lines that resulted from the clonal selection. Alternatively, it could be due to mutations or altered gene expression due to the genomic

integration site of the lentiviral vectors. The more recently developed CRISPR/Cas9 technology could be used to overcome the problem of random insertion sites by lentiviral transduction (*256*).

An increase in $CD45^+$ cell infiltration in tumours was seen in CT26 sm, fm and mbm TNF expressing tumours, especially myeloid cells ($CD45^+$ $CD11b^+$). Furthermore, a non statistically significant trend towards more infiltration of MDSCs ($CD11b^+$ $Gr1^+$ cells) was seen in TNF expressing tumours. Unfortunatetly, due to the limited amount of channels on the BD Calibur FACS machine used in this chapter, it was not possible to combine activation markers with cell markers. Further studies are necessary to see whether changes in activation of myeloid cells occur between tumours expressing sm TNF, fm TNF, mbm TNF and control.

Myeloid cells are a very heterogeneous population of cells and depending on their maturation and activation status, myeloid cells can have very different functions (*93-95*). Contrary to results found in this chaper, in a syngeneic lung carcinoma model expression of mbm TNF within the tumour microenvironment reduced myeloid cell infiltration and $F4/80^+$ cell infiltration (*194*). Also, an increase in myeloid infiltration and was seen in tumours expressing sm TNF in this study. Furthermore, a reduction of tumour growth was seen in mbm expressing tumours, whereas increased tumour growth was seen in tumours that express sm TNF (*194*). The tumour growth in this model was thought to positively correlate with myeloid infiltration. In this model, myeloid cell death by mbm TNF expressing tumours was mediated through a ROS-dependent mechanism. The increase in MDSCs observed the syngeneic mammary tumours expressing mbm TNF was also correlated to increased in tumour growth (*196*). Contrary to these previous findings linking myeloid cells to tumour growth in

TNF expressing tumours, in the CT26 model used in this study, tumour growth do not correlate with the amount of myeloid infiltration; CT26 sm TNF, fm TNF and mbm TNF all increased myeloid infiltration and only expression of mbm TNF altered tumour growth. This may indicate a different role in myeloid cell populations in different types of cancer. High infiltration of macrophages has been linked to poor patient outcomes, in most types of cancers. Several tumour promoting actions by macrophages have been shown, including the promotion of angiogenesis, tumour cell invasion, metastasis and the induction of chemotherapy resistance (*100-102*). However, peritumoural $CD68^+$ macrophages have been linked to good prognosis in CRC patients (*103-105*). Moreover, in a syngeneic rat CRC model, inhibition of immature monocyte and macrophage infiltration into peritoneal tumours, using the flavanoids rutin and luteolin, promoted tumour growth (*257*). Additionally, the response to TNF may be highly dependent on other immunoregulatory molecules in the tumour microenvironement. For example, the expression of the chemokine CXCL16 causes an upregulation of IRF8 and sensitizes CRC to apoptosis due to TNF secreted by tumor infiltrating macrophages (*258*).

Previous studies have shown, increased $CD4^+$ and $CD8^+$ lymphocyte infiltration in sm TNF expressing tumours and decrease in lymphocyte infiltration in 4T1 mbm TNF exprssing tumours. *In vitro*, the expression of mbm TNF showed an induction of MDSC activity, which inhibited T cell proliferation, and increase in the arginase, iNOS and NO levels (*196*). In the studies performed this chapter, no significant differences were found in $CD45^+$ $CD8^+$ or $CD45^+$ $CD4^+$ infiltration between the mice treated with Dox.

Different levels of TNF expression between the different models may contribute to dissimilar effects on immune infiltration and tumour growth. Unfortunately, previous studies using constructs expressing TNF under a constitutive promoter, such as CMV, have not reported the levels of TNF in the tumour lysates (*194, 196*). Moreover, the timing of transgene expression may influence the effects of cytokines. Previous studies by Dr. Aliaa Alamoudi, using the Dox-inducible system to express IL-10 and TGFβ scavengers, found a significant decrease in tumour growth when Dox was adminstered at the same time as tumour cell implantation, whereas administering Dox to mice with established tumours did not cause a significant decrease in tumour growth (*259*).

Administration of recombinant soluble TNF is known to target the tumour-associated vasculature (*183, 184, 202, 207*). Further studies are necessary to see wether the decreased tumour growth observed in CT26 tumours expressing mbm TNF was mediated through changes in the tumour-associated vasculature.

No statistically significant differences were found in the composition of immune cells in the spleen between control and Dox mice of any group. This may suggest that increased infiltration of tumours by immune cells is due to local changes of the microenvironment and not due systemic changes caused by TNF. However, due to the small group sizes, subtle differences may not have been detected.

Interestingly, no statistically significant differences in body weight were found in mice expressing TNF compared to the CT26 ni Dox group. TNF is known to cause cachexia (*260*), and the absence of weight loss in TNF expressing mice compared to CT26 ni Dox mice may indicate that the local expression of TNF in the tumour microenvironment could potentially reduce the systemic side-effects seen with

systemic delivery of TNF. Alternatively, the levels of TNF produced by the inducible cell lines may be below the levels that cause weight loss.

3.4.1 Limitations

In vivo, TNF expression from the cell lines is dependent on the availability of Dox in the tumours. Therefore, any factor altering the availability of Dox in the tumours will influence the expression of TNF.

A disadvantage of the syngeneic tumour implantation model is that this model does not fully mimic the tumour microenvironment of spontaneous tumours and the multistep tumour development that occurs in spontaneous tumours (*261*). Specifically, in these transplantable models, the immunoediting process is not recapitulated (*261*). These limitations may be particularly relevant when developing agents that rely on modification of tumour immunity and the tumour microenvironment. More recently, mouse models that imitate the natural tumorigenesis process have been developed. For example, mouse models with conditional overexpression of oncogenes or deletions tumour suppressor genes under the control of inducible promoters, such as the Cre/Loxp system, have been made. A major disadvantage of these models is that experiments using these models are more time-consuming.

Finally, the mouse model used in this study, BALB/c mice may have influenced the immunological response to TNF expression, as BALB/c mice have stronger humoral responses than C57BL/6 mice (*261*).

3.5 Chapter conclusion

Expression of soluble, full length and membrane-bound TNF leads to increased immune infiltration into tumours. An increase in myeloid cells in the tumours is seen upon TNF expression.

Inducing the expression of soluble or full length TNF by administering Dox to mice bearing CT26 sm TNF or CT26 fm TNF did not influence tumour growth. A minor reduction in tumour growth was seen in mice bearing CT26 mbm TNF tumours treated with Dox, compared to non Dox controls. Moreover, systemic toxicity by inducing local TNF expression was not observed, this may suggest that inducing local intratumoural TNF expression could be safe.

Chapter 4: Armed ColoAd1

4.1 Introduction

Oncolytic virotherapy uses viruses to preferentially infect and replicate in cancer cells and destroy these cells in the process. Numerous viruses have been tested in preclinical and clinical studies, including herpes simplex virus, measles virus, Newcastle disease virus, reovirus, vaccinia virus and adenovirus (*21*). Most studies on oncolytic adenoviruses have used an Ad5-based vector. However, due to the high prevalence of pre-existing immunity against Ad5 in the general population, this species might not be ideal for oncolytic therapy (*64*). ColoAd1 is a novel species B adenovirus, derived from Ad11p and Ad3, made by using a bioselection approach on a CRC cell line (*62*). Preexisting immunity against Ad11p is much less frequent in the general population compared to Ad5 (*64*). Moreover, increased cytotoxic effects have been observed during Ad11p infection compared to Ad5, in certain ovarian cancer cell lines (*262*). A more detailed overview of ColoAd1 can be found in the chapter 1.

To increase the efficacy of oncolytic virotherapy, viruses have been armed with numerous immune modulatory molecules. Chapter 1, paragraph 1.2.1 gives an overview of oncolytic viruses armed with immune-modulatory proteins. Several non-replicating adenoviruses expressing TNF have been made to date. The most advanced replication deficient vector expressing TNF is TNFerade. TNFerade expresses TNF from a radiation inducible promoter.

The aim of this chapter is to arm a replicating virus with TNF, to see whether efficacy can be increased, while maintaining a good safety profile.

Based on the reduced tumour growth observed in CT26 cell expression mbm TNF, ColoAd1 will be armed with this form of TNF. However, as cells infected with ColoAd1 will die rather quickly, using this unsecretable form may lead to low intratumoral levels of TNF. Thus, ColoAd1 will also be armed with soluble and full length TNF.

TNFerade

Previously, a non-replicating Ad5 vector expressing TNF, called TNFerade has been made. Xenograft models using cervical or prostate tumours expressing TNF in combination with brachytherapy, show enhanced tumour regression when TNF and radiation are combined in vivo (*263*). Moreover, the combination of radiation therapy and recombinant human TNF has been shown to be synergistic in humans (*264, 265*). However, TNF cannot be used for systemic treatment of cancer, due to dose-limiting toxicity.

Based on the synergy between radiation and TNF, TNFerade, a non-replicating Ad5 based vector, expressing human soluble TNF under the early growth response protein 1 (Egr1) promoter, has been developed. This vector has deletions of the E1 and E4 region, and a partial deletion in E3. Radiation induces the Egr1 promoter, via the induction of reactive oxygen intermediates (ROI) (*266*). In preclinical models, intratumoural administration of TNFerade, twice weekly, combined with 30 Gy (fractioned as 5 Gy per day, 4 times a week) resulted in complete tumour regression in approximately 70% of mice bearing subcutaneous glioma xenografts. No cures were seen in mice treated with only TNFerade or a combination of an Ad-vector without TNF and radiation. Mice treated with TNFerade and radiation had 345 ± 179 pg human TNF/mg protein

by day 4 and up to 1033 ± 201 pg TNF/mg protein by day 7 (*206*). An increase of thrombosis in tumour-associated vasculature and necrosis within tumours has been observed in mice treated with a combination of TNFerade and radiation, whereas vessels in normal tissues seem unaffected (*205, 206*).

In a melanoma model, mice treated with TNFerade and 20 Gy of radiation (given as a single dose) had 547.4 (± 10.4) pg/mg of protein human TNF 24h after treatment (*267*). Mice treated with a combination of TNFerade and radiation had significantly lower tumour burden at day 11 than IR alone or TNFerade alone on day 8. When mice were treated with etanercept, no difference in tumour growth between mice treated with IR and TNFerade or IR was observed. Tumours in mice with germline deletions of TNF were also responsive to the IR and TNFerade combination, suggesting that the effects were mediated through TNF expressed from the adenovirus vector. Rather than endogenously produced TNF. Interestingly, TNF KO mice seemed more radiosensitive than wt mice, indicating that both an increase in TNF concentrations and blocking of endogenous TNF can increase radiosensitivity. Furthermore, in mice with germline deletions of TNFR1 and TNFR2, the combination of TNFerade with IR showed no additional benefit over IR alone. Moreover, tumours with silencing of the TNFR1 using an shRNA still showed sensitivity to the combination of TNFerade and IR, even when the tumours were more resistant to TNF as a monotherapy.

Increased caspase 3 in tumour-associated endothelial cells was seen in mice treated with TNFerade and IR compared to either treatment alone. Together these results suggest host-mediated effects of TNF rather than direct cytotoxicity of TNF to the tumours as an underlying mechanism. Interestingly, combination

of IR and TNFerade also reduces tumour growth in TNF-resistant cell lines, such as PC3 (*268*).

Besides radiation, chemotherapeutic agents, including cisplatin and doxorubicin have also been shown to activate the Egr1 promoter. Studies, combining TNFerade with Egr1 activating drugs have shown increased anti-tumour activity compared to TNFerade or chemotherapy alone (*269, 270*).

Phase I and phase II studies on TNFerade in combination with radiation for solid tumours were promising. In a phase I study, 21 out of 30 patients showed an objective tumour responses (*271*). Yet, in 2010, Genvec stopped a phase III trial on the efficacy of TNFerade for patients with locally advanced pancreatic cancer, based on a lack of effectiveness revealed during the interim analysis (*240*).

4.2 Chapter objectives and hypotheses

1) Engineer cDNA encoding murine soluble, full length and membrane-bound TNF, murine mLTA and human full length TNF into a ColoAd1 vector, under a splice acceptor site under the control of the major late promoter.
2) Characterize the viruses made *in vitro*.
3) Expression of mTNF and mLTA from ColoAd1 decreases tumour growth, and increases immune infiltration and vascular permeability compared to parental ColoAd1 *in vivo*

4.3 Results

Adenoviruses encode several proteins that interfere with TNF signalling during infection, see chapter 1 paragraph 1.3.1 for a summary. ColoAd1 has large deletions in the E3 region, which encodes the adenoviral proteins that interfere with host immunity and interfere with TNF signalling in infected cells. Thus, it is important to test whether treating ColoAd1 infected cells leads to cell lysis and whether ColoAd1 replication can still take place in the presence of TNF. Thus, before arming ColoAd1 with TNF or LTA, studies to test viral infection and replication in the presence of TNF or LTA were conducted.

4.3.1 Effects of TNF treatment on Ad infections, *in vitro*

4.3.1.1 TNF effects on Ad5 adenovirus uptake and transgene expression

To determine the impact of TNF on the ability of an adenovirus to infect tumour cells a non-replicating reporter virus (Ad5-CMV-luciferase: AdLuc) was used. E1A-deficient, non-replicating Ad5-CMV-luciferase (AdLuc), A549 cells were treated with two different concentrations of human recombinant TNF (50 ng/ml or 100 ng/ml) 2 hours before infection with a range of AdLuc concentrations. TNF was added either 2h before (see figure 4) or at the time of infection (data not shown). The cells were treated with 0, 0.1, 1, 10, 100 or 200 vp/cell. 24 h (figure A) or 48 h (figure B) after AdLuc infection, the cells were washed and lysed in cell lysis buffer and frozen at -80°C. A luciferase assay was conducted on the cell lysate and the luciferase activity was normalized to protein concentrations in the cell lysate. As expected, a dose dependent increase in luciferase activity was seen in AdLuc infected cells. As figure 4.1 shows, treatment of A549 cells with high levels of TNF did not alter luciferase at 24 h or

48 h. Similarly, simultaneous treatment of A549 cells with AdLuc and TNF did not affect luciferase activity either (data not shown). The bioactivity of the human recombinant TNF was confirmed by a L929 cytotoxicity assay.

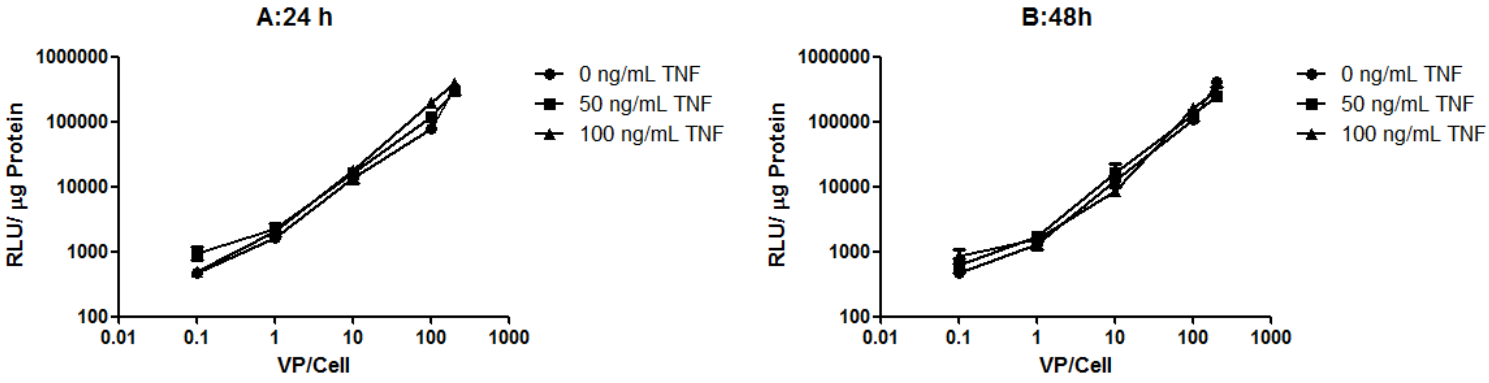

Figure 4.1: Effects of TNF on the infection and expression efficiency of Ad5luc. A549 cells were treated with human recombinant 50 ng/ml or 100 ng/ml TNF 2h before infection. The cells were then treated with 0, 0.1, 1, 10, 100 or 200 vp/cell of Ad5luc. After a further 24 h (A) or 48 h (B), the cells were washed and lysed in cell lysis buffer and frozen at -80°C before analysis by luminometry. Luciferase activity (RLU) was normalized per µg protein. The luciferase activity was normalized to protein concentrations in the cell lysate. Studies were performed in triplicate well. A two way ANOVA was used to analyse the data. No significant differences were observed across virus or TNF concentrations Mean and SEM are shown, n=3.

4.3.1.2 Effects of TNF/LTA on replication of Ad5, Ad11, and ColoAd1

The previous experiment revealed no discernible effect of TNF on infection or early gene expression. To determine if TNF has any effects on later events in adenovirus replication, a further study was conducted with replication competent virus. TNF has been shown kill to adenovirus-infected cells. To test whether TNF and LTA influenced replication of adenoviruses a q-PCR study was set up.

HT29 (human CRC) cells were treated with 0, 10 or 100 ng/ml TNF or LTA and 0, 1, 10 or 100 vp/cell Ad5, Ad11p or ColoAd1. The supernatant was collected 48h after the start of infection and stored at -80°C. The cells were washed and an MTS assay was done to assess cell viability. Subsequently, the cells were washed again and lysed in lysis buffer and stored at -80°C. Viral DNA was extracted from the cell lysate and supernatant using a DNA extraction kit and a QPCR for viral genome copies was done to assess viral replication. The bioactivity of the human recombinant TNF used in this experiment was confirmed by a cytotoxicity assay on L929 cells.

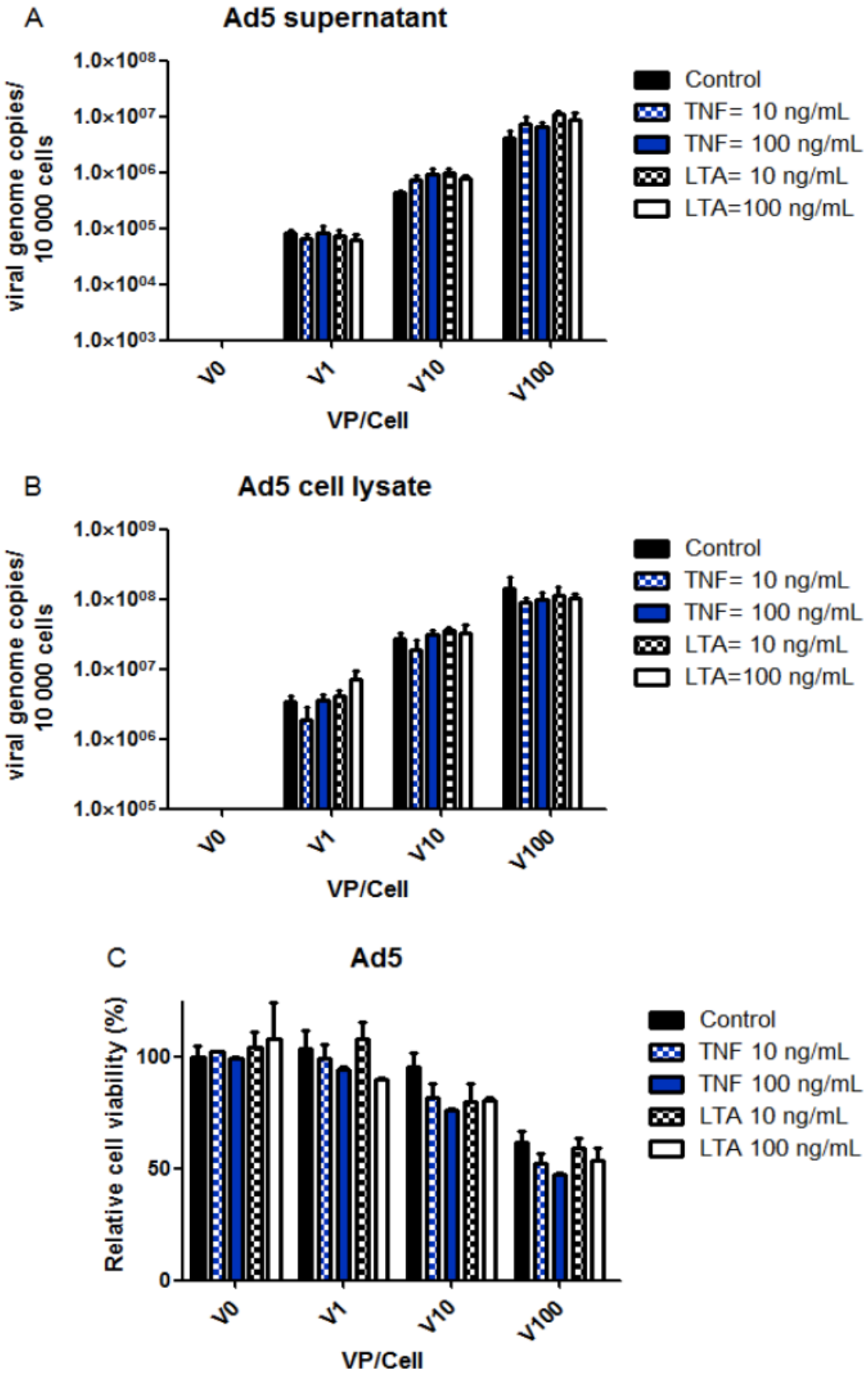
A
Ad5 supernatant
viral genome copies/ 10 000 cells
1.0×10^08
1.0×10^07
1.0×10^06
1.0×10^05
1.0×10^04
1.0×10^03
V0
V1
V10
V100
VP/Cell
Control
TNF= 10 ng/mL
TNF= 100 ng/mL
LTA= 10 ng/mL
LTA=100 ng/mL
B
Ad5 cell lysate
viral genome copies/ 10 000 cells
1.0×10^09
1.0×10^08
1.0×10^07
1.0×10^06
1.0×10^05
V0
V1
V10
V100
VP/Cell
Control
TNF= 10 ng/mL
TNF= 100 ng/mL
LTA= 10 ng/mL
LTA=100 ng/mL
C
Ad5
Relative cell viability (%)
100
50
0
V0
V1
V10
V100
VP/Cell
Control
TNF 10 ng/mL
TNF 100 ng/mL
LTA 10 ng/mL
LTA 100 ng/mL

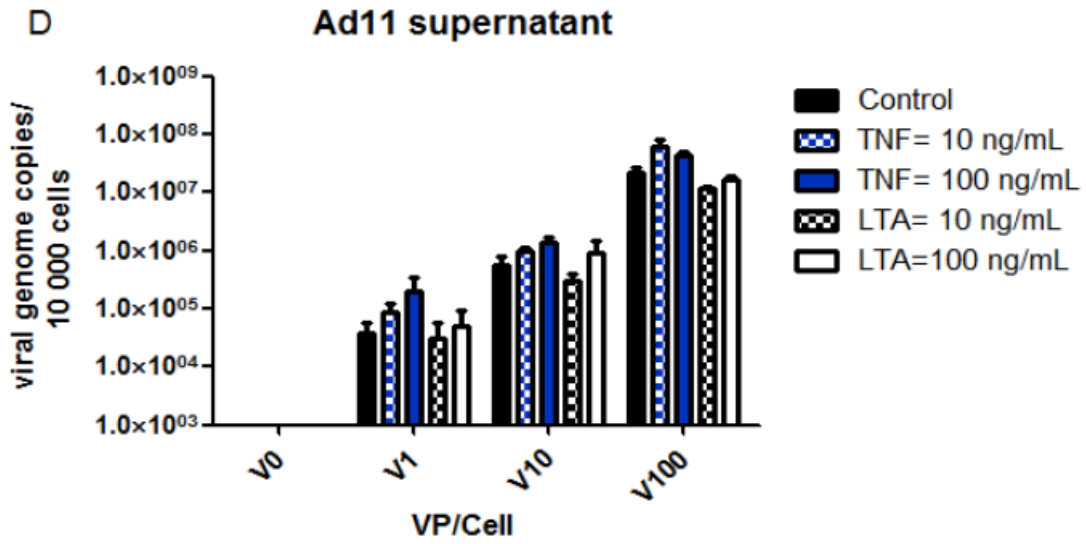
D
Ad11 supernatant
viral genome copies/ 10 000 cells
1.0×10^09
1.0×10^08
1.0×10^07
1.0×10^06
1.0×10^05
1.0×10^04
1.0×10^03
V0
V1
V10
V100
VP/Cell
Control
TNF= 10 ng/mL
TNF= 100 ng/mL
LTA= 10 ng/mL
LTA=100 ng/mL

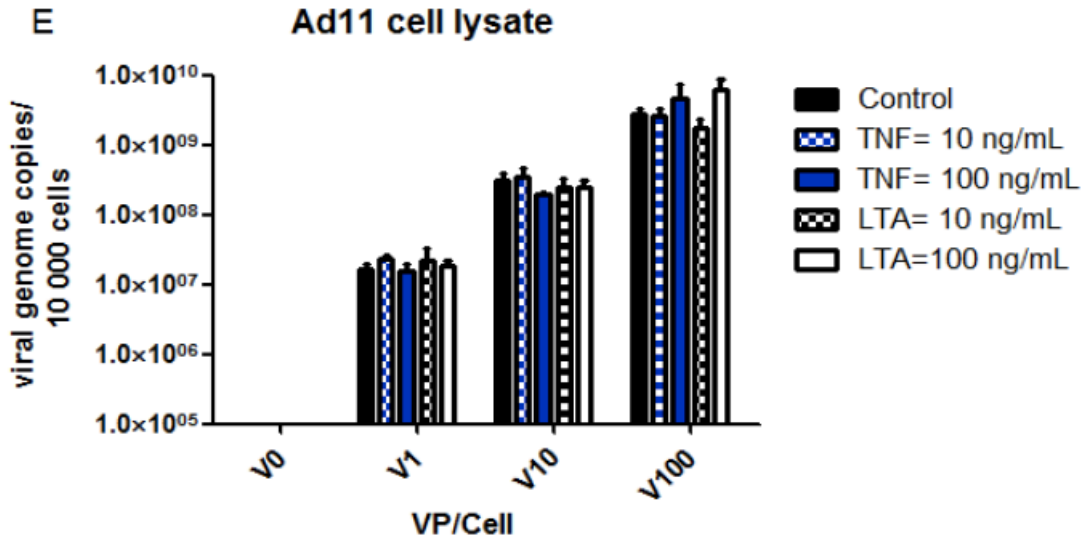
E
Ad11 cell lysate
viral genome copies/ 10 000 cells
1.0×10^10
1.0×10^09
1.0×10^08
1.0×10^07
1.0×10^06
1.0×10^05
V0
V1
V10
V100
VP/Cell
Control
TNF= 10 ng/mL
TNF= 100 ng/mL
LTA= 10 ng/mL
LTA=100 ng/mL

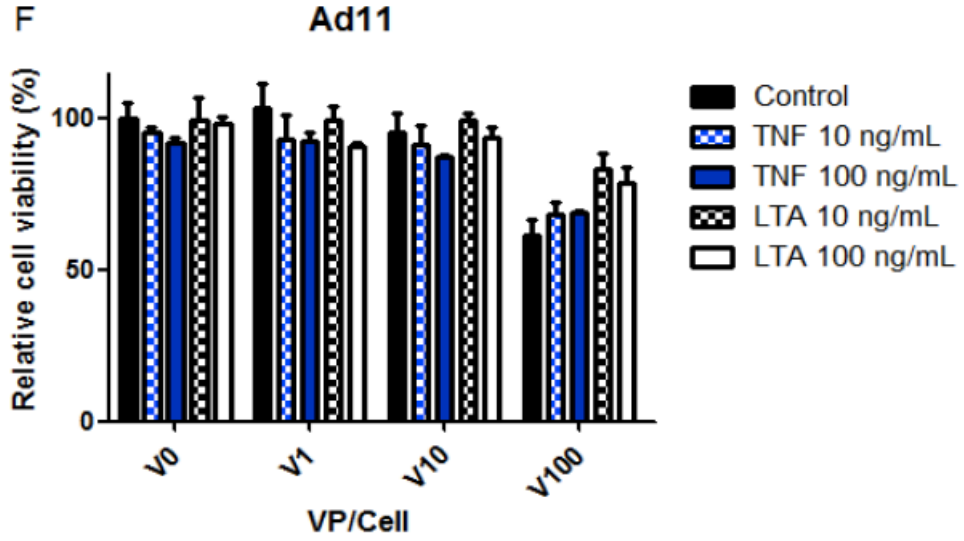
F
Ad11
Relative cell viability (%)
100
50
0
V0
V1
V10
V100
VP/Cell
Control
TNF 10 ng/mL
TNF 100 ng/mL
LTA 10 ng/mL
LTA 100 ng/mL

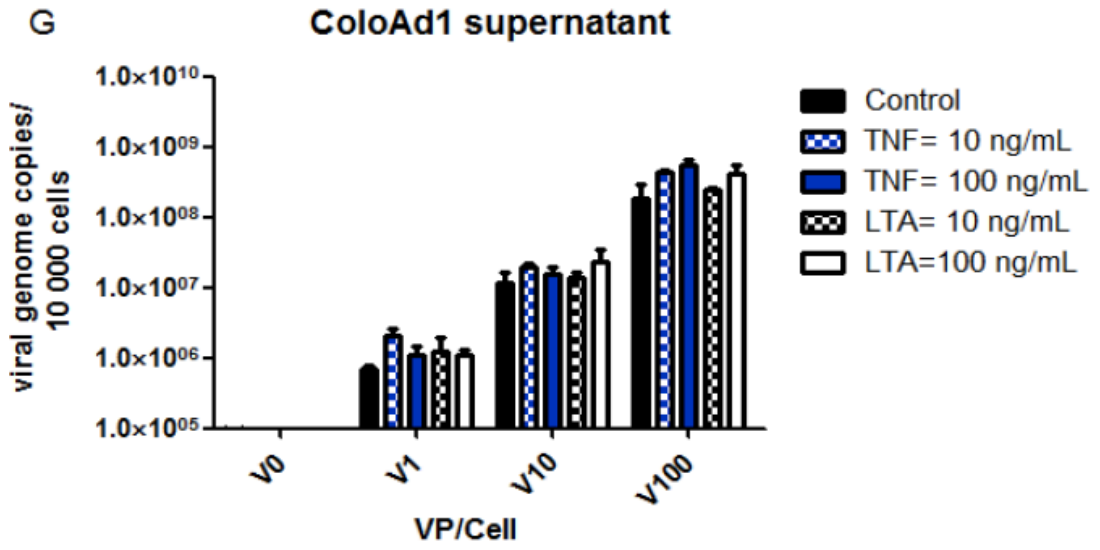
G
ColoAd1 supernatant
viral genome copies/ 10 000 cells
1.0×10¹⁰
1.0×10⁰⁹
1.0×10⁰⁸
1.0×10⁰⁷
1.0×10⁰⁶
1.0×10⁰⁵
V0
V1
V10
V100
VP/Cell
Control
TNF= 10 ng/mL
TNF= 100 ng/mL
LTA= 10 ng/mL
LTA=100 ng/mL

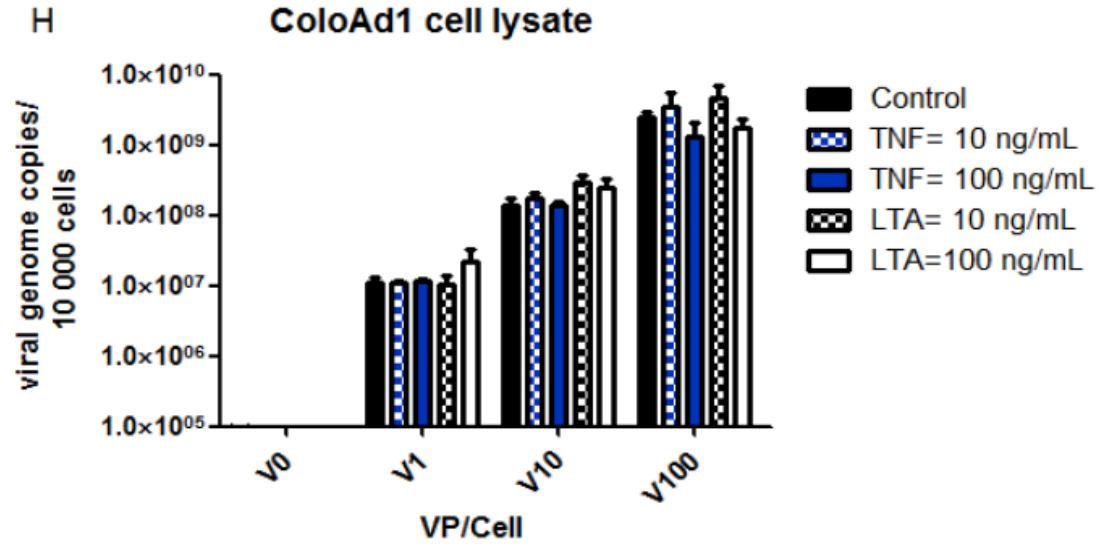
H
ColoAd1 cell lysate
viral genome copies/ 10 000 cells
1.0×10¹⁰
1.0×10⁰⁹
1.0×10⁰⁸
1.0×10⁰⁷
1.0×10⁰⁶
1.0×10⁰⁵
V0
V1
V10
V100
VP/Cell
Control
TNF= 10 ng/mL
TNF= 100 ng/mL
LTA= 10 ng/mL
LTA=100 ng/mL

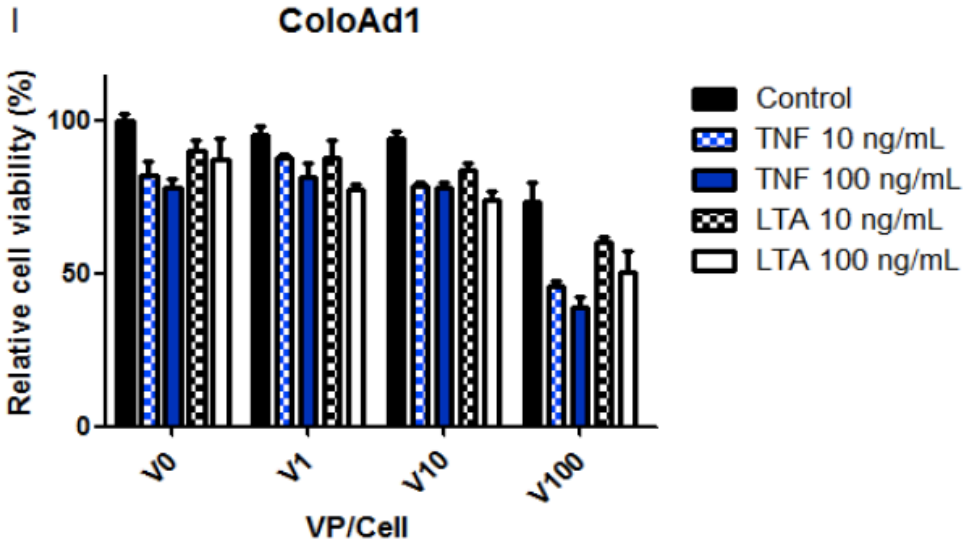
I
ColoAd1
Relative cell viability (%)
100
50
0
V0
V1
V10
V100
VP/Cell
Control
TNF 10 ng/mL
TNF 100 ng/mL
LTA 10 ng/mL
LTA 100 ng/mL

Figure 4.2: The effects of TNF on Ad5, Ad11p and ColoAd1 replication and cytotoxicity in HT29 cells. HT29 cells ($1x10^4$ cells/well) were seeded overnight. Subsequently, the cells were treated with 0, 10 or 100 ng/ml TNF or LTA and infected at 0, 1, 10 or 100 vp/cell Ad5 (A, B, C), Ad11p (D, E, F) or ColoAd1 (G, H, I). At 48h post infection and treatment, the supernatant was harvested and an MTS assay was performed (C, F, I) to assess cell viability. Subsequently, the cells were washed and lysed. A QPCR was performed to analyse viral genome copies (A; B; D; E; G; H). A 2-way ANOVA was used to test for the effects of TNF and LTA on viral replication. Statistically significant effects on supernatant were found with Ad11p and ColoAd1 but not Ad5. Additionally, statistically significant effects on cell viability were found in Ad5, Ad11p and ColoAd1 cells treated with TNF or LTA.

As expected, treatment with higher amounts of virus led to increased genome copies with all three viruses. Also, a dose dependent decrease in cell viability was seen in treatment in Ad5, Ad11p and ColoAd1 infection after 48h.

Using 2-way ANOVAs, the effects of TNF and LTA on adenovirus infection were tested. A significant ($p=0.015$) effect of TNF and LTA treatment on ColoAd1 genome copies in the supernatant was found. Using separate t-tests, a significant increase in ColoAd1 genome copies in the supernatant at was found in cells infected at 100 vp/cell and 100 ng/ml TNF ($p=0.045$). However, a decrease in the ColoAd1 cell lysate was found at this condition (although not statistically significant by 2-way ANOVA) and increased cell death on the MTS assay was found. This indicates the cell released the virus quicker upon cell death when treated with high levels of TNF. In the cell viability assay, a statistically significant effect of TNF and LTA, vp/cell and statistically significant interaction between them was found for ColoAd1.

For Ad11, a statistically significant effect of TNF and LTA ($p=0.0001$) was and statistically significant interaction factor ($p=0.0008$) was found for Ad11p genome copies in the supernatant. Using separate t-tests, a borderline not significant ($p=0.07$) increase between 10 ng/ml of TNF and control was found

and a statistically significant increase (p=0.0453) between 100 ng/ml of TNF and control was seen at 100 vp/cell. No statistically significant differences between LTA treated cells and control cells were seen. Additionally, no statistically significant differences were seen at lower viral concentrations between TNF, LTA and PBS controls in the supernatant. No differences in Ad11p genome copies in the cell lysate were found. A statistically significant effect of TNF and LTA was found on cell survival ($p<0.001$) and a statistically significant interaction between TNF and LTA and Ad11p was found (p=0.0015). Using t-tests, a statistically significant increase in cell survival was seen in cells infected with 100 vp/cell Ad11p and 10 ng/ml or 100 ng/ml of LTA. No statistically significant effects of TNF on cell viability were seen during Ad11p infection.

For Ad5, no statistically significant differences in viral genome copies in the supernatant or cell lysate were found. However, a statistically significant decrease in cell viability in infected cells treated with TNF was seen (p=0.0008) and a significant interaction (p=0.0429) between the cytokines and Ad5 were found.

4.4.2 Cloning TNF and LTA into the ColoAd1 vector

With no strong evidence of TNF or LTA inhibiting the virus *in vitro*, the next step was to clone human full length TNF and murine soluble, full length and membrane-bound TNF and LTA into a ColoAd1 vector.

TNF and LTA were cloned under a splice-acceptor (SA) site under the control of the major late promoter (MLP). The MLP is switched on during the later stages of viral infection, when replication begins. Thus, this promoter was hypothesized to be safer as TNF would not be expressed in cells that are not permissive for

adenovirus replication. Additionally, higher levels of GFP were found when expressed under the MLP compared to a CMV promoter (PsiOxus Ltd, personal communications).

Priority to cloning different forms of mouse TNF was given, because human TNF cannot activate signalling through the murine TNFR2, leading to much decreased toxicity of hTNF in mice. Additionally, *in vitro*, TNF and LTA do not have major cytotoxic effects on CRC cell lines. Thus, we expect effects of TNF and LTA to be mediated through host immunity and effects on the vasculature. An SA site and kozak sequence were added prior to the TNF and LTA cDNA sequence by insertional mutagenesis PCR. Hf length TNF, sm and fm TNF and mLTA were inserted into the ColoAd1 vector, via 2 shuttle vectors, using endonuclease enzymes. Cloning of these viruses was done at PsiOxus Therapeutics, UK, and help was kindly provided by Dr. Alice Bown and Prithvi Kodialbail. Mbm TNF was inserted into a shuttle vector using endonuclease enzymes. From this shuttle vector, mbm TNF was inserted into the ColoAd1 backbone using Gibson assembly. For details on the cloning strategy, please see the materials and methods.

All ColoAd1 plasmids were sent off for sequencing to confirm the correct sequence was inserted. Upon correct sequencing, the virus was rescued by transfecting the linearized plasmids into 293 A cells. Once significant cytopathic effect (CPE) developed, the cells and supernatant was collected. Repeated freeze-thawing cycles were used to release the virus from the cells and the supernatant and cell lysate was filtered to exclude cellular debris. The rescued virus was then used to infect 2 hyperflasks of 293 A cells per virus stock. Between 48-72 h after the start of infection of the hyperflasks significant CPE developed. Upon CPE, the

virus was harvested from the cells and purified. Concentrations of the virus particles concentrations of these virus stocks was determined using the PicoGreen® method.

These data support earlier findings that TNF express does not impact the virus or packaging cells to the point where yield is unduly effected. The modest variability in yield between batches is consistent with typical of the variation between bulk preparations of viruses in the research laboratory.

Virus Stock	**Titer**
ColoAd1	2.14 x 10^{12} vp/ml
ColoAd1 SA mLTA	7.78 x 10^{12} vp/ml
ColoAd1 SA sm TNF	1.49 x 10^{12} vp/ml
ColoAd1 SA fm TNF	3.04 x 10^{12} vp/ml
ColoAd1 SA mbm TNF	7.38 x 10^{11} vp/ml
ColoAd1 SA fh TNF	4.79 x 10^{12} vp/ml

Table 4.1: The titer of viral stocks made for this thesis. The vp concentration of viral stock made for this thesis as determined by the PicoGreen® method. A serial dilution of known amounts of bacteriophage λ DNA was used as a standard curve. Viral dilutions were made in SDS and incubated at 56 °C for 30 min to disintegrate the viral capsid. Subsequently, fluorescence was of the standard curve and samples were measured using PicoGreen® reagent. DNA concentrations of viral stocks were calculated and the vp was calculated, assuming 1 µg/ml of DNA equals 2.7 x 10^{10} vp (*245*).

4.4.2. In vitro characterization of the viruses

A PicoGreen® assay will detect viral particles based on DNA concentrations. This approach does not distinguish inactive particles from particles capable of infecting cells. To assess whether the virus produced was infectious, 293A cells were infection with different concentrations of the viral stocks. Cells were fixed 48h after the start of infection and stained for hexon to confirm successful viral infection.

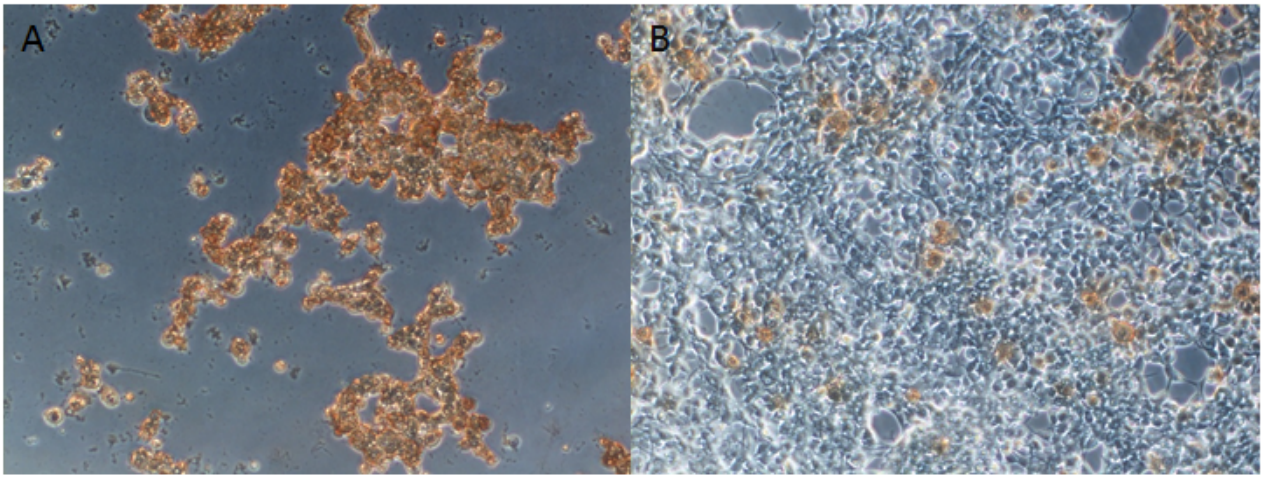

Figure 4.3: Hexon staining of HT29 cells infected with ColoAd1 fm TNF. HT29 cells were infected with a high MOI (A) or low MOI (B) of ColoAd1 fm TNF. After 48h, the cells were fixed in methanol and staining for adenovirus hexon protein was performed.

To test the cytotoxicity of the viral stocks produced, 293A or DLD cells were infected with 1000, 100, 10, 1, 0.1 or 0.01 vp/cell. The cell viability was measured 5 days after the start of infection by MTS assay. As expected, 293A cells were more sensitive to ColoAd1 infection than DLD cells. Furthermore, on both 293A and DLD cells, ColoAd1 fm TNF, ColoAd1 hf TNF and ColoAd1 mbm TNF induced more cell death than ColoAd1 or ColoAd1 sm TNF. The reduced cell viability seen in cells treated with viral stocks of ColoAd1 expressing TNF is consistent with the data from paragraph 4.3.2.1, where simultaneous treatment of ColoAd1 with TNF reduced cell viability towards the end of the replication cycle although this does not appear to overly impact on yield.

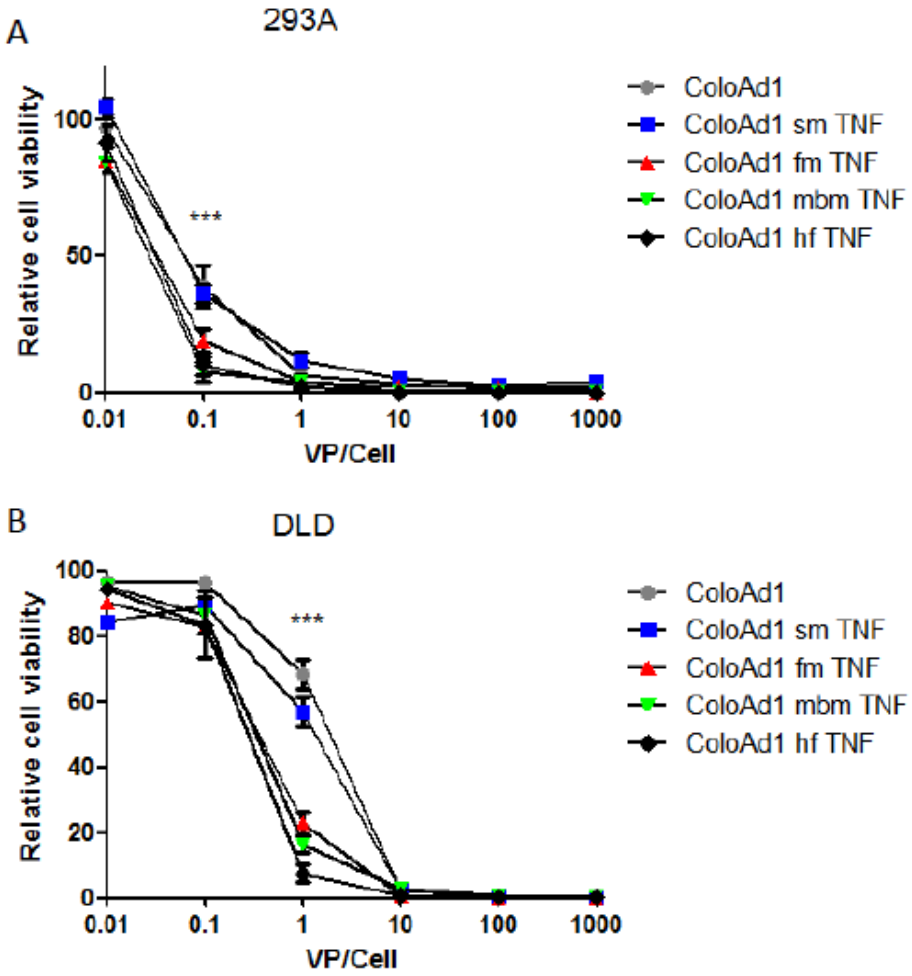

Figure 4.4: Cell viability 293A or DLD cells infected with TNF expressing ColoAd1. 293A (A) or DLD (B) cells ($1x10^4$ cells/well) were seeded overnight. Subsequently the cells were infected with a serial dilution of ColoAd1, ColoAd1 sm TNF, ColoAD1 fm TNF, ColoAd1 mbm TNF or ColoAd1 hf TNF. Five days after the start of infection, cell viability was measured using an MTS assay. Data was analysed using a 1-way ANOVA. A statistically significant decrease in cell viability was found in cells treated with ColoAd1 fm TNF, ColoAd1 mbm TNF or ColoAd1 hf TNF compared to ColoAd1 or ColoAd1 sm TNF in 293A cells (0.1 vp/cell) or DLD cells (1 vp/cell). ***$p<0.001$. Mean and SD shown, n=3.

4.4.2.2 Transgene production of TNF and LTA from ColoAd1

The characterized and purified stocks of recombinant viruses were then evaluated for expression of TNF isoforms. In the first study, expression levels in either the supernatant of cell lysate was quantified by ELISA (see figure 4.5).

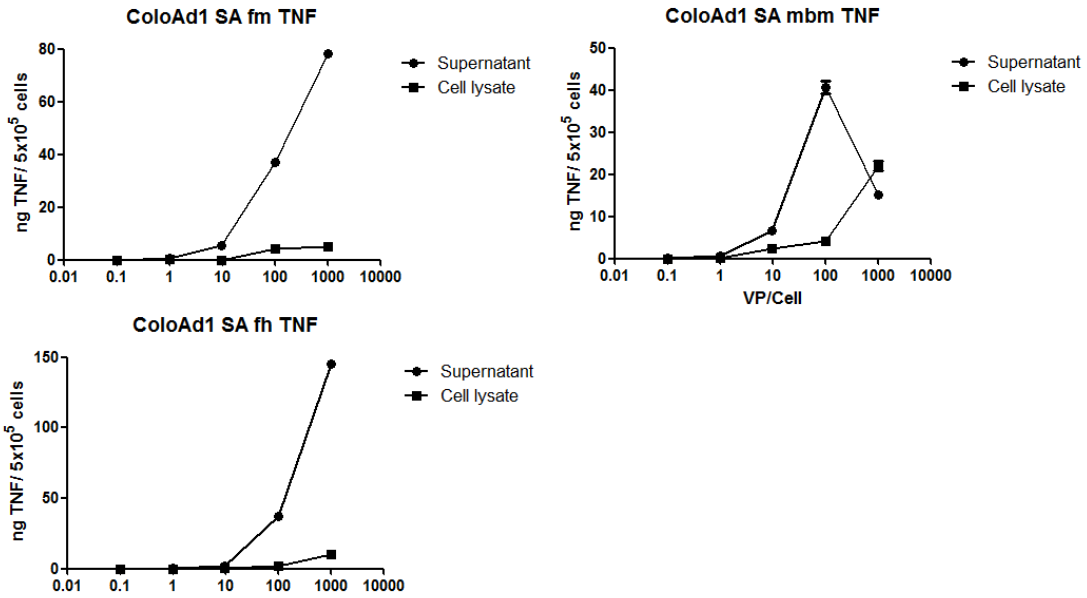

Figure 4.5: In vitro TNF expression from serial dilutions of ColoAd1 expressing TNF. DLD cells ($5x10^5$ cells/well) were seeded overnight. The next day, the cells were infected with a serial dilution (1000, 100, 10, 1 or 0.1 vp/cell) of ColoAd1 fm TNF, ColoAd1 mbm TNF or ColoAd1 fh TNF. The cells were incubated for 48h, before harvesting the supernatant. TNF expression was quantified using a sandwich ELISA. A dose-dependent relationship between vp/cell and TNF produced was observed. Mean and SEM shown, n=3.

The data show that, TNF expression from a ColoAd1 is dose-dependent and expression continues to increase up to 48 hours under the control of the MLP, see figures 4.5 and 4.6.

Surprisingly, a decrease in mbm TNF in the supernatant produced from ColoAd1 was seen when cells were treated with 1000 vp/cell compared to a 100 vp/cell. The total amount of TNF produced, so adding supernatant and cell lysate, was

also lower in cells treated with 1000 vp/cell ColoAd1 mbm TNF (37.20 ng/5x10^5) cells compared to 100 vp/cell (44.84 ng/5x10^5). The decrease in TNF production could be through speadier cell kill in cells treated with more virus. Cells may have died due to particle toxicity or died sooner after infection, thereby decreasing the amount of TNF produced and released into the supernatant, whereas the cells that are still alive produced more TNF, thus TNF in the cell lysate still increased between 100 vp/cell and 1000 vp/cell ColoAd1 mbm TNF.

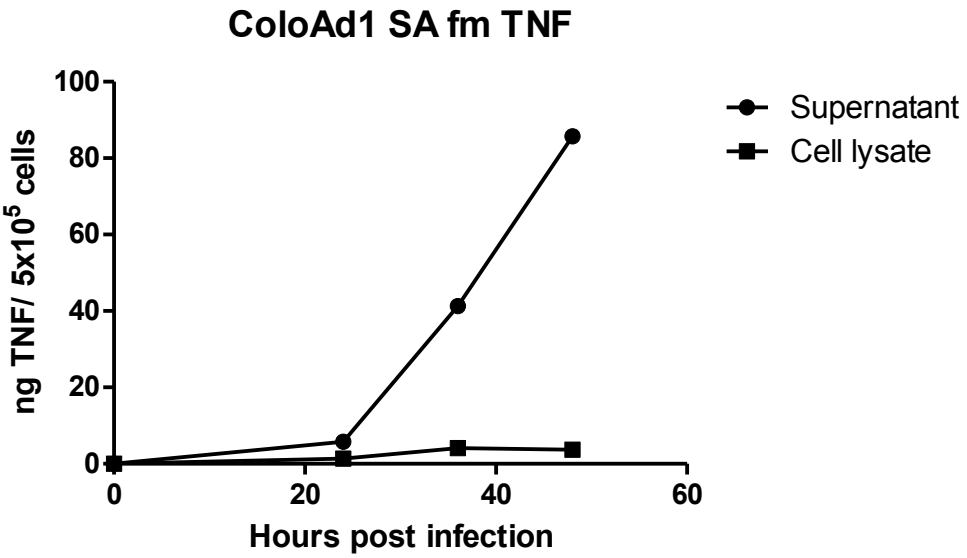

Figure 4.6: fm TNF expression from ColoAd1 over time. DLD cells (5x10^5 cells/well) were seeded overnight. The next day, the cells were infected with 100, vp/cell ColoAd1 fm TNF. The cells were incubated for 0h, 24h, 36h or 48h, before harvesting the supernatant. TNF expression was quantified using a sandwich ELISA. TNF production was first observed after 24h and increased until 48h. Mean and SEM shown, n=3.

Using an ELISA, mLTA protein expression from ColoAd1 mLTA could not be detected, at a range of different time points and MOIs (data not shown).

4.4.2.3 Membrane-associated TNF

To test whether TNF is expressed on the cell surface, flow cytometry analysis was used. DLD Cells were infected with 100 vp/cell ColoAd1 (grey), ColoAd1 fm TNF (red) or ColoAd1 mbm TNF (green) or mock (black) infected. 24h after the start of infected, the cells were scraped off the plates, washed and stained with an isotype control antibody (A) or a TNF antibody (B). 24h was picked, as at 48h large amounts of dead cells and cellular debris occur in ColoAd1 treated cells. The cells were stained without prior permeabilisation to limit staining to membrane-associated TNF. Cellular debris was excluded from the analysis based on the Forward/Side scatter plot. As can been seen in figure 4.7, ColoAd1 mbm TNF showed slightly higher TNF staining than ColoAd1 fm TNF.

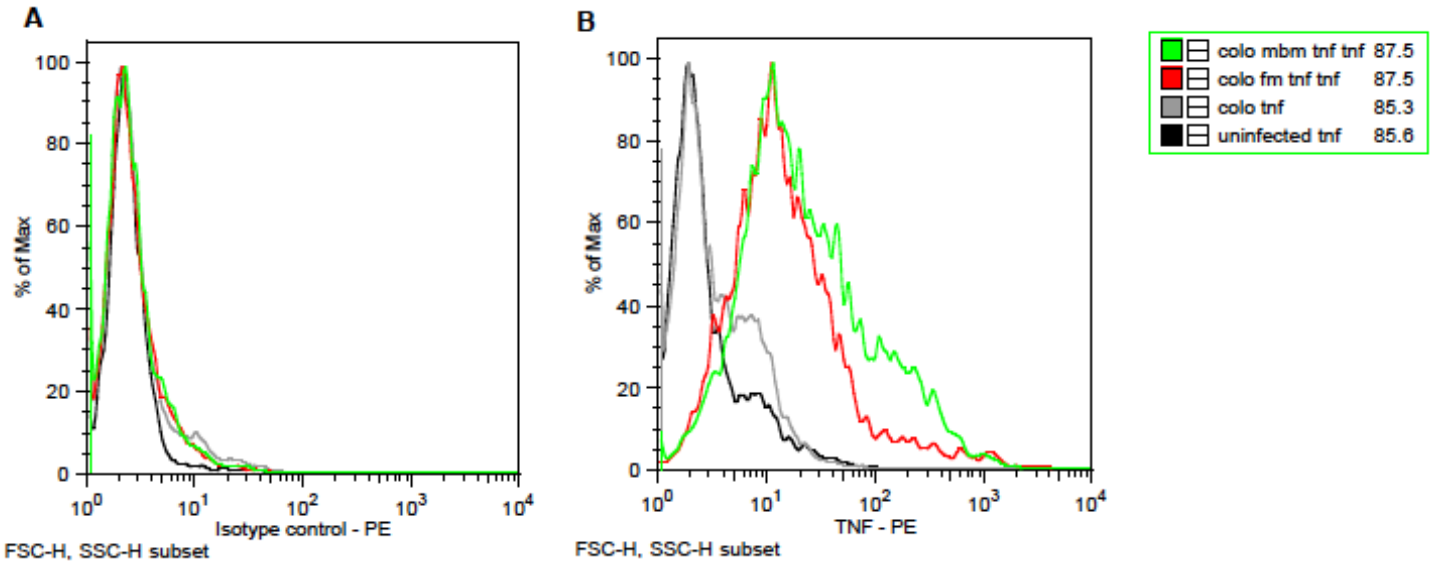

Figure 4.7: Flow cytometry analysis of membrane-associeted TNF in DLD cells infected with ColoAd1 mTNF. DLD cells ($5x10^5$ cells/well; in triplicates) were seeded overnight. The cells were infected with 100 vp/cell ColoAd1 (grey), ColoAd1 fm TNF (red) or ColoAd1 mbm TNF (green) or mock (black). The cells were incubated for 24h and scraped off the plates. Subsequently, the triplicates were pooled and stained with isotype control (A) or TNF (B) antibody. The staining was analysed using flow-cytometry.

Thus, TNF and LTA were successfully cloned into ColoAd1. Expression of mLTA was very low and therefore this virus was not taken forward to animal studies. *In vitro*, all TNF armed viruses were infectious and expressing the transgene.

4.4.3 *In vivo* studies

In vitro, high TNF expression was seen from the ColoAd1 vectors. Additionally, using flow-cytometry, expression of TNF the cell membrane was seen with the ColoAd1 fm TNF and ColoAd1 mbm TNF vectors. Next, *in vivo* studies were done to see the effects of expressing ColoAd1 on tumour growth and immune infiltration into the tumours.

4.4.3.1 Pilot: TNF expression and ColoAd1 fm replication in different xenograft CRC models

A small pilot study was set up to test whether replication of ColoAd1 fm TNF and TNF expression occur *in vivo* and to pick a human CRC cell line to use for subsequent xenograft studies. HCT116, HT29 or DLD cells were implanted subcutaneously in female BALB/c nude mice. Once tumours were approximately 100 mm^3, the mice were injected i.t. with 5 x 10^9 vp ColoAd1 fm TNF or PBS (day 0). Tumour size was measured frequently.

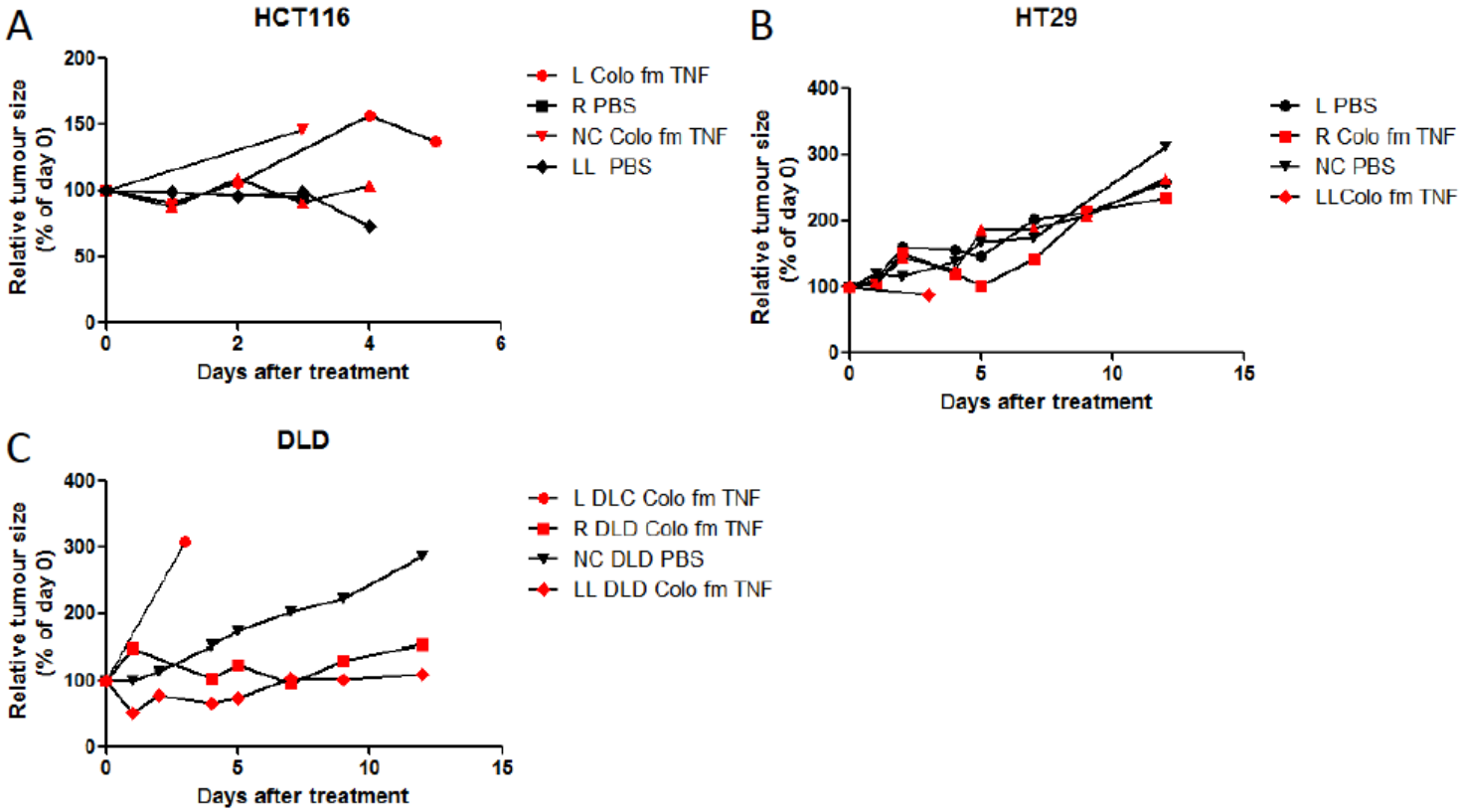

Figure 4.8: Effects of ColoAd1 fm TNF on human CRC xenografts. Mice were implanted subcutaneously with HCT116 (A; n=4), HT29 (B; n=4) or DLD (C; n=4) cells. The tumours were allowed to approximately 100 mm^3. Mice were injected at day 0 with 5 x 10^9 vp ColoAd1 fm TNF (red) or PBS (black) i.t. Two HCT116 mice developed an ulcer and one HCT116 mouse developed a cyst. From the mice bearing DLD and HT29 tumours, 2 ColoAd1 fm TNF mice were kept for 12 days after treatment and one ColoAd1 fm TNF mouse was euthanized after 3 days.

Two mice bearing HCT116 tumours developed an ulcer and one mouse developed a cyst. Thus, these mice were euthanized earlier than the DLD and HT29 mice.

At the time of euthanasia, the tumours were harvested and snap frozen for further analysis.

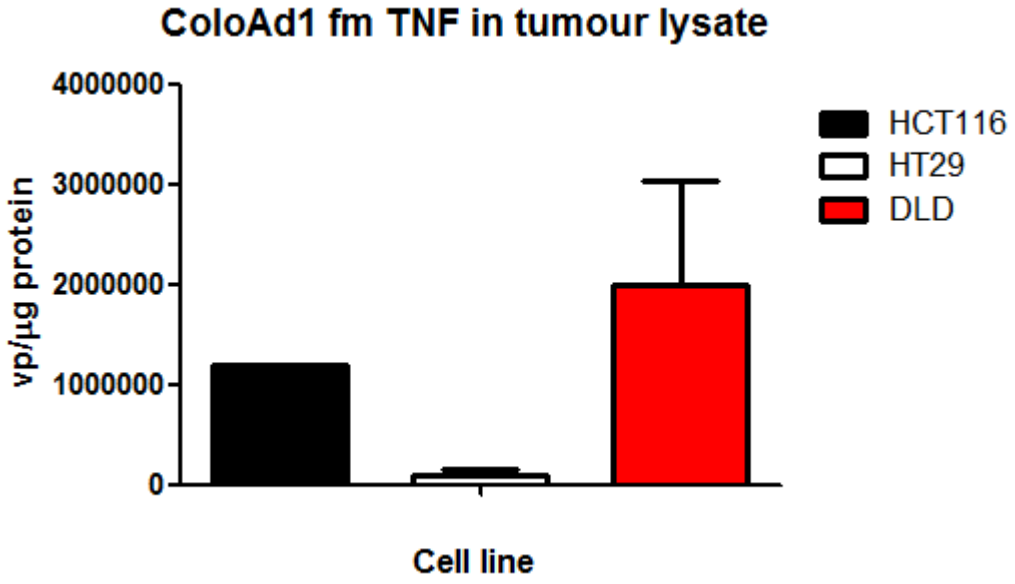

Figure 4.9: Viral genome copies in the tumour lysate of ColoAd1 fm TNF treated HCT116, HT29 and DLD xenograft tumours. The tumours were harvested and homogenized. Viral genomes were detected using QPCR and the data was normalized to protein content using a protein assay. Mean and SEM are shown.

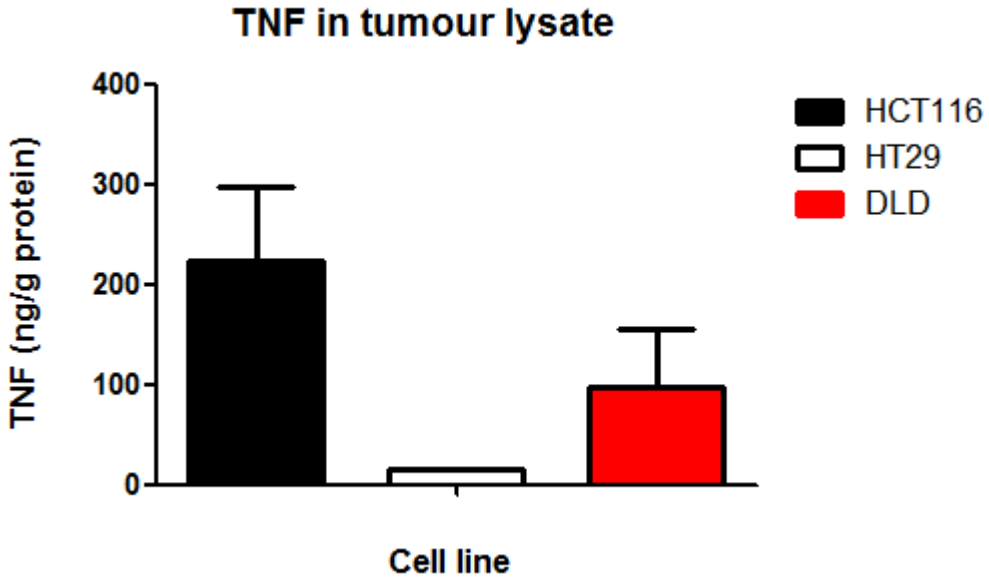

Figure 4.10: TNF protein expression in the tumour lysate of ColoAd1 fm TNF treated HCT116, HT29 and DLD xenograft tumours. The tumours were harvested and homogenized. TNF levels were measured using a sandwich ELISA and the data was normalized to protein content using a protein assay. Mean and SEM are shown.

In all three CRC xenograft models, TNF expression could be detected after ColoAd1 fm TNF treatment. Additionally, viral genomes could be detected by QPCR up to 12 days after treatment in HT29 and DLD tumours. Based on the higher amount of TNF and viral genome copies found in the tumour lysate of DLD tumours compared to HT29, DLD tumours were used for further studies. In the HCT116 xenograft model, a high rate of adverse events occcured in our pilot study, as two mice developed an ulcer and one mouse developed a cyst out of the 5 mice implanted with this cell line. Additionally, a high percentage of mice not suitable for inclusion in studies after HCT116 implantation were also observed by PsiOxus Ltd (personal communications). Thus, using this model would mean increasing the number of mice necessary to perform experiments. Therefore, the HCT116 model was not used for further studies.

4.4.3.2 Pilot: TNF expression and ColoAd1 genome copies at day 9, 15 and 30 post treatment

Based on the findings of the first pilot study, the DLD xenograft was chosen for further studies. A small second pilot study was done to compare ColoAd1 with ColoAd1 fm TNF. Additionally, the TNF levels and viral genome copies in the tumour were assessed at several time points after i.t. injections with the virus. For this study, subcutaneous DLD tumour cells were implanted on the flanks of 27 mice. Once tumours reached approximately 100 mm^3

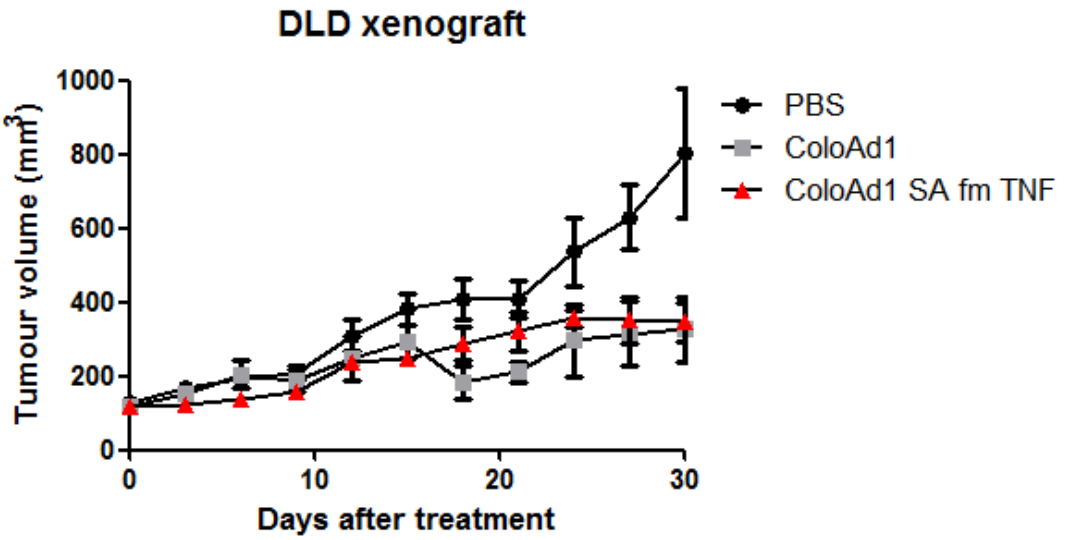

Figure 4.11: Pilot study tumour growth of DLD xenografts treated with ColoAd1 or ColoAd1 fm TNF. DLD cells were implanted on the flanks of BALB/c mice (n=9 for each group). The tumours were allowed to grow until approximately 100 mm^3. The mice were randomized into treatment groups and injected with 5 x 10^9 vp of ColoAd1 or ColoAd1 mbm TNF at day 0, day 3 and day 9, intratumourally. At day 9, day 15 and day 30, 3 mice of each group were euthanized and tumours were harvested for analysis. Mean and SEM shown.

The tumours were harvested and snap frozen on dry ice. The tumours were stored at -80°C until further processing. Using a tissue-homogenizer, the tumours were homogenized and spun at 2000 g. The supernatants were used for subsequent analysis. Using a sandwich ELISA, the levels of murine TNF were quantified. Genomic DNA extractions were done and a QPCR on the purified DNA was done to quantify viral genome copies in the tumour lysate. Additionally, an ELISA for TNF levels within the tumours was done, see figure 4.13.

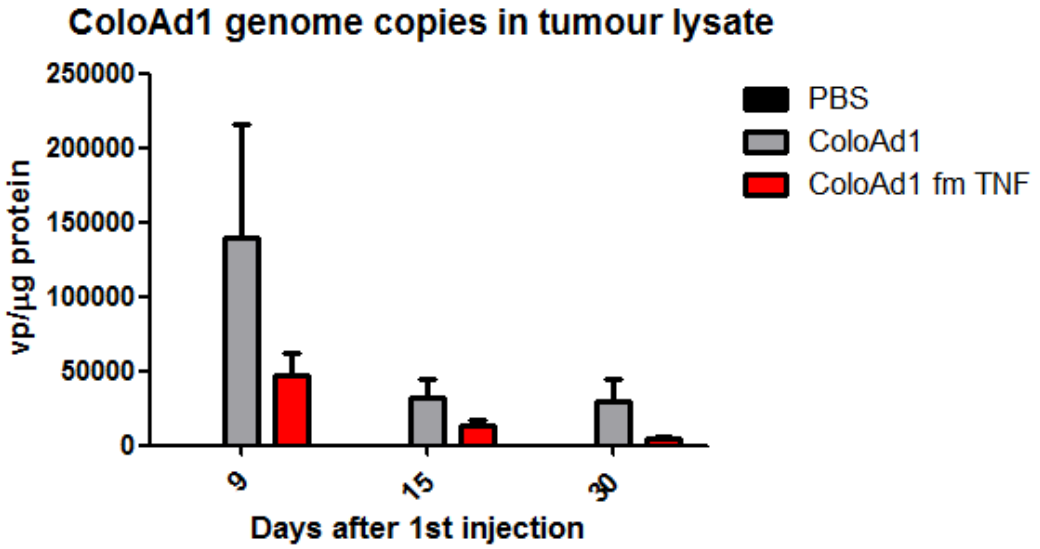

Figure 4.12: Viral genome copies in the tumour lysate at day 9, 15 and 30. Mice bearing DLD tumours were injected with PBS or $5x10^9$ vp ColoAd1 or ColoAd1 fm TNF on day 0, day 3 and day 6. Mice were euthanized at day 9, day 15 and day 30 (n=3 for each group). Viral genome copies were detected using a QPCR and the results were normalized to protein content of the tumour lysate. Mean and SEM are shown.

As can be seen in figure 4.12, ColoAd1 levels drop off quickly between day 9 and day 15. Interestingly, the ColoAd1 levels between day 15 and day 30 are very similar, suggesting a persistent infection. The ColoAd1 fm TNF levels reduced compared to ColoAd1. Furthermore, the levels of ColoAd1 fm TNF seem to decrease between day 15 and day 30, suggesting that arming ColoAd1 with TNF may increase viral clearance.

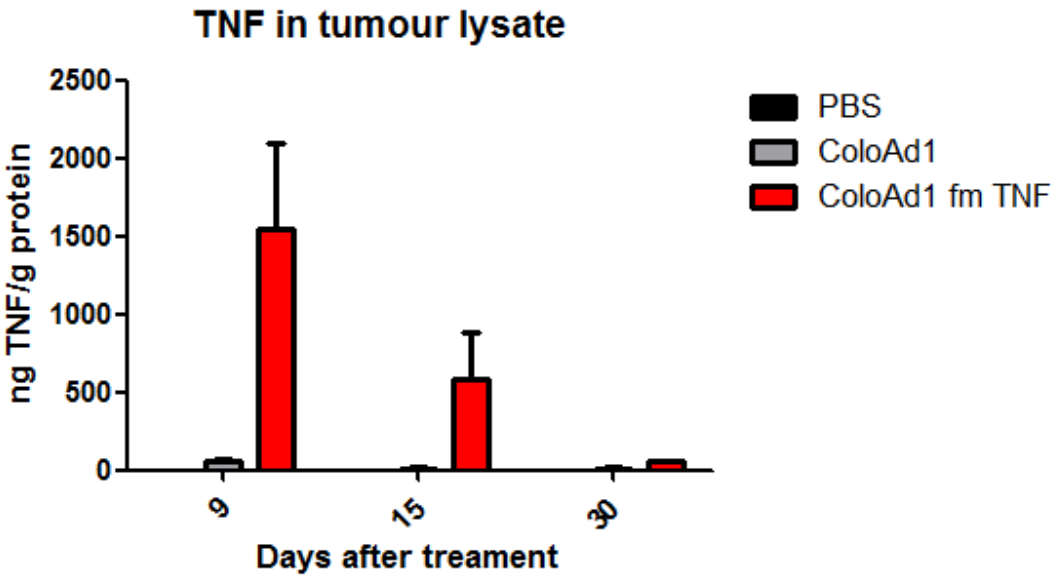

Figure 4.13: TNF protein expression in the tumour lysate at day 9, 15 and 30. Mice bearing DLD tumours were injected with PBS or $5x10^9$ vp ColoAd1 or ColoAd1 fm TNF on day 0, day 3 and day 6. Mice were euthanized at day 9, day 15 and day 30 (n=3 for each group). A sandwich ELISA was done to quantify TNF protein in the tumour lysate and the expression was normalized to protein content of the tumour lysate. Mean and SEM are shown.

As can be seen in figure 4.13, TNF levels are high 3 days after the last injection with ColoAd1 fm TNF (day 9) and these levels drop off quickly over time, with approximately 3-fold reduction in TNF levels between day 9 and day 15.

4.4.3.3 DLD Tumour Growth study

To assess the effects of ColoAd1 fm TNF and ColoAd1 mbm TNF on DLD tumour growth, 50 female BALC/c nude mice were injected with 5 $x10^6$ cells subcutaneously. To reduce variability, the mice bearing the 10 per cent largest tumours and 10 per cent smallest tumours were excluded from this study. After exclusion, 37 mice were divided between the PBS (n=9), ColoAD1 (n=9), ColoAd1 fm TNF (n=9), ColoAd1 mbm TNF (n=10) once their tumours reached approximately 100 mm^3. Mice were injected with 5 x 10^9 vp or PBS at day 0, day

3 and day 6. Mice were kept until the tumours reached 1200 mm^3, or until they developed an ulcer (ColoAd1, n=1; ColoAd1 fm TNF n=3, ColoAd1 mbm TNF n=2) or when they lost more than 15 per cent body weight for more than 72 h (PBS n=1; ColoAd1 mbm TNF n=1).

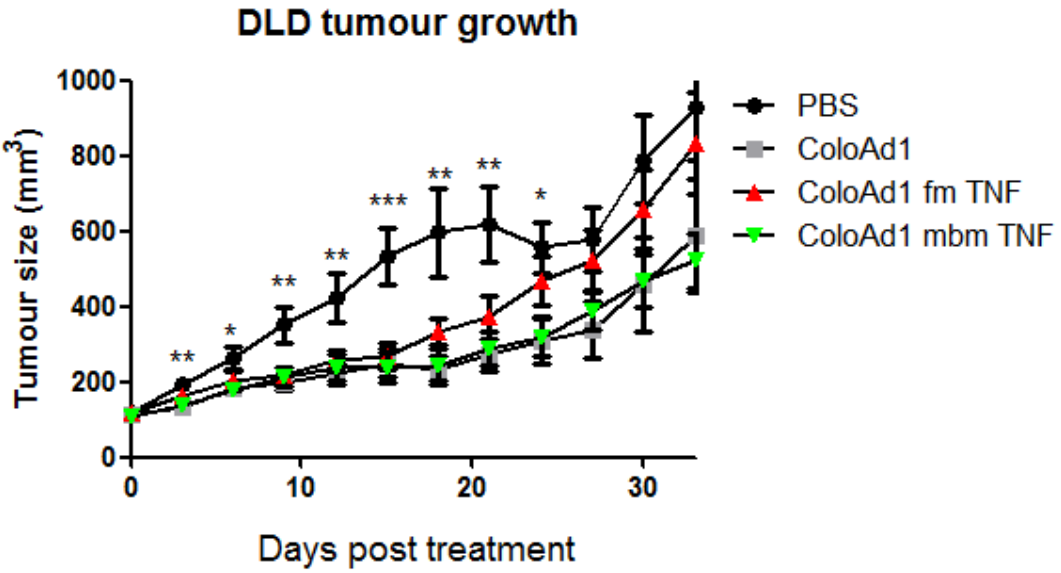

Figure 4.14: Effects of ColoAd1 and ColoAd1 mTNF on DLD xenograft tumour growth. DLD cells were implanted subcutaneously on the flanks of BALB/c mice. Tumours were allowed to grow until approximately 100 mm^3. Subsequently, PBS (n=9), ColoAd1 ($5x10^9$ vp; n=9), ColoAd1 fm TNF ($5x10^9$ vp; n=9) or ColoAd1 mbm TNF ($5x10^9$ vp; n=10) was injected at day 0, 3 and 6, intratumourally. Tumour size was measured every 3 days. At day 33, more than 50 per cent (n=5) of the PBS mice were euthanized due to tumour size. A 1-way ANOVA was performed for each time point to assess statistical significance. *=p<0.05, **=p<0.01. Mean and SEM are shown.

At each time point, a 1-way ANOVA, followed by a Bonferroni multiple comparison post test was done to assess statistically significant differences in tumour growth.

PBS mice had statistically significant larger tumour burden than the ColoAd1, ColoAd1 fm TNF and ColoAd1 mbm TNF mice. No statistically significant differences in tumour size were found between the ColoAd1, ColoAd1 fm TNF or ColoAd1 mbm TNF mice at any time.

Concurrent with the decreased tumour growth, a slight increase in survival was seen in mice treated with ColoAd1, however survival analysis showed the difference was not statistically significant (p=0.0626).

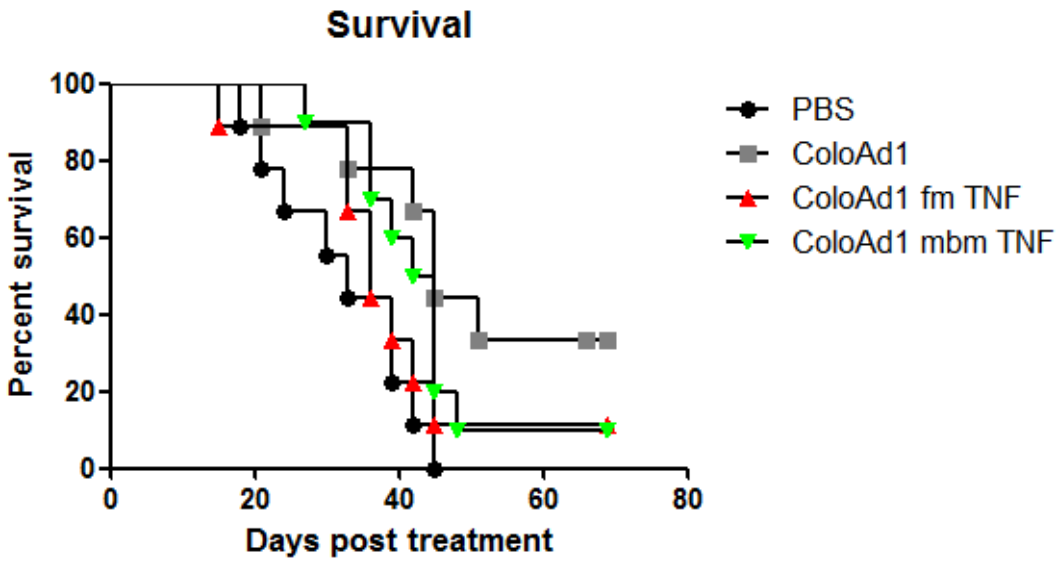

Figure 4.15: Effects of ColoAd1 and ColoAd1 mTNF on animal survival. DLD cells were implanted subcutaneously on the flanks of BALB/c mice. Tumours were allowed to grow until approximately 100 mm^3. Subsequently, PBS (n=9; black), ColoAd1 ($5x10^9$ vp; n=9; grey), ColoAd1 fm TNF ($5x10^9$ vp; n=9; red) or ColoAd1 mbm TNF ($5x10^9$ vp; n=10; green) was injected at day 0, 3 and 6, intratumourally. Survival was assessed as time until reaching humane endpoints, including tumour size more than 1200 mm^3 or ulceration of tumours. Survival was analysed using Log-rank (Mantel Cox) analysis. A borderline not significant (p=0.0626) increase in survival was observed.

An important indicator for health is the body weight of mice. Additionally, TNF is known to cause weight loss in both humans and mice. The body weight of mice was assessed every 3 days. Using a 1-way ANOVA, no statistically significant differences were found between treatment groups.

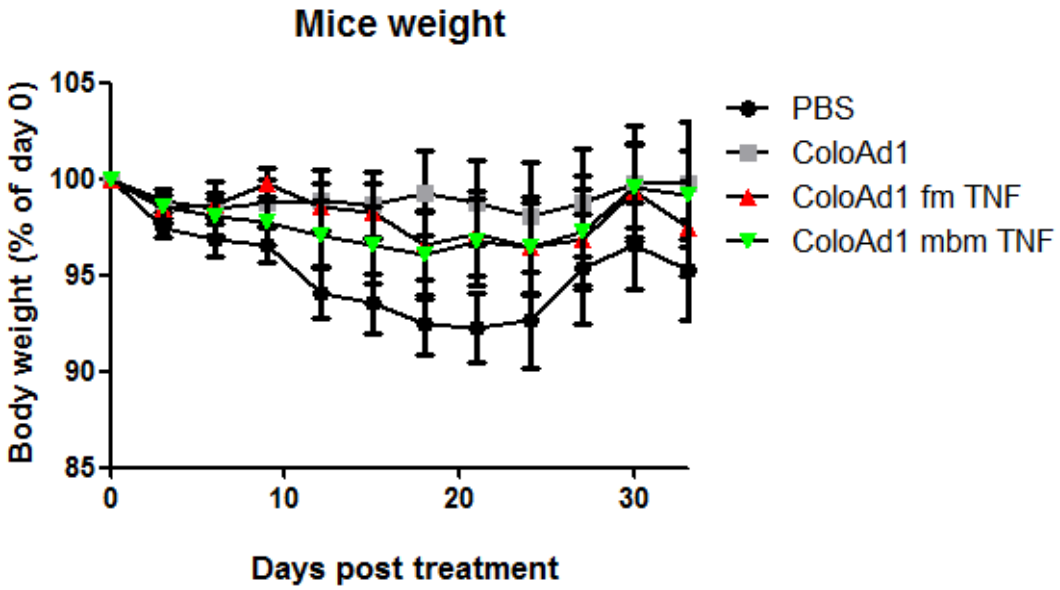

Figure 4.16: The body weight of mice treated with ColoAd1 or ColoAd1 mTNF. The body weight is expressed as a percentage of the last pre treatment measurement (day 0). PBS (n=9; black), ColoAd1 ($5x10^9$ vp; n=9; grey), ColoAd1 fm TNF ($5x10^9$ vp; n=9; red) or ColoAd1 mbm TNF ($5x10^9$ vp; n=10; green) was injected at day 0, 3 and 6. Body weight was measured every 3 days. At day 33, more than 50 per cent (n=5) of the PBS mice were euthanized due to tumour size. A 1-way ANOVA was performed for each time point to assess statistical significance. No statistically significant differences were found.

Interestingly, the PBS mice had lower body weights than the ColoAd1, ColoAd1 fm TNF and ColoAd1 mbm TNF mice, although this difference was not statistically significant. A possible explanation for the lower body weight is the higher tumour burden PBS mice had compared to the virus treated groups. A significant correlation between body weight and tumour burden was found between tumour burden and body weight in mice at day 18, see figure 4.17. At day 18, the first PBS mouse was put down due to tumour size.

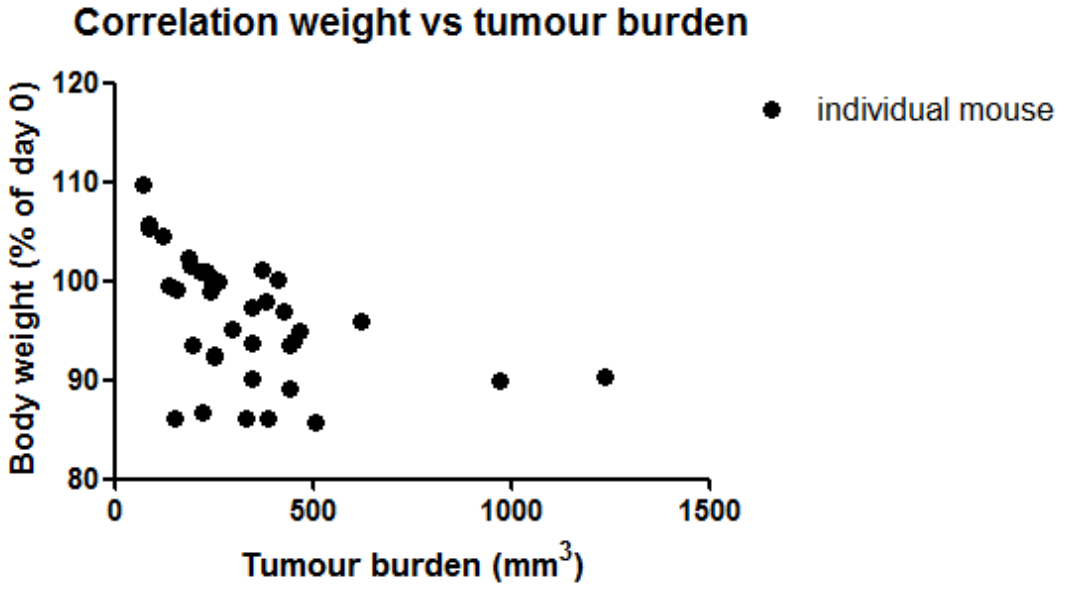

Figure 4.17: The negative correlation between body weight and DLD tumour burden. Body weight (normalized to the last pre-treatment measurement; day 0) plotted against tumour burden of each individual mouse at day 18. Using a Spearman correlation test, a highly significant correlation between tumour burden and body weight was found (p=0.0004).

To test whether arming ColoAd1 with TNF influenced viral replication, a QPCR for viral genome copies was done, see figure 4.18.

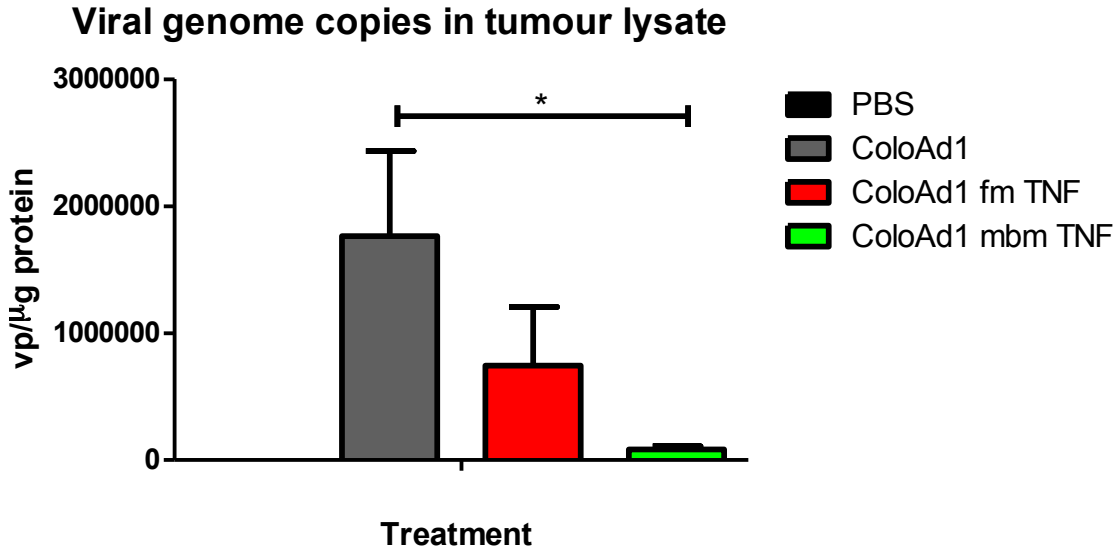

Figure 4.18: Long-term viral genome copies in the tumour lysate. DLD cells were implanted subcutaneously on the flanks of BALB/c mice. Tumours were allowed to grow until approximately 100 mm^3. Subsequently, PBS (n=9; black), ColoAd1 ($5x10^9$ vp; n=9; grey), ColoAd1 fm TNF ($5x10^9$ vp; n=9; red) or ColoAd1

mbm TNF ($5x10^9$ vp; n=10; green) was injected at day 0, 3 and 6, intratumourally. Mice were euthanized when tumours reached 1200 mm^3 or when ulceration occurred. Tumours were harvested and homogenized. Viral genome copies were analysed using QPCR and normalized to protein concentration. Using a 1-way ANOVA, statistically significance was found. Further comparisons between treatment groups were made using students T tests. A statistically significant increase in viral genome copies in ColoAd1 mice compared to ColoAd1 mbm TNF mice was found. Mean and SEM are shown. *=$p<0.05$

To analyse TNF levels within the tumour at the time of euthanized, an ELISA was done, see figure 4.19. In concurrence with the lower amount of viral genome copies in the tumour in ColoAd1 mbm TNF treated mice compared to mice treated with ColoAd1 fm TNF, lower TNF levels were seen in tumours of mice treated with ColoAd1 mbm TNF.

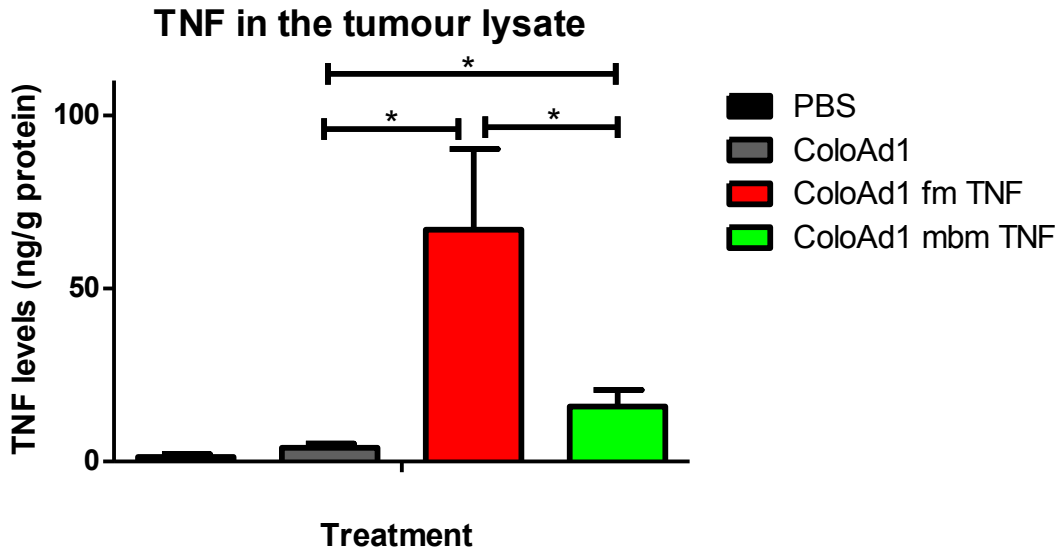

Figure 4.19: Long-term TNF expression in the DLD tumour lysate. DLD cells ($5x10^6$) were implanted subcutaneously on the flanks of nude BALB/c mice. Tumours were allowed to grow until approximately 100 mm^3. Subsequently, PBS (n=9; black), ColoAd1 ($5x10^9$ vp; n=9; grey), ColoAd1 fm TNF ($5x10^9$ vp; n=9; red) or ColoAd1 mbm TNF ($5x10^9$ vp; n=10; green) was injected at day 0, 3 and 6, intratumourally. Mice were euthanized when they reached the humane endpoints and tumours were harvested at this time. TNF concentrations were measured in homogenized tumour lysate and normalized to protein concentration. Using a 1-way ANOVA a statistically significant differences were

found (p=0.0011). Further comparisons between treatment groups were made using students T tests. A statistically significant increase in TNF levels was seen in mice treated with ColoAd1 fm TNF compared to ColoAd1 mbm TNF and ColoAd1. Furthermore, an increase in TNF levels was seen in mice treated with ColoAd1 mbm TNF compared to mice treated with ColoAd1. Mean and SEM are shown. *=p<0.05.

Liver toxicity

A cardiac bleed was performed on mice at the time of euthanasia. The blood was allowed to clot at RT and spun at 2000 g to separate blood cells from the serum. The serum was stored at -80°C until further processing. Alanine aminotransferase (ALT) is normally found in low levels in the serum. The majority of ALT is in the liver, although some other organs also express ALT. Upon liver damage, ALT is released into the blood stream. TNF can induce apoptosis and necroptosis in hepatocytes, due to an upregulation in ROS (*272*).

Thus, ALT activity in the serum was quantified to assess hepatotoxicity (see materials and methods). Low levels of ALT activity were observed in the serum of most mice. However, increased levels of ALT were seen in 1 mouse treated with PBS, 2 mice treated with ColoAd1, 3 mice treated with ColoAd1 fm TNF and 1 mouse treated with ColoAd1 mbm TNF at the time of euthanasia. Using a Kruskal-Wallis test (rather than an ANOVA, due to the non-normal distribution of the data), no statistically significant (p=0.847) increase in ALT activity in the serum was detected, see figure 4.20.

Notably, murine hepatocytes do not express CD46, an important cellular entry receptor for ColoAd1. To exclude liver toxicity from ColoAd1, ColoAd1 fm TNF or ColoAd1 mbm TNF, studies using transgenic CD46 mice should be used. Additionally, TNF is expressed under a splice acceptor and will only be

expressed from cell in which the virus can replicate and thus activate the MLP. Murine cells are not permissive to human adenovirus replication and this may also decrease the liver toxicity seen in mice.

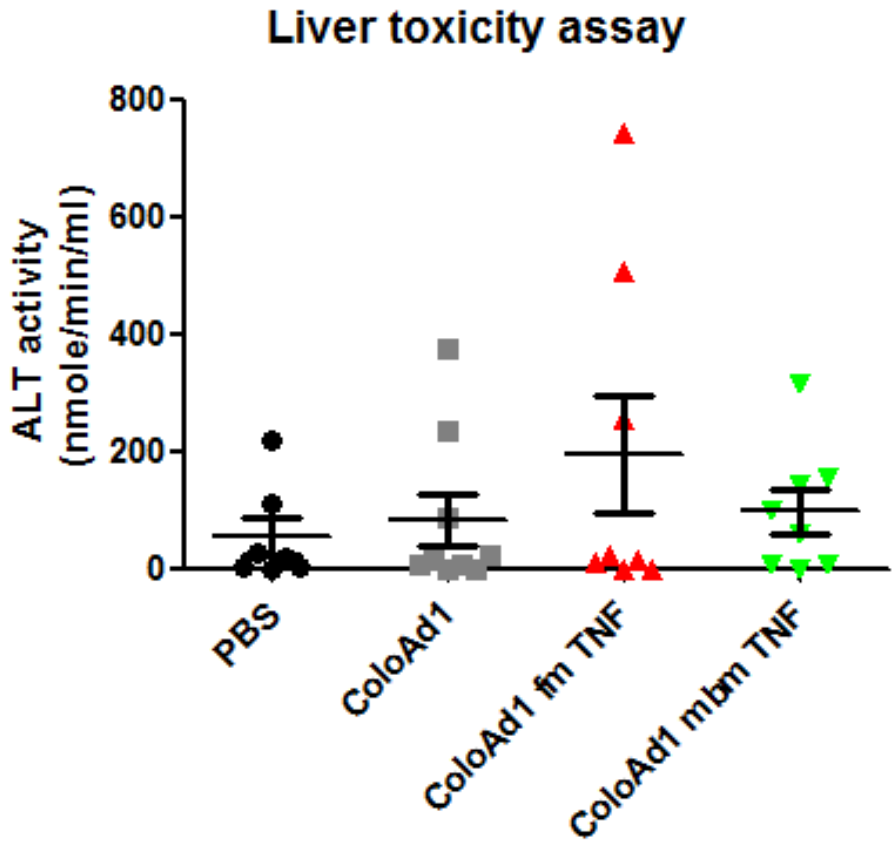

Figure 4.20: Absence of liver toxicity in ColoAd1 and ColoAd1 TNF treated mice. Once mice reached the humane endpoint, a cardiac bleed was performed. The serum was immediately isolated and the ALT activity in the serum was used as a measure for liver toxicity. Due to the non-normal distribution of the data, a Kruskal-Wallis test was performed to assess statistical significance. No statistically significant increase (p=0.847) in liver toxicity was seen between ColoAd1, ColoAd1 fm TNF, ColoAd1 mbm TNF and PBS mice.

4.4.3.4 Tumour immune infiltration

The effects of expressing TNF from ColoAd1 on innate immune cell infiltration into the tumour were studied using flow-cytometry analysis. Antibody concentrations and combinations of antibodies were optimized on BALB/c nude mice carrying DLD tumours. Once the conditions for flow-cytometry were

optimized, 47 female BALC/c nude mice were injected with 5 x 10^6 DLD cells subcutaneously. The largest and smallest 10% of tumours were excluded from flow cytometry analysis to reduce the variability. Like previous studies, mice were injected with PBS (n=10), ColoAd1 (5x 10^9 vp; n=9), ColoAd1 fm TNF (5x 10^9 vp; n=9) or ColoAd1 mbm TNF (5x 10^9 vp; n=9). Tumour growth was measured every 3 days, and at day 15, mice were euthanized and tumours were harvested for flow cytometry analysis and a small piece of the tumour was snap frozen on dry ice for protein analysis and QPCR. One ColoAd1 mbm TNF mouse was euthanized due to an ulcer before day 16.

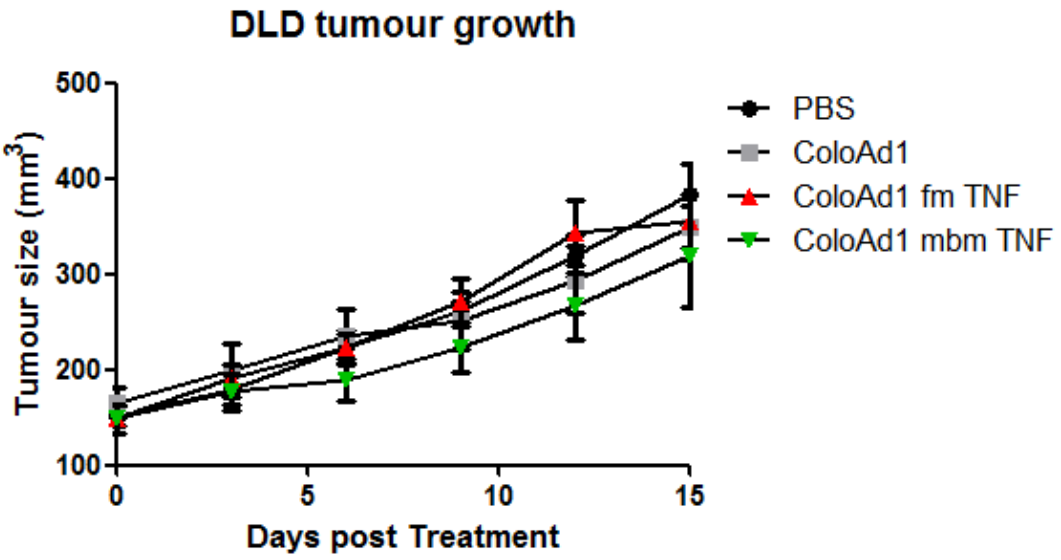

Figure 4.21: Tumour growth of DLD xenograft tumours treated with ColoAd1 or ColoAd1 mTNF for flow-cytometry. PBS (n=10), ColoAd1 (5x10^9 vp; n=9), ColoAd1 fm TNF (5x10^9 vp; n=9) or ColoAd1 mbm TNF (5x10^9 vp; n=9) was injected at day 0, 3 and 6. Tumour size was measured every 3 days. At day 26, tumours were harvested for flow cytometry analysis. A 1-way ANOVA was performed for each time point to assess statistical significance. No differences in tumour growth were seen between treatment groups. Mean and SEM are shown.

Contrary to the previous *in vivo* experiment, no effects on tumour growth were seen in the mice treated with ColoAd1 or ColoAd1 expressing TNF compared to the control PBS group.

The body weight of the mice was measured every 3 days. The body weight was normalized to the last measurement before treatment started (day 0). Similar to the DLD tumour growth experiment, no statistically significant differences were found between treatment groups, see figure 4.22.

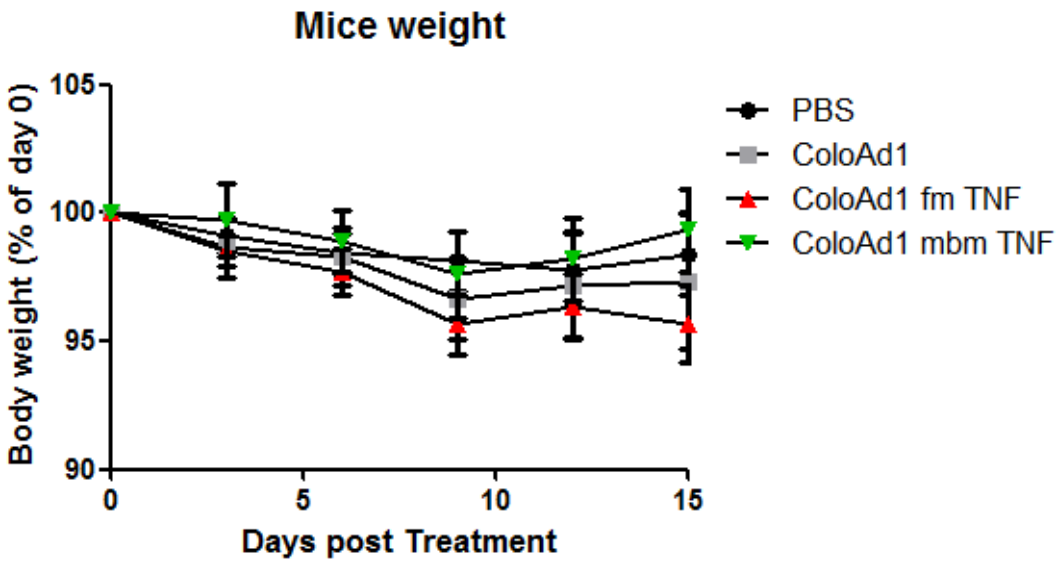

Figure 4.22: The body weight of tumour bearing mice treated with ColoAd1 or ColoAd1 mTNF. Mice were injected with DLD tumours and treated with PBS (n=), ColoAd1 ($5x10^9$ vp; n=9), ColoAd1 fm TNF ($5x10^9$ vp; n=9) or ColoAd1 mbm TNF ($5x10^9$ vp; n=10) was injected at day 0, 3 and 6, once tumours reached 100 mm^3. The body weight was measured every 3 days and expressed as a percentage of the last pre treatment measurement (day 0). A 1-way ANOVA was performed for each time point to assess statistical significance. No statistically significant differences were found. Mean and SEM shown.

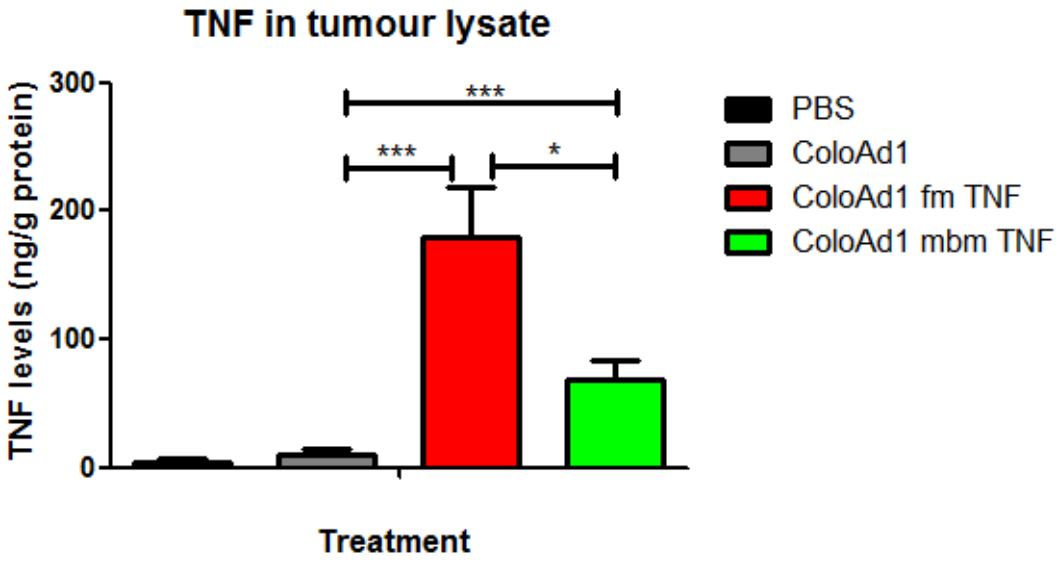

Figure 4.23: TNF levels in the DLD tumour lysate at day 16 post treatment initiation. $5x10^6$ DLD cells were injected subcutaneously on the flanks of BALB/c nude mice. Once tumours reached approximately 100 mm^3, mice were treated with PBS, ColoAd1, ColoAd1 fm TNF or ColoAd1 mbm TNF on day 0, 3 and 6. Tumours were harvested for flow-cytometry analysis at day 16 post the start of treatment. A part of the tumour was snap frozen and stored for protein analysis. Tumours were homogenized and a sandwich ELISA was performed to determine TNF protein expression and TNF levels were normalized to protein concentration of the sample. Using a 1-way ANOVA a statistically significant differences were found. Using subsequent student T-tests, higher level of TNF was found in mice treated with ColoAd1 fm TNF or ColoAd1 mbm TNF than PBS or ColoAd1 mice. Moreover a statistically significant increase in TNF levels was seen in mice treated with ColoAd1 fm TNF compared to ColoAd1 mbm TNF. Mean and SEM are shown. *=$p<0.05$, *** $p<0.001$.

Similar to expression from CT26 cells (Chapter 3) and literature, lower levels of TNF were found in mice treated with the ColoAd1 mbm virus compared to the ColoAd1 fm TNF virus.

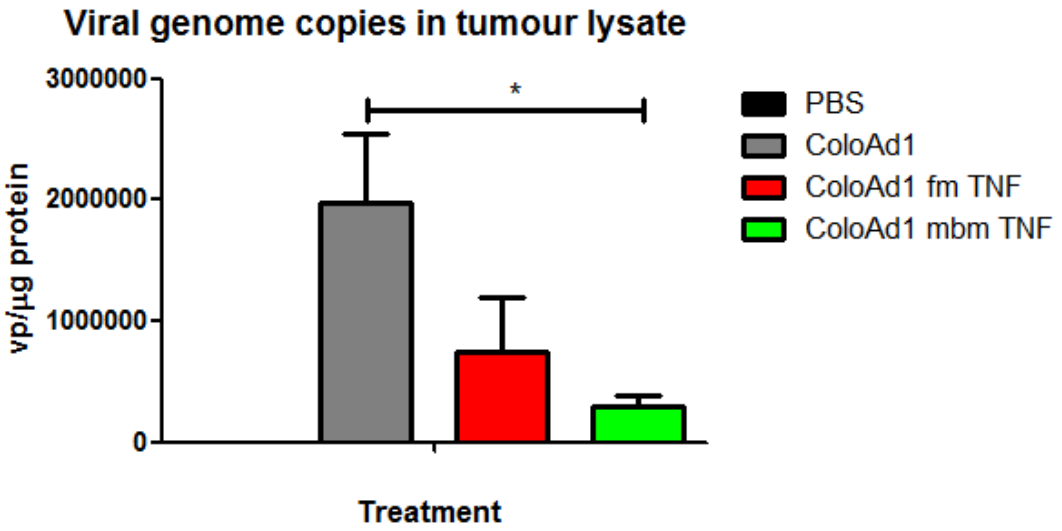

Figure 4.24: Viral genome copies in DLD tumours treated with ColoAd1 or ColoAd1 mTNF at day 16. $5x10^6$ DLD cells were injected subcutaneously on the flanks of BALB/c nude mice. Once tumours reached approximately 100 mm^3, mice were treated with PBS, ColoAd1, ColoAd1 fm TNF or ColoAd1 mbm TNF on day 0, 3 and 6. Tumours were harvested for flow-cytometry analysis at day 16 post the start of treatment. A part of the tumour was snap frozen and stored for QPCR analysis. Tumours were homogenized and a DNA extraction was performed. Viral genome copies were analysed using QPCR analysis and normalized to protein concentration. Using an 1-way ANOVA, a statistically significant difference in genome copies was found. Using a student T test, an increase in viral genome copies in ColoAd1 mice compared to ColoAd1 mbm TNF mice was found. Mean and SEM are shown. *=$p<0.05$

The largest part of the dissected tumours was used for flow-cytometry analysis. Tumours were transferred to serum-free RPMI-1640. Tumours were dissociated mechanically, followed by an enzymatic dissociation. Once dissociated, a single cell suspension was obtained by filtering the cells through a cell strainer. Cells were stained with CD45, CD11b, F4/80, CD64, CD11c, Ly6C, Ly6G and NK1.1 antibodies. The staining conditions were optimized using BALB/c nude mice bearing tumours (data not shown).

Some monocytes will also stain positively for the staining used for macrophages, CD45+, CD11b+ F4/80+. To increase the specificity for macrophage staining, CD14 was tested. Unfortunately, CD14 expression was seen during optimization. To differentiate M1 from M2 macrophages, the conventional CD86 antibody was

tested. During optimization, CD86 could not be detected in tumour infiltrating macrophages. Therefore CD64 (FcγR1) was used as a marker for M1 macrophages (*273, 274*).

A

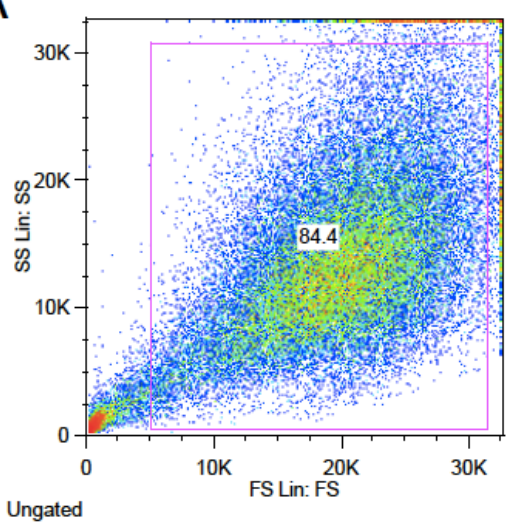
30K
20K
10K
0
SS Lin: SS
84.4
0
10K
20K
30K
FS Lin: FS
Ungated

B

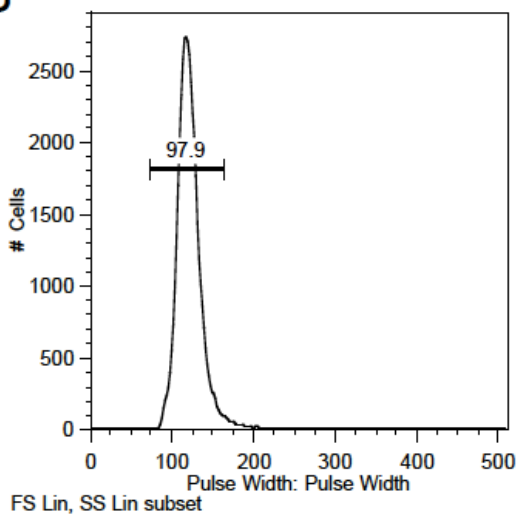
2500
2000
1500
1000
500
0
Cells
97.9
0
100
200
300
400
500
Pulse Width: Pulse Width
FS Lin, SS Lin subset

C

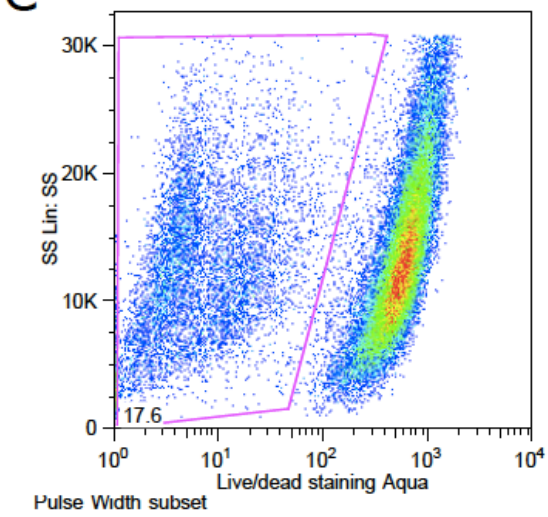
30K
20K
10K
0
SS Lin: SS
17.6
10^0
10^1
10^2
10^3
10^4
Live/dead staining Aqua
Pulse Width subset

D

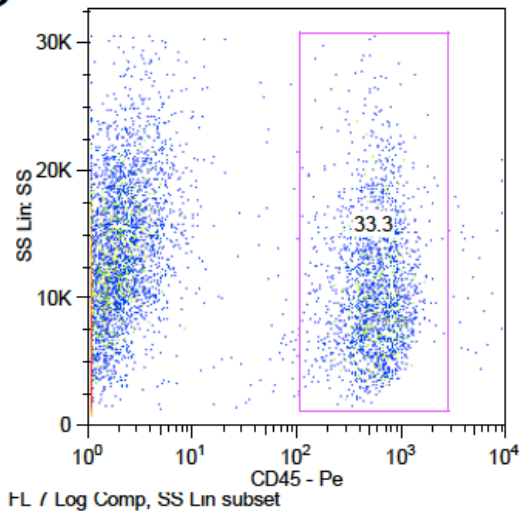
30K
20K
10K
0
SS Lin: SS
33.3
10^0
10^1
10^2
10^3
10^4
CD45 - Pe
FL 7 Log Comp, SS Lin subset

E

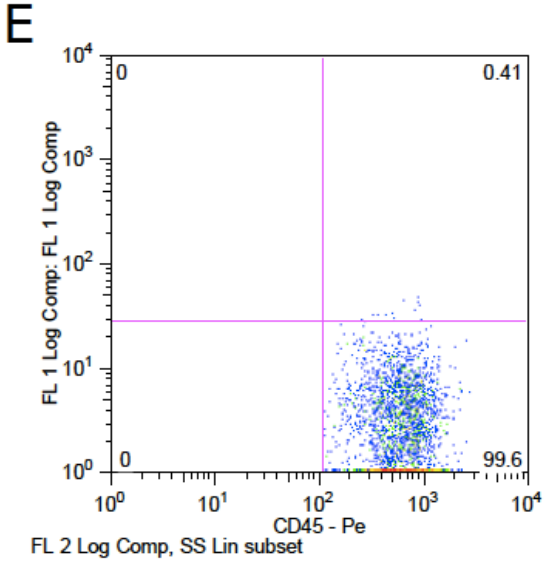
10^4
10^3
10^2
10^1
10^0
FL 1 Log Comp: FL 1 Log Comp
0
0.41
0
99.6
10^0
10^1
10^2
10^3
10^4
CD45 - Pe
FL 2 Log Comp, SS Lin subset

F

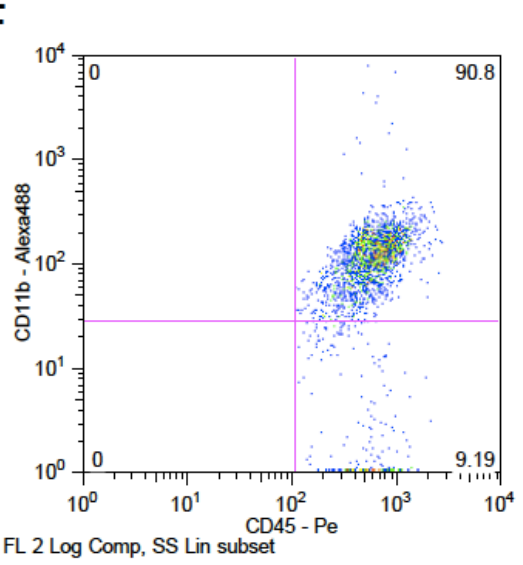
10^4
10^3
10^2
10^1
10^0
CD11b - Alexa488
0
90.8
0
9.19
10^0
10^1
10^2
10^3
10^4
CD45 - Pe
FL 2 Log Comp, SS Lin subset

G

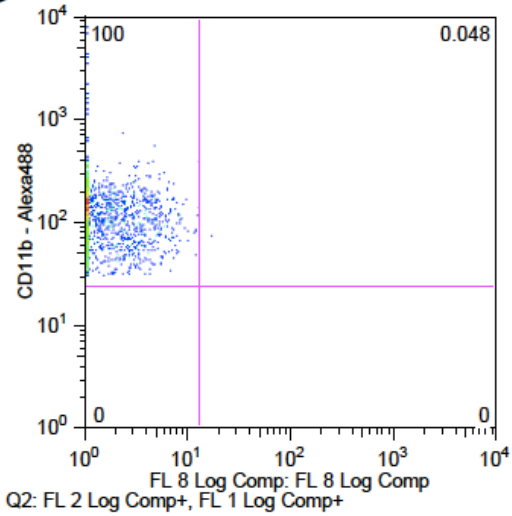
100
0.048
0
0
CD11b - Alexa488
FL 8 Log Comp: FL 8 Log Comp
Q2: FL 2 Log Comp+, FL 1 Log Comp+

H

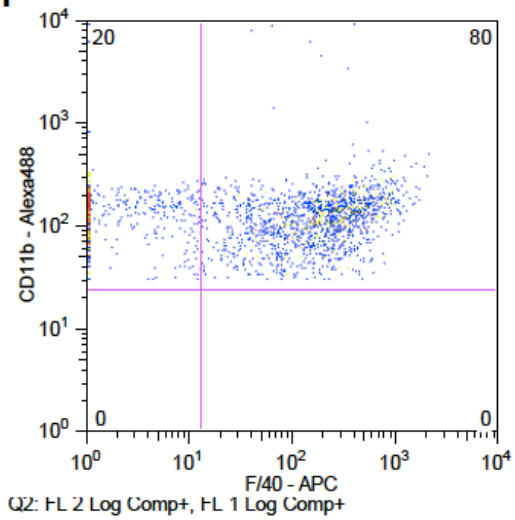
20
80
0
0
CD11b - Alexa488
F/40 - APC
Q2: FL 2 Log Comp+, FL 1 Log Comp+

I

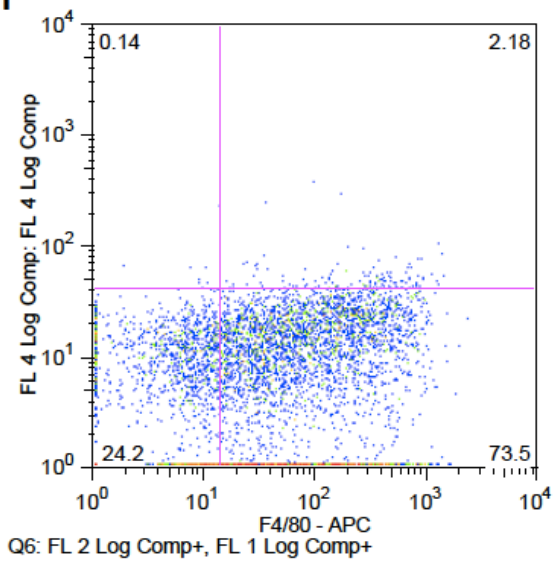
0.14
2.18
24.2
73.5
FL 4 Log Comp: FL 4 Log Comp
F4/80 - APC
Q6: FL 2 Log Comp+, FL 1 Log Comp+

J

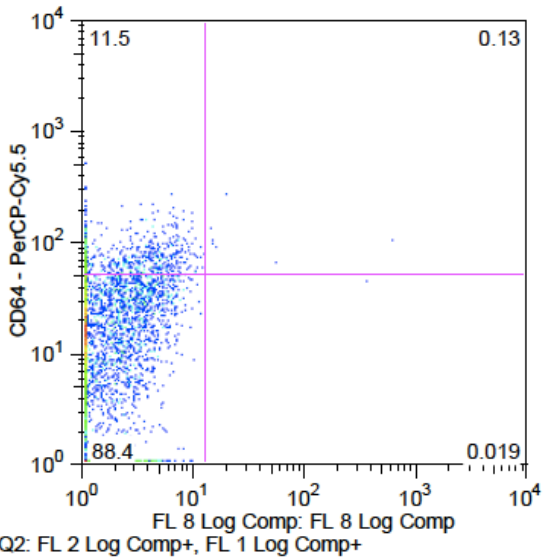
11.5
0.13
88.4
0.019
CD64 - PerCP-Cy5.5
FL 8 Log Comp: FL 8 Log Comp
Q2: FL 2 Log Comp+, FL 1 Log Comp+

K

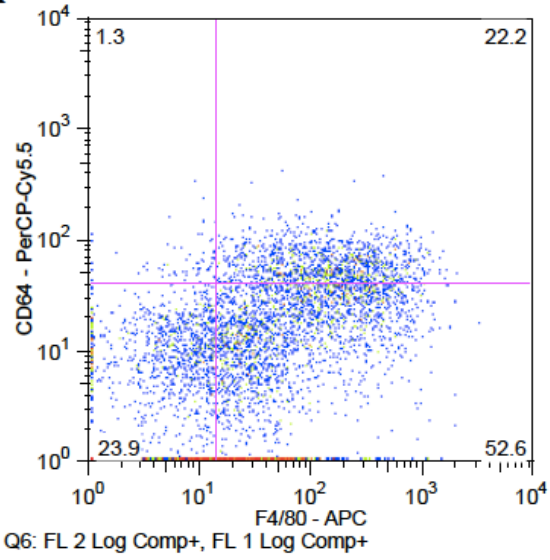
1.3
22.2
23.9
52.6
CD64 - PerCP-Cy5.5
F4/80 - APC
Q6: FL 2 Log Comp+, FL 1 Log Comp+

L

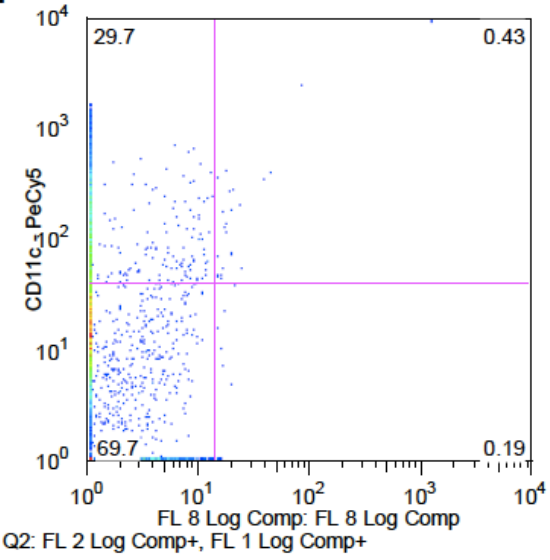
29.7
0.43
69.7
0.19
CD11c - PeCy5
FL 8 Log Comp: FL 8 Log Comp
Q2: FL 2 Log Comp+, FL 1 Log Comp+

M

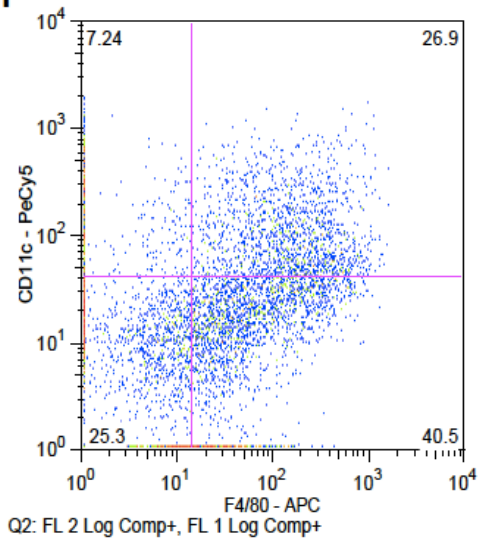
7.24
26.9
25.3
40.5
CD11c - PeCy5
F4/80 - APC
Q2: FL 2 Log Comp+, FL 1 Log Comp+

N

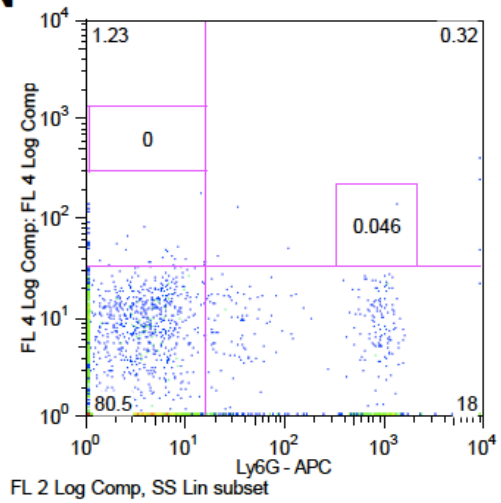
1.23
0.32
0
0.046
80.5
18
FL 4 Log Comp: FL 4 Log Comp
Ly6G - APC
FL 2 Log Comp, SS Lin subset

O

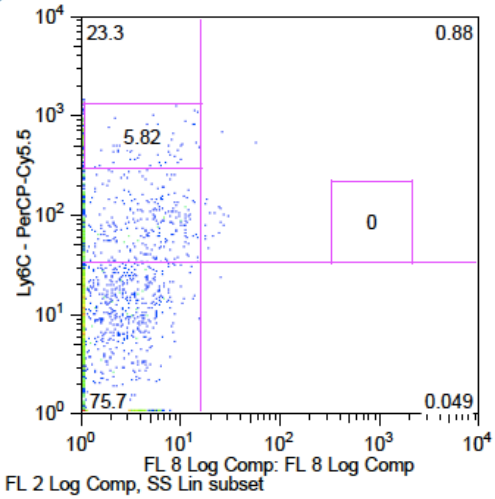
23.3
0.88
5.82
0
75.7
0.049
Ly6C - PerCP-Cy5.5
FL 8 Log Comp: FL 8 Log Comp
FL 2 Log Comp, SS Lin subset

P

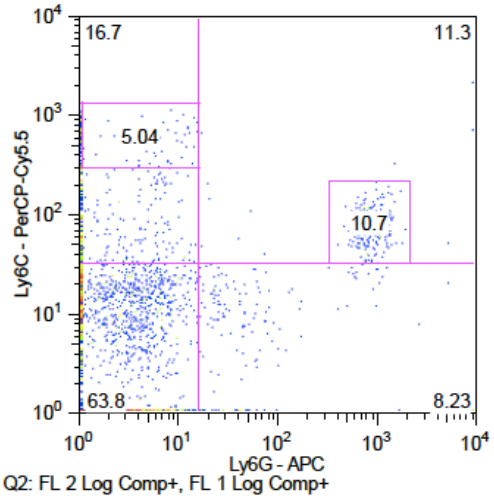
16.7
11.3
5.04
10.7
63.8
8.23
Ly6C - PerCP-Cy5.5
Ly6G - APC
Q2: FL 2 Log Comp+, FL 1 Log Comp+

Q

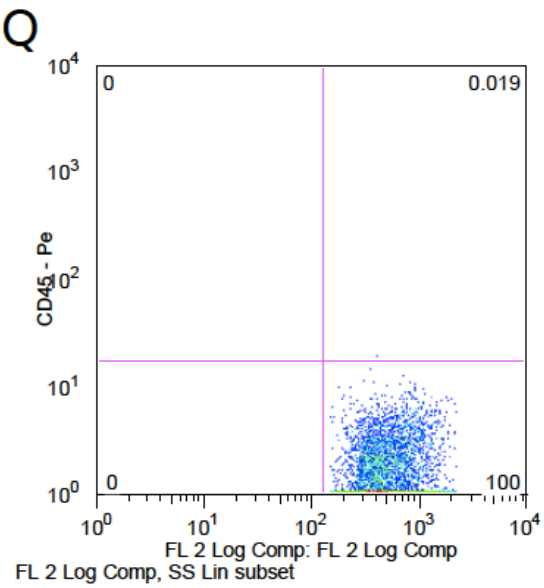
0
0.019
0
100
CD45 - Pe
FL 2 Log Comp: FL 2 Log Comp
FL 2 Log Comp, SS Lin subset

R

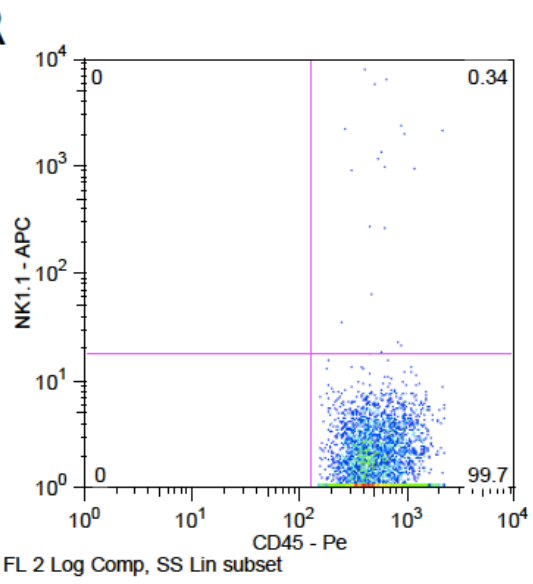
0
0.34
0
99.7
NK1.1 - APC
CD45 - Pe
FL 2 Log Comp, SS Lin subset

Figure 4.25: Flow-cytometry analysis of DLD xenograft tumours. $5x10^6$ DLD cells were injected subcutaneously on the flanks of BALB/c nude mice. Once tumours reached approximately 100 mm^3, mice were treated with PBS, ColoAd1, ColoAd1 fm TNF or ColoAd1 mbm TNF on day 0, 3 and 6. Tumours were harvested and dissociated. Cells were subsequently stained and analysed using flow-cytometry. The gating used for stained cells is shown. A: forward/side scatter plot of dissociated tumour cells; cellular debris was gated out. B: Pulse-width histogram; doublets were gated out. C: live/dead staining; live cells were gated for further analysis. D: gating of $CD45^+$ cells. E: $CD45^+$ cells. F: $CD45^+$ $CD11b^+$ gating. G: $CD45^+$ $CD11b^+$ cells. H: gating of $CD45^+$ $CD11b^+$ $F4/80^+$. I: $CD45^+$ $CD11b^+$ $F4/80^+$ stained cells: J: Gating of CD45+ $CD11b^+$ $CD11c^+$ cells. K: Gating of $CD45^+$ CD11b+ $CD11c^+$ $F4/80^-$ cells. L: $CD45^+$ $CD11b^+$ $CD64^+$ cells. M: $CD45^+$ $CD11b^+$ $F4/80^+$ $CD64^+$ cells. N: $CD45^+$ $CD11b^+$ $Ly6G^+$. O: Staining of $CD45^+$ $CD11b^+$ $Ly6C^+$. P: Gating of $CD45^+$ $CD11b^+$ $Ly6C^{high}$ $Ly6G^-$ and $CD45^+$ $CD11b^+$ $Ly6C^{low}$ $Ly6G^+$. Q: $CD45^+$ cells. R: $CD45^+$ $NK1.1^+$ cells.

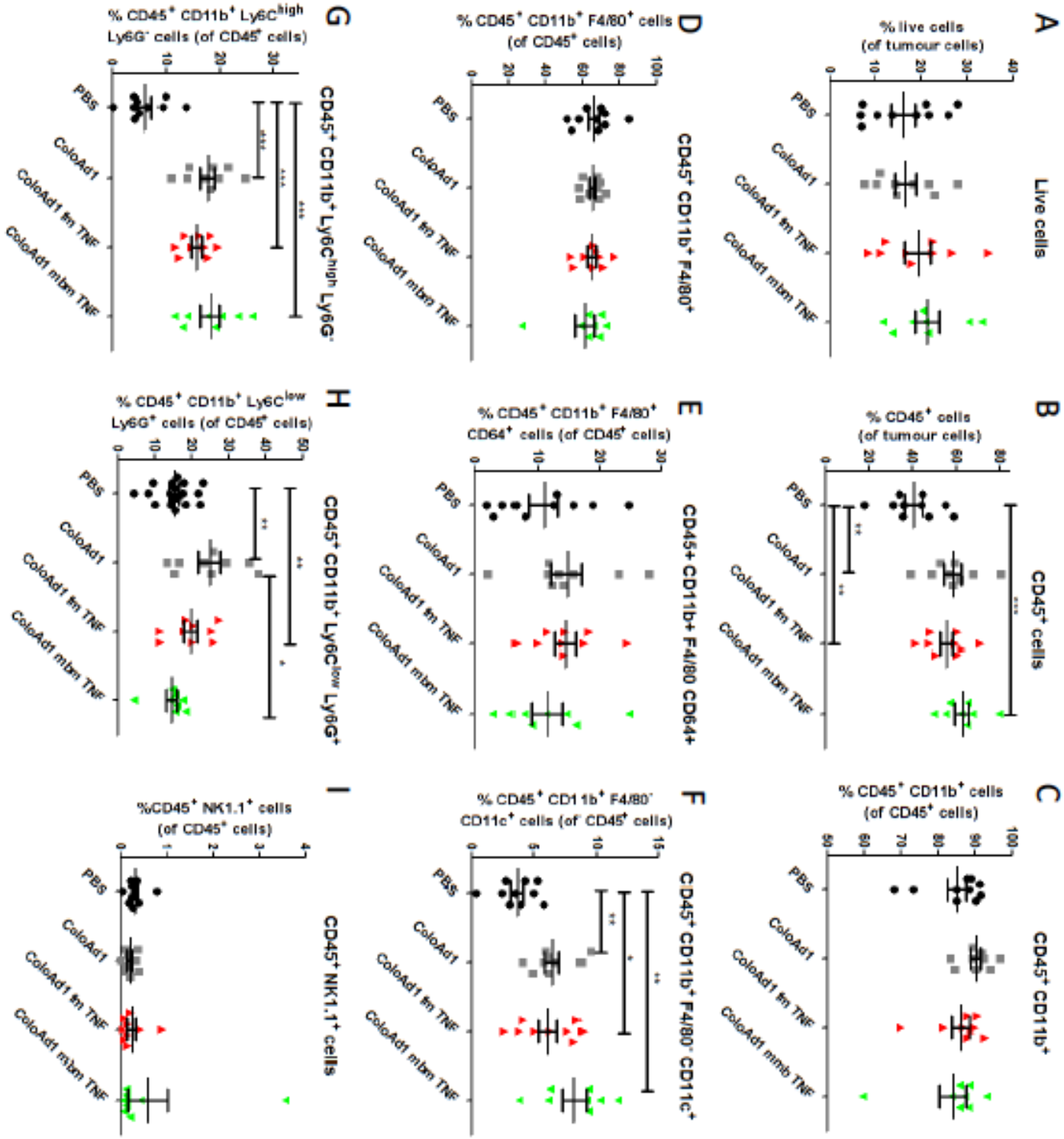

Figure 4.26: Quantification of immune infiltration in DLD tumours treated with ColoAd1 or ColoAd1 mTNF. 5x10^6 DLD cells were injected subcutaneously on the flanks of BALB/c nude mice. Once tumours reached approximately 100 mm^3, the tumours were injected with 5 x 10^9 vp ColoAd1, ColoAd1 fm TNF or ColoAd1 mbm TNF or with PBS control at day 0, 3 and 6. At day 16, tumours were harvested, dissociated and stained. Staining was analysed using flow cytometry. Analysis of live cells (A), CD45$^+$ cells (B), CD45$^+$ CD11b$^+$ cells (C), CD45$^+$ CD11b$^+$ F4/80$^+$ cells (D), CD45$^+$ CD11b$^+$ F4/80$^+$ CD64$^+$ (E), CD45$^+$ CD11b$^+$ F4/80$^-$ CD11c$^+$ (F), CD45$^+$ CD11b$^+$ Ly6C^{high} Ly6G$^-$ (G), CD45$^+$ CD11b$^+$ Ly6C^{low}

Ly6G$^+$ (H) and CD45$^+$ NK1.1+ (I) is shown. A 1-way ANOVA was done to assess statistical significance. If the $p<0.05$ in the ANOVA, separate student's t-tests were done to assess the statistical significance of differences between all the treatment groups. An increase in immune infiltration was seen in tumours treated with ColoAd1 or ColoAd1 expressing mTNF compared to PBS (B). Specifically, CD11b$^+$ F4/80$^-$ CD11c$^+$ (F) and CD45$^+$ CD11b$^+$ Ly6C^{high} Ly6G$^-$ (G) infiltration is increased in tumours treated with all viruses compared to PBS (F). Increased CD45$^+$ CD11b$^+$ Ly6C^{low} Ly6G$^+$ (H) was seen in tumours treated with ColoAd1 or ColoAd1 fm TNF compared to PBS. *=$p<0.05$, **$p<0.01$, ***$p<0.001$.

Compared to PBS, ColoAd1, ColoAd1 fm TNF and ColoAd1 mbm TNF all increased the infiltration of immune (CD45$^+$) cells. The percentage of myeloid cells (CD45$^+$ CD11b$^+$), macrophages (CD45$^+$ CD11b$^+$ F4/80$^+$), M1 macrophages (CD45$^+$ CD11b$^+$ F4/80$^+$ CD64$^+$) of all CD45$^+$ cell infiltrated in tumours is approximately equal in all mice groups. An increase in myeloid-derived DCs (CD45$^+$ CD11b$^+$ F4/80$^-$ CD11c$^+$) cells was found in ColoAd1, ColoAd1 fm TNF and ColoAd1 mbm TNF compared to PBS. An increase in monocytic MDSCs (CD45$^+$ CD11b$^+$ Ly6C^{high} Ly6G$^-$ was found in ColoAd1, ColoAd1 fm TNF and ColoAd1 mbm TNF mice compared to the PBS control group. No statistically significant differences were found between ColoAd1 or ColoAd1 expressing TNF.

Both ColoAd1 and ColoAd1 fm TNF had a statistically significant higher percentage of granulocytic MDSCs (CD45$^+$ CD11b$^+$ Ly6C^{low} Ly6G$^+$) compared to PBS. Tumours treated with ColoAd1 also had significantly more granulocytic MDSCs than tumours treated with ColoAd1 mbm TNF. As ColoAd1 causes an increase in granulocytic MDSCs compared to PBS, the reduced levels of reduced levels of viral genome copies found in tumours from mice treated with ColoAd1 mbm TNF compared to ColoAd1 are the cause of the lower infiltration of granulocytic MDSCs in ColoAd1 mbm TNF tumours. Alternatively, the presences

of membrane-bound TNF may reduce granulocytic MDSCs, either by reducing tumour infiltration or increasing cell death.

One ColoAd1 mbm TNF spleen was excluded from the analysis due to human error during the staining process.

.

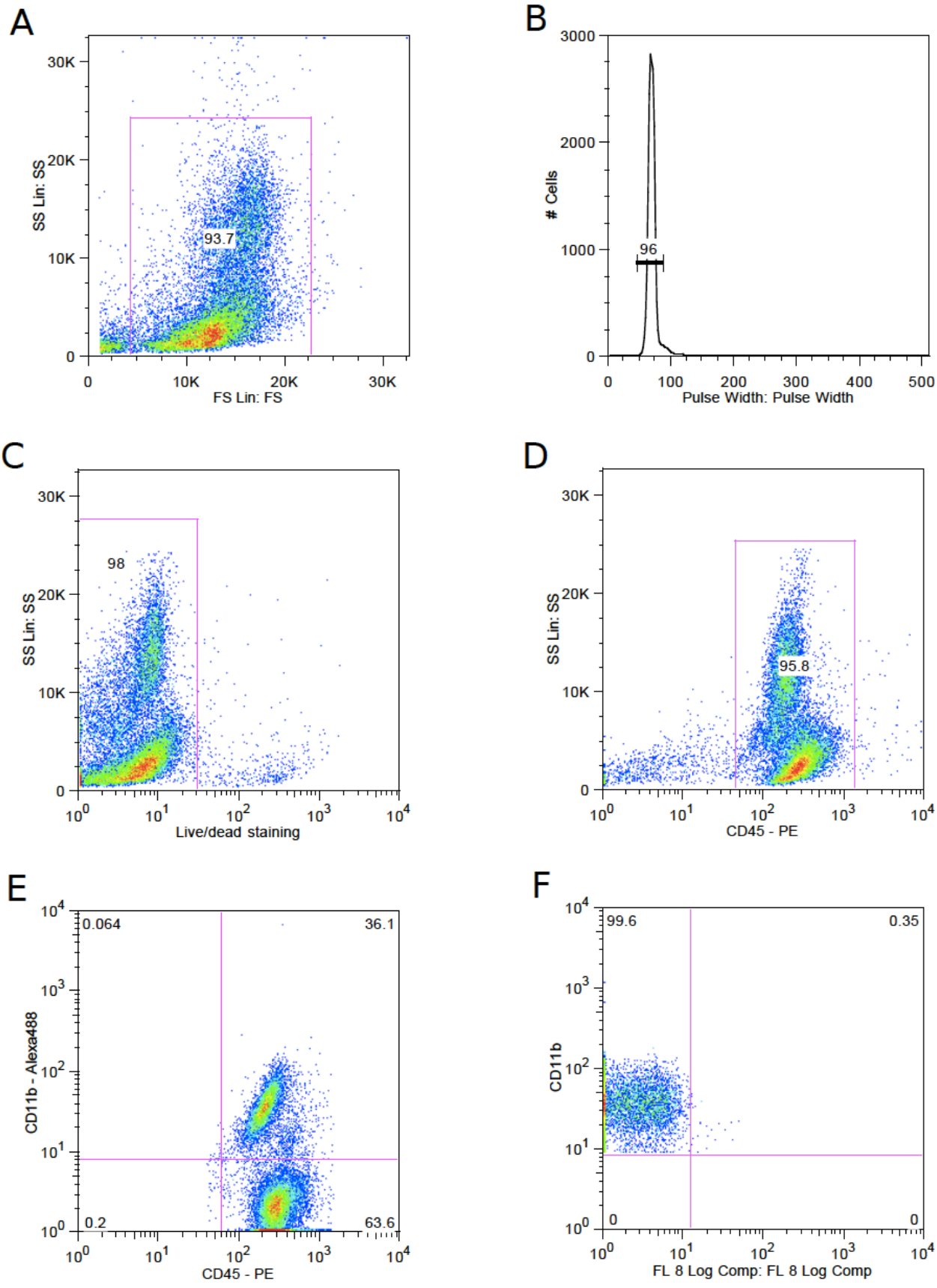
A
SS Lin: SS
FS Lin: FS
93.7
B
Cells
Pulse Width: Pulse Width
96
C
SS Lin: SS
Live/dead staining
98
D
SS Lin: SS
CD45 - PE
95.8
E
CD11b - Alexa488
CD45 - PE
0.064
36.1
0.2
63.6
F
CD11b
FL 8 Log Comp: FL 8 Log Comp
99.6
0.35
0
0

G

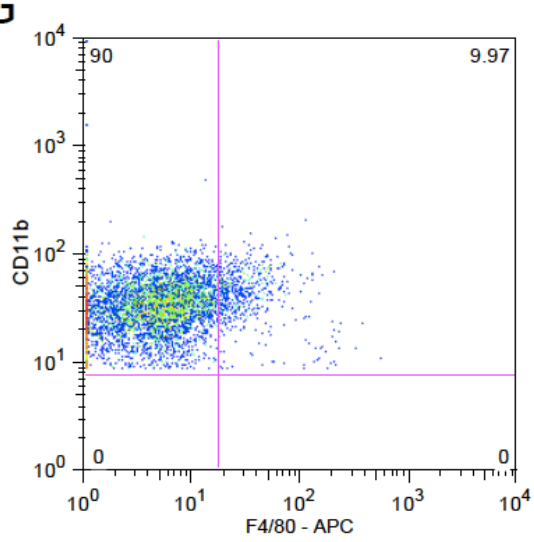
90
9.97
0
0
CD11b
F4/80 - APC

H

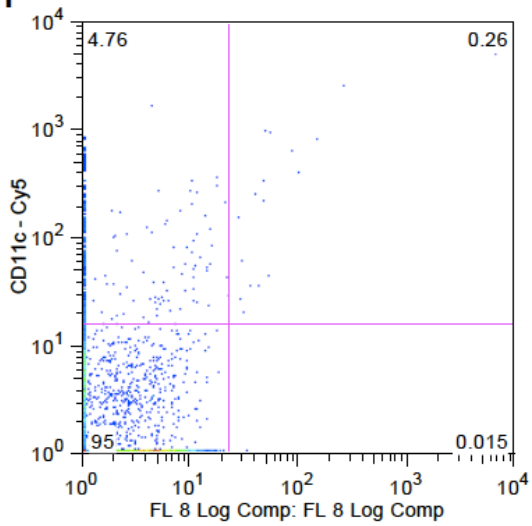
4.76
0.26
95
0.015
CD11c - Cy5
FL 8 Log Comp: FL 8 Log Comp

I

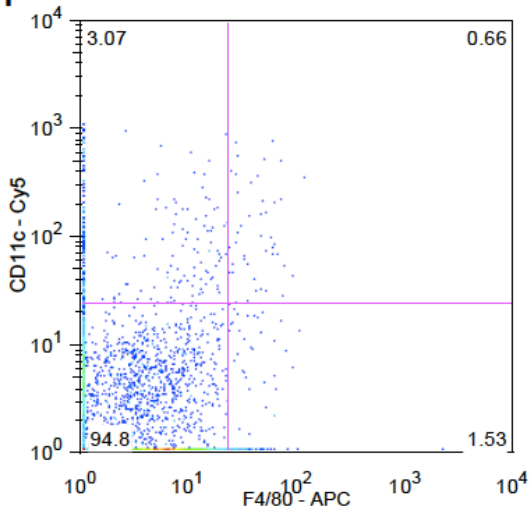
3.07
0.66
94.8
1.53
CD11c - Cy5
F4/80 - APC

J

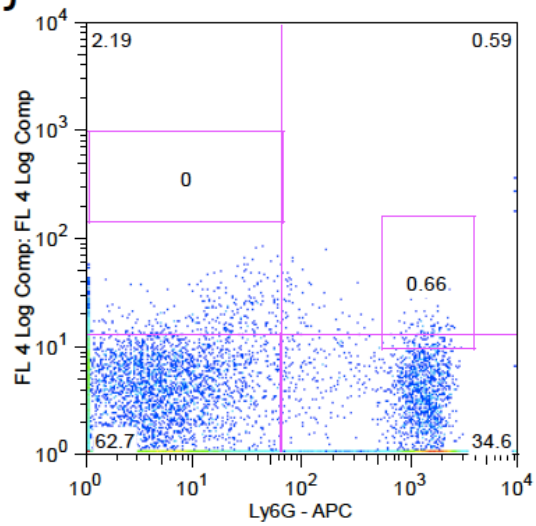
2.19
0.59
0
0.66
62.7
34.6
FL 4 Log Comp: FL 4 Log Comp
Ly6G - APC

K

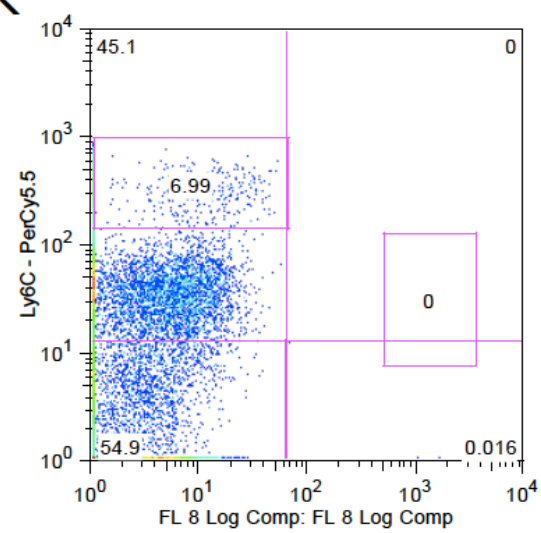
45.1
0
6.99
0
54.9
0.016
Ly6C - PerCy5.5
FL 8 Log Comp: FL 8 Log Comp

L

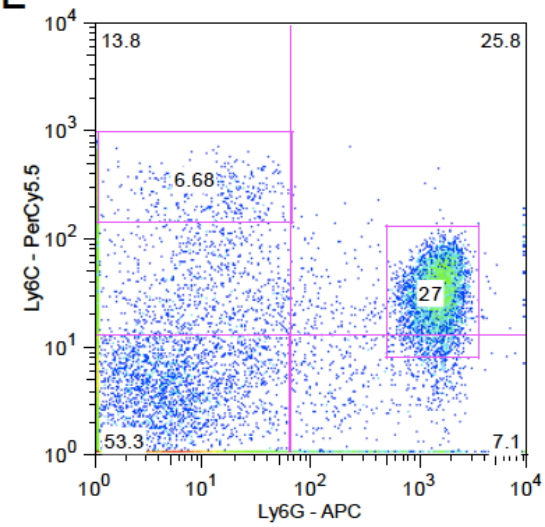
13.8
25.8
6.68
27
53.3
7.1
Ly6C - PerCy5.5
Ly6G - APC

Figure 4.27: Flow-cytometry on splenocytes of mice bearing DLD tumours. $5x10^6$ DLD cells were injected subcutaneously on the flanks of BALB/c nude mice. Once tumours reached approximately 100 mm^3, tumours were injected with 5 x 10^9 vp ColoAd1, ColoAd1 fm TNF or ColoAd1 mbm TNF or with PBS control at day 0, 3 and 6. At day 16, tumours were harvested, dissociated and stained. Splenocytes were gated based on Forward and Side scatter (A). Doublets were excluded based on pulse width (B). Live/dead staining on splenocytes (C). $CD45^+$ were gated (D). $CD45^+$ $CD11b^+$ cells were gated (E). $CD45^+$ $CD11b^+$ cells and gating (F). $CD45^+$ $CD11b^+$ $F4/80^+$ cells (G). $CD11b^+$ $CD11b^+$ cells were gated. $CD11b^+$ $CD11c^+$ $F4/80^+$ staining (H). I: $Ly6G^+$ cells. J: $Ly6C^{high.}$ K: $CD11b^+$ $Ly6G^+$ $Ly6C^{high}$.

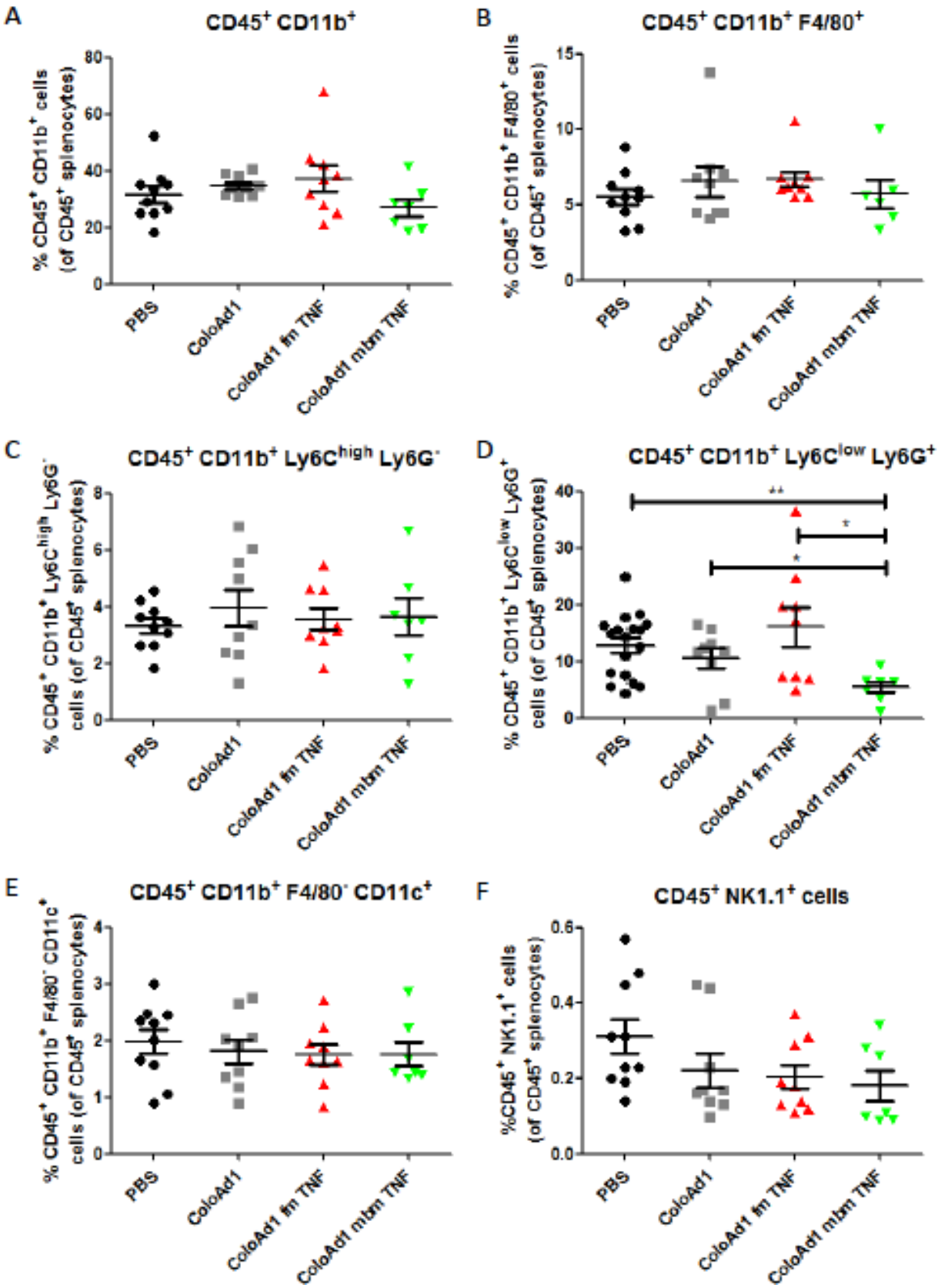

Figure 4.28: Quantification of flow-cytometry on splenocytes of mice bearing DLD tumours. Mice were treated on day 0, day 3 and day 6 with PBS or 5 x 10^9 vp ColoAd1, ColoAd1 fm TNF or ColoAd1 mbm TNF, i.t.. Spleens were harvested at day 16 and dissociated and stained. Analysis was done for $CD45^+$ $CD11b^+$ (A), $CD45^+$ $CD11b^+$ $F4/80^+$ (B), $CD45^+$ $CD11b^+$ $Ly6C^{high}$ $Ly6G^-$ (C), $CD45^+$ $CD11b^+$ $Ly6C^{low}$ $Ly6G^+$ (D), $CD45^+$ $CD11b^+$ $F4/80^-$ $CD11c^+$ (E) or $CD45^+$ $NK1.1^+$ (F)

populations. The data is represented as the percentage of $CD45^+$ splenocytes with positive markers. A 1-way ANOVA was performed, followed by student's t-tests. *=$p<0.05$, **$p<0.01$

The percentage of myeloid cells, macrophages, monocytic MDSCs, dendritic cells and NK cells are not affected by treatment with ColoAd1 or TNF expressing ColoAd1. Interestingly, a statistically significant decrease in granulocytic MDSCs was seen in mice treated with ColoAd1 mbm TNF compared to PBS, ColoAd1 or ColoAd1 fm TNF.

4.4.3.5 Immunosuppressive cytokines in the tumour microenvironment

An increase in monocytic MDSC infiltration in tumours treated with ColoAd1, ColoAd1 fm TNF and ColoAd1 mbm TNF was seen. Additionally, an increase in granulocytic MDSCs was seen in mice treated with ColoAd1 and ColoAd1 fm TNF. Two very important immunosuppressive cytokines in tumours are TGF-β1 and IL-10. These cytokines can suppress pro-inflammatory cytokine production, suppress alter activation and maturation and differentiation of numerous immune cells including NK cells, DC cells, macrophages, neutrophils and cells mediating adaptive immunity (*275, 276*).

To test whether more immunosuppressive cytokines are produced in tumours treated with ColoAd1 or TNF expressing ColoAd1, a sandwich ELISA for murine TGF-β1 and IL-10 on the tumour lysate was done. The concentrations of these cytokines were normalized to protein content, using a Bradford protein assay, see figure 4.29.

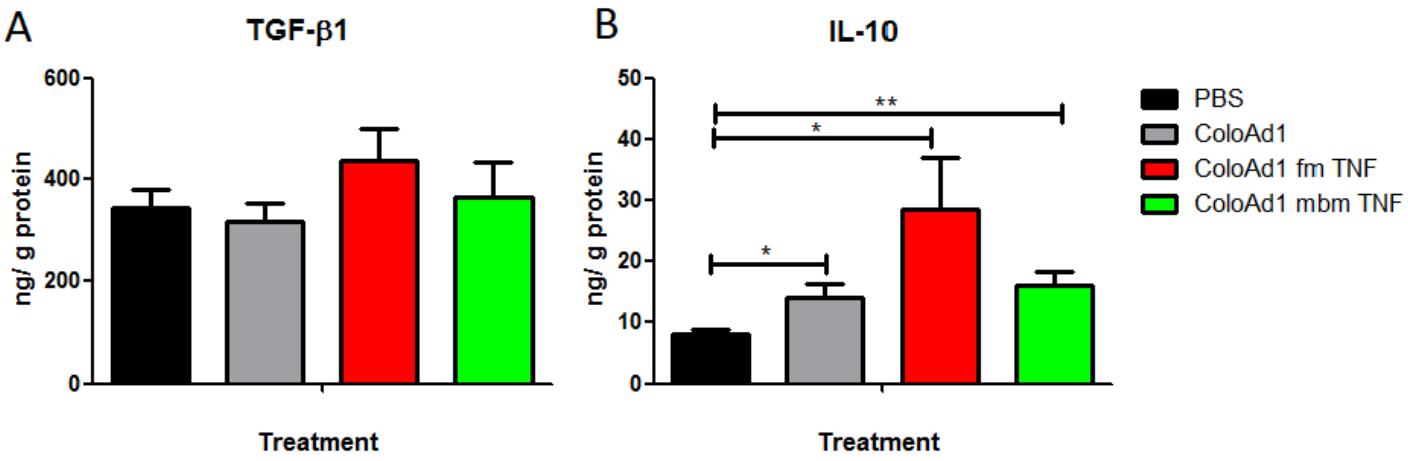

Figure 4.29: Quantification of immune suppressive cytokines in ColoAd1 or ColoAd1 mTNF treated DLD tumours. $5x10^6$ DLD cells were injected subcutaneously on the flanks of BALB/c nude mice. Once tumours reached approximately 100 mm^3, tumours were injected with 5 x 10^9 vp ColoAd1, ColoAd1 fm TNF or ColoAd1 mbm TNF or with PBS control at day 0, 3 and 6. Tumours were harvested for flow-cytometry analysis at day 16 post the start of treatment. A part of the tumour was snap frozen and stored for protein analysis. Murine TGF-β1 (A) and IL-10 (B) protein levels in the tumour lysate were quantified using a sandwich ELISA and normalized to protein content of the sample. A 1-way ANOVA was used to test for statistical significance, followed by student's tests when the ANOVA was significant. No statistically significant differences were found in TGF-β1 levels between treatment groups. A statistically significant increase in IL-10 levels was seen in tumours treated with ColoAd1, ColoAd1 fm TNF and ColoAd1 mbm TNF was seen compared to PBS. No statistically significant differences were found between ColoAd1, ColoAd1 fm TNF or ColoAd1 mbm TNF were found. Mean and SEM are shown. *=$p<0.05$, **=$p<0.01$.

As can be seen in figure 4.29, an increase in IL-10 levels was seen in ColoAd1, ColoAd1 fm TNF and ColoAd1 mbm TNF treated tumours compared to the control group. IL-10 levels were highest in mice treated with ColoAd1 fm TNF, although the increase was not statistically significant compared to ColoAd1 ($p=0.11$) or ColoAd1 mbm TNF ($p=0.16$). ColoAd1 fm TNF treated tumours also had the highest levels of TGF-β1 expression, but this difference was not statistically significant (1-way ANOVA; $p=0.3889$).

ColoAd1 fm TNF and vascular permeability

To test the influence of ColoAd1 expressing TNF, an MRI study was set up in collaboration with Dr. Stavros Melemenidis and Professor Nicola Sibson.

Briefly, mice were injected 5 x 10^9 vp ColoAd1 (n=5) or ColoAd1 fm TNF (n=6) or PBS (n=5), intratumourally, three times three days apart at the Biomedical Services, John Radcliffe Hospital. Mice were subsequently transported to the RRI for imaging. One mouse injected with ColoAd1 fm TNF was euthanized before transport to the RRI, due to ulceration of the tumour.

Based on the high levels of TNF expression seen on day 9 post the start of treatment in the pilot study (figure 4.13) a dynamic contrast enhanced (DCE) MRI scan using gandolinium was planned on this day. Due to technical failure of both the T4.7 and T9 MRI machines at the RRI, the MRI study was aborted.

To assess the effects of ColoAd1 and ColoAd1 fm TNF, 3 mice in each group were euthanized 4 days after the last i.t. injections and the tumours were harvested and snap frozen for IHC analysis. Unfortunately, due to time constraints the IHC analysis could not be included in this thesis.

To assess vascular permeability, Evans blue was injected 4 days after the last injection in the tail vein of mice (n=2 per group). Evans blue is a dye that binds to serum albumin and Evans blue extravasation can be used as a measure of vascular protein leakage. Six hours after Evans blue injection, mice were euthanized and the tumours were harvested and snap frozen on dry ice. The tumours were thawed on ice and Evans blue was extracted using formamide. The amount of Evans blue extravasation was measured by analysing the amount of Evans blue in the formamide using a spectrophotometer.

As can be seen in figure 4.30, Evans blue extravasation was highest in mice treated with ColoAd1 fm TNF, and also elevated in mice treated with ColoAd1 compared to PBS controls. Possibly due to the small group size, the differences were not statistically significant (p=0.11; analysed using a one-way ANOVA).

Inflammation causes vasodilation, increased blow flow and increased vascular permeability. The increase of Evans blue extravasation in mice treated with ColoAd1 or ColoAd1 fm TNF compared to PBS may be due to increased immune cell infiltration and inflammation in these tumours.

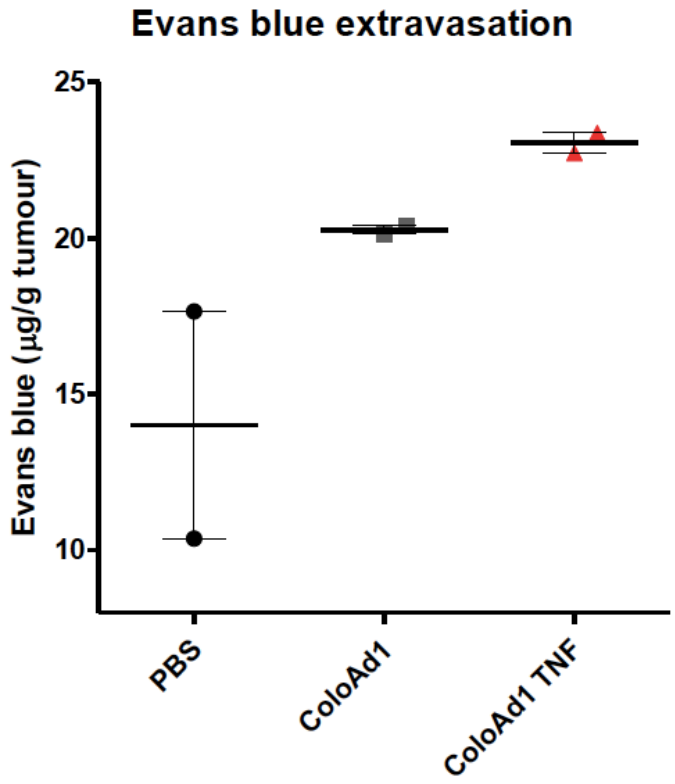

Figure 4.30: Vascular permeability of ColoAd1 or ColoAd1 fm TNF treated tumours. Mice were injected with 5 x 10^6 DLD cells subcutaneously. Tumours were allowed to grow for 21 days. Tumours were injected with 5 x 10^9 vp ColoAd1 (n=2), ColoAd1 fm TNF (n=2) or PBS (n=2) at day 0, 3 and 6. At day 10, mice were injected i.v. with 10 mg/kg Evans blue. Six hours later, mice were euthanized, tumours were harvested and Evans blue was extracted from the tumours. Evans Blue extravasation was quantified using a spectrophotometer and normalize to sample weight. An increase of Evans blue extravasation was seen in mice treated with ColoAd1 or ColoAd1 fm TNF compared to PBS. The data was analysed using a one-way ANOVA.

4.5 Discussion

ColoAd1 is a novel chimeric species B adenovirus that is currently in clinical trials for metastatic carcinoma. The work performed in this chapter sought to improve its efficacy by arming ColoAd1 with TNF and LTA.

TNF is an important cytokine during adenoviral infection and the virus expresses several proteins that can inhibit lysis by TNF during infection (*56*). Hence, before cloning TNF into the ColoAd1 virus, which has E3 deletions, TNF, the ability of ColoAd1 to infect and replicate in the presence of TNF *in vitro* was confirmed by QPCR.

Based on this QPCR study, we proceeded to clone TNF and LTA into the ColoAd1 genome, under the MLP. To the best of our knowledge, we were developing the first replication competent adenoviral vector expressing TNF. However, a paper using a replicating Ad5 virus expressing TNF was published in March 2015 (*242*). Results obtained with this virus will be discussed later in this section.

The newly cloned viruses were rescued and purified. High levels of TNF expression could be seen from ColoAd1 sm TNF, fm TNF and mbm TNF *in vitro*. Additionally, *in vivo* expression of TNF from ColoAd1 TNF viruses could be confirmed using an ELISA. Unfortunatlely, expression of mLTA from ColoAd1 was very low *in* vitro and therfore this virus was not used for further testing.

In vivo, a borderline not significant (p=0.0626) increase in survival was seen between mice treated with virus and PBS. Moreover, a statistically significant decrease in tumour growth was observed ColoAd1, ColoAd1 fm TNF and ColoAd1 mbm TNF compared to PBS. However, no statistically significant differences in tumour growth were observed between ColoAd1 and ColoAd1 fm TNF or ColoAd1 mbm TNF.

Interestingly, no weight loss was observed in mice treated with ColoAd1, ColoAd1 fm TNF or ColoAd1 mbm TNF compared to PBS mice. Weight loss is a well-known side effect of systemic TNF treatment (*260*). The absence of weight loss upon treatment with ColoAd1 suggests that local expression may reduce systemic toxicity. Additionally, no evidence of liver toxicity was found in mice treated with ColoAd1, ColoAd1 fm TNF or ColoAd1 mbm TNF compared to PBS control mice. However, it should be noted that CD46, an important receptor for Ad11p and ColoAd1 infection, is not expressed in murine liver tissue. Moreover, murine cells are not permissive for human adenovirus replication, thus transgenes under the control of the MLP will not be expressed in murine cells. Thus, the studies performed in this chapter have underestimated liver toxicity.

In the DLD xenograft tumours, treatment with ColoAd1, ColoAd1 fm TNF or ColoAd1 mbm TNF leads to increased immune infiltration compared to PBS. Specifically, the dendritic ($CD11b^+$ $F4/80^-$ $CD11c^+$), granulocytic MDSC ($CD11b^+$ $Ly6C^{low}$ $Ly6G^+$) and monocytic MDSC ($CD11b^+$ $Ly6C^{high}$ $Ly6G^-$) populations are enriched after virotherapy. Moreover, arming ColoAd1 with TNF did not lead increase in immune infiltration or alter the composition of immune infiltrates. The exact role of these cell populations in the context of oncolytic virus therapy is still contentious. Traditionally, granulocytic and monocytics MDSC are thought to contribute tumour progression (*93*). Granulocytic cells are known to induce angiogenesis, secrete matrix degrading proteins and promote tumour growth (*113, 114*). However, anti-cancer effects by neutrophils have also been reported (*116-119*). In the context of oncolytic virus therapy, neutrophils may contribute to antitumour responses. Using VSV and vaccinia virus (VV), killing of uninfected tumour cells by neutrophils was observed. Increased neutrophil infiltration was

seen in virally treated tumours and neutrophil depletion reduced apoptosis. Besides tumoricidal actions of neutrophils in this model, neutrophils also helped clear the virus as an increase in viral replication and viral spread was seen in neutrophil depleted mice (*277*). Arming an oncolytic measles virus (MV) with GM-CSF decreased tumour growth, whilst increasing $Ly6G^+$ cell infiltration in SCID mice bearing Burkitt's lymphoma tumours compared to unarmed MV. Grote et al. suggested an antitumour effect by neutrophils in this model (*278*). In this model, macrophages (Mac-3) and NK cell (CD49b) infiltration was not detected. Finally, a conditionally replicating Ad5 expressing *Helicobacter pylori* neutrophil-activating protein (HP-NAP) decreased tumour growth and increased survival compared to control virus in a neuroendocrine nude mouse model (*279*). Thus, the increase in granulocytic monocytes may increase the efficacy of ColoAd1. Studies administering ColoAd1 to neutrophil-depleted mice may help clear up the role these cells play during ColoAd1 treatment.

Besides the increase in granulocytic cell infiltration, increased infiltration of myeloid-derived DCs ($CD45^+$ $CD11b^+$ $F4/80^-$ $CD11c^+$) was observed in ColoAd1, ColoAd1 fm TNF and ColoAd1 mbm TNF tumours compared to PBS treated controls. DCs can engulf apoptotic or necrotic tumour cells and process tumour-associated antigens for presentation (*106*). Mature and fully activated DCs are crucial for inducing and maintaining an antitumoural immune response. Immature DCs and DCs not expressing co-stimulatory molecules, such as CD80 and CD86, can induce tolerance and hinder the antitumoural immunity. IL-10 has been implicated in generating tolerogenic DCs and can reduce the expression of co-stimulatory molecules and increase $CD4^+$ and $CD8^+$ T cells that suppress antigen-specific proliferation of other T cells through cell-to-cell contact (*280*). In

a mouse model, IL-10 is a major factor in DC malfunctioning (*281*). A statistically significant increase in the immunosuppressive IL-10 cytokine was observed in mice treated with ColoAd1, ColoAd1 fm TNF and ColoAd1 mbm TNF compared to control mice. The combination of increased DC infiltration and increased IL-10 levels upon ColoAd1 treatment may be detrimental to the induction of anti-tumour immunity. Further studies, combining activation and maturation markers to flow-cytometry analysis of tumour-infiltrating DCs are necessary to understand the role DCs play in ColoAd1 treatment. Additionally, it would be interseting to assess the effects of co-administering a IL-10 scavenger on these acitvation and maturation markers.

In studies performed in this chapter, arming ColoAd1 with TNF did not reduce tumour growth compared to parental ColoAd1. Studies using replicating Ad5, with an Ad3 fiber, armed with human TNF showed reduced tumour growth compared to unarmed virus in murine xenograft PC3-MM2 (prostate carcinoma) as well as in a syngeneic B16-OVA model (a melanoma cell line expressing a chicken ovoalbumin) (*242*). ColoAd1 kills has increased potency and kills many cancer cell lines faster than Ad5 does (62). Also, in the Ad5-based virus, TNF was inserterd into the E3 region, an early adenovirus gene, whereas TNF was cloned under the control of the MLP in the studies performed in this chapter. Perhaps, the relatively short timespan of TNF expression from the MLP of ColoAd1 has contributed to lack of efficacy of TNF expression from ColoAd1 compared to parental ColoAd1. Unfortunately, TNF kinetics from the Ad5-TNF virus were not reported (*242*). The kinetics of TNF expression from TNFerade has been well documented. From the pilot study data performed in this chapter, TNF levels are highest a shortly after treatment and decline over time. The highest levels of TNF

expressed *in vivo* from TNFerade (1033 ± 201 ng TNF/g protein by day 7) are similar to the levels seen in our pilot study, 3 days after the last injection (day 9) (*206*). However, using ColoAd1 expressing TNF, the levels of TNF decline after treatment, whereas an increase in TNF levels over the first week was seen with TNFerade (345 ± 179 ng human TNF/g protein by day 4) (*206*). Differences in TNF kinetics may explain why TNFerade was more efficacious than ColoAd1 espressing TNF.

A statistically significant reduction in ColoAd1 mbm TNF genome copies was found 16 days after treatment compared to ColoAd1. A reduction in ColoAd1 fm TNF genome copies, compared to ColoAd1, was also found consistently in all animal experiment, although this difference was not statistically significant. One of the major benefits of oncolytic virus therapy compared to conventional therapy is the ability of the virus to spread and replicate within the tumour. However, lack of viral spread is a major hurdle for oncolytic virus therapy (*282*). The reduced viral load in the tumours may have been a major contributor to the lack of efficacy seen by arming ColoAd1 TNF compared to ColoAd1. The reduction in viral genome copies seen in tumours treated with ColoAd1 mbm TNF may be due to increased virual clearance or due to reduced viral replication.

ColoAd1 has deletions in the E3 region. Human adenoviruses encode several proteins that help evade the host's immunity in the E3 region (*49*). In species C adenovirus, the 17.K E3 protein inhibits cell lysis by TNF in adenovirus infected cells (*56*). However, in human cancer cell lines, the E1B-19K protein can protect from lysis by TNF when infected with Ad5 virus lacking E3 (*59*). In *in vitro* studies performed in this chapter, viral replication of ColoAd1 did not seem

impaired by adding TNF to HT29 cells. However, perhaps the deletions in the E3 region may have led to increased viral clearance or decreased replication in ColoAd1 TNF *in vivo*. This is further discussed in chapter 6.3.

Although not statistically significant, the increase in Evans blue extravasation suggests that ColoAd1 and ColoAd1 fm TNF may increase vascular permeability of the tumours, compared to PBS control. A study using a larger group size is necessary to confirm the effects of the virus on vascular permeability, preferably by using DCE-MRI. The suspected increase of vascular permeability may be due to the inflammatory response to these viruses. The inability of drugs to penetrate the tumour and reach all viable cells can contribute to failure of therapy (*201*). An increase in vascular permeability may help to increase drug delivery to tumour sites and combination of ColoAd1 or ColoAd1 fm TNF may synergize with chemotherapy.

4.5.1 Limitations

One of the major limitations in *in vivo* work with human adenoviruses is the host-specific nature of the virus. Murine cells are not permissive for adenovirus replication. Due to this non-permissiveness, all studies in this chapter were done using immune compromised xenograft tumour models. Thus, the virus could replicate in the tumour cells, and thus expression of TNF was strictly limited to the tumour site. Using the xenograft model, no evidence of toxic side effects from expressing TNF from a replicating adenovirus was found. Possibly, toxic side effects of TNF expression from ColoAd1 were missed due to inactivity of the MLP in murine cells.

Besides potentially missing the side effects of ColoAd1 or ColoAd1 expressing TNF, important anticancer efficacy mediated by the adapted immune response may be missed in an immune-impaired nude mouse model. Studies have shown that TNF is involved in both $CD8^+$ cell and NK cell activity against tumour cells (*150, 187-189*). To circumvent this problem, the syngeneic inducible cell line model (see chapter 2) was made. However, the highest intratumoural levels of fm TNF measured in this model (approximately 60 ng TNF/g protein) were more than 20-fold lower than the levels of TNF achieved 3 days after the last injection with ColoAd1 fm TNF (approximately 1500 ng/g protein). Thus, due to the large differences in TNF expression, the inducible model may not have revealed the actions of high local doses of TNF as seen by expression from a viral vector.

On the other hand, viral clearance may be impaired in mice lacking adaptive immunity. TNF, as pro-inflammatory cytokine, may help clear the virus by the adaptive immune response.

4.6 Chapter Conclusion

Expression of TNF from ColoAd1 did not result in observed systemic toxicity. However, expression of full length or membrane-bound TNF from ColoAd1 did not reduce tumour growth or increase survival compared to ColoAd1. A statistically significant decrease in viral genome copies was found in ColoAd1 mbm TNF compared to ColoAd1, and a consistent, yet not statistically significant decrease was seen with ColoAd1 fm TNF.

Increased immune infiltration ($CD45^+$ cells) was seen in tumours treated with virus compared to PBS control mice. Specifically, increased monocytic MDSC and DC infiltration into tumours was seen in ColoAd1, ColoAd1 fm and ColoAd1 mbm TNF treated tumours compared to PBS. Increased infiltration of granulocytic MDSCs were seen in ColoAd1 and ColoAd1 fm TNF, but not ColoAd1 mbm TNF, compared to control.

Chapter 5: ColoAd1, ColoAd1 fm TNF and Radiation

5.1 Introduction

Ionizing radiation (IR) is a major component of cancer therapy and palliative care, with more than 50% of cancer patients receiving radiation therapy (*283*). IR can, either directly or indirectly, damage DNA or disrupt DNA division, replication and transcription. Effective DNA repair is necessary as endogenous and exogenous substances constantly cause DNA damage. Cells have five major pathways to repair DNA damage, base excision repair (BER), nucleotide excision repair (NER), mismatch repair (MMR), nonhomologous end joining (NHEJ) and homologous recombination (HR). Both NHEJ and HR are used to repair double strand breaks (DSB). Decreased DNA repair has been linked to increased risk of developing cancers in humans.

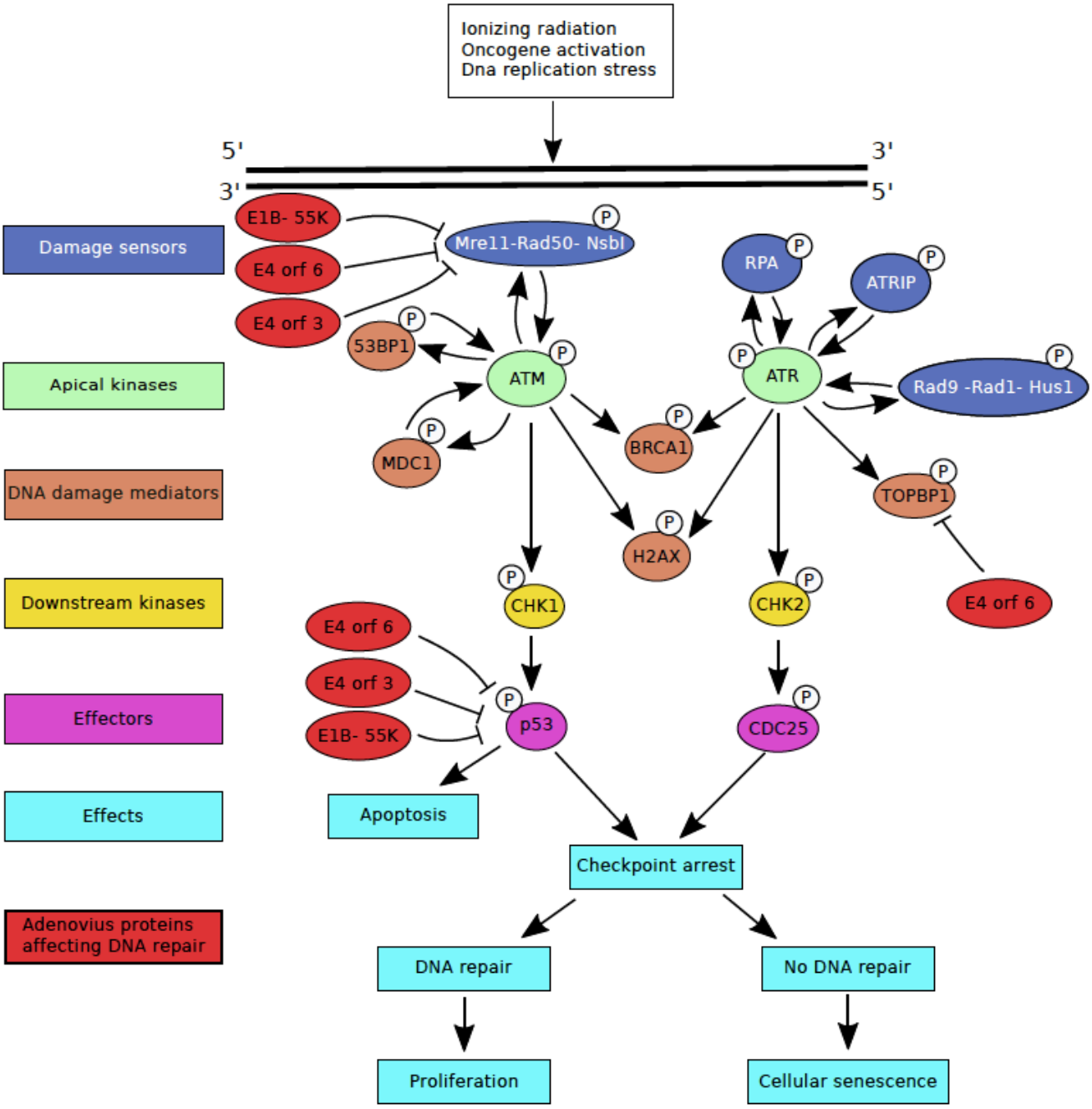

Figure 5.1: Schematic overview of DNA damage response. The DNA damage response consists of two major sensors of DNA damage, the MRN complex and the RPA and RAD9-RAD1-HUS1 complex. The MRN complex recruits ATM and ATR is recruited through the RPA and RAD9-RAD1-HUS1 complex. Through downstream signalling, ATM and ATR regulate the cellular response to DNA damage and DNA repair. Figure adapted from Sulli et al (*284*).

5.1.1 Adenovirus and DNA repair mechanisms

Like most studies on adenovirus biology, the majority of studies on adenovirus and DNA repair mechanisms have been performed with Ad5 (species C) serotype. Synergy between oncolytic virotherapy and radiation has been found in numerous studies (*285*). Several viruses, including adenoviruses and herpes simplex virus (HSV) have been shown to have radiosensitizing properties. As Ads are double-stranded DNA viruses, they need to interfere with DSB repair to achieve successful infection, replication and avoidance of genome concatamerization. The interference with DNA repair sensitizes infected cells to IR.

Adenoviruses have evolved several mechanisms to interfere with DNA repair proteins and avoid the formation of viral genome concatemers. In the absence of viral proteins inhibiting concatermers, the viral genome is too large to be packaged into new virions (*286*). Concatemerization requires functional cellular Mre11 and NbsI proteins and these proteins are found close to viral replication centers (*286*). Mre11 and NbsI form the MRN complex together with Rad50. This complex is one of the earliest and major sensors of DSBs. The MRN complex also activates checkpoint-signalling pathways and acts as an effector complex to repair DNA (*287*).

In E4 mutant virus, the DNA damage response is activated and concatemer formation occurs (*288*). Ad5 uses the E1B-55K and E4orf6 proteins for ubiquitin mediated, proteasome-dependent degradation of the MRN complex and E4orf3 for relocalization and sequestration of MRN within the nucleus of infected cells (*286, 289, 290*). E1B-55K and E4orf6 assemble with the cellular, Elongins B and C, Cullin (CUL) 5 and RBX1 proteins to form E3 ubiquitin-protein ligase, which

ubiquinates both p53 and the MRN complex (*291*). Also, during later stages of infection, NsbI is localized at viral replication centers, whereas Mre11 is degraded and Rad50 is colocalized with E4orf3 (*290*).

E1B-55K is reported to form aggresomes, in which the MRN complex and p53 are degraded. Aggresomes are cytoplasmic inclusion bodies consisting of dynein-dependent aggregation of proteins. Either E4orf6 or E4orf3 is needed to help E1B-55K form these aggresomes (*292*). Finally, SUMOlation of proteins in the MRN complex also occurs (*289*).

During Ad5 infection, the degradation and mislocalization of Mre11 also reduces the ATM-Rad3-related (ATR) protein kinase activation. ATR is normally activated in response to genotoxic stress, DNA damage and viral infection (*293*). During Ad12 infection (a species A virus), Mre11 is also degraded in a proteasome-dependent manner. However, contrary to Ad5, topoisomerase IIβ binding protein (TOPBP1) is also degraded in this way during Ad12 infection. The degradation of TOPBP1 inhibits ATR activation in Ad12. Moreover, Ad12 forms CUL2/RBX1/Elongin-C ubiquitin ligases, whereas Ad5 forms Cul5/RBX1/Elongins B ubiquitin ligases (*294*). Ad16, a species B virus, has been reported to bind both Cul5 and Cul2 (*295*). This indicates that different species or strains of Ad may have evolved slightly different ways of interfering with DNA repair. Additionally, an upregulation in p53 and no degradation of the Mre11 complex were seen in Hela cells infected with either Ad3 or Ad11p (*296*).

In cells infected with recombinant non-replicating Ad5, expressing E4orf3 or E4orf6 under the CMV promoter, persistent γH2AX levels were observed 24h after treatment, indicating inhibition of DSB repair (*297*). In a control virus expressing GFP and luciferase under the CMV, persistent γH2AX was not

observed after radiation, suggesting E4orf4 and E4orf6 may be responsible for the prolonged γH2AX levels. H2AX is phosphorylated at serine 139, by the PI3K-related kinases ATM, ATR and DNA-PK. This phosphorylation is one of the earliest events in DNA damage sensing and repair and γH2AX acts as a scaffold for other proteins involved in DNA repair, including the MRN complex and 53BP1 (*298-300*). Stalled replication and replication stress also induce γH2AX at sites of replication arrest (*301, 302*).

Besides the proteins in the MRN complex, the cellular DNA-dependent protein kinase (DNA PK) are also important in the formation of concatemers. In cells devoid of DNA-PK concatemer formation does not occur, even in the absence of viral E4 proteins. E4orf6 can inhibit V(D)J recombination in the absence of other adenoviral proteins. Finally, E4orf3 and E4or6 proteins colocalize with DNA-PK (*303*).

Besides the role in DNA repair, Mre11 and Rad50 also have a role in detecting cytosolic dsDNA and activating an antiviral type I interferon response via a STING-dependent mechanism (*304*).

5.1.2 Adenoviruses and radiation therapy

OBP-301, a selectively replicating Ad5 vector expressing E1A and E1B under the hTERT promoter, was used to study the synergy between IR and oncolytic adenovirus therapy. *In vitro*, a dose-dependent decrease in Mre11 and Rad50 was seen after OBP-301 treatment, whereas NbsI levels were not affected by the infection (*305*). Radiation induced the expression of these three proteins, whereas combination of radiation and OBP-301 led to degradation of these proteins. *In vivo*, injections of OBP-301 combined with 5 Gy every 2 days

decreased tumour growth, increased survival and increased the amount of apoptotic cells present in the tumours compared to OBP-301 monotherapy or IR monotherapy.

In a GBM model, in vitro infection of with an Ad5-Δ24RGD virus potentiated the effects of irradiation on GBM cell lines and primary glioma cultures. Moreover 10 out of 10 mice bearing subcutaneous tumours were treated with 10^6 pfu Ad5-Δ24RGD and 5 Gy TBI for 5 consecutive days showed tumour regression, whereas TBI alone had no effect on tumour growth and virus alone had 6 out of 9 mice with a response (*306*). Furthermore, combination of dl520, an E1A mutated adenovirus with radiation (4 Gy total, 2 Gy per fraction, administered 6 h before infection) was superior on a GBM xenograft model compared to either agent alone (*307*).

Onyx-015 has a deletion in the E1B-55kDa; the E1B-55kDa protein interferes with the p53 to avoid cells undergoing apoptosis upon infection. Thus, this virus can selectively replicate in p53 deficient cells and it was the first genetically engineered replication selective virus used in humans. An adenovirus vector very similar Onyx-015, H101, is now approved for clinical use in China. Synergy between low doses of Onyx-015 and a single dose of 10 Gy radiation in the decrease of growth of thyroid carcinoma xenograft tumours occurred (*308*). Additionally, total body irradiation (5 Gy per fraction) and i.t. injection of Onyx-015, daily for 5 consecutive days reduces tumour growth in p53 deficient glioma xenograft model. Interestingly, Onyx-015 also potentiates radiation in p53 functional glioma xenograft tumours at low doses (*309*). In this study, radiation did not increase viral replication *in vivo* or *in vitro* and had no effect on infectivity *in vitro*.

Combination of 10 Gy of radiation in a single dose and CV706, an Ad5-based prostate-specific antigen (PSA)-selectively replicating vector, reduced tumour growth in a prostate cancer xenograft model (*310*). Interestingly, this study also looked at the timing of combination of radiation and infection. Mice receiving radiation 24 h before or 24 h or 72 h after infection have similar tumour burden in the long term. However, administration of radiation 7 days after infection did reduce efficacy. Additionally, fractioning the radiation into 2.5 Gy on day 1, 3, 6 and 8 after infection has similar effects on tumour growth as 10 Gy 1 day after infection.

An increase in necrotic cells was seen in tumours treated with both CV706 and radiation, compared to either agent alone. Similarly, CG7870, another PSA-selective replicating adenovirus, also showed synergy between ad infection and 10 Gy of radiation (*311*).

5.1.4 TNF and IR

In vitro, synergy between TNF and x-ray radiation is seen, when TNF is added 4-12 hours before irradiation in several tumour cell lines (*312*). However, not all cell lines show synergy between TNF and radiation, *in vitro* (*313*). In a clinical phase I study, tumour response to a combination of systemic TNF and x-ray irradiation were measured in 20 patients. Of these 20 patients, a total tumour regression was seen in 4 patients, as well as a partial response in 4 patients and a minimal response in 4 patients. A trend towards greater tumour regression at higher doses of TNF was seen (*265*). One possible mechanism for the synergy between TNF and radiation is the formation of hydroxyl radicals upon TNF treatments.

Based on synergy between TNF and radiation, the non-replicating TNFerade adenoviral vector was made. A more in-depth review of TNFerade can be found in chapter 4.

5.2 Chapter objectives and hypotheses

1) Species B adenovirus, Ad11p and ColoAd1, alter the DNA repair response proteins *in vitro*
2) Similar to species C adenovirus, synergy exists between radiation and ColoAd1 *in vivo*
3) Expression of TNF from ColoAd1, combined with radiation increases efficacy of ColoAd1

5.3 Results

5.3.1. Radiation and virus replication *in vitro*

For Ad5, an increase in viral uptake after radiation *in vitro* has been reported, due to an upregulation in dynamin 2 and subsequent macropinocytosis (*314*). Additionally, an increase in Ad5 viral replication and release was seen after radiation, *in vitro*. The increase in virus replication was reported to be due to an increase in YB-1, a human transcription factor that enables E1-independent replication by targeting of the E2 promoter (*307*).

To test whether radiation affects Ad5, Ad11p and ColoAd1 replication in DLD cells, *in vitro*, a QPCR study was performed. DLD cells were infected 6 or 24h before radiation or 6 or 24h after radiation (5 Gy). The supernatant and cell lysate were harvested 48h after the start of infection. DNA extraction was performed and viral replication was assessed using QPCR.

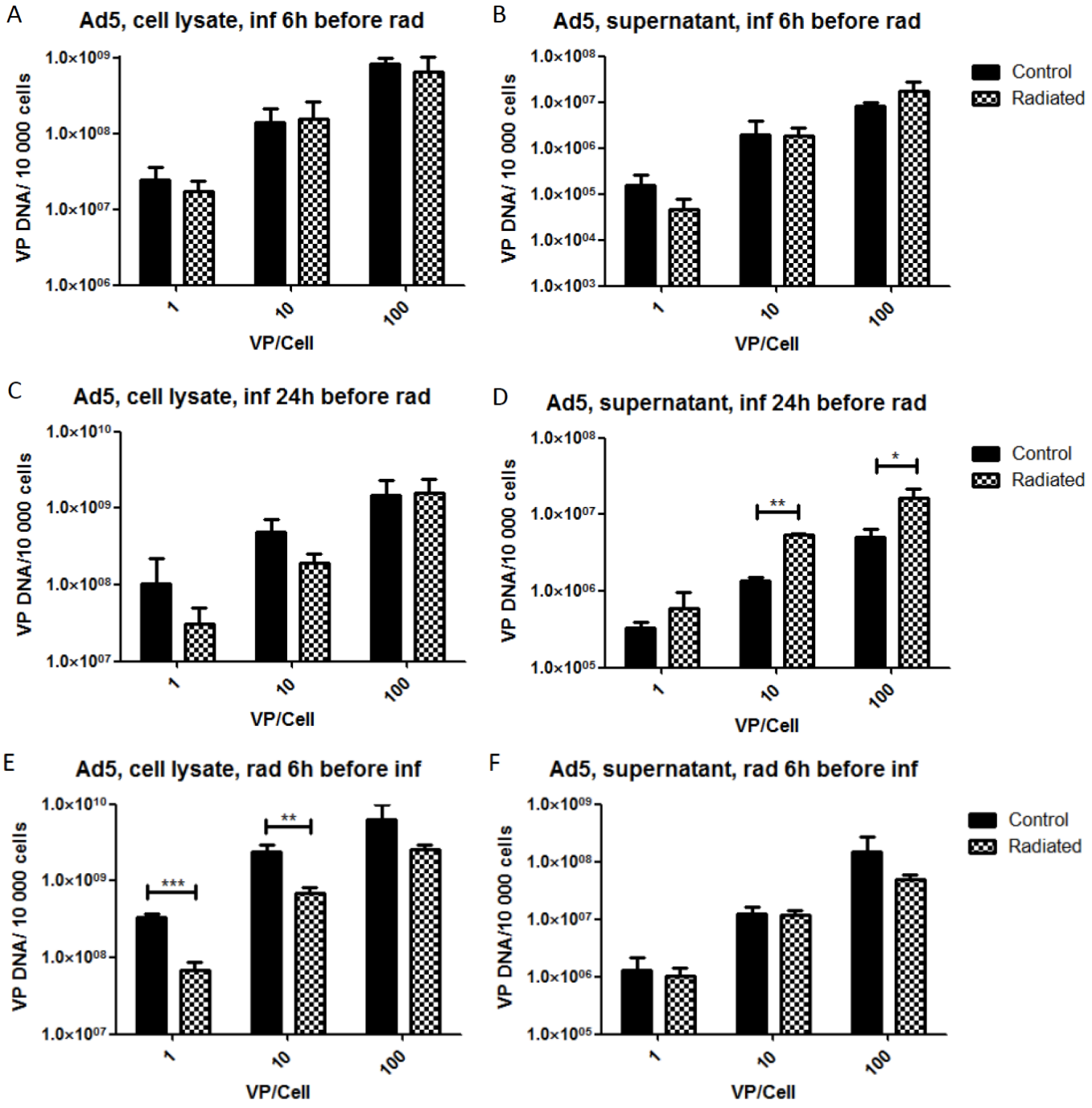
A
Ad5, cell lysate, inf 6h before rad
VP DNA/ 10 000 cells
1.0×10^09
1.0×10^08
1.0×10^07
1.0×10^06
1
10
100
VP/Cell
B
Ad5, supernatant, inf 6h before rad
VP DNA/ 10 000 cells
1.0×10^08
1.0×10^07
1.0×10^06
1.0×10^05
1.0×10^04
1.0×10^03
1
10
100
VP/Cell
Control
Radiated
C
Ad5, cell lysate, inf 24h before rad
VP DNA/10 000 cells
1.0×10^10
1.0×10^09
1.0×10^08
1.0×10^07
1
10
100
VP/Cell
D
Ad5, supernatant, inf 24h before rad
VP DNA/10 000 cells
1.0×10^08
1.0×10^07
1.0×10^06
1.0×10^05
**
*
1
10
100
VP/Cell
Control
Radiated
E
Ad5, cell lysate, rad 6h before inf
VP DNA/ 10 000 cells
1.0×10^10
1.0×10^09
1.0×10^08
1.0×10^07
***
**
1
10
100
VP/Cell
F
Ad5, supernatant, rad 6h before inf
VP DNA/10 000 cells
1.0×10^09
1.0×10^08
1.0×10^07
1.0×10^06
1.0×10^05
1
10
100
VP/Cell
Control
Radiated

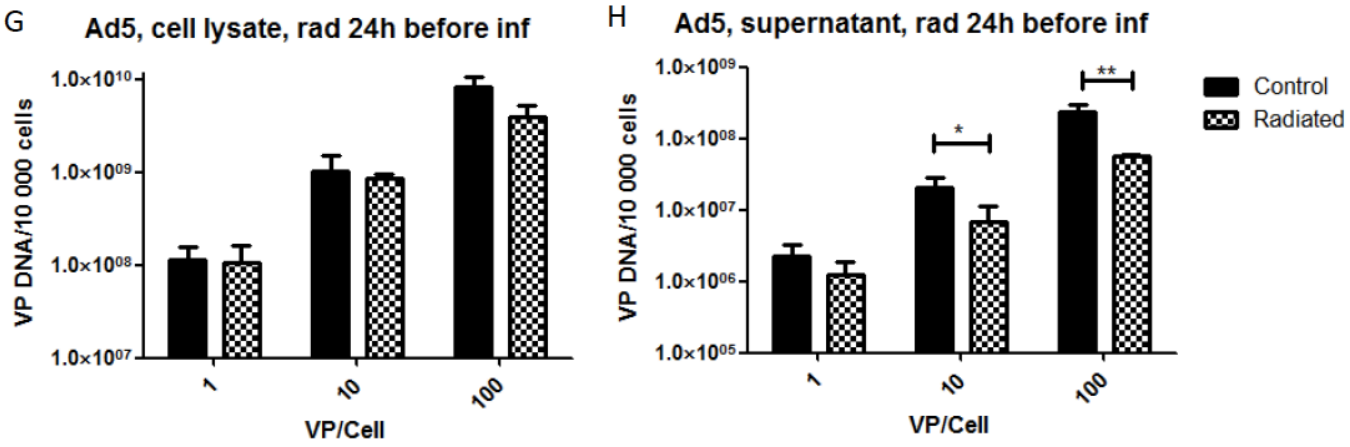

Figure 5.2: Effects of radiation of Ad5 replication, in vitro. DLD cells (1x 10^4 cells/well) were seeded overnight, subsequently cells were infected with Ad5 (100 vp/cell) 6h or 24h before or after radiation (5 Gy). Cells and supernatant were harvested 48h after the start of infection and viral replication was measured using QPCR analysis. A statistically significant increase in viral genome copies was seen in the supernatant of cells infected with Ad5 infected 24h before radiation. A statistically significant decrease in the cell lysate of cells radiated 6h before infection and the supernatant of cells radiated 24h before infection was observed. A two-way ANOVA was done to assess statistical significance. Upon statistical significance, student t-test were performed to compare radiated and control conditions. Inf=infected; rad=radiated; *$p<0.05$, **$p<0.01$.

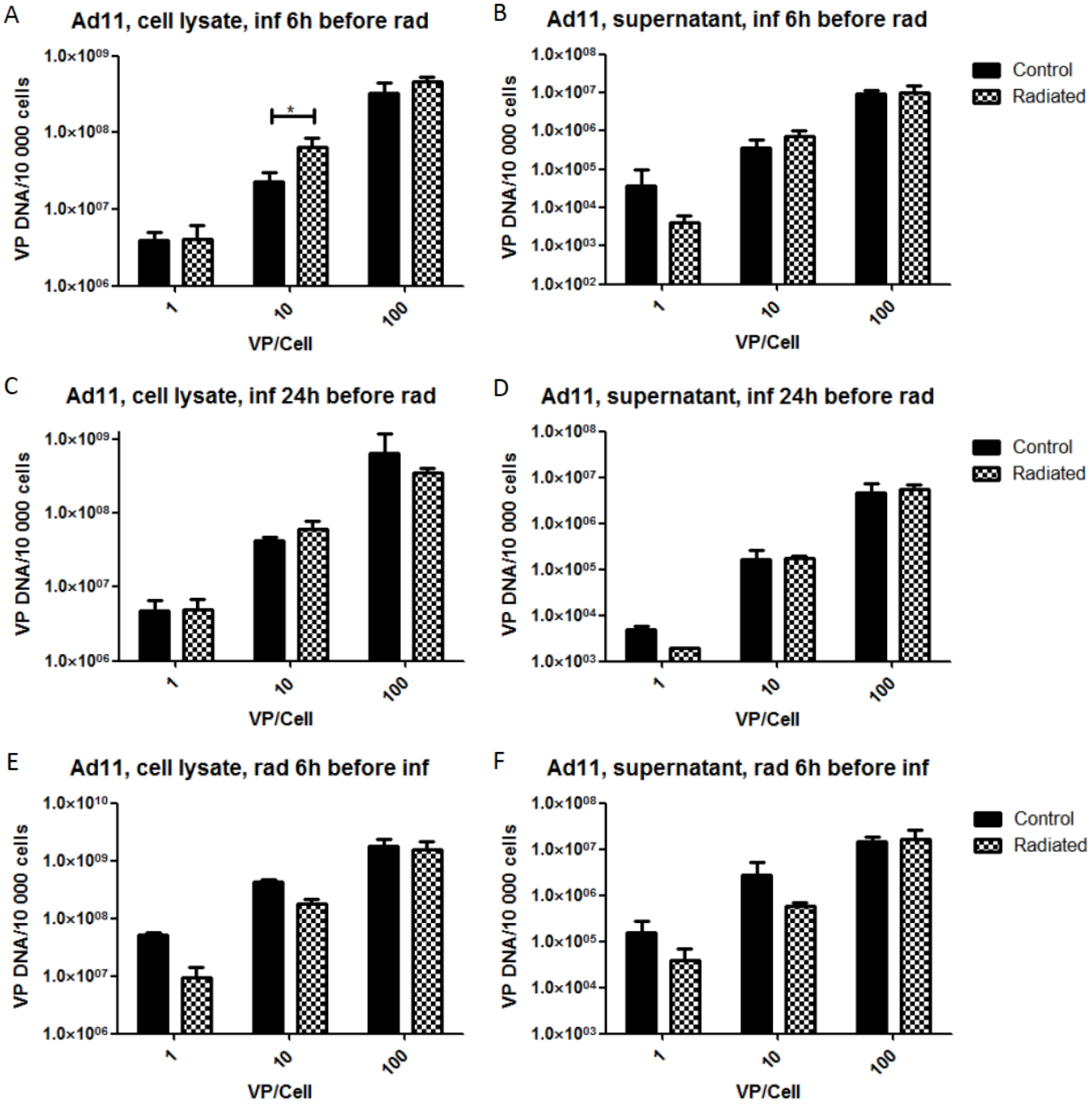
A
Ad11, cell lysate, inf 6h before rad
VP DNA/10 000 cells
1.0×10^09
1.0×10^08
1.0×10^07
1.0×10^06
*
1
10
100
VP/Cell
B
Ad11, supernatant, inf 6h before rad
VP DNA/10 000 cells
1.0×10^08
1.0×10^07
1.0×10^06
1.0×10^05
1.0×10^04
1.0×10^03
1.0×10^02
1
10
100
VP/Cell
Control
Radiated
C
Ad11, cell lysate, inf 24h before rad
VP DNA/10 000 cells
1.0×10^09
1.0×10^08
1.0×10^07
1.0×10^06
1
10
100
VP/Cell
D
Ad11, supernatant, inf 24h before rad
VP DNA/10 000 cells
1.0×10^08
1.0×10^07
1.0×10^06
1.0×10^05
1.0×10^04
1.0×10^03
1
10
100
VP/Cell
Control
Radiated
E
Ad11, cell lysate, rad 6h before inf
VP DNA/10 000 cells
1.0×10^10
1.0×10^09
1.0×10^08
1.0×10^07
1.0×10^06
1
10
100
VP/Cell
F
Ad11, supernatant, rad 6h before inf
VP DNA/10 000 cells
1.0×10^08
1.0×10^07
1.0×10^06
1.0×10^05
1.0×10^04
1.0×10^03
1
10
100
VP/Cell
Control
Radiated

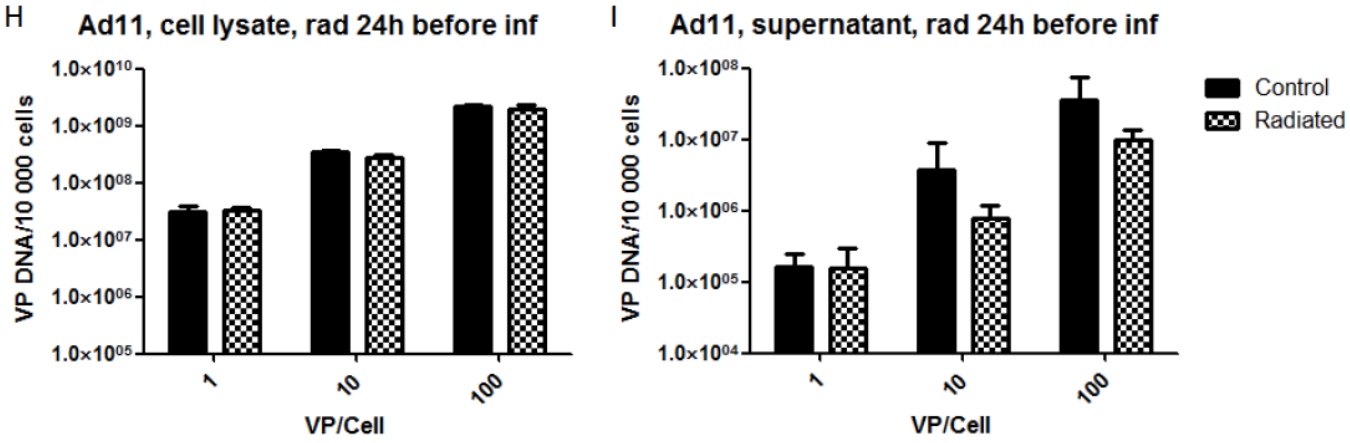

Figure 5.3: Effects of radiation of Ad11p replication, in vitro. DLD cells (1x 10^4/well) were seeded overnight. Cells were subsequently infected with Ad11p (100 vp/cell) 6h or 24h before or after radiation (5 Gy). Cells and supernatant were harvested 48h after the start of infection and viral replication was measured using QPCR analysis. A two-way ANOVA was done to assess statistical significance. A statistically significant increase in genome copies in the cell lysate of cells infected 6h before radiation (10 vp/cell) was found**.** No statistically significant differences between radiated and non-radiated cells were seen in the supernatant or in the cell lysate of cells radiated 6 or 24h before infection or the cell lysate of cells infected 24h before radiation. Inf=infected; rad=radiated; *= $p<0.05$.

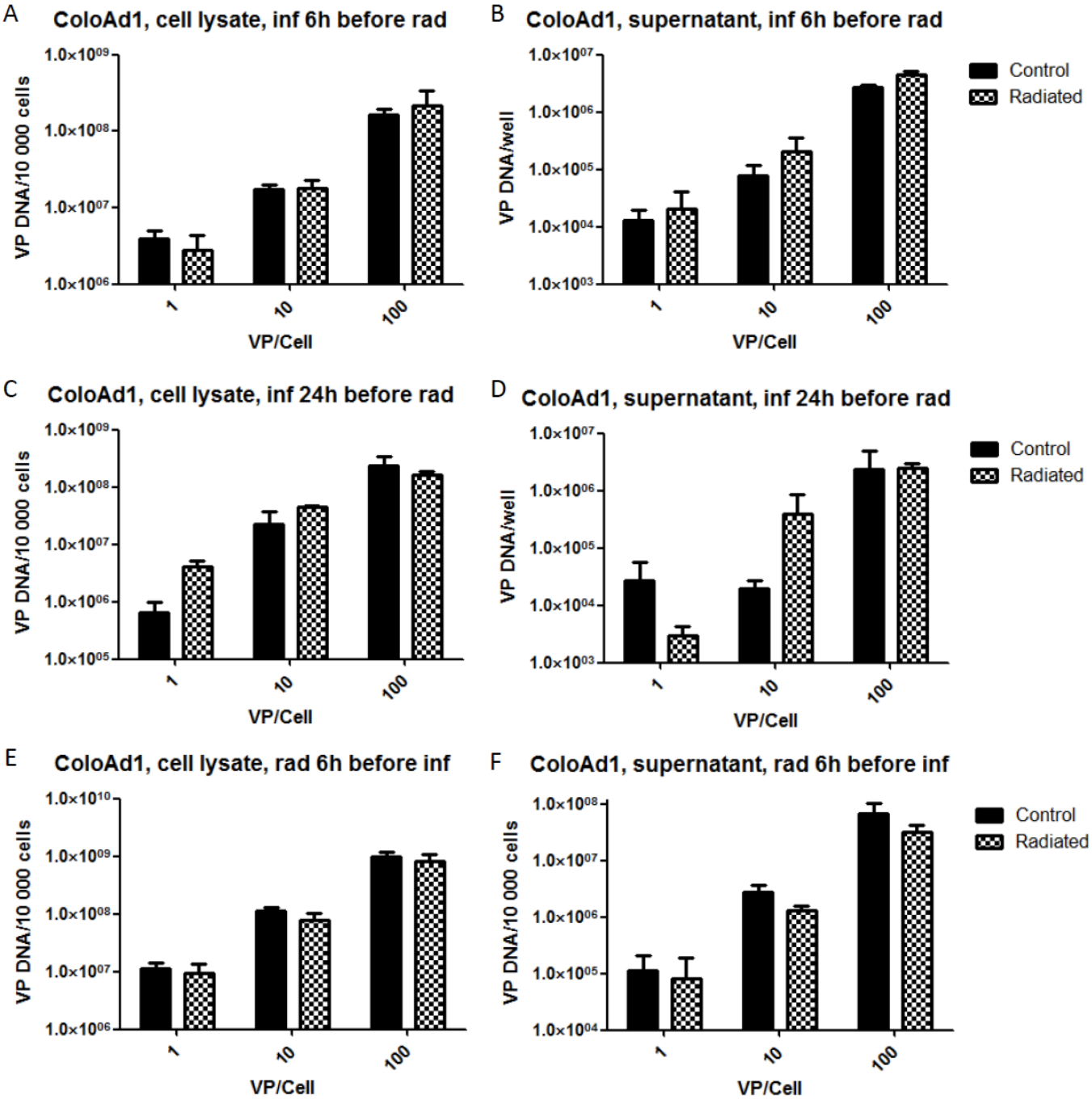
A
ColoAd1, cell lysate, inf 6h before rad
VP DNA/10 000 cells
1.0×10^09
1.0×10^08
1.0×10^07
1.0×10^06
1
10
100
VP/Cell
B
ColoAd1, supernatant, inf 6h before rad
VP DNA/well
1.0×10^07
1.0×10^06
1.0×10^05
1.0×10^04
1.0×10^03
1
10
100
VP/Cell
Control
Radiated
C
ColoAd1, cell lysate, inf 24h before rad
VP DNA/10 000 cells
1.0×10^09
1.0×10^08
1.0×10^07
1.0×10^06
1.0×10^05
1
10
100
VP/Cell
D
ColoAd1, supernatant, inf 24h before rad
VP DNA/well
1.0×10^07
1.0×10^06
1.0×10^05
1.0×10^04
1.0×10^03
1
10
100
VP/Cell
Control
Radiated
E
ColoAd1, cell lysate, rad 6h before inf
VP DNA/10 000 cells
1.0×10^10
1.0×10^09
1.0×10^08
1.0×10^07
1.0×10^06
1
10
100
VP/Cell
F
ColoAd1, supernatant, rad 6h before inf
VP DNA/10 000 cells
1.0×10^08
1.0×10^07
1.0×10^06
1.0×10^05
1.0×10^04
1
10
100
VP/Cell
Control
Radiated

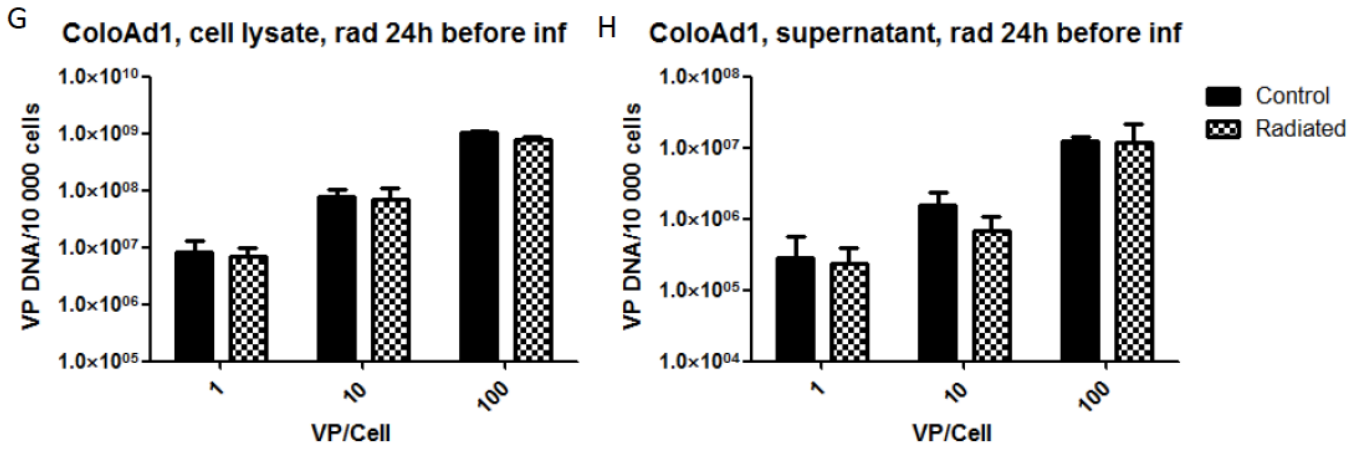

Figure 5.4: Effects of radiation on ColoAd1 replication, in vitro. DLD cells (1x 10^4/well) were seeded overnight. Cells were subsequently infected with ColoAd1 (100 vp/cell) 6h or 24h before or after radiation (5 Gy). Cells and supernatant were harvested 48h after the start of infection and viral replication was measured using QPCR analysis. A two-way ANOVA was used to assess statistical significance. No statistically significant differences were found between radiated and non-radiated cells. Inf=infected; rad=radiated.

Previous studies using Ad5 have shown increased viral uptake and replication when combining radiation with virotherapy (*314*). In the experiments reported here using DLD cells, a statistically significant increase in Ad5 genome copies was found in the supernatant of cells radiated 24h after the start of infection compared to non-radiated cells, see figure 5.2. However, this may be due to an increased or speedier release of viral particles from infected cells rather than increased replication, as no increase in the cell lysate was seen in of cells radiated 24h after infection was seen. For Ad5, a statistically significant decrease in genome copies was found in the cell lysate of cells radiated 6h before the start of infection and in the supernatant of cells radiated 24h before infection compared to non-radiated cells. For Ad11p, a statistically significant increase in genome copies was found in the cell lysate of cells infected (10 vp/cell) 6h before radiation, see figure 5.3. No statistically significant differences were found in

viral replication, as measured by QPCR, ColoAd1 radiated either 6 or 24h before or after infection, see figure 5.4.

5.3.2 Effects of radiation and virotherapy on cell viability

To assess whether the combination of radiation and ColoAd1 infection showed any interaction in affecting cell viability, cells were infected with a serial dilution of ColoAd1 for 24h and then irradiation with 5 Gy. Five days after the start of infection, cell viability was measured using an MTS assay. The irradiation of ColoAd1 infected cells did not reduce the cell viability compared to non-irradiated cells infected with ColoAd1, see figure 5.5.

Due to the fast killing of DLD cells by ColoAd1 (as well as Ad5, and Ad11; see also figure 5.20) it was not possible to combine virotherapy with radiation and perform a colony formation assay. This standard assay in radiation biology measures the effects of radiation on the ability of cells to produce progeny and thus cell colonies, a process that would take a few weeks. Thus, ColoAd1 infected cells will be killed before colony formation can be assessed and would therefore not give useful data.

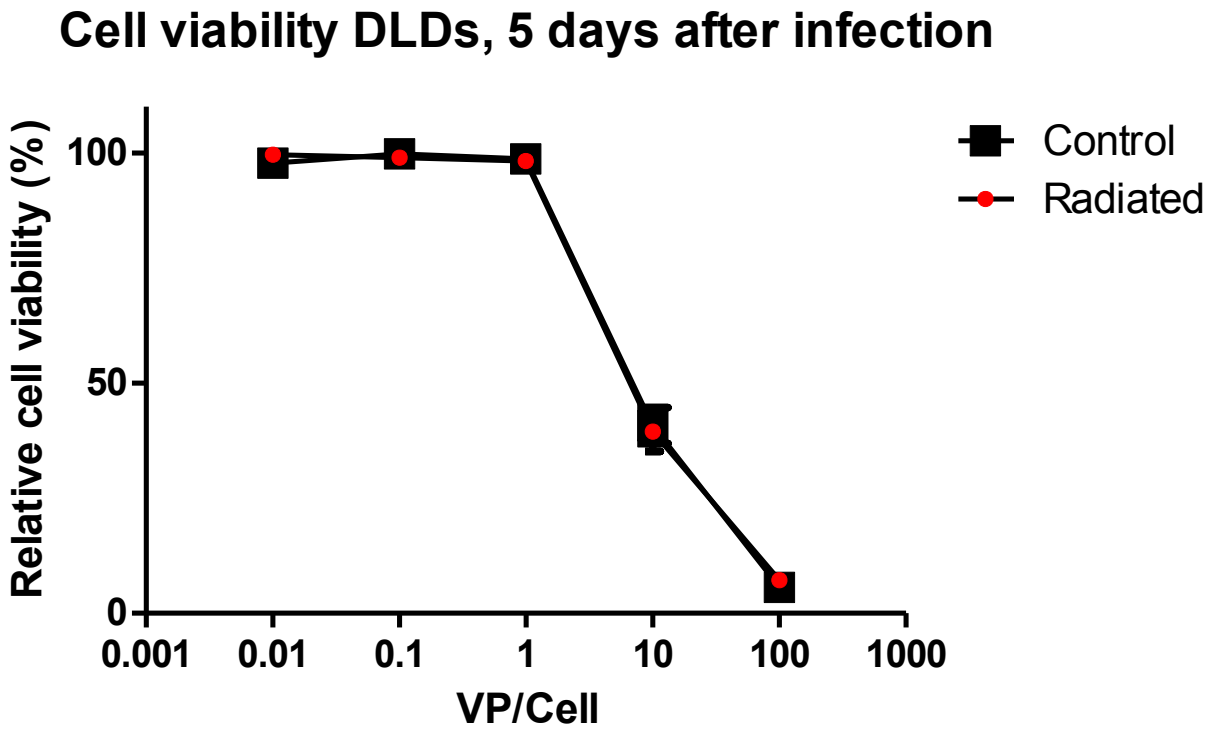

Figure 5.5: Cell viability of radiated cells infected with ColoAd1. DLD cells ($1x10^4$ cells/well) were seeded overnight. Next, the cells were infected with ColoAd1 (100 vp/cell). After 24h, the cells were irradiated (5 Gy) or received no irradiation (control). Cell viability was measured 5 days after the start of infection using and MTS assay and normalized to non-infected, non radiated cells. No differences between radiated and non-radiated cells were seen. Mean and SEM are depicted.

5.3.3 Comet assay

The most direct way to measure cellular DNA damage is the comet assay. In this assay, cells are embedded in an agarose gel, lysed and subsequently subjected to electrophoresis to separate shorter DNA fragments from the nucleus. Finally, ds DNA is stained using cyber gold. As can be seen in figure 5.6, DNA damage by radiation (B) is visible 15 minutes after irradiation of DLD cells with 5 Gy as a tail appears that is not visible in non-radiated cells (A). However, in adenovirus infected cells (C; infected with Ad11p for 24h) extensive clustering of cells was seen and despite vigorous pipetting before and during agarose embedding it was not possible to produce a suspension of single cells, which is necessary for accurate analysis of DNA tails. Additionally, DNA tails were visible in a subpopulation of non-radiated adenovirus infected cells. It is unclear whether this tail is due to double stranded DNA from the adenovirus itself, induction of genomic DNA damage due to cellular stress due to infection or due to apoptotic events.

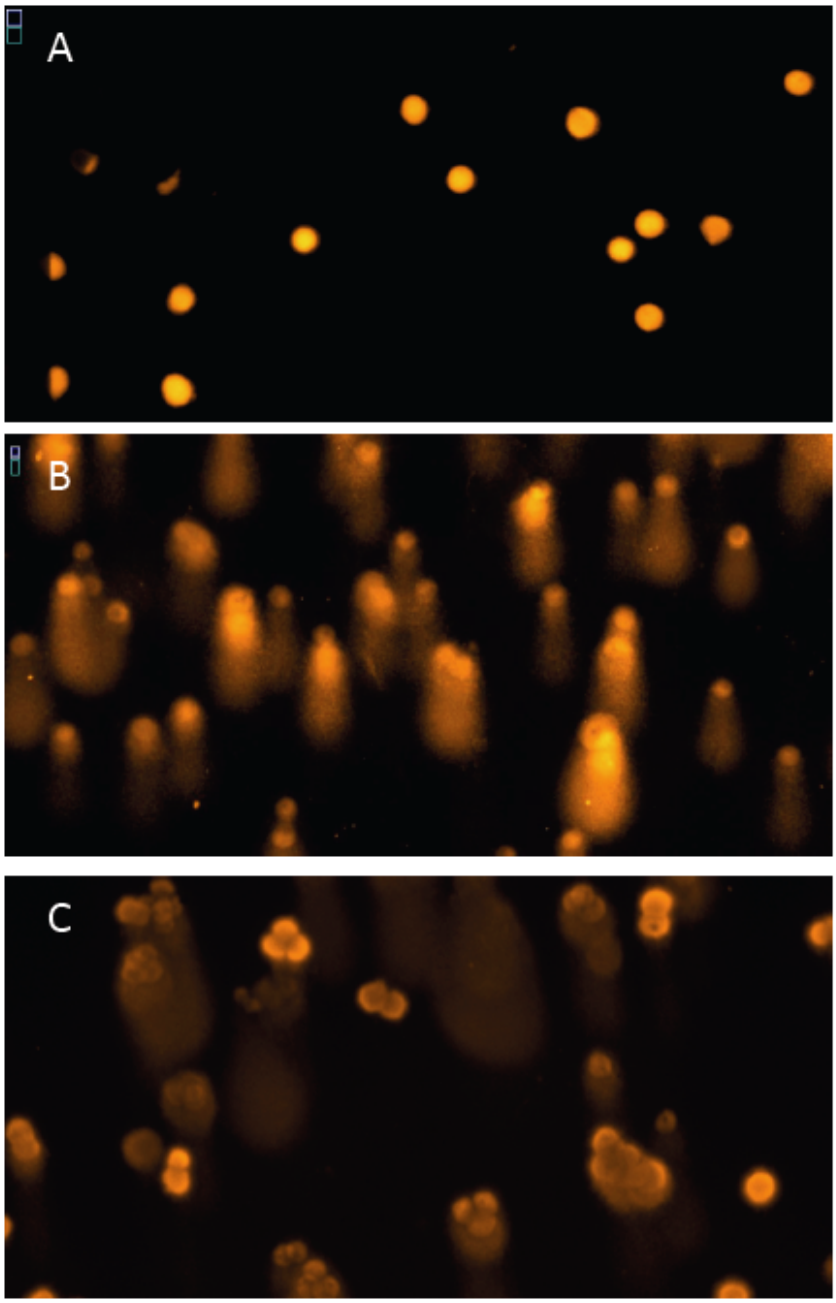

Figure 5.6: Comet assay on DLD cells infected with Ad11p. DLD cells ($1x10^5$ cells/well) were seeded over night. Cells were mock infected (A and B), mock or infected with Ad11p (C; 100 vp/cell) for 24 h. Subsequently cells were irradiated (5 Gy; B and C) or mock irradiated (A). Cells were harvested and embedded in an agarose gel 15 min post radiation. Cells were lysed and a comet assay was performed to assess DNA damage.

5.3.4 DNA repair proteins and adenovirus infection *in vitro*

For Ad5 and Ad12, it is known that viral infection leads to high levels of phosphorylation of H2AX at serine 139, called γH2AX (*298, 315, 316*). To test whether infection with ColoAd1 induce a similar phosphorylation of H2AX, cells were infected with 100 vp/cell ColoAd1 and harvested at several time points post infection. As can be seen in figure 5.7, H2AX phosphorylation did not occur 8h after infection but was visible from 24h onwards. Using immunocytochemistry, the phosphorylation of γH2AX was shown to be pan-nuclear in cells infected with Ad5, Ad11p or ColoAd1, see figure 5.8.

The timescale of γH2AX production suggest it is not purposefully mediated by early infection by adenovirus or adenovirus early genes, but rather a cellular response during the later stages of infection. Activation of the MLP and thus ColoAd1 replication occurs from 24h onward in DLD cells, suggesting that γH2AX may occur as a result of ColoAd1 replication and/or replication stress. Alternatively, pan-nuclear γH2AX may be due to apoptotic events.

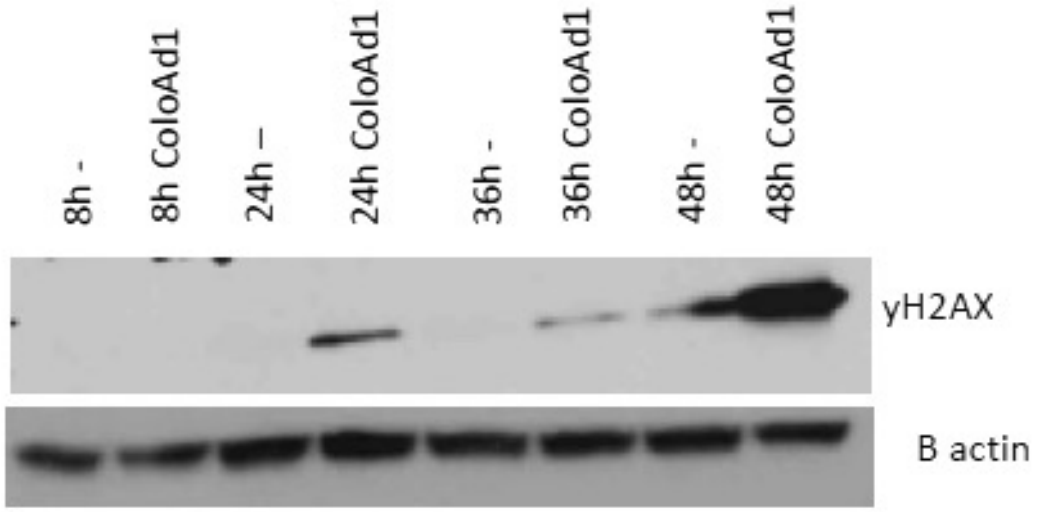

Figure 5.7: γH2AX during ColoAd1 infection of DLD cells. DLD cells (5 x 10^5 cells/well) were seeded overnight. The cells were infected with 100 vp/cell of ColoAd1 or mock (-) and collected 8, 24, 36 or 48h after the start of infection. Western blot analysis on whole cell lysates was performed for phosphorylated

H2AX (γH2AX). B-actin was used as a loading control. At 24h post ColoAd1 infection, γH2AX is first observed.

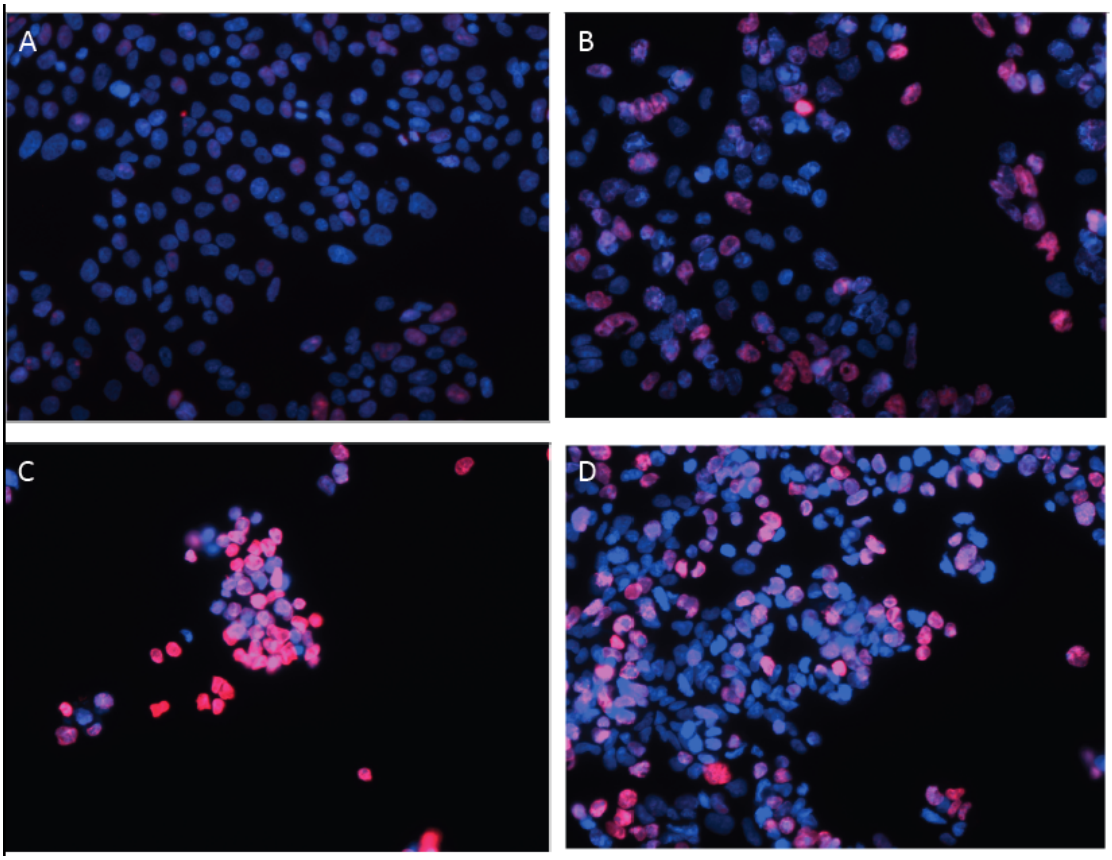

Figure 5.8: γH2AX staining of adenovirus infected DLD cells. DLD cells ($1x10^4$ cells/well) were seeded overnight. Cells were mock infected (A) or infected with 100 vp/cell Ad5 (B), Ad11p (C) or ColoAd1 (D). At 24h after the start of infection, the cells were fixed in PFA and stained for γH2AX (red) and counterstained with DAPI (blue). An increase in γH2AX staining was seen in cells infected with adenovirus compared to PBS control.

During Ad5 infection, mre11 degradation inhibits the phosphorylation of ATM. To test ATM phosphorylation in cells infected with Ad11p and ColoAd1, a western blot on whole cell lysate was done.

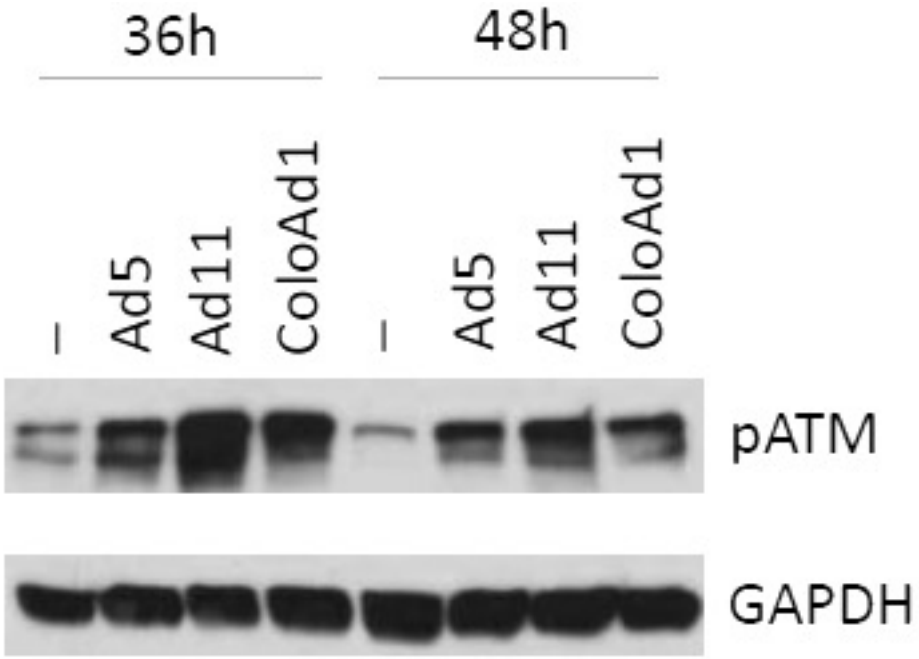

Figure 5.9: ATM phosphorylation in adenovirus infected DLD cells. DLD cells (5 x 10^5 cells/well) were seeded overnight. The cells were mock infected (-) or infected with 100 vp/cell of A5, Ad11p or ColoAd1 or mock (-) and collected 36h (left side) or 48h (right side) after the start of infection. Western blot analysis on whole cell lysates were done for phospho-ATM (pATM; Ser-1981) and GAPDH was used a loading control. Cells infected with adenovirus showed an increase in ATM phosphorylation compared to mock.

Using immunocytochemistry, the ATM phosphorylation was shown to be in distinct nuclear foci, see figure 5.10. Previously, inhibition of ATM activation by Ad5 has been described in A549 cells (*288*). As both the western blot and ICC show, infection of DLD cells with Ad5, Ad11p or ColoAd1 leads to phosphorylation of ATM at later stages of infection. Using ICC, staining is seen in a subpopulation of the cells.

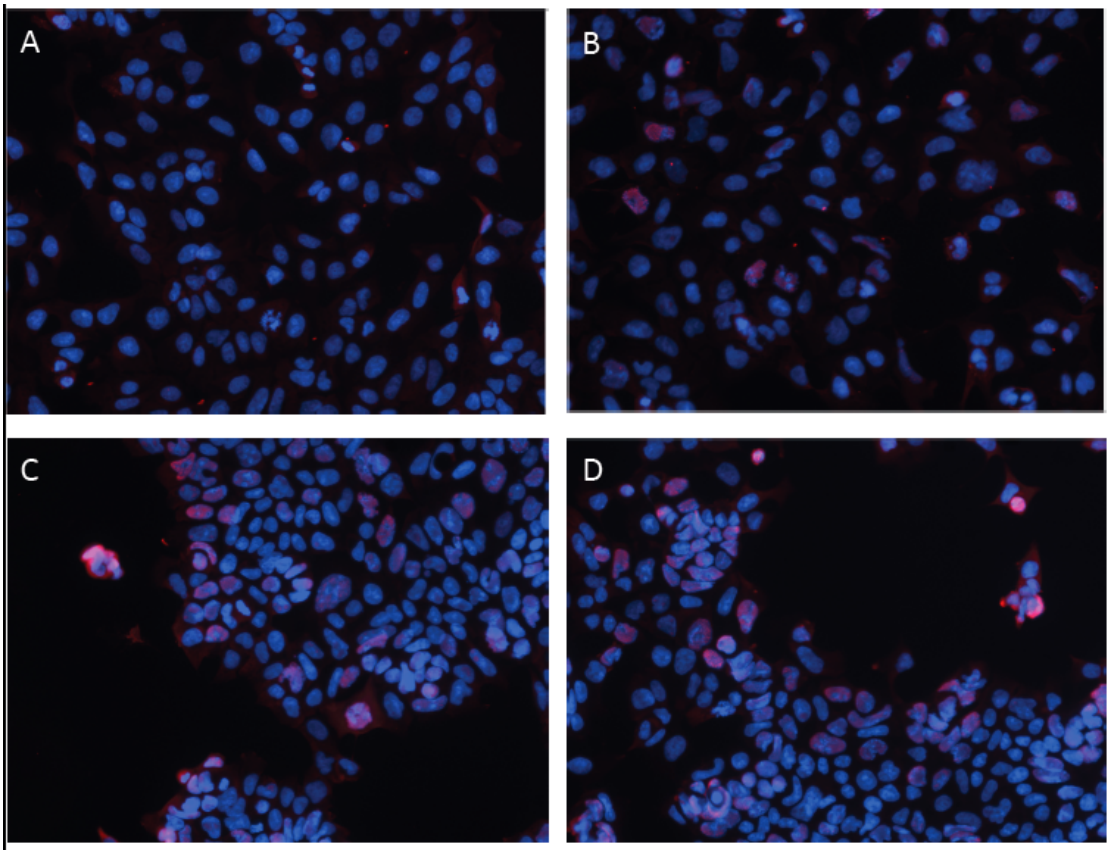

Figure 5.10: Phospho-ATM staining of adenovirus infected DLD cells. DLD cells ($1x10^4$ cells/well) were seeded overnight. Cells were mock infected (A) or infected with 100 vp/cell Ad5 (B), Ad11p (C) or ColoAd1 (D). 36 h post infection, the cells were fixed in PFA and stained for pATM (red) and counterstained with DAPI (blue). An increase in γH2AX staining was seen in cells infected with adenovirus compared to PBS control. Compared to PBS control, increased pATM foci in the nucleus were seen in adenovirus-infected cells.

E4orf6 from Ad5 forms E3 ubiquitin ligase complexes with Cullin5. For Ad12, Ad16 and Ad40 association of E4orf6 with Cul2 has been found using immunoprecipitation (*295*). E4orf6 from Ad16, a species B virus, associates with both Cul2 and Cul5. Possibly due to differences in E3 ubiquitin ligase complexes, different efficiency of degradation of p53 and mre11 is observed in different Ad serotypes.

The effects of Ad11p and ColoAd1 on downstream mediators of DNA repair of ATM, were analysed by western blot on whole cell lysate was done. Cells were

infected with Ad5, Ad11p or ColoAd1 for 36 or 48 hours, before harvesting. Cells were lysed and a western blot was performed. As previously described in the literature, Ad5 degrades Mre11, Rad50 and DNA ligase IV. Reduced Rad50 levels may be due to Mre11 degradation as Mre11 stabilizes Rad50 (*317*). In agreement with literature describing DNA ligase IV degradation by all adenovirus species studied, Ad11p and ColoAd1 also degrade this protein. Contrary, Mre11 and Rad50 are not targeted as efficiently by Ad11p and ColoAd1 as by Ad5. Similarly, p53 is degraded by Ad5 whereas Ad11p does not seem to target this protein. Interestingly, a minor decrease in p53 levels may occur in ColoAd1 infected cells compared to controls.

To confirm that the results found on DLD cells were not cell line specific, a western blot on HT29 cells was also performed. Similar results between DLD and HT29 infected cells were found.

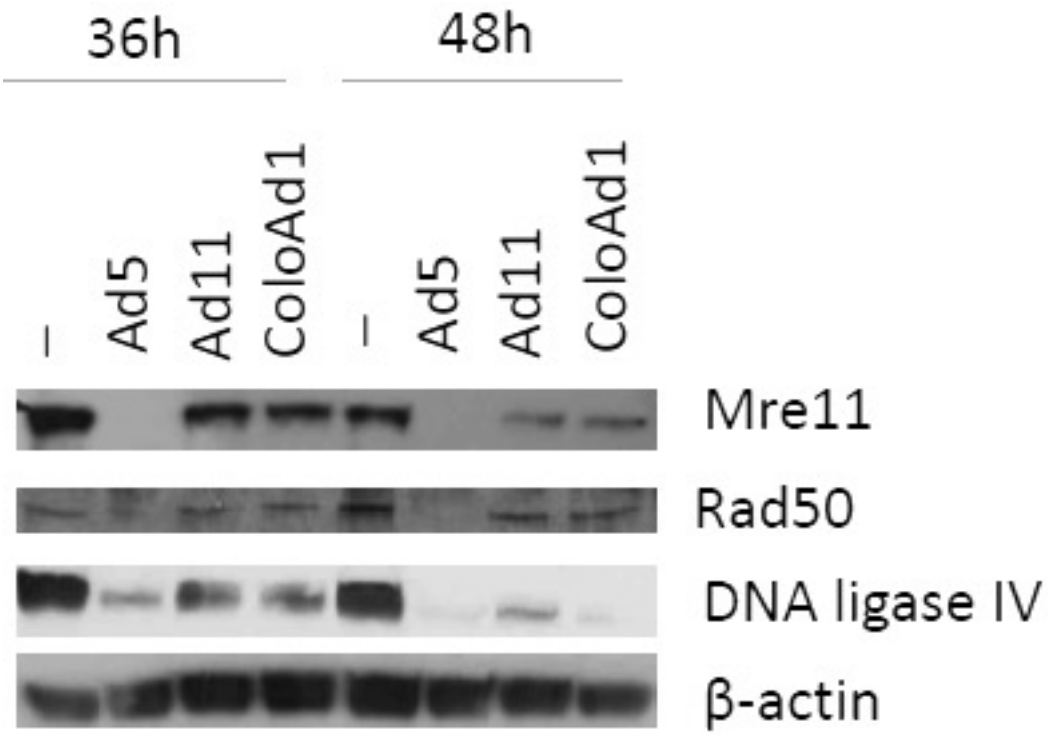

Figure 5.11: DNA repair proteins in adenovirus infected DLD cells. DLD cells ($5x10^5$ cells/well) were seeded overnight. DLD cells were infected with Ad5, Ad11p, ColoAd1 (100 vp/cell) or mock (-) for 36h (left side) or 48h (right side). A western blot analysis was performed on whole cell lysate. Reduced levels of Mre11, Rad50 and DNA ligase IV were seen in cells infected with Ad5. Degradation of Mre11 and Rad50 was less efficient in cells infected with Ad11p or ColoAd1, compared to Ad5.

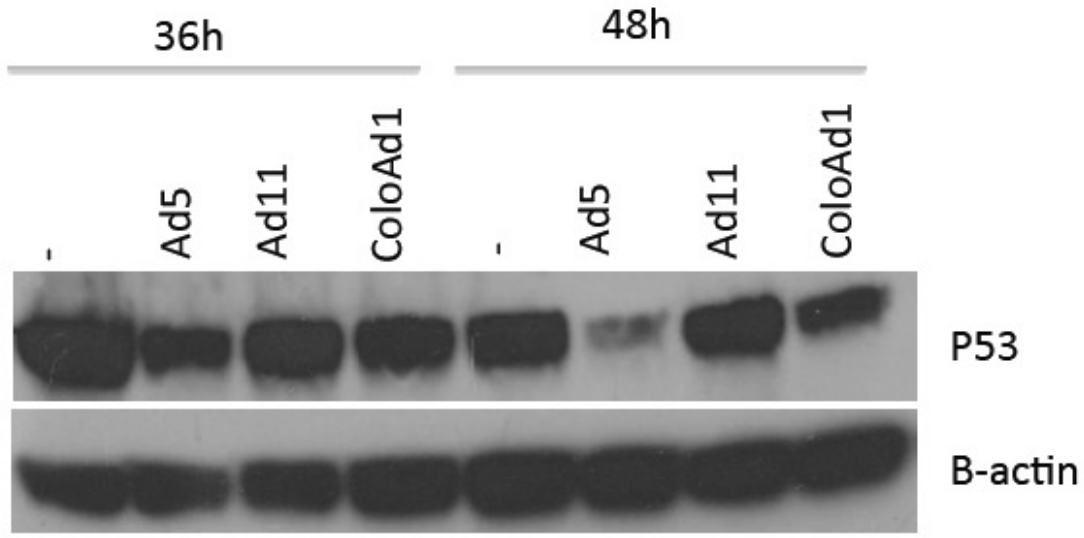

Figure 5.12: P53 in adenovirus infected DLD cells. DLD cells ($5x10^5$ cells/well) were seeded overnight. DLD cells were mock infected (-) or infected with Ad5, Ad11, ColoAd1 (100 vp/cell) or mock (-) for 36 (left side) or 48h (right side). Cells were harvested and a western blot analysis was done on whole cell lysate. Reduced levels of p53 were observed in adenovirus infected DLD cells.

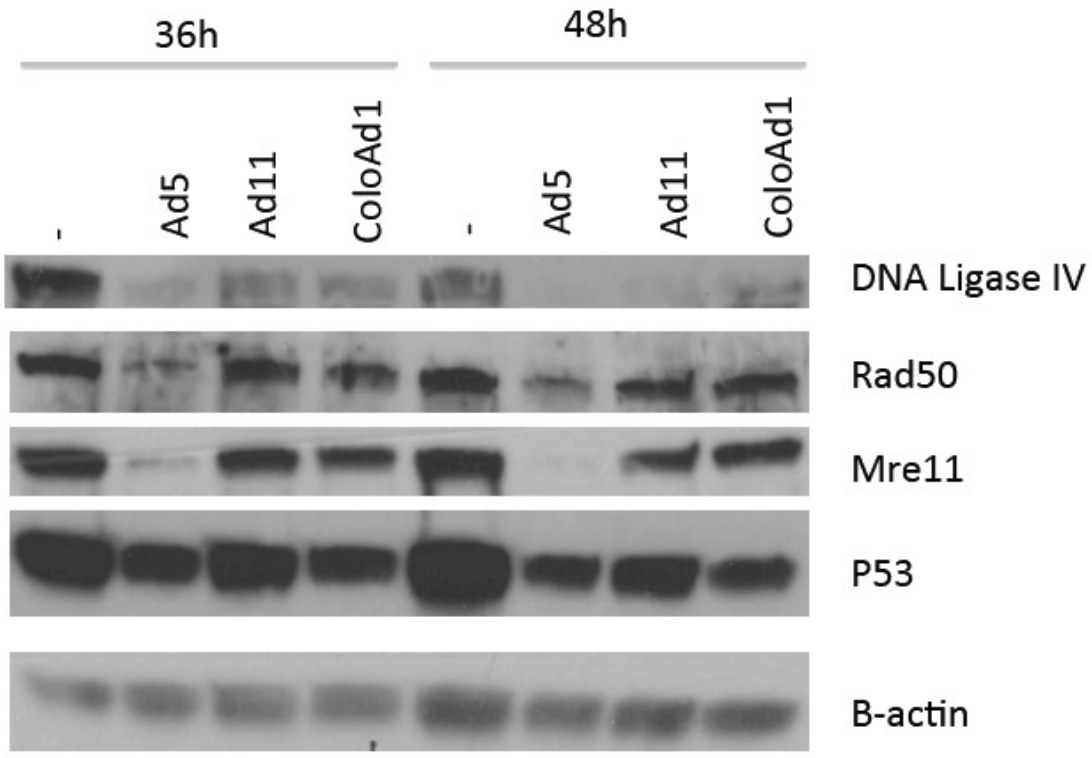

Figure 5.13: DNA repair proteins in adenovirus infected HT29 cells. HT29 cells ($5x10^5$ cells/well) were seeded overnight. The cells were infected with Ad5, Ad11p, ColoAd1 (100 vp/cell) or mock (-) for 36 (left side) or 48h (right side). A western blot analysis was performed on whole cell lysate. Reduced levels of Mre11, Rad50 and DNA ligase IV were seen in cells infected with Ad5. Reduced levels of Mre11, Rad50 and DNA ligase IV were seen in cells infected with Ad5. Degradation of Mre11 and Rad50 was less efficient in cells infected with Ad11p or ColoAd1, compared to Ad5

As p53 degradation is more efficient during Ad5 infection than infection with either ColoAd1 or Ad11, this raises the question whether p53 inactivation occurs via a different mechanism. Cells were irradiated with 5 Gy and harvested either 1h or 8h after radiation or control. A western blot was done and the membrane was stained for phosphorylated p53 (serine 15). As expected, radiation induced a strong phosphorylation 1h after radiation. In Ad5, concurrent with p53 degradation, reduced levels of phosphorylated p53 were seen. In Ad11p and ColoAd1 infected cells, phosphorylation of p53 still occurred upon radiation, suggesting p53 might still be functional and phosphorylation is not inhibited. Similar results were seen after 8h.

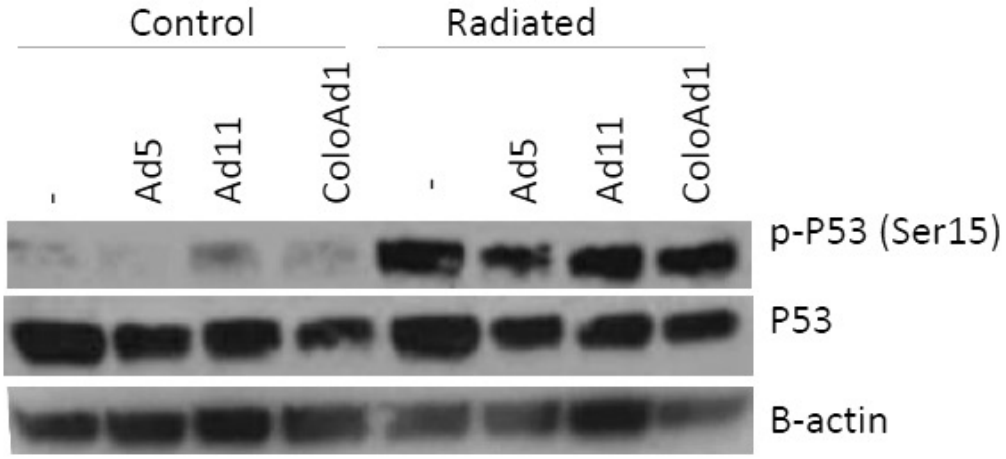

Figure 5.14: p53 phosphorylation in adenovirus infected cells, 1h after irradiation. DLD cells (5 x10^5) were seeded overnight and subsequently mock infected (-) or infected with Ad5, Ad11p or ColoAd1 (all at 100 vp/cell). Cells were irradiated (5 Gy) or mock irradiated 24h post infection and harvested 1h after irradiation. A western blot analysis was performed on whole cell lysate for phospho-p53 and p53 levels. B-actin was used as a loading control.

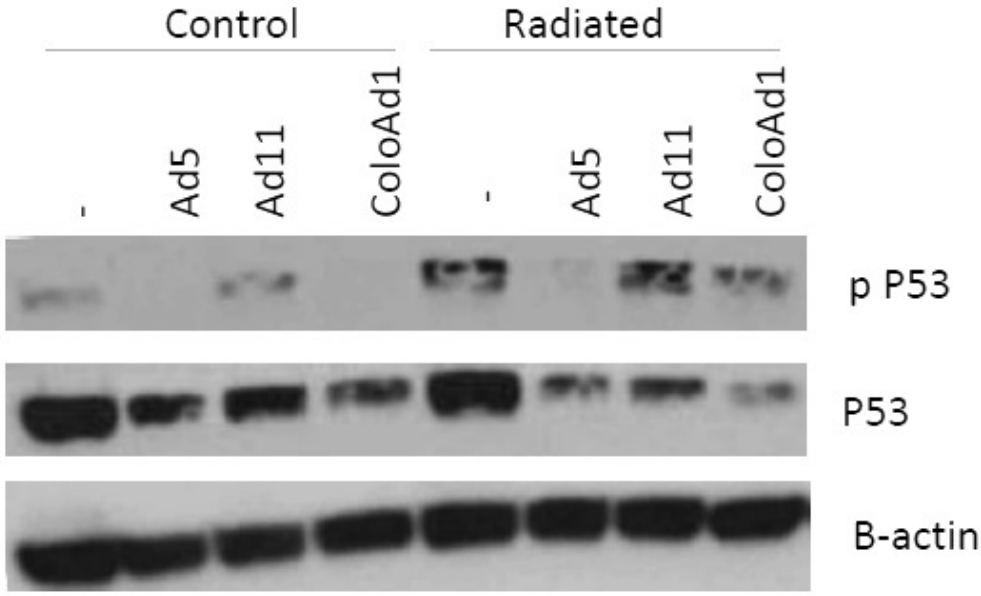

Figure 5.15: p53 phosphorylation in adenovirus infected cells, 8h after irradiation. DLD cells (5 x10^5) were seeded overnight and subsequently mock infected (-) or infected with Ad5, Ad11p or ColoAd1 (all at 100 vp/cell). Cells were mock irradiated or irradiated (5 Gy) 24h post infection and harvested 8h after irradiation. A western blot analysis was performed on whole cell lysate for phospho-p53 and p53 levels. B-actin was used as a loading control.

Mre11

Based on western blotting results, Mre11 was not degraded to the same extent by Ad11p and ColoAd1 as it is by Ad5. To test whether foci formation was affected by adenovirus infection, cells were infected with 100 vp/cell Ad5, Ad11p or ColoAd1 or mock infected for 24h, before radiation with 5 Gy. Cells were fixed 2h after irradiation and staining for Mre11. Due to the high amount of cytosolic Mre11, an accurate count of Mre11 foci in the nucleus was not possible, see figure 5.16.

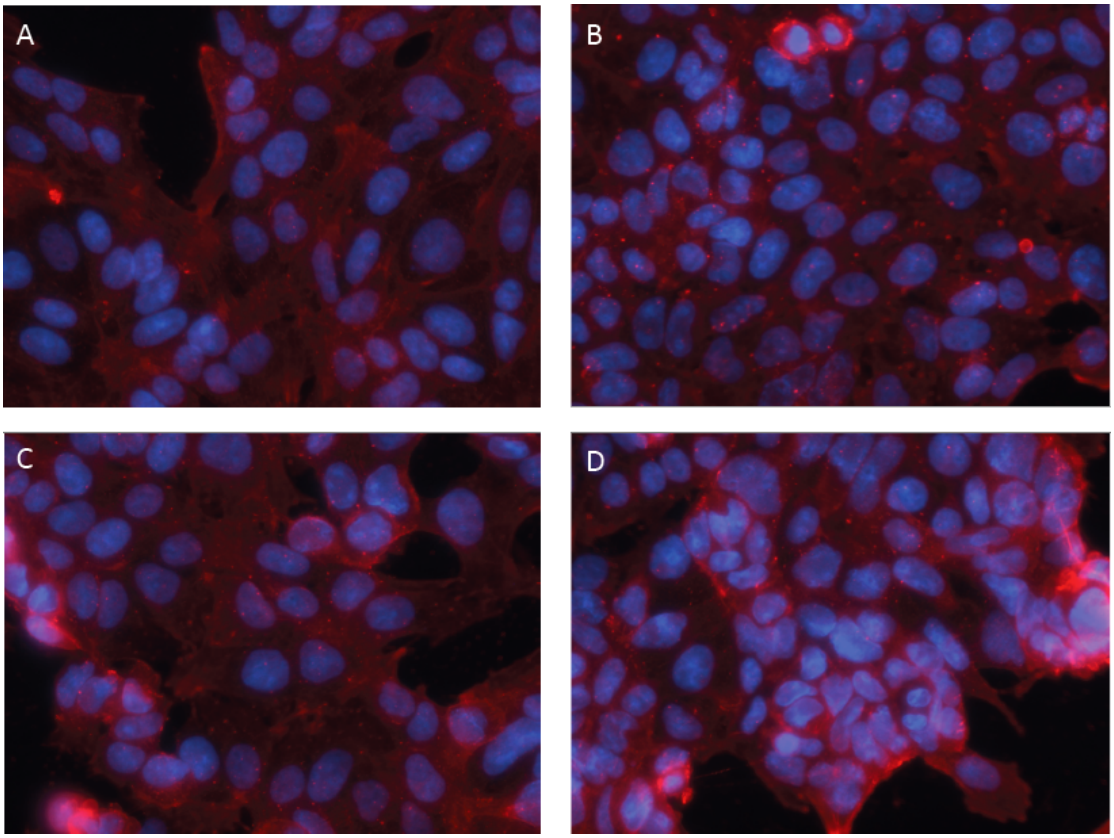

Figure 5.16: Mre11 staining of adenovirus infected DLD cells. DLD cells ($1x10^4$ cells/well) were seeded overnight. Next, cells were mock infected (A), or infected with Ad5 (B), Ad11p (C) or ColoAd1 (D) at 100/vp cell for 24h. Cells were then irradiated and fixed in PFA, 2h after radiation. Cells were stained for Mre11 (red) and counterstained for DAPI (blue). High levels of cytosolic Mre11 were observed.

DNA repair protein foci formation

As infection of DLD cells with Ad5, Ad11p and ColoAd1 leads to pan-nuclear γH2AX staining and pATM foci, ICC for these proteins could not be used to study the DNA damage response in virus infected cells. To test the effects of virus infection on the formation of DNA repair protein foci after radiation, ICC for 53BP1 was performed. 53BP1 is an important protein for the maintenance of genomic integrity (*318*). 53BP1 can be phosphorylated by ATM (*319*). 53BP1 has several functions, including acting as a scaffold to recruit other DNA repair proteins to the damaged chromatin and amplifying ATM activity to promote checkpoint signalling and regulation of NHEJ-mediated DSB repair (*318*).

Cells were infected with Ad5, Ad11p or ColoAd1 for 24h before radiation (4 Gy). The cells were fixed at several time points (15 min – 12h) after radiation and staining for 53BP1. Foci formation was analysed automatically using the Incel microscope and automated foci counting software. A decrease in 53BP1 foci formation is seen in virally infected cells at early time points after radiation in DLD cells. Furthermore, the decrease in 53BP1 formation was confirmed in A549 cells, using the same assay.

Previously, reduced numbers of 53BP1 foci have been reported at early time points in ATM deficient cells, whereas equal numbers of 53BP1 foci were seen at later time points after irradiation (*320*).

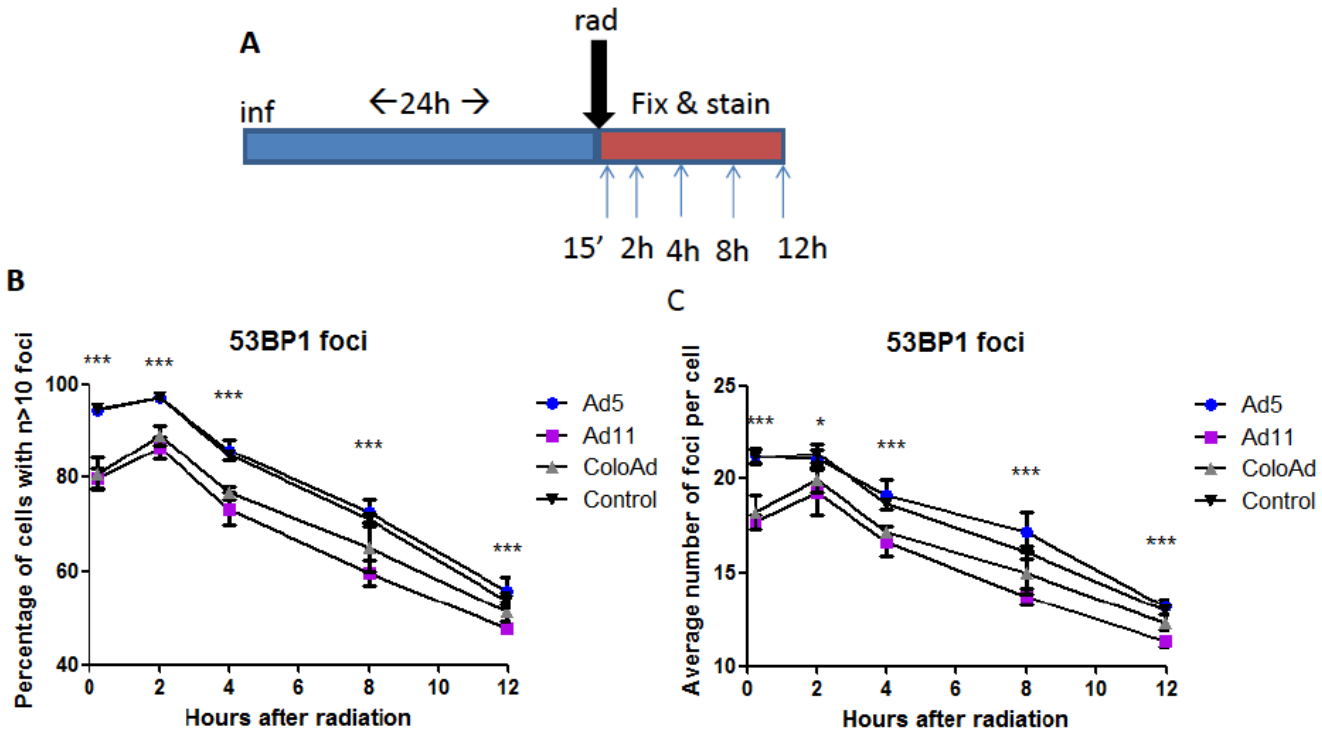

Figure 5.17: Time course of 53BP1 foci formation in adenovirus infected DLD cells upon radiation. A: schematic overview of the experiment. Cells ($1x10^4$ cells/well) were seeded overnight. Next, DLD cells were infected with Ad5, Ad11p, ColoAd1 (all 100 vp/cell) or control for 24h before radiation with 5 Gy. Cells were fixed in PFA 15 minutes to 12h after irradiation and 53BP1 foci were stained and automatically analysed using InCell software. B: quantification of the percentage of cells with more than 10 53BP1 foci in the nucleus at several time points after radiation. C: quantification of the average amount of foci in the nucleus of radiated cells at several time points after radiation. The experiment was performed in quadruplicates. Mean and SD shown.

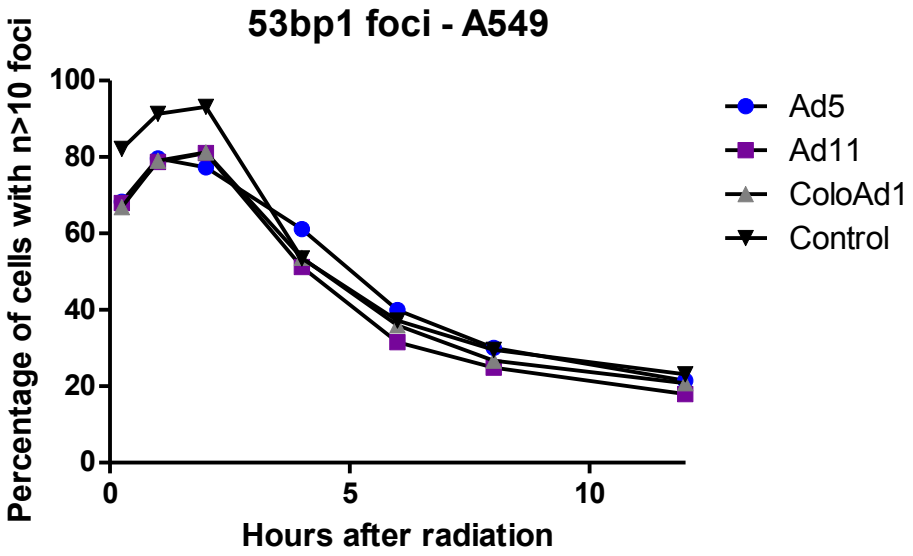

Figure 5.18: Time course of 53BP1 foci formation in adenovirus infected A549 cells after radiation. A549 cells were seeded ($1x10^4$ cells/well) overnight. Next, cells were infected with Ad5, Ad11p, ColoAd1 (100 vp/cell) or mock infected for 24h before radiation with 5 Gy. Cells were fixed in PFA 15 minutes to 12h after irradiation and 53BP1 foci were stained and automatically analysed using InCell software. The quantification of the percentage of cells with more than 10 53BP1 foci in the nucleus at several time points after radiation is shown. The experiment was performed in quadruplicates. Mean and SD shown.

To test how long cells needed to be infected with adenovirus before the virus would inhibit the cell's ability to form 53BP1 foci, an experiment was designed that exposed cells to virus at various times up to 24h prior to irradiation. Accordingly, cells were infected (100 vp/cell) with Ad5, Ad11p or ColoAd1 (0 h - 24 h), irradiated (4 Gy) and then fixed 2h after radiation. Cells infected for approximately 16h with Ad11p and ColoAd1 or 24h with Ad5 showed decreased 53BP1 foci formation at early time points after irradiation, suggesting the viruses required these lengths of time to inhibit 53BP1 foci formation.

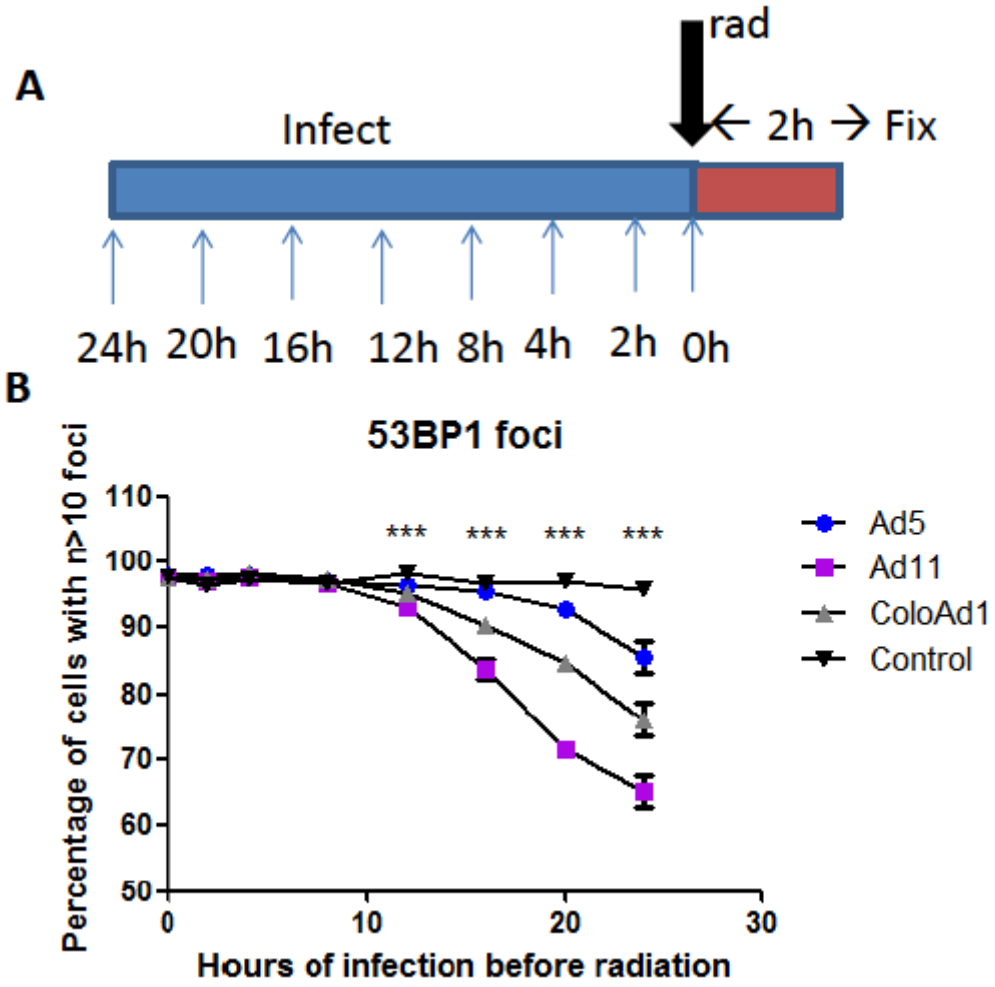

Figure 5.19: Effects of adenovirus infection time on 53BP1 foci formation in DLD cells. A: schematic overview of the experiment. Cells were seeded overnight and subsequently infected 24h to 0h before radiation with 5 Gy. Cells were fixed 2h after irradiation and 53BP1 foci were stained and automatically analysed using InCell software. B: quantification of the percentage of cells with more than 10 53BP1 foci in the nucleus at several time points after radiation. C: quantification of the average amount of foci in the nucleus of radiated cells at several time points after radiation. The experiment was performed in quadruplicates. Mean and SD shown.

Ad5, Ad11p and ColoAd1 all inhibited 53BP1 foci formation on early time points after radiation. However, on later time points after irradiation, no differences in 53BP1 foci count were seen between adenovirus infected cells and non-infected cells.

Ad11p and ColoAd1 inhibit foci formation earlier during infection compared to Ad5. Comparison of 53BP1 foci formation in cell infected with all three viruses at

later after irradiation was not possible, due to the fast cell death induced by infection with 100 vp/cell of ColoAd1 or Ad11p. To compare the speed of infection of all three viruses, cell viability was assessed in real-time using an XCelligence system. Cells were plated and incubated over night, before starting infection (blue arrow in figure 5.20). As can be seen in figure 5.20, both Ad11p and ColoAd1 kill DLD cells faster than Ad5. Most likely the slower onset of inhibition of the cell's ability to produce 53BP1 foci in the case of Ad5 infection compared to the other viruses, is due to the slower progression of Ad5 adenovirus infection and subsequent cytotoxicity compared to Ad11p and ColoAd1 in DLD cells.

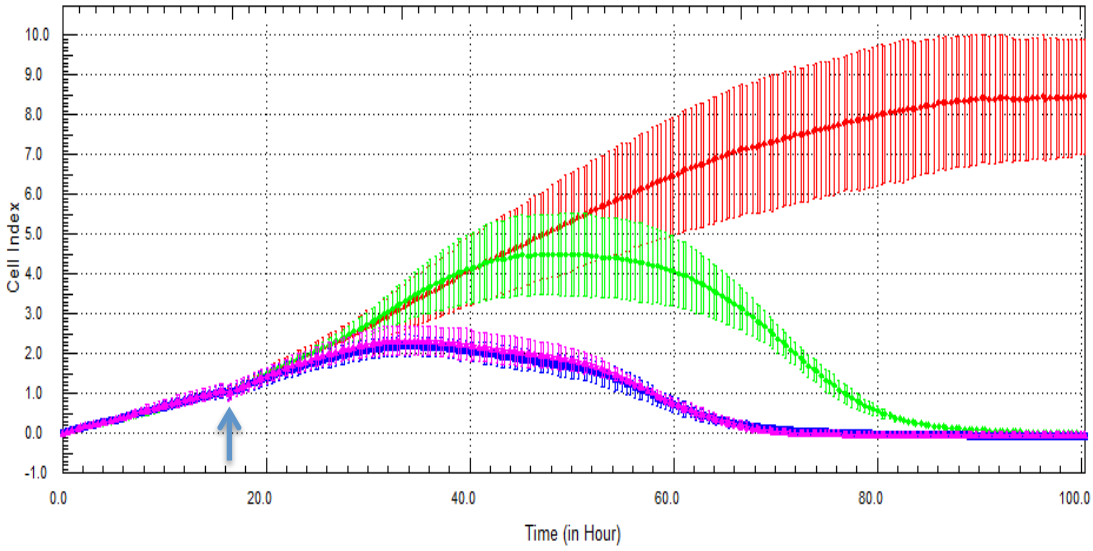

Figure 5.20: Cytotoxicity time course of adenovirus infection in DLD cells. Cells ($5x10^3$ cells/well) were seeded at 0h and left overnight. 16h after seeding cells were infected (see blue arrow) with 100 vp/cell Ad5 (green), Ad11p (blue) or ColoAd1 (purple) or control (red). Cell viability was measured every 15 min using the XCelligence. Both ColoAd1 and Ad11p killed cells quicker than Ad5 infection. The experiment was performed in quadruplicates. Mean and SD shown.

5.3.5 *In vivo* study combining ColoAd1 and ColoAd1 fm TNF with radiation

Multiple studies have shown synergy between Ad5-based viruses and radiation therapy *in vivo*. Some *in vitro* studies have been done to look at the effects other adenovirus species have on DNA repair pathways. However, to the best of our knowledge, no *in vivo* studies have been performed combining a species B virus with radiation therapy. To test whether ColoAd1, a species B-derived virus, or ColoAd1 fm TNF synergize with radiation *in vivo* an animal experiment was set up. Mice were implanted with 5 x 10^6 DLD cells subcutaneously. At day 15 and 16 post tumour implantation, when tumours were small but well-established, mice were started on treatment (5 x 10^9 VP ColoAd1, ColoAd1 fm TNF or PBS; three intratumoural injections, every 3 days). The mice were radiated with 15 Gy, at the site of the tumour, whilst having their bodies shielded with led, 24 h after receiving the last virus injection. The radiation dose was chosen based on a study showing reduced tumour growth when administering 15 Gy in a single fraction to DLD xenograft tumours (*321*). The 24 h time point of radiation after injection was based on previous study showing synergy between radiation and Ad5 when radiation was administered 24h after viral injection (*310*).

Data was analyzed using SPSS (IBM), using a multilevel regression model testing changes in tumour growth over time between groups. The hierarchy in data is that time points were nested within individual mice.

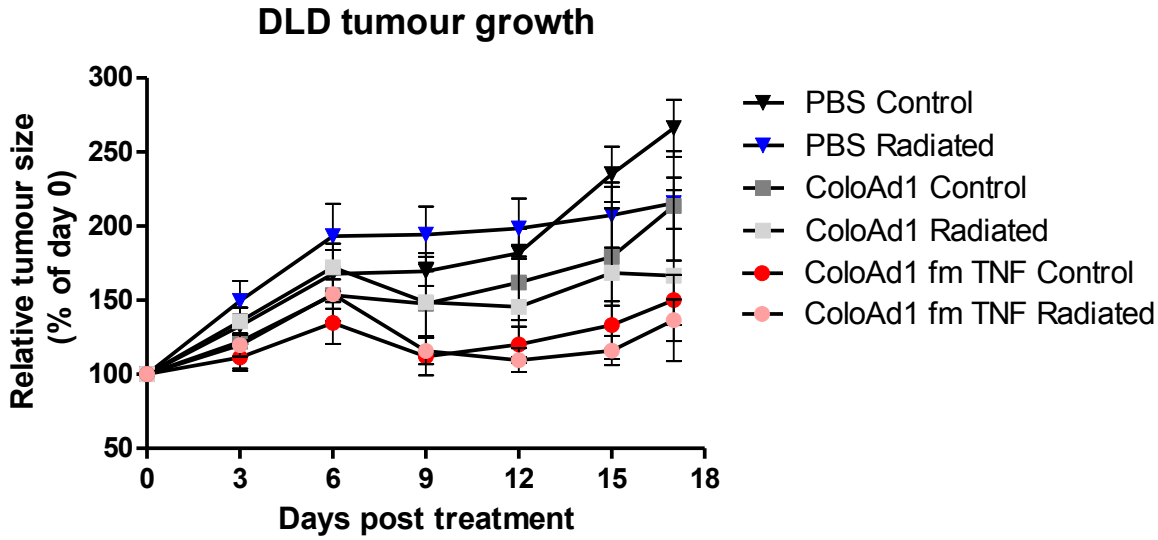

Figure 5.21: *In vivo* effects of combining radiation and ColoAd1 or ColoAd1 fm. BALB/c mice were injected s.c. with DLD cells ($5x10^6$) and at day 15 or 16 post tumour implantation (day 0 post treatment), the tumours were injected with 5 x 10^9 vp ColoAd1 (n=5 for control; n=6 for radiation) or ColoAd1 fm TNF (n=6 for control; n=7 for radiation) or PBS (n=6 for control, n=7 for radiation) on day 0, day 3 and day 6. Subsequently, 24h after the last injection (day 7), tumours were radiated with 15 Gy (squares) or not radiated (control, circles). Tumour size was measured every 2-3 days and expressed and as a percentage of the last pre-treatment measurement (day 0). A multilevel longitudinal regression analysis was performed using SPSS, a borderline not significant group effect over time was found (p=0.061).

Similar to results seen by Williams et al., 15 Gy radiation reduced tumour growth of DLD cells treated with PBS (*321*). Similarly, tumours treated with ColoAd1 or ColoAd1 fm TNF treated with 15 Gy radiation showed little tumour growth after radiation. However, no statistically significant differences in tumour growth between groups were observed (p=0.061). No additive effects or synergy were seen on tumour growth in mice treated with a combination of radiation and viral therapy in this DLD xenograft model.

Using Ad5-based viruses, an increase in viral genome copies has been seen *in vivo* when combining virotherapy with radiation. To test whether irradiation had an effect on ColoAd1 genome copies, tumours were homogenized and a QPCR was done to compare treatment groups.

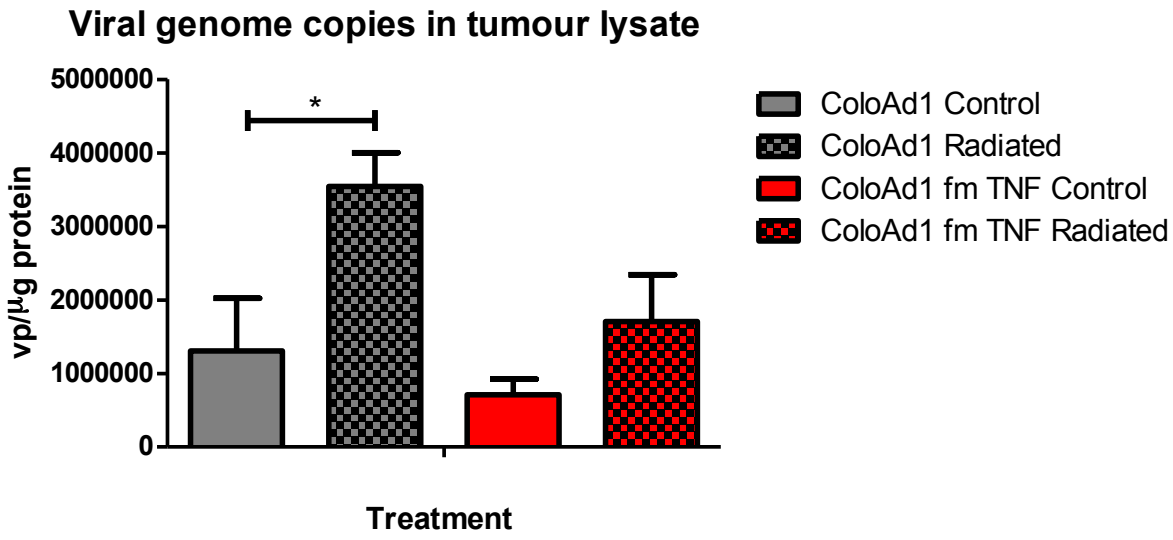

Figure 5.22: Viral genome copies in tumours 10 days post radiation or control, normalized to protein concentration. Using a 1-way ANOVA, statistically significant difference in viral genome copies was found (p=0.0338). Using a student T test, an increase in viral genome copies was found in mice treated with ColoAd1 and radiation compared to mice treated with ColoAd1 and no radiation (p=0.0491). An increase in genome copies was also seen in mice treated with ColoAd1 fm TNF and radiation compared to control mice, although this difference was not statistically significant (p=0.19).

At 10 days post irradiation, an increase in viral genome copies in the tumour lysate is observed in mice treated with ColoAd1, compared to non-irradiated controls (figure 5.22). This result is discussed in more detail in section 5.4. Similar to previous studies comparing viral genome copies of ColoAd1 and ColoAd1 fm TNF *in vivo*, a non-statistically significant (p=0.44) decrease in ColoAd1 fm TNF viral genome copies was seen in the tumour lysate, compared to ColoAd1, see figure 5.22.

Finally, TNF levels were assessed in the tumour lysate using an ELISA. In concurrence with the increased viral genome copies of ColoAd1 fm TNF in irradiated tumours compared to non-irradiated tumours, an increase in TNF levels was seen in these tumours. However this increase was not statistically significant (p=0.08), see figure 5.23.

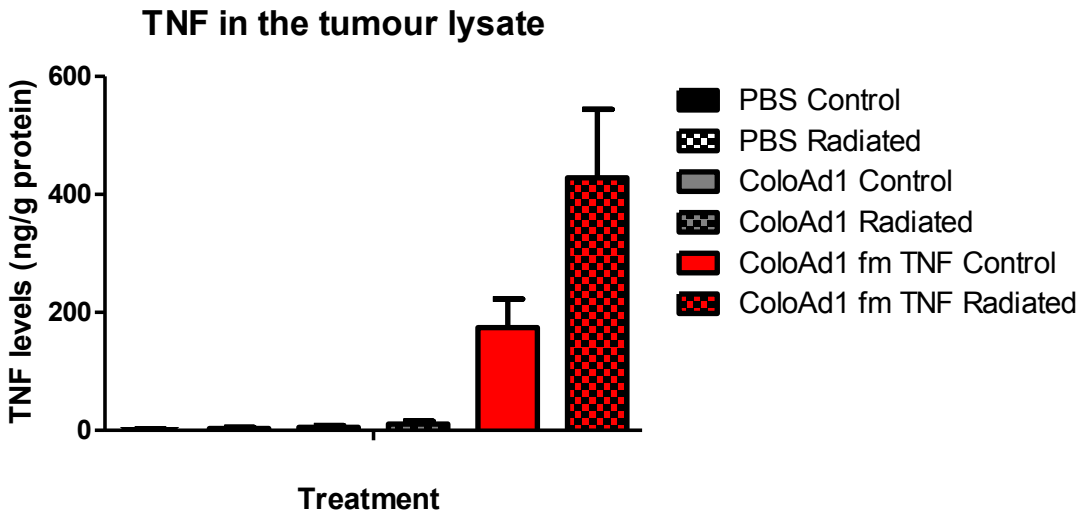

Figure 5.23: TNF levels in the tumours 10 days post radiation. TNF was quantified in the tumour lysate of mice treated with PBS (black), ColoAd1 (grey) or ColoAd1 fm TNF (red) and 15 Gy of radiation (checked bars) or control (even coloured bars) using an ELISA. Statistical significance was tested using a one-way ANOVA. A borderline not significant (p=0.0837) increase in TNF levels was seen in tumour of mice treated with ColoAd1 fm TNF that were irradiated compared to controls. Mean and SEM are depicted.

5.4 Discussion

The combination of radiotherapy with virotherapy may be beneficial because both modalities can be applied locoregionally.

Two main DNA damage sensors are involved in the DNA damage response; one pathway is mediated through MRN activation and subsequent ATM activation, leading to CHK2 and p53 activation. The other pathway is mediated through ATR and subsequent CHK1 activation. ATR is activated through single strand (ss) DNA, DSB and replication stress (*322*). For Ad5, degradation of Mre11 and Rad50, two components of the MRN complex and p53 degradation have been described. Concurrent with literature about other cell lines, in DLD and HT29 cells Ad5 infection leads to the degradation of Mre11, Rad50 and p53 proteins (*286, 289, 290*). Both Ad11p and ColoAd1 infection of DLD or HT29 cells do not lead to the degradation of these proteins. Additionally, Ad11p infection does not lead to p53 degradation. Lack of degradation of MRN complex proteins and p53 has also been shown previously for Ad11p (*296*). Furthermore, upon ionizing radiation, phosphorylation of p53 still occurs in Ad11p infected cells, suggesting that p53 may still be functional in Ad11p infected cells. Interestingly, ColoAd1 infection leads to a decrease in p53 levels, whereas Ad11p does not.

Adenoviruses need to interfere with the cellular DNA damage response to avoid genome concatamerization (*286*). As discussed in section 5.1, the DNA damage response has two major sensors of DNA damage, the ATM pathway and the ATR pathway. Ad12 has been shown to interfere with TOPBP1 and thereby ATR activation (*315*). As Ad11p and ColoAd1 do not degrade Mre11 (in the ATM pathway) to the same extend as Ad5, it would be interesting to investigate

whether preferential interference with the ATR pathway occurs in species B adenovirus.

For Ad5 based vectors, increase in viral uptake and transcription of viral DNA have been reported (*314, 323*). In vitro, radiation with 5 Gy either 6 or 24 h before or after infection with ColoAd1 did not result in statistically significant changes in viral replication in DLD cells, as measured by QPCR.

Interestingly, an increase in viral genome copies was found in tumours treated with radiation compared to non-radiated controls in ColoAd1 ($p=0.0338$). An increase in viral genome copies of irradiated tumours treated with ColoAd1 fm TNF was also seen, compared to non-radiated ColoAd1 fm TNF controls, however this difference was not statistically significant. Yet, despite an increase in viral genome copies in radiated tumours compared to non-radiated tumours, viral therapy did not have a synergistic or additive effect on tumour growth in DLD xenografts. For Ad5, synergy between virotherapy and radiation has been found in multiple preclinical tumour models (*307-311*). Perhaps as a result of reduced p53 and MRN-complex degradation, no synergy between radiation and ColoAd1 or ColoAd1 fm TNF was seen in the *in vivo* study using a DLD xenograft model. However, the *in vivo* study did not include an Ad5 control to test synergy in this model. Thus, the lack of synergy might also be due to the tumour model and cell line used or due to the treatment regimen used in this study.

The increase in viral genome copies in irradiated tumours may, however, be very useful for successful virotherapy, as lack of viral spread is an important hurdle for successful virotherapy. Increased viral particles or viral genomes have been seen previously upon Ad5 treatment (*308, 310*). Moreover, Portella et al. found a synergistic effect when combining the selectively replicating ONYX-015 with 10

Gy of radiation, but not when using a non-replicating Ad5 vector (*308*). Suggesting that the synergy between virotherapy and radiation may be due to increased replication. Additionally, increased viral spread and viral particles *in vivo* have also been found after radiation with other double-stranded DNA oncolytic virus treatments, such as HSV1 (*324, 325*). Radiation changes the cellular processes such as gene expression and posttranslational modifications. These changes might lead to increased susceptibility to virotherapy and increased replication of viruses (*285*). Alternatively, increase release of viral particles from cells damaged by IR has also been postulated as a cause for the increased viral particles found when combining IR and oncolytic virotherapy (*285*).

As mentioned in chapter 4, treatment with TNF expressing Ad5-based viruses and radiation therapy have shown synergy. Contrary to these studies, no synergy between ColoAd1 fm TNF and radiation was observed. TNFerade, a non-replicating vector expressing TNF under the Egr1 promoter, has shown large reductions in tumour volume when combining radiation with viral therapy, compared to either agent alone. Although the highest levels of TNF with both viruses are roughly equal, the TNF kinetics of this vector differs from the kinetics seen with ColoAd1. Using TNFerade, TNF levels go up within the first week after treatment with TNFerade (*206*), whereas TNF expressed from ColoAd1 seems to drop off quickly after treatment, see figure 4.13. Thus, the area under the curve for TNF expression may be larger for TNFerade than for ColoAd1. The differences in kinetics and total production of TNF expression may explain why synergy was seen between TNFerade and radiation, whereas synergy was not seen between ColoAd1 fm TNF and radiation. It should be noted that this pilot

data was obtained without including radiation, whereas radiation showed a significant increase in ColoAd1 genome copies and a non-statistically significant increase in ColoAd1 fm TNF at day 10 post radiation. Thus, the viral kinetics post radiation may differ compared to non-radiated controls.

5.4.1 Limitations

More time-consuming radiobiology assays, such as clonogenic assays, were not possible due to the fast killing seen with adenovirus infection of colorectal cancer cell lines. To study the effects of species B adenovirus on DNA repair, assays with cells stably transduced with adenoviral proteins, such as E4 proteins, will be necessary for more conclusive results on the interaction between species B viruses and DNA repair. Furthermore, due to time constraints, generation of E4 deleted ColoAd1 or Ad11p viruses was not possible. Using these mutant viruses, might provide better insight into the effects species B proteins have.

5.5 Chapter conclusion

Ad11p and ColoAd1 do not degrade the MRN complex and p53 to the same extend as Ad5 does.

A synergetic reduction of tumour growth between radiation therapy and ColoAd1 or ColoAd1 fm TNF was not observed in a DLD xenograft model. However, an increase in ColoAd1 genome copies was seen in irradiated tumours compared to non-radiated tumours at day 10 post radiation ($p=0.0338$). An increase in ColoAd1 fm TNF genome copies was also observed, although this was not statistically significant ($p=0.19$).

Chapter 6: Discussion

6.1 Preface

Despite advances in cancer therapy, the prognosis for patients with advanced metastatic cancers is still very poor. Lack of efficacy in the clinic is still a major hurdle for the treatment of cancer patients with oncolytic virus therapy. The overarching aim of this thesis was to improve the efficacy of ColoAd1 by arming this virus with TNF and LTA. As all three results chapters of this thesis explored different aspects of local TNF expression and virotherapy, most results and limitations of the work done are discussed at the end of each chapter. This section attempts to summarize the principal findings and general discussion, as well as the implications and possible areas for future research.

6.2 Principal findings

6.2.1 Chapter 3

- The Lenti-X-Tet-ON system shows inducible expression of TNF in CT26 cell, both *in vitro* and *in vivo*.
- Expression of sm, fm and mbm TNF leads to increased immune infiltration into syngeneic CT26 tumours. Mostly myeloid cell infiltration is increased in these tumours upon TNF expression.
- *In vivo*, expression of mbm TNF leads to a reduction in tumour growth of CT26 cells compared to non-Dox controls.

- Using the inducible cell lines, no signs of systemic toxicity were observed, suggesting that local expression of TNF from tumours may be a safe strategy.
- The highest levels of fm TNF expression seen from inducible cell lines is approximately 20-fold lower than the levels seen 3 days after injection 3 ColoAd1 fm TNF injections, three days apart.

6.2.2 Chapter 4

- High levels of TNF were found at early time points after intratumoural injections with ColoAd1 fm TNF and these levels dropped over time. However, the expression of fm or mbm TNF from ColoAd1 did not reduce tumour growth or increase survival compared to ColoAd1. Statistically significant lower amounts of ColoAd1 mbm TNF genome copies were found in tumour compared to ColoAd1. Additionally, a decrease in ColoAd1 fm TNF genome copies was found consistently in every *in vivo* study, although this reduction was not statistically significant.
- Evidence of systemic toxicity was not observed using ColoAd1 expressing TNF in athymic BALB/c nude mice.
- A borderline not significant increase in survival was seen in mice treated with virotherapy compared to PBS ($p=0.0626$).
- In virus treated tumours, an increase in immune cells within the tumours was observed. Specifically, increased monocytic MDSC and DC infiltration into tumours was seen in ColoAd1, ColoAd1 fm and ColoAd1 mbm TNF treated tumours compared to PBS. Additionally, an increase in the

granulocytic MDSC population within tumours treated with ColoAd1 and ColoAd1 fm TNF compared to control was seen. IL-10 expression is increased in tumours treated with ColoAd1 or ColoAd1 fm TNF compared to PBS control.

- Unfortunately, mLTA expression from ColoAd1 was not seen at high levels, *in vitro*. Therefore, this virus was not used in subsequent *in vivo* studies.

6.2.2 Chapter 5

- Contrary to Ad5, Ad11p and ColoAd1 do not degrade Mre11 and Rad50 in HT29 and DLD cells. Additionally, p53 degradation is more efficient in cells infected Ad5 than Ad11p or ColoAd1.
- Similar to other adenoviruses, Ad11p and ColoAd1 degrade DNA ligase IV.
- H2AX and ATM are phosphorylated during late stages of Ad5, Ad11p and ColoAd1 infection.
- At early time points after radiation, 53BP1 foci formation is reduced in adenovirus infected cells.
- Combination of radiation with ColoAd1 therapy resulted in an increase in viral genome copies in irradiated tumours, 10 days post radiation. Despite an increase in viral genome copies, no synergistic effects between virotherapy and radiation therapy were seen on tumour growth.

6.2.3 Main findings thesis

- Arming ColoAd1 did not improve anticancer efficacy in xenograft CRC model compared to unarmed ColoAd1. Lower viral genome copies were

found in tumours treated with ColoAd1 TNF compared to ColoAd1, which may have been a major contributor to the failure to improve the efficacy by arming ColoAd1. This decrease may be due to decreased replication or increased viral clearance.

6.3 General discussion

Arming oncolytic viruses to enhance the efficacy has received a lot of attention lately, especially as T-Vec, an oncolytic herpes virus encoding GM-CSF has recently been shown clinical efficacy and has now been approved for melanoma therapy (*25, 26*). T-Vec serves as a proof-of-concept for arming oncolytic viruses to enhance the immune response to tumour. Following T-Vec, several different oncolytic viruses encoding immune modulatory proteins are currently in clinical trials (*25, 26, 28-31*).

The aim of this thesis was to improve ColoAd1 cancer therapy by arming this adenovirus with TNF and LTA, two powerful pro-inflammatory cytokines.

Previous attempt to use adenoviruses armed with TNF as cancer therapy have also been made. A non-replicating Ad5 based vector expressing TNF under the control of a radiation inducible Egr1 promoter, named TNFerade, has been developed previously. Using this vector, good efficacy was seen in preclinical mouse studies when combined with radiation (*205, 206, 267*). However, this vector ultimately failed in phase III studies for the treatment of locally advanced pancreatic cancer, due to lack of effectiveness (*240*). More recently, a replicating Ad5 virus expressing TNF from the E3 region reduced tumour growth compared to unarmed Ad5 virus in both a xenograft postate carcinoma model and a

syngeneic melanoma mouse model (*242*). Contrary to these studies with TNF-armed adenovirus, arming ColoAd1 with TNF did not increase the anti-tumour efficacy in a preclinical xenograft model. ColoAd1 has been selected on its increased ability to kill cancer cells (62). Perhaps, due to the optimization that has already occurred in ColoAd1, it is more difficult to improve oncolytic virus therapy with this virus than with Ad5, which naturally infects repiratory epithelial cells and has not been subjected to selective pressure on speedy killing of tumour cells (*326*). Moreover, due to increased speed of kill, the expression of transgenes by ColoAd1 may be limited. TNF kinetics compared to TNF from TNFerade is discussed in more detail in chapter 4.4.

In vitro, treatment with TNF and infection with ColoAd1 did not reduce viral replication. Also, cell viability was reduced in both 293A cells and DLD cells treated with ColoAd1 fm TNF or ColoAd1 mbm TNF compared to parental ColoAd1. Compared to parental ColoAd1, decreased viral genome copies were found in xenograft tumours treated with ColoAd1 expressing TNF. Perhaps, an increased ability to kill infected cells has reduced the ability of ColoAd1 to replicate and produce active progeny virus *in vivo*. Alternatively, ColoAd1 TNF may be cleared more rapidly through the host immune response. There may be an inevitable trade-off between immune stimulation and/or increased cytotoxic potential and the ability of adenoviruses to replicate and spread in tumours.

The loss of E3 proteins may have contributed to the decrease in viral genome copies seen from ColoAd1 TNF *in vivo*. E3 proteins, amongst other immune modulatory functions, inhibit cell lysis by TNF in cells infected by adenovirus (*56*). Additionally, E3 proteins also inhibit MHC-I molecule loading and transport of this receptor to the cell surface (*50-54*). Additionally, inhibition of

apoptosis by Fas ligand by E3 14.7K has also been reported. *In vitro*, these proteins seem redundant, as the E1B-19K protein can also protect cells infected with E3-deleted virus from lysis by TNF (*59*). However, it is possible that E3 proteins are not redundant *in vivo* and contributed to increased viral clearance of ColoAd1 TNF. Arming a vaccinia virus with Ad2 14.7K and mTNF in SCID mice increased its virulence compared to VV armed with only TNF (*327*). This suggests that E3 has a role in maintaining viral infections even in severely immunecompromised environments *in vivo.* Moreover, deletion of E3 proteins decreased the persistance of AD5 in a permissive. Immunocompetent Syrian hamster model of pancreatic cancer (*328*). A study that included the herpes virulence factor glycoprotein G (gG), a broad-spectrum viral chemokine binding protein into the VSV genome saw increased efficacy of the VSV-gG virus compared to wt VSV (*329*). Thus, virulence factors may be important for oncolytic virus therapy and further studies are necessary to confirm the role of E3 deletions in ColoAd1 biology. PsiOxus Ltd. has recently developed Ad-Backs; these viruses have replace the mutations found in ColoAd1 back to the parental Ad11p sequences (personal communications). Arming an Ad-Back with a restored E3 region with TNF could help determine whether the E3 deletion has made armed ColoAd1 more susceptible to immune clearance *in vivo*.

The degradation of Mre11 and Rad50 by Ad5 proteins has been well documented. (*286, 289, 290*). In studies performed in this thesis, Ad11p and ColoAd1 do not degrade these two proteins. Previous studies have also shown that Ad11 does not degrade the MRN complex or p53 (*296*). Interestingly, Ad5, Ad11p and ColoAd1 all reduce 53BP1 foci upon radiation, at early time point

after radiation. 53BP1 is an important protein in regulation of the DNA damage response; it acts as a scaffold for other DNA repair proteins, amplifies ATM signalling and promotes checkpoint signalling and is also requiered for NHEJ (*318*). 53BP1 is downstream of ATM and needs the MRN complex, ATM, MDC1, RNF8, RNF168 and HERC2 to get translocated to DSB sites (*330-333*). Perhaps, through targetting MDC1, RNF8, RNF168 or HERC2, Ad11p and ColoAd1 decrease the accumulation of 53BP1 at damage sites, whereas Ad5 achieves this through targetting the MRN complex. Additionally, Ad12, a species A adenovirus, has shown interference with the ATR pathway through degradation of TOPBP1 (*294*). It is possible that species B virus also preferentially target the ATR pathway instead of the ATM pathway. Further studies are necessary to confirm the mechanism of action of DNA damage repair interference of species B adenovirus.

To date, most research on oncolytic adenovirus therapy and adenovirus biology has been conducted on species C virus, such as Ad2 and Ad5. The use of species B, such as ColoAd1, Ad11p and Ad3, virus could have several potential benefits such as lower levels of pre-existing immunity and decreased liver toxicity (*64, 65*). Moreover, CAR, the entry receptor for species C adenovirus, is often downregulated in cancer cells, whereas CD46 is often expressed by CRC cells (*334*). Better understanding of species B adenovirus biology and its therapeutic properties, such as pharmacokinetics and pharmacodynamics, might help improve the development of species B adenoviruses as oncolytic agents.

6.4 Future directions

Administration of TNF can increase the uptake of many therapeutic agents, including small molecules, antibodies, liposomes and viruses into tumour sites (*183, 202, 207, 208, 210, 211*). Additionally, several therapeutic agents synergize with TNF, including doxorubicin and melphalan (*230*). More recently, synergy between TNF and SMAC mimetic compounds has been shown as well. These drugs sensitize cells to apoptosis by blocking the activity of inhibitors of apoptosis (*335*). The increase extravasation in tumours treated with ColoAd1 or ColoAd1 fm TNF, as seen with Evans blue, suggest there may be an increase in vascular permeability in tumours treated. The combination of the aforementioned therapeutic agents with ColoAd1 TNF may lead to synergy due to increased drug extravasation at tumour sites.

As discussed in section 4.5, increased IL-10 expression and increased infiltration of dendritic cells, granulocytic and monocytic myeloid derived suppressor cells were seen in tumours treated with ColoAd1 or ColoAd1 TNF compared to PBS. It would be interesting to see whether arming ColoAd1 with molecules targeting the immune suppression (for example with IL-10 or TGFβ scavengers) would cause a decrease in MDSC infiltration and increase the efficacy of ColoAd1 treatment. Additionally, arming ColoAd1 with cytokines that drive the infiltrating myeloid cells towards a more pro-inflammatory and anti-tumoural phenotype may improve the efficacy of ColoAd1. An example of such a cytokine would be IFNγ, which polarizes macrophages towards an M1 activated phenotype (*96*). This strategy is currently investigated by Philip Jakeman (Len Seymour laboratory). Cancer cells and their stroma cells create a complex immunosuppressive environment by secretion of multiple immunosuppressive

cytokines, such as IL-6 IL-10, TGFβ and other molecules such adenosine (*275, 276*). Perhaps, the expression of a single pro-inflammatory cytokine from an oncolytic virus is not the most efficient approach to overcome the immunosuppression by the immunosuppressive molecules present in the tumour microenvironment. Encoding a combination of molecules targeting immune suppressive cytokines together with immune stimulatory proteins such as TNF or IFNγ within an adenovirus may improve oncolytic virus therapy. Alternatively, arming oncolytic viruses with immune checkpoint inhibitors, such as anti-CTLA-4 or PD1 antibodies may be more beneficial than arming with cytokines (*336*). Further studies are necessary to assess the best arming strategy for oncolytic virus therapy.

For Ad5, interference with the ATM/Chk2/p53 pathway is well established (*286, 289, 290*). Ad11p and ColoAd1 appear to have a different mechanism of action to avoid concatemerization and do not degrade the MRN complex and p53 to the same extent as Ad5. Further studies into the mechanism of interference with DNA repair proteins by Ad11p and ColoAd1 are necessary. Generation of cell lines stably expressing E1 and E4 proteins might help study the effects species B virus have on DNA repair. Perhaps as a result of not degrading MRN and p53, no evidence was found for synergy between ColoAd1 and radiation therapy in a DLD xenograft model. It would be interesting to see whether targeting of the MRN complex, by for example short hairpin RNA sites incorporated in ColoAd1 would lead to sensitization to radiotherapy.

6.5 Final conclusion

Oncolytic viruses therapy utilizes viruses that selectively replicate in tumour cells, leading to cell death. A desirable feature of virotherapy is encoding a gene that will affect cells surrounding the infected cell, thus causing a bystander effect. Prolonged local expression and reduced systemic toxicity obtained by this strategy is potentially a major benefit over systemic delivery or intratumoural injection of cytotoxic proteins. The work in this thesis sought to improve the efficacy of ColoAd1 therapy by arming ColoAd1 with TNF and LTA. TNF is an interesting gene to encode in an oncolytic virus as it has shown several potent mechanisms of action against tumour cells, including destruction of tumour-associated vasculature, enhanced tumour immunity and in some cases direct cytotoxic effects on cancer cells.

A syngeneic model was set up to study TNF in a immune-competent host. Using a CT26 Dox-inducible model, expression of sm, fm and mbm TNF leads to increased immune infiltration, most of which were myeloid cells. Expression of sm TNF or fm TNF did not influence tumour growth, whereas, expression of mbm TNF leads to a reduction in tumour growth of CT26 cells compared to non-Dox controls. Unfortunately, the TNF levels seen with this model are far lower than TNF levels seen shortly after treatment with ColoAd1 fm TNF.

In vitro, TNF treatment did not reduce ColoAd1 infection or replication. Additionally, increased cytotoxicity was seen in 293A and DLD cells infected with ColoAd1 fm TNF or ColoAd1 mbm compared to ColoAd1 infected cells.

High levels of TNF were found at early time points after intratumoural injections with ColoAd1 fm TNF and these levels dropped over time. The expression of fm or mbm TNF from ColoAd1 did not reduce tumour growth, or increase survival

compared to treatment with ColoAd1. Perhaps as a result of the absence of adaptive immunity, ColoAd1 mbm TNF did not reduce tumour growth, whereas mbm TNF expression reduced CT26 tumour growth. The development of better pre-clinical models is needed to study the full effects of arming human adenoviruses in an immune comptetent host. Statistically significant lower amounts of ColoAd1 mbm TNF genome copies were found in tumour compared to ColoAd1. Additionally, decreased ColoAd1 fm TNF genome copies compared to ColoAd1 were found consistently, although this difference was not statistically significant.

In ColoAd1 or ColoAd1 fm TNF treated tumours, increased monocytic and granulocytic MDSC and DC infiltration into tumours was seen, compared to PBS. Additionally, IL-10 expression is increased in tumours treated with ColoAd1 or ColoAd1 fm TNF compared to PBS control. Together these results suggest an immune suppressive phenotype upon virus treatment.

Expression of TNF from ColoAd1 was well tolerated and hepatic or systemic toxicity were not observed, suggesting that virotherapy can be used to express molecules that may not be suitable for systemic delivery.

The combination ColoAd1 with irradiation lead to increased viral genome copies in irradiated tumours, 10 days post radiation. Yet, a synergistic decrease in tumour growth between radiation and ColoAd1 or ColoAd1 fm TNF was not observed.

Unfortunately, both CT26 mLTA cells and ColoAd1 armed with mLTA did not produce mLTA protein expression, *in vitro*. Therefore, the effects of inducing expression of LTA intratumourally could not be tested.

In conclusion, ColoAd1 can be used to deliver powerful cytokines, such as TNF, to the tumour microenvironment without inducing systemic toxicity. Arming ColoAd1 with immunemodulatory proteins may increase its clinical potential.

References:

1. A. Jemal *et al.*, Global cancer statistics. *CA Cancer J Clin* **61**, 69 (Mar-Apr, 2011).
2. D. Hanahan, R. A. Weinberg, The hallmarks of cancer. *Cell* **100**, 57 (Jan 7, 2000).
3. D. Hanahan, R. A. Weinberg, Hallmarks of cancer: the next generation. *Cell* **144**, 646 (Mar 4, 2011).
4. W. C. Hahn, R. A. Weinberg, Modelling the molecular circuitry of cancer. *Nat Rev Cancer* **2**, 331 (May, 2002).
5. C. E. DeSantis *et al.*, Cancer treatment and survivorship statistics, 2014. *CA Cancer J Clin* **64**, 252 (Jul-Aug, 2014).
6. M. M. Center *et al.*, Worldwide variations in colorectal cancer. *CA Cancer J Clin* **59**, 366 (Nov-Dec, 2009).
7. H. Brenner *et al.*, Colorectal cancer. *Lancet* **383**, 1490 (Apr 26, 2014).
8. D. H. Kim *et al.*, CT colonography versus colonoscopy for the detection of advanced neoplasia. *N Engl J Med* **357**, 1403 (Oct 4, 2007).
9. D. R. Rudy, M. J. Zdon, Update on colorectal cancer. *Am Fam Physician* **61**, 1759 (Mar 15, 2000).
10. D. F. Ransohoff *et al.*, Colorectal cancer screening: clinical guidelines and rationale. *Gastroenterology* **113**, 1423 (Oct, 1997).
11. Y. Miyoshi *et al.*, Somatic mutations of the APC gene in colorectal tumors: mutation cluster region in the APC gene. *Hum Mol Genet* **1**, 229 (Jul, 1992).
12. S. M. Powell *et al.*, APC mutations occur early during colorectal tumorigenesis. *Nature* **359**, 235 (Sep 17, 1992).
13. B. Vogelstein *et al.*, Genetic alterations during colorectal-tumor development. *N Engl J Med* **319**, 525 (Sep 1, 1988).
14. S. J. Baker *et al.*, p53 gene mutations occur in combination with 17p allelic deletions as late events in colorectal tumorigenesis. *Cancer Res* **50**, 7717 (Dec 1, 1990).
15. R. Tang *et al.*, Mutations of p53 gene in human colorectal cancer: distinct frameshifts among populations. *Int J Cancer* **91**, 863 (Mar 15, 2001).
16. S. B. Edge *et al.*, in *American Joint Committee on Cancer (AJCC) Staging Manual*. (2010), vol. 7, pp. 143-163.
17. G. Wilkes, K. Hartshorn, Clinical update: colon, rectal, and anal cancers. *Semin Oncol Nurs* **28**, e1 (Nov, 2012).
18. M. A. Khattak *et al.*, Survival differences in patients with metastatic colorectal cancer and with single site metastatic disease at initial presentation: results from South Australian clinical registry for advanced colorectal cancer. *Clin Colorectal Cancer* **11**, 247 (Dec, 2012).
19. M. S. Roberts *et al.*, Naturally oncolytic viruses. *Curr Opin Mol Ther* **8**, 314 (Aug, 2006).
20. E. A. Chiocca, Oncolytic viruses. *Nat Rev Cancer* **2**, 938 (Dec, 2002).
21. K. A. Parato *et al.*, Recent progress in the battle between oncolytic viruses and tumours. *Nat Rev Cancer* **5**, 965 (Dec, 2005).
22. S. J. Russell *et al.*, Oncolytic virotherapy. *Nat Biotechnol* **30**, 658 (Jul, 2012).

23. G. Hallden, G. Portella, Oncolytic virotherapy with modified adenoviruses and novel therapeutic targets. *Expert Opin Ther Targets* **16**, 945 (Oct, 2012).
24. J. W. Choi *et al.*, Evolution of oncolytic adenovirus for cancer treatment. *Adv Drug Deliv Rev* **64**, 720 (Jun 1, 2012).
25. H. L. Kaufman, S. D. Bines, OPTIM trial: a Phase III trial of an oncolytic herpes virus encoding GM-CSF for unresectable stage III or IV melanoma. *Future Oncol* **6**, 941 (Jun, 2010).
26. R. H. Andtbacka *et al.*, Talimogene Laherparepvec Improves Durable Response Rate in Patients With Advanced Melanoma. *J Clin Oncol*, (May 26, 2015).
27. R. Eager, J. Nemunaitis, GM-CSF gene-transduced tumor vaccines. *Mol Ther* **12**, 18 (Jul, 2005).
28. O. Hemminki *et al.*, Immunological data from cancer patients treated with Ad5/3-E2F-Delta24-GMCSF suggests utility for tumor immunotherapy. *Oncotarget* **6**, 4467 (Feb 28, 2015).
29. J. M. Burke *et al.*, A first in human phase 1 study of CG0070, a GM-CSF expressing oncolytic adenovirus, for the treatment of nonmuscle invasive bladder cancer. *J Urol* **188**, 2391 (Dec, 2012).
30. J. Heo *et al.*, Randomized dose-finding clinical trial of oncolytic immunotherapeutic vaccinia JX-594 in liver cancer. *Nat Med* **19**, 329 (Mar, 2013).
31. J. L. Li *et al.*, A phase I trial of intratumoral administration of recombinant oncolytic adenovirus overexpressing HSP70 in advanced solid tumor patients. *Gene Ther* **16**, 376 (Mar, 2009).
32. S. M. Wold, M. G. Ison, in *Fields Virology,* D. M. Knipe, P. M. Howley, Eds. (Wolther Kluwer Health, Philadelphia, USA, 2013), pp. 1732-1767.
33. K. Toth *et al.*, Oncolytic (replication-competent) adenoviruses as anticancer agents. *Expert Opin Biol Ther* **10**, 353 (Mar, 2010).
34. H. Liu *et al.*, Atomic structure of human adenovirus by cryo-EM reveals interactions among protein networks. *Science* **329**, 1038 (Aug 27, 2010).
35. G. R. Nemerow *et al.*, Insights into adenovirus host cell interactions from structural studies. *Virology* **384**, 380 (Feb 20, 2009).
36. P. W. Roelvink *et al.*, The coxsackievirus-adenovirus receptor protein can function as a cellular attachment protein for adenovirus serotypes from subgroups A, C, D, E, and F. *J Virol* **72**, 7909 (Oct, 1998).
37. A. Gaggar *et al.*, CD46 is a cellular receptor for group B adenoviruses. *Nat Med* **9**, 1408 (Nov, 2003).
38. H. Wang *et al.*, Desmoglein 2 is a receptor for adenovirus serotypes 3, 7, 11 and 14. *Nat Med* **17**, 96 (Jan, 2011).
39. T. J. Wickham *et al.*, Integrins alpha v beta 3 and alpha v beta 5 promote adenovirus internalization but not virus attachment. *Cell* **73**, 309 (Apr 23, 1993).
40. B. Amstutz *et al.*, Subversion of CtBP1-controlled macropinocytosis by human adenovirus serotype 3. *EMBO J* **27**, 956 (Apr 9, 2008).
41. S. Kalin *et al.*, Macropinocytotic uptake and infection of human epithelial cells with species B2 adenovirus type 35. *J Virol* **84**, 5336 (May, 2010).

42. J. G. Smith *et al.*, Insight into the mechanisms of adenovirus capsid disassembly from studies of defensin neutralization. *PLoS Pathog* **6**, e1000959 (2010).
43. N. Miyazawa *et al.*, Adenovirus serotype 7 retention in a late endosomal compartment prior to cytosol escape is modulated by fiber protein. *J Virol* **75**, 1387 (Feb, 2001).
44. C. J. Bailey *et al.*, Association of adenovirus with the microtubule organizing center. *J Virol* **77**, 13275 (Dec, 2003).
45. U. F. Greber *et al.*, The role of the nuclear pore complex in adenovirus DNA entry. *EMBO J* **16**, 5998 (Oct 1, 1997).
46. A. J. Berk, in *Fields Virology,* D. M. Knipe, P. M. Howley, Eds. (Wolther Kluwer Health, Philadelphia, USA, 2013), pp. 1704-1731.
47. S. M. Berget *et al.*, Spliced segments at the 5' terminus of adenovirus 2 late mRNA. *Proc Natl Acad Sci U S A* **74**, 3171 (Aug, 1977).
48. L. Lenaerts *et al.*, Clinical features and treatment of adenovirus infections. *Rev Med Virol* **18**, 357 (Nov-Dec, 2008).
49. D. L. Lichtenstein *et al.*, Functions and mechanisms of action of the adenovirus E3 proteins. *Int Rev Immunol* **23**, 75 (Jan-Apr, 2004).
50. M. Andersson *et al.*, Impaired intracellular transport of class I MHC antigens as a possible means for adenoviruses to evade immune surveillance. *Cell* **43**, 215 (Nov, 1985).
51. H. G. Burgert, S. Kvist, An adenovirus type 2 glycoprotein blocks cell surface expression of human histocompatibility class I antigens. *Cell* **41**, 987 (Jul, 1985).
52. H. G. Burgert *et al.*, "E3/19K" protein of adenovirus type 2 inhibits lysis of cytolytic T lymphocytes by blocking cell-surface expression of histocompatibility class I antigens. *Proc Natl Acad Sci U S A* **84**, 1356 (Mar, 1987).
53. F. C. Rawle *et al.*, Mouse anti-adenovirus cytotoxic T lymphocytes. Inhibition of lysis by E3 gp19K but not E3 14.7K. *J Immunol* **143**, 2031 (Sep 15, 1989).
54. E. M. Bennett *et al.*, Cutting edge: adenovirus E19 has two mechanisms for affecting class I MHC expression. *J Immunol* **162**, 5049 (May 1, 1999).
55. R. S. Ames *et al.*, Induction of sensitivity to the cytotoxic action of tumor necrosis factor alpha by adenovirus E1A is independent of transformation and transcriptional activation. *J Virol* **64**, 4115 (Sep, 1990).
56. L. R. Gooding *et al.*, A 14,700 MW protein from the E3 region of adenovirus inhibits cytolysis by tumor necrosis factor. *Cell* **53**, 341 (May 6, 1988).
57. W. Schneider-Brachert *et al.*, Inhibition of TNF receptor 1 internalization by adenovirus 14.7K as a novel immune escape mechanism. *J Clin Invest* **116**, 2901 (Nov, 2006).
58. L. R. Gooding *et al.*, The 10,400- and 14,500-dalton proteins encoded by region E3 of adenovirus function together to protect many but not all mouse cell lines against lysis by tumor necrosis factor. *J Virol* **65**, 4114 (Aug, 1991).
59. L. R. Gooding *et al.*, The E1B 19,000-molecular-weight protein of group C adenoviruses prevents tumor necrosis factor cytolysis of human cells but not of mouse cells. *J Virol* **65**, 3083 (Jun, 1991).

60. J. Shisler *et al.*, The adenovirus E3-10.4K/14.5K complex mediates loss of cell surface Fas (CD95) and resistance to Fas-induced apoptosis. *J Virol* **71**, 8299 (Nov, 1997).
61. C. A. Benedict *et al.*, Three adenovirus E3 proteins cooperate to evade apoptosis by tumor necrosis factor-related apoptosis-inducing ligand receptor-1 and -2. *J Biol Chem* **276**, 3270 (Feb 2, 2001).
62. I. Kuhn *et al.*, Directed evolution generates a novel oncolytic virus for the treatment of colon cancer. *PLoS One* **3**, e2409 (2008).
63. C. O'Shea *et al.*, Adenoviral proteins mimic nutrient/growth signals to activate the mTOR pathway for viral replication. *EMBO J* **24**, 1211 (Mar 23, 2005).
64. R. Vogels *et al.*, Replication-deficient human adenovirus type 35 vectors for gene transfer and vaccination: efficient human cell infection and bypass of preexisting adenovirus immunity. *J Virol* **77**, 8263 (Aug, 2003).
65. E. V. Shashkova *et al.*, Characterization of human adenovirus serotypes 5, 6, 11, and 35 as anticancer agents. *Virology* **394**, 311 (Nov 25, 2009).
66. K. W. Kinzler, B. Vogelstein, Lessons from hereditary colorectal cancer. *Cell* **87**, 159 (Oct 18, 1996).
67. K. E. de Visser *et al.*, Paradoxical roles of the immune system during cancer development. *Nat Rev Cancer* **6**, 24 (Jan, 2006).
68. F. Balkwill *et al.*, Smoldering and polarized inflammation in the initiation and promotion of malignant disease. *Cancer Cell* **7**, 211 (Mar, 2005).
69. E. A. Engels *et al.*, Spectrum of cancer risk among US solid organ transplant recipients. *JAMA* **306**, 1891 (Nov 2, 2011).
70. D. Collett *et al.*, Comparison of the incidence of malignancy in recipients of different types of organ: a UK Registry audit. *Am J Transplant* **10**, 1889 (Aug, 2010).
71. C. G. Clemente *et al.*, Prognostic value of tumor infiltrating lymphocytes in the vertical growth phase of primary cutaneous melanoma. *Cancer* **77**, 1303 (Apr 1, 1996).
72. L. Zhang *et al.*, Intratumoral T cells, recurrence, and survival in epithelial ovarian cancer. *N Engl J Med* **348**, 203 (Jan 16, 2003).
73. K. Schumacher *et al.*, Prognostic significance of activated CD8(+) T cell infiltrations within esophageal carcinomas. *Cancer Res* **61**, 3932 (May 15, 2001).
74. Y. Naito *et al.*, CD8+ T cells infiltrated within cancer cell nests as a prognostic factor in human colorectal cancer. *Cancer Res* **58**, 3491 (Aug 15, 1998).
75. F. Pages *et al.*, Effector memory T cells, early metastasis, and survival in colorectal cancer. *N Engl J Med* **353**, 2654 (Dec 22, 2005).
76. V. Shankaran *et al.*, IFNgamma and lymphocytes prevent primary tumour development and shape tumour immunogenicity. *Nature* **410**, 1107 (Apr 26, 2001).
77. R. D. Schreiber *et al.*, Cancer immunoediting: integrating immunity's roles in cancer suppression and promotion. *Science* **331**, 1565 (Mar 25, 2011).
78. J. Galon *et al.*, Type, density, and location of immune cells within human colorectal tumors predict clinical outcome. *Science* **313**, 1960 (Sep 29, 2006).

79. M. Bouvier, Accessory proteins and the assembly of human class I MHC molecules: a molecular and structural perspective. *Mol Immunol* **39**, 697 (Jan, 2003).
80. M. Tosolini *et al.*, Clinical impact of different classes of infiltrating T cytotoxic and helper cells (Th1, th2, treg, th17) in patients with colorectal cancer. *Cancer Res* **71**, 1263 (Feb 15, 2011).
81. F. Pages *et al.*, Immune infiltration in human tumors: a prognostic factor that should not be ignored. *Oncogene* **29**, 1093 (Feb 25, 2010).
82. H. Pere *et al.*, Comprehensive analysis of current approaches to inhibit regulatory T cells in cancer. *Oncoimmunology* **1**, 326 (May 1, 2012).
83. G. Zhou *et al.*, Amplification of tumor-specific regulatory T cells following therapeutic cancer vaccines. *Blood* **107**, 628 (Jan 15, 2006).
84. D. A. Vignali *et al.*, How regulatory T cells work. *Nat Rev Immunol* **8**, 523 (Jul, 2008).
85. S. Kim *et al.*, In vivo natural killer cell activities revealed by natural killer cell-deficient mice. *Proc Natl Acad Sci U S A* **97**, 2731 (Mar 14, 2000).
86. M. J. Smyth *et al.*, New aspects of natural-killer-cell surveillance and therapy of cancer. *Nat Rev Cancer* **2**, 850 (Nov, 2002).
87. K. J. Malmberg *et al.*, NK cell-mediated targeting of human cancer and possibilities for new means of immunotherapy. *Cancer Immunol Immunother* **57**, 1541 (Oct, 2008).
88. E. Carbone *et al.*, HLA class I, NKG2D, and natural cytotoxicity receptors regulate multiple myeloma cell recognition by natural killer cells. *Blood* **105**, 251 (Jan 1, 2005).
89. M. A. Cooper *et al.*, The biology of human natural killer-cell subsets. *Trends Immunol* **22**, 633 (Nov, 2001).
90. S. Coca *et al.*, The prognostic significance of intratumoral natural killer cells in patients with colorectal carcinoma. *Cancer* **79**, 2320 (Jun 15, 1997).
91. M. H. Sandel *et al.*, Natural killer cells infiltrating colorectal cancer and MHC class I expression. *Mol Immunol* **42**, 541 (Feb, 2005).
92. R. Tallerico *et al.*, Human NK cells selective targeting of colon cancer-initiating cells: a role for natural cytotoxicity receptors and MHC class I molecules. *J Immunol* **190**, 2381 (Mar 1, 2013).
93. D. I. Gabrilovich *et al.*, Coordinated regulation of myeloid cells by tumours. *Nat Rev Immunol* **12**, 253 (Apr, 2012).
94. S. Gordon, P. R. Taylor, Monocyte and macrophage heterogeneity. *Nat Rev Immunol* **5**, 953 (Dec, 2005).
95. A. Mantovani *et al.*, Macrophage polarization: tumor-associated macrophages as a paradigm for polarized M2 mononuclear phagocytes. *Trends Immunol* **23**, 549 (Nov, 2002).
96. M. Stein *et al.*, Interleukin 4 potently enhances murine macrophage mannose receptor activity: a marker of alternative immunologic macrophage activation. *J Exp Med* **176**, 287 (Jul 1, 1992).
97. A. Mantovani, From phagocyte diversity and activation to probiotics: back to Metchnikoff. *Eur J Immunol* **38**, 3269 (Dec, 2008).
98. F. O. Martinez *et al.*, Transcriptional profiling of the human monocyte-to-macrophage differentiation and polarization: new molecules and patterns of gene expression. *J Immunol* **177**, 7303 (Nov 15, 2006).

99. J. W. Pollard, Trophic macrophages in development and disease. *Nat Rev Immunol* **9**, 259 (Apr, 2009).
100. E. Y. Lin *et al.*, Macrophages regulate the angiogenic switch in a mouse model of breast cancer. *Cancer Res* **66**, 11238 (Dec 1, 2006).
101. B. Qian *et al.*, A distinct macrophage population mediates metastatic breast cancer cell extravasation, establishment and growth. *PLoS One* **4**, e6562 (2009).
102. Y. Zheng *et al.*, Macrophages are an abundant component of myeloma microenvironment and protect myeloma cells from chemotherapy drug-induced apoptosis. *Blood* **114**, 3625 (Oct 22, 2009).
103. C. Lackner *et al.*, Prognostic relevance of tumour-associated macrophages and von Willebrand factor-positive microvessels in colorectal cancer. *Virchows Arch* **445**, 160 (Aug, 2004).
104. J. Forssell *et al.*, High macrophage infiltration along the tumor front correlates with improved survival in colon cancer. *Clin Cancer Res* **13**, 1472 (Mar 1, 2007).
105. Q. Zhou *et al.*, The density of macrophages in the invasive front is inversely correlated to liver metastasis in colon cancer. *J Transl Med* **8**, 13 (2010).
106. D. Gabrilovich, Mechanisms and functional significance of tumour-induced dendritic-cell defects. *Nat Rev Immunol* **4**, 941 (Dec, 2004).
107. P. Chaux *et al.*, Tumor-infiltrating dendritic cells are defective in their antigen-presenting function and inducible B7 expression in rats. *Int J Cancer* **72**, 619 (Aug 7, 1997).
108. J. I. Youn *et al.*, Subsets of myeloid-derived suppressor cells in tumor-bearing mice. *J Immunol* **181**, 5791 (Oct 15, 2008).
109. H. L. Sun *et al.*, Increased frequency and clinical significance of myeloid-derived suppressor cells in human colorectal carcinoma. *World J Gastroenterol* **18**, 3303 (Jul 7, 2012).
110. B. Zhang *et al.*, Circulating and tumor-infiltrating myeloid-derived suppressor cells in patients with colorectal carcinoma. *PLoS One* **8**, e57114 (2013).
111. Y. S. Khaled *et al.*, Myeloid-derived suppressor cells in cancer: recent progress and prospects. *Immunol Cell Biol* **91**, 493 (Sep, 2013).
112. Z. Y. Chen *et al.*, Cytokine profile and prognostic significance of high neutrophil-lymphocyte ratio in colorectal cancer. *Br J Cancer* **112**, 1088 (Mar 17, 2015).
113. F. Shojaei *et al.*, Role of Bv8 in neutrophil-dependent angiogenesis in a transgenic model of cancer progression. *Proc Natl Acad Sci U S A* **105**, 2640 (Feb 19, 2008).
114. L. A. Pekarek *et al.*, Inhibition of tumor growth by elimination of granulocytes. *J Exp Med* **181**, 435 (Jan 1, 1995).
115. M. Kowanetz *et al.*, Granulocyte-colony stimulating factor promotes lung metastasis through mobilization of Ly6G+Ly6C+ granulocytes. *Proc Natl Acad Sci U S A* **107**, 21248 (Dec 14, 2010).
116. F. Pericle *et al.*, Direct killing of interleukin-2-transfected tumor cells by human neutrophils. *Int J Cancer* **66**, 367 (May 3, 1996).
117. Z. Granot *et al.*, Tumor entrained neutrophils inhibit seeding in the premetastatic lung. *Cancer Cell* **20**, 300 (Sep 13, 2011).

118. K. Morikawa *et al.*, Hydrogen peroxide as a tumoricidal mediator of murine polymorphonuclear leukocytes induced by a linear beta-1,3-D-glucan and some other immunomodulators. *Cancer Res* **45**, 3482 (Aug, 1985).
119. D. B. Learn, E. L. Thomas, Inhibition of tumor cell glutamine uptake by isolated neutrophils. *J Clin Invest* **82**, 789 (Sep, 1988).
120. Z. G. Fridlender *et al.*, Polarization of tumor-associated neutrophil phenotype by TGF-beta: "N1" versus "N2" TAN. *Cancer Cell* **16**, 183 (Sep 8, 2009).
121. E. Peranzoni *et al.*, Myeloid-derived suppressor cell heterogeneity and subset definition. *Curr Opin Immunol* **22**, 238 (Apr, 2010).
122. E. Schlecker *et al.*, Tumor-infiltrating monocytic myeloid-derived suppressor cells mediate CCR5-dependent recruitment of regulatory T cells favoring tumor growth. *J Immunol* **189**, 5602 (Dec 15, 2012).
123. T. Tachibana *et al.*, Increased intratumor Valpha24-positive natural killer T cells: a prognostic factor for primary colorectal carcinomas. *Clin Cancer Res* **11**, 7322 (Oct 15, 2005).
124. M. Corvaisier *et al.*, V gamma 9V delta 2 T cell response to colon carcinoma cells. *J Immunol* **175**, 5481 (Oct 15, 2005).
125. T. Hehlgans, K. Pfeffer, The intriguing biology of the tumour necrosis factor/tumour necrosis factor receptor superfamily: players, rules and the games. *Immunology* **115**, 1 (May, 2005).
126. C. F. Ware, Network communications: lymphotoxins, LIGHT, and TNF. *Annu Rev Immunol* **23**, 787 (2005).
127. K. J. Tracey, in *The cytokine handbook,* A. Thomson, Ed. (Academic Press, London, United Kingdom, 1994), pp. 289-304.
128. B. B. Aggarwal, Signalling pathways of the TNF superfamily: a double-edged sword. *Nat Rev Immunol* **3**, 745 (Sep, 2003).
129. F. Balkwill, TNF-alpha in promotion and progression of cancer. *Cancer Metastasis Rev* **25**, 409 (Sep, 2006).
130. M. Grell *et al.*, Induction of cell death by tumour necrosis factor (TNF) receptor 2, CD40 and CD30: a role for TNF-R1 activation by endogenous membrane-anchored TNF. *EMBO J* **18**, 3034 (Jun 1, 1999).
131. R. A. Black *et al.*, A metalloproteinase disintegrin that releases tumour-necrosis factor-alpha from cells. *Nature* **385**, 729 (Feb 20, 1997).
132. M. Grell *et al.*, The transmembrane form of tumor necrosis factor is the prime activating ligand of the 80 kDa tumor necrosis factor receptor. *Cell* **83**, 793 (Dec 1, 1995).
133. C. Richter *et al.*, The tumor necrosis factor receptor stalk regions define responsiveness to soluble versus membrane-bound ligand. *Mol Cell Biol* **32**, 2515 (Jul, 2012).
134. M. Karin, A. Lin, NF-kappaB at the crossroads of life and death. *Nat Immunol* **3**, 221 (Mar, 2002).
135. X. Wang, Y. Lin, Tumor necrosis factor and cancer, buddies or foes? *Acta Pharmacol Sin* **29**, 1275 (Nov, 2008).
136. V. Baud, M. Karin, Signal transduction by tumor necrosis factor and its relatives. *Trends Cell Biol* **11**, 372 (Sep, 2001).

137. Y. Lin *et al.*, Tumor necrosis factor-induced nonapoptotic cell death requires receptor-interacting protein-mediated cellular reactive oxygen species accumulation. *J Biol Chem* **279**, 10822 (Mar 12, 2004).
138. N. Holler *et al.*, Fas triggers an alternative, caspase-8-independent cell death pathway using the kinase RIP as effector molecule. *Nat Immunol* **1**, 489 (Dec, 2000).
139. Y. S. Kim *et al.*, TNF-induced activation of the Nox1 NADPH oxidase and its role in the induction of necrotic cell death. *Mol Cell* **26**, 675 (Jun 8, 2007).
140. K. Imamura *et al.*, Expression of tumor necrosis factor receptors on human monocytes and internalization of receptor bound ligand. *J Immunol* **139**, 2989 (Nov 1, 1987).
141. M. Tsujimoto *et al.*, Tumor necrosis factor: specific binding and internalization in sensitive and resistant cells. *Proc Natl Acad Sci U S A* **82**, 7626 (Nov, 1985).
142. N. Watanabe *et al.*, Continuous internalization of tumor necrosis factor receptors in a human myosarcoma cell line. *J Biol Chem* **263**, 10262 (Jul 25, 1988).
143. S. Vuk-Pavlovic, J. S. Kovach, Recycling of tumor necrosis factor-alpha receptor in MCF-7 cells. *FASEB J* **3**, 2633 (Dec, 1989).
144. S. Xanthoulea *et al.*, Tumor necrosis factor (TNF) receptor shedding controls thresholds of innate immune activation that balance opposing TNF functions in infectious and inflammatory diseases. *J Exp Med* **200**, 367 (Aug 2, 2004).
145. T. W. Williams, G. A. Granger, Lymphocyte in vitro cytotoxicity: lymphotoxins of several mammalian species. *Nature* **219**, 1076 (Sep 7, 1968).
146. C. F. Ware *et al.*, Expression of surface lymphotoxin and tumor necrosis factor on activated T, B, and natural killer cells. *J Immunol* **149**, 3881 (Dec 15, 1992).
147. N. Etemadi *et al.*, Lymphotoxin alpha induces apoptosis, necroptosis and inflammatory signals with the same potency as TNF. *FEBS J*, (Jul 2, 2013).
148. M. Matsumoto *et al.*, Involvement of distinct cellular compartments in the abnormal lymphoid organogenesis in lymphotoxin-alpha-deficient mice and alymphoplasia (aly) mice defined by the chimeric analysis. *J Immunol* **163**, 1584 (Aug 1, 1999).
149. D. Ito *et al.*, Mice with a targeted mutation in lymphotoxin-alpha exhibit enhanced tumor growth and metastasis: impaired NK cell development and recruitment. *J Immunol* **163**, 2809 (Sep 1, 1999).
150. Y. Kashii *et al.*, Constitutive expression and role of the TNF family ligands in apoptotic killing of tumor cells by human NK cells. *J Immunol* **163**, 5358 (Nov 15, 1999).
151. D. Schrama *et al.*, Targeting of lymphotoxin-alpha to the tumor elicits an efficient immune response associated with induction of peripheral lymphoid-like tissue. *Immunity* **14**, 111 (Feb, 2001).
152. M. Lukashev *et al.*, Targeting the lymphotoxin-beta receptor with agonist antibodies as a potential cancer therapy. *Cancer Res* **66**, 9617 (Oct 1, 2006).
153. D. Yang *et al.*, Targeting lymphotoxin beta receptor with tumor-specific T lymphocytes for tumor regression. *Clin Cancer Res* **13**, 5202 (Sep 1, 2007).

154. Y. Huang *et al.*, Four genetic polymorphisms of lymphotoxin-alpha gene and cancer risk: a systematic review and meta-analysis. *PLoS One* **8**, e82519 (2013).
155. T. Hehlgans *et al.*, Lymphotoxin-beta receptor immune interaction promotes tumor growth by inducing angiogenesis. *Cancer Res* **62**, 4034 (Jul 15, 2002).
156. J. Haybaeck *et al.*, A lymphotoxin-driven pathway to hepatocellular carcinoma. *Cancer Cell* **16**, 295 (Oct 6, 2009).
157. M. Ammirante *et al.*, B-cell-derived lymphotoxin promotes castration-resistant prostate cancer. *Nature* **464**, 302 (Mar 11, 2010).
158. L. Martinet *et al.*, Human solid tumors contain high endothelial venules: association with T- and B-lymphocyte infiltration and favorable prognosis in breast cancer. *Cancer Res* **71**, 5678 (Sep 1, 2011).
159. A. Kratz *et al.*, Chronic inflammation caused by lymphotoxin is lymphoid neogenesis. *J Exp Med* **183**, 1461 (Apr 1, 1996).
160. P. W. Gray *et al.*, Cloning and expression of cDNA for human lymphotoxin, a lymphokine with tumour necrosis activity. *Nature* **312**, 721 (Dec 20-1985 Jan 2, 1984).
161. B. Feinberg *et al.*, A phase I trial of intravenously-administered recombinant tumor necrosis factor-alpha in cancer patients. *J Clin Oncol* **6**, 1328 (Aug, 1988).
162. A. Ferrajoli *et al.*, The clinical significance of tumor necrosis factor-alpha plasma level in patients having chronic lymphocytic leukemia. *Blood* **100**, 1215 (Aug 15, 2002).
163. S. Kim *et al.*, Circulating levels of inflammatory cytokines and risk of colorectal adenomas. *Cancer Res* **68**, 323 (Jan 1, 2008).
164. P. W. Szlosarek *et al.*, Expression and regulation of tumor necrosis factor alpha in normal and malignant ovarian epithelium. *Mol Cancer Ther* **5**, 382 (Feb, 2006).
165. M. I. Ahmed *et al.*, Human papillomavirus infection among Egyptian females with cervical carcinoma: relationship to spontaneous apoptosis and TNF-alpha. *Clin Biochem* **34**, 491 (Sep, 2001).
166. B. Bel Hadj Jrad *et al.*, Tumor necrosis factor promoter gene polymorphism associated with increased susceptibility to non-Hodgkin's lymphomas. *Eur J Haematol* **78**, 117 (Feb, 2007).
167. S. Y. Ho *et al.*, Increased risk of developing hepatocellular carcinoma associated with carriage of the TNF2 allele of the -308 tumor necrosis factor-alpha promoter gene. *Cancer Causes Control* **15**, 657 (Sep, 2004).
168. I. Duarte *et al.*, G-308A TNF-alpha polymorphism is associated with an increased risk of invasive cervical cancer. *Biochem Biophys Res Commun* **334**, 588 (Aug 26, 2005).
169. M. M. Garrity-Park *et al.*, Tumor necrosis factor-alpha polymorphisms in ulcerative colitis-associated colorectal cancer. *Am J Gastroenterol* **103**, 407 (Feb, 2008).
170. C. M. Shih *et al.*, Association of TNF-alpha polymorphism with susceptibility to and severity of non-small cell lung cancer. *Lung Cancer* **52**, 15 (Apr, 2006).

171. W. H. Jang *et al.*, The -238 tumor necrosis factor-alpha promoter polymorphism is associated with decreased susceptibility to cancers. *Cancer Lett* **166**, 41 (May 10, 2001).
172. R. J. Moore *et al.*, Mice deficient in tumor necrosis factor-alpha are resistant to skin carcinogenesis. *Nat Med* **5**, 828 (Jul, 1999).
173. B. K. Popivanova *et al.*, Blocking TNF-alpha in mice reduces colorectal carcinogenesis associated with chronic colitis. *J Clin Invest* **118**, 560 (Feb, 2008).
174. H. Kitakata *et al.*, Essential roles of tumor necrosis factor receptor p55 in liver metastasis of intrasplenic administration of colon 26 cells. *Cancer Res* **62**, 6682 (Nov 15, 2002).
175. A. Komori *et al.*, Tumor necrosis factor acts as a tumor promoter in BALB/3T3 cell transformation. *Cancer Res* **53**, 1982 (May 1, 1993).
176. E. Pikarsky *et al.*, NF-kappaB functions as a tumour promoter in inflammation-associated cancer. *Nature* **431**, 461 (Sep 23, 2004).
177. H. Yang *et al.*, TNF-alpha inhibits asbestos-induced cytotoxicity via a NF-kappaB-dependent pathway, a possible mechanism for asbestos-induced oncogenesis. *Proc Natl Acad Sci U S A* **103**, 10397 (Jul 5, 2006).
178. N. Babbar, R. A. Casero, Jr., Tumor necrosis factor-alpha increases reactive oxygen species by inducing spermine oxidase in human lung epithelial cells: a potential mechanism for inflammation-induced carcinogenesis. *Cancer Res* **66**, 11125 (Dec 1, 2006).
179. B. Yan *et al.*, Tumor necrosis factor-alpha is a potent endogenous mutagen that promotes cellular transformation. *Cancer Res* **66**, 11565 (Dec 15, 2006).
180. P. O. Esteve *et al.*, Protein kinase C-zeta regulates transcription of the matrix metalloproteinase-9 gene induced by IL-1 and TNF-alpha in glioma cells via NF-kappa B. *J Biol Chem* **277**, 35150 (Sep 20, 2002).
181. T. Hagemann *et al.*, Enhanced invasiveness of breast cancer cell lines upon co-cultivation with macrophages is due to TNF-alpha dependent up-regulation of matrix metalloproteases. *Carcinogenesis* **25**, 1543 (Aug, 2004).
182. M. Egeblad, Z. Werb, New functions for the matrix metalloproteinases in cancer progression. *Nat Rev Cancer* **2**, 161 (Mar, 2002).
183. J. J. Connell *et al.*, Selective permeabilization of the blood-brain barrier at sites of metastasis. *J Natl Cancer Inst* **105**, 1634 (Nov 6, 2013).
184. H. Mueller, Tumor necrosis factor as an antineoplastic agent: pitfalls and promises. *Cell Mol Life Sci* **54**, 1291 (Dec, 1998).
185. J. B. Swann *et al.*, Demonstration of inflammation-induced cancer and cancer immunoediting during primary tumorigenesis. *Proc Natl Acad Sci U S A* **105**, 652 (Jan 15, 2008).
186. B. Zhang *et al.*, IFN-gamma- and TNF-dependent bystander eradication of antigen-loss variants in established mouse cancers. *J Clin Invest* **118**, 1398 (Apr, 2008).
187. E. A. Havell *et al.*, The antitumor function of tumor necrosis factor (TNF), I. Therapeutic action of TNF against an established murine sarcoma is indirect, immunologically dependent, and limited by severe toxicity. *J Exp Med* **167**, 1067 (Mar 1, 1988).

188. M. A. Palladino, Jr. *et al.*, Characterization of the antitumor activities of human tumor necrosis factor-alpha and the comparison with other cytokines: induction of tumor-specific immunity. *J Immunol* **138**, 4023 (Jun 1, 1987).
189. N. Larmonier *et al.*, The inhibition of TNF-alpha anti-tumoral properties by blocking antibodies promotes tumor growth in a rat model. *Exp Cell Res* **313**, 2345 (Jul 1, 2007).
190. G. Aversa *et al.*, The 26-kD transmembrane form of tumor necrosis factor alpha on activated CD4+ T cell clones provides a costimulatory signal for human B cell activation. *J Exp Med* **177**, 1575 (Jun 1, 1993).
191. T. P. Birkland *et al.*, Soluble TNF and membrane TNF expressed on CD4+ T lymphocytes differ in their ability to activate macrophage antileishmanial defense. *J Leukoc Biol* **51**, 296 (Mar, 1992).
192. F. S. Kleijwegt *et al.*, Critical role for TNF in the induction of human antigen-specific regulatory T cells by tolerogenic dendritic cells. *J Immunol* **185**, 1412 (Aug 1, 2010).
193. R. Peck *et al.*, Cell surface tumor necrosis factor (TNF) accounts for monocyte- and lymphocyte-mediated killing of TNF-resistant target cells. *Cell Immunol* **122**, 1 (Aug, 1989).
194. S. Ardestani *et al.*, Membrane versus Soluble Isoforms of TNF-alpha Exert Opposing Effects on Tumor Growth and Survival of Tumor-Associated Myeloid Cells. *Cancer Res*, (Jun 21, 2013).
195. R. A. Marr *et al.*, Tumour immunotherapy using an adenoviral vector expressing a membrane-bound mutant of murine TNF alpha. *Gene Ther* **4**, 1181 (Nov, 1997).
196. X. Hu *et al.*, Transmembrane TNF-alpha promotes suppressive activities of myeloid-derived suppressor cells via TNFR2. *J Immunol* **192**, 1320 (Feb 1, 2014).
197. Q. Li *et al.*, Mechanism of action differences in the antitumor effects of transmembrane and secretory tumor necrosis factor-alpha in vitro and in vivo. *Cancer Immunol Immunother* **55**, 1470 (Dec, 2006).
198. A. L. Asher *et al.*, Murine tumor cells transduced with the gene for tumor necrosis factor-alpha. Evidence for paracrine immune effects of tumor necrosis factor against tumors. *J Immunol* **146**, 3227 (May 1, 1991).
199. S. E. Karp *et al.*, In vivo activity of tumor necrosis factor (TNF) mutants. Secretory but not membrane-bound TNF mediates the regression of retrovirally transduced murine tumor. *J Immunol* **149**, 2076 (Sep 15, 1992).
200. O. Tredan *et al.*, Drug resistance and the solid tumor microenvironment. *J Natl Cancer Inst* **99**, 1441 (Oct 3, 2007).
201. A. I. Minchinton, I. F. Tannock, Drug penetration in solid tumours. *Nat Rev Cancer* **6**, 583 (Aug, 2006).
202. T. Seki *et al.*, Tumour necrosis factor-alpha increases extravasation of virus particles into tumour tissue by activating the Rho A/Rho kinase pathway. *J Control Release* **156**, 381 (Dec 20, 2011).
203. M. Clauss *et al.*, A permissive role for tumor necrosis factor in vascular endothelial growth factor-induced vascular permeability. *Blood* **97**, 1321 (Mar 1, 2001).

204. C. A. Kristensen *et al.*, Reduction of interstitial fluid pressure after TNF-alpha treatment of three human melanoma xenografts. *Br J Cancer* **74**, 533 (Aug, 1996).
205. H. J. Mauceri *et al.*, Tumor necrosis factor alpha (TNF-alpha) gene therapy targeted by ionizing radiation selectively damages tumor vasculature. *Cancer Res* **56**, 4311 (Oct 1, 1996).
206. M. J. Staba *et al.*, Adenoviral TNF-alpha gene therapy and radiation damage tumor vasculature in a human malignant glioma xenograft. *Gene Ther* **5**, 293 (Mar, 1998).
207. S. Folli *et al.*, Tumor-necrosis factor can enhance radio-antibody uptake in human colon carcinoma xenografts by increasing vascular permeability. *Int J Cancer* **53**, 829 (Mar 12, 1993).
208. A. H. van der Veen *et al.*, TNF-alpha augments intratumoural concentrations of doxorubicin in TNF-alpha-based isolated limb perfusion in rat sarcoma models and enhances anti-tumour effects. *Br J Cancer* **82**, 973 (Feb, 2000).
209. J. H. de Wilt *et al.*, Tumour necrosis factor alpha increases melphalan concentration in tumour tissue after isolated limb perfusion. *Br J Cancer* **82**, 1000 (Mar, 2000).
210. P. Brouckaert *et al.*, Tumor necrosis factor-alpha augmented tumor response in B16BL6 melanoma-bearing mice treated with stealth liposomal doxorubicin (Doxil) correlates with altered Doxil pharmacokinetics. *Int J Cancer* **109**, 442 (Apr 10, 2004).
211. A. L. Seynhaeve *et al.*, Tumor necrosis factor alpha mediates homogeneous distribution of liposomes in murine melanoma that contributes to a better tumor response. *Cancer Res* **67**, 9455 (Oct 1, 2007).
212. T. F. Logan *et al.*, Biologic response modulation by tumor necrosis factor alpha (TNF alpha) in a phase Ib trial in cancer patients. *J Immunother* **20**, 387 (Sep, 1997).
213. W. L. Furman *et al.*, Phase I clinical trial of recombinant human tumor necrosis factor in children with refractory solid tumors: a Pediatric Oncology Group study. *J Clin Oncol* **11**, 2205 (Nov, 1993).
214. K. W. Zamkoff *et al.*, A phase I trial of subcutaneously administered recombination tumor necrosis factor to patients with advanced malignancy. *J Biol Response Mod* **8**, 539 (Oct, 1989).
215. H. Lenk *et al.*, Phase II clinical trial of high-dose recombinant human tumor necrosis factor. *Cancer Chemother Pharmacol* **24**, 391 (1989).
216. N. Kemeny *et al.*, A phase II trial of recombinant tumor necrosis factor in patients with advanced colorectal carcinoma. *Cancer* **66**, 659 (Aug 15, 1990).
217. R. P. Whitehead *et al.*, A phase II trial of recombinant tumor necrosis factor in patients with metastatic colorectal adenocarcinoma: a Southwest Oncology Group study. *J Biol Response Mod* **9**, 588 (Dec, 1990).
218. T. D. Brown *et al.*, A phase II trial of recombinant tumor necrosis factor in patients with adenocarcinoma of the pancreas: a Southwest Oncology Group study. *J Immunother (1991)* **10**, 376 (Oct, 1991).
219. G. T. Budd *et al.*, A Southwest Oncology Group phase II Trial of recombinant tumor necrosis factor in metastatic breast cancer. *Cancer* **68**, 1694 (Oct 15, 1991).

220. E. R. Feldman *et al.*, Phase II trial of recombinant tumor necrosis factor in disseminated malignant melanoma. *Am J Clin Oncol* **15**, 256 (Jun, 1992).
221. P. J. Creaven *et al.*, Phase I clinical trial of recombinant human tumor necrosis factor. *Cancer Chemother Pharmacol* **20**, 137 (1987).
222. H. Gamm *et al.*, Phase I trial of recombinant human tumour necrosis factor alpha in patients with advanced malignancy. *Eur J Cancer* **27**, 856 (1991).
223. M. Blick *et al.*, Phase I study of recombinant tumor necrosis factor in cancer patients. *Cancer Res* **47**, 2986 (Jun 1, 1987).
224. A. M. Eggermont *et al.*, Isolated limb perfusion with tumor necrosis factor and melphalan for limb salvage in 186 patients with locally advanced soft tissue extremity sarcomas. The cumulative multicenter European experience. *Ann Surg* **224**, 756 (Dec, 1996).
225. J. M. Seinen, H. J. Hoekstra, Isolated limb perfusion of soft tissue sarcomas: A comprehensive review of literature. *Cancer Treat Rev* **39**, 569 (Oct, 2013).
226. D. J. Grunhagen *et al.*, Isolated limb perfusion with TNF-alpha and melphalan in locally advanced soft tissue sarcomas of the extremities. *Recent Results Cancer Res* **179**, 257 (2009).
227. J. P. Deroose *et al.*, 20 years experience of TNF-based isolated limb perfusion for in-transit melanoma metastases: TNF dose matters. *Ann Surg Oncol* **19**, 627 (Feb, 2012).
228. D. W. Kim *et al.*, Immunohistological analysis of immune cell infiltration of a human colon tumor xenograft after treatment with Stealth liposome-encapsulated tumor necrosis factor-alpha and radiation. *Int J Oncol* **21**, 973 (Nov, 2002).
229. D. W. Kim *et al.*, Liposome-encapsulated tumor necrosis factor-alpha enhances the effects of radiation against human colon tumor xenografts. *J Interferon Cytokine Res* **21**, 885 (Nov, 2001).
230. T. L. ten Hagen *et al.*, Pegylated liposomal tumor necrosis factor-alpha results in reduced toxicity and synergistic antitumor activity after systemic administration in combination with liposomal doxorubicin (Doxil) in soft tissue sarcoma-bearing rats. *Int J Cancer* **97**, 115 (Jan 1, 2002).
231. M. A. Lyu, M. G. Rosenblum, The immunocytokine scFv23/TNF sensitizes HER-2/neu-overexpressing SKBR-3 cells to tumor necrosis factor (TNF) via up-regulation of TNF receptor-1. *Mol Cancer Ther* **4**, 1205 (Aug, 2005).
232. Y. Liu *et al.*, The antimelanoma immunocytokine scFvMEL/TNF shows reduced toxicity and potent antitumor activity against human tumor xenografts. *Neoplasia* **8**, 384 (May, 2006).
233. O. Christ *et al.*, Efficacy of local versus systemic application of antibody-cytokine fusion proteins in tumor therapy. *Clin Cancer Res* **7**, 985 (Apr, 2001).
234. C. Halin *et al.*, Synergistic therapeutic effects of a tumor targeting antibody fragment, fused to interleukin 12 and to tumor necrosis factor alpha. *Cancer Res* **63**, 3202 (Jun 15, 2003).
235. C. Larbouret *et al.*, Radiocurability by targeting tumor necrosis factor-alpha using a bispecific antibody in carcinoembryonic antigen transgenic mice. *Int J Radiat Oncol Biol Phys* **69**, 1231 (Nov 15, 2007).

236. F. Curnis *et al.*, Coupling tumor necrosis factor-alpha with alphaV integrin ligands improves its antineoplastic activity. *Cancer Res* **64**, 565 (Jan 15, 2004).
237. A. Sacchi *et al.*, Synergistic antitumor activity of cisplatin, paclitaxel, and gemcitabine with tumor vasculature-targeted tumor necrosis factor-alpha. *Clin Cancer Res* **12**, 175 (Jan 1, 2006).
238. H. W. van Laarhoven *et al.*, Effects of the tumor vasculature targeting agent NGR-TNF on the tumor microenvironment in murine lymphomas. *Invest New Drugs* **24**, 27 (Jan, 2006).
239. N. Zarovni *et al.*, Inhibition of tumor growth by intramuscular injection of cDNA encoding tumor necrosis factor alpha coupled to NGR and RGD tumor-homing peptides. *Hum Gene Ther* **15**, 373 (Apr, 2004).
240. J. M. Herman *et al.*, Randomized phase III multi-institutional study of TNFerade biologic with fluorouracil and radiotherapy for locally advanced pancreatic cancer: final results. *J Clin Oncol* **31**, 886 (Mar 1, 2013).
241. Z. Q. Han *et al.*, Development of a second-generation oncolytic Herpes simplex virus expressing TNFalpha for cancer therapy. *J Gene Med* **9**, 99 (Feb, 2007).
242. M. Hirvinen *et al.*, Immunological effects of a tumor necrosis factor alpha-armed oncolytic adenovirus. *Hum Gene Ther* **26**, 134 (Mar, 2015).
243. Promega. (2012).
244. V. L. Singer *et al.*, Characterization of PicoGreen reagent and development of a fluorescence-based solution assay for double-stranded DNA quantitation. *Analytical Biochemistry* **249**, 228 (1997).
245. P. Murakami, M. T. McCaman, Quantitation of adenovirus DNA and virus particles with the PicoGreen fluorescent Dye. *Anal Biochem* **274**, 283 (Oct 15, 1999).
246. Y. Matsumura, H. Maeda, A new concept for macromolecular therapeutics in cancer chemotherapy: mechanism of tumoritropic accumulation of proteins and the antitumor agent smancs. *Cancer Res* **46**, 6387 (Dec, 1986).
247. S. Goverdhana *et al.*, Regulatable gene expression systems for gene therapy applications: progress and future challenges. *Mol Ther* **12**, 189 (Aug, 2005).
248. Z. Zhu *et al.*, Tetracycline-controlled transcriptional regulation systems: advances and application in transgenic animal modeling. *Semin Cell Dev Biol* **13**, 121 (Apr, 2002).
249. Clontech. (http://www.clontech.com, 2010), vol. 2013.
250. L. C. Trost, J. J. Lemasters, A cytotoxicity assay for tumor necrosis factor employing a multiwell fluorescence scanner. *Anal Biochem* **220**, 149 (Jul, 1994).
251. S. Urlinger *et al.*, Exploring the sequence space for tetracycline-dependent transcriptional activators: novel mutations yield expanded range and sensitivity. *Proc Natl Acad Sci U S A* **97**, 7963 (Jul 5, 2000).
252. Y. H. Jeon *et al.*, Immune response to firefly luciferase as a naked DNA. *Cancer Biol Ther* **6**, 781 (May, 2007).

253. C. Cawthorne *et al.*, Comparison of doxycycline delivery methods for Tet-inducible gene expression in a subcutaneous xenograft model. *J Biomol Tech* **18**, 120 (Apr, 2007).
254. H. Liu *et al.*, TNF-alpha gene expression in macrophages: regulation by NF-kappa B is independent of c-Jun or C/EBP beta. *J Immunol* **164**, 4277 (Apr 15, 2000).
255. F. R. Balkwill, Tumour necrosis factor and cancer. *Prog Growth Factor Res* **4**, 121 (1992).
256. A. A. Dominguez *et al.*, Beyond editing: repurposing CRISPR-Cas9 for precision genome regulation and interrogation. *Nat Rev Mol Cell Biol* **17**, 5 (Jan, 2016).
257. G. J. van der Bij *et al.*, Tumor infiltrating macrophages reduce development of peritoneal colorectal carcinoma metastases. *Cancer Lett* **262**, 77 (Apr 8, 2008).
258. J. Y. Kee *et al.*, CXCL16 suppresses liver metastasis of colorectal cancer by promoting TNF-alpha-induced apoptosis by tumor-associated macrophages. *BMC Cancer* **14**, 949 (2014).
259. A. Alamoudi, University of Oxford (2014).
260. J. K. Onesti, D. C. Guttridge, Inflammation based regulation of cancer cachexia. *Biomed Res Int* **2014**, 168407 (2014).
261. S. Budhu *et al.*, The importance of animal models in tumor immunity and immunotherapy. *Curr Opin Genet Dev* **24**, 46 (Feb, 2014).
262. C. M. M. Thoma, University of Oxford (2011).
263. M. Jung *et al.*, Combining radiation therapy with interstitial radiation-inducible TNF-alpha expression for locoregional cancer treatment. *Cancer Gene Ther* **18**, 189 (Mar, 2011).
264. G. Sersa *et al.*, Anti-tumor effects of tumor necrosis factor alone or combined with radiotherapy. *Int J Cancer* **42**, 129 (Jul 15, 1988).
265. D. E. Hallahan *et al.*, Phase I dose-escalation study of tumor necrosis factor-alpha and concomitant radiation therapy. *Cancer J Sci Am* **1**, 204 (Sep-Oct, 1995).
266. R. Datta *et al.*, Ionizing radiation activates transcription of the EGR1 gene via CArG elements. *Proc Natl Acad Sci U S A* **89**, 10149 (Nov 1, 1992).
267. H. J. Mauceri *et al.*, Translational strategies exploiting TNF-alpha that sensitize tumors to radiation therapy. *Cancer Gene Ther* **16**, 373 (Apr, 2009).
268. T. D. Chung *et al.*, Tumor necrosis factor-alpha-based gene therapy enhances radiation cytotoxicity in human prostate cancer. *Cancer Gene Ther* **5**, 344 (Nov-Dec, 1998).
269. J. O. Park *et al.*, Transcriptional control of viral gene therapy by cisplatin. *J Clin Invest* **110**, 403 (Aug, 2002).
270. C. A. Lopez *et al.*, Chemoinducible gene therapy: a strategy to enhance doxorubicin antitumor activity. *Mol Cancer Ther* **3**, 1167 (Sep, 2004).
271. N. Senzer *et al.*, TNFerade biologic, an adenovector with a radiation-inducible promoter, carrying the human tumor necrosis factor alpha gene: a phase I study in patients with solid tumors. *J Clin Oncol* **22**, 592 (Feb 15, 2004).

272. R. F. Schwabe, D. A. Brenner, Mechanisms of Liver Injury. I. TNF-alpha-induced liver injury: role of IKK, JNK, and ROS pathways. *Am J Physiol Gastrointest Liver Physiol* **290**, G583 (Apr, 2006).
273. K. D. Grugan *et al.*, Tumor-associated macrophages promote invasion while retaining Fc-dependent anti-tumor function. *J Immunol* **189**, 5457 (Dec 1, 2012).
274. M. Beyer *et al.*, High-resolution transcriptome of human macrophages. *PLoS One* **7**, e45466 (2012).
275. R. A. Flavell *et al.*, The polarization of immune cells in the tumour environment by TGFbeta. *Nat Rev Immunol* **10**, 554 (Aug, 2010).
276. G. T. Motz, G. Coukos, Deciphering and reversing tumor immune suppression. *Immunity* **39**, 61 (Jul 25, 2013).
277. C. J. Breitbach *et al.*, Targeted inflammation during oncolytic virus therapy severely compromises tumor blood flow. *Mol Ther* **15**, 1686 (Sep, 2007).
278. D. Grote *et al.*, Neutrophils contribute to the measles virus-induced antitumor effect: enhancement by granulocyte macrophage colony-stimulating factor expression. *Cancer Res* **63**, 6463 (Oct 1, 2003).
279. M. Ramachandran *et al.*, An infection-enhanced oncolytic adenovirus secreting H. pylori neutrophil-activating protein with therapeutic effects on neuroendocrine tumors. *Mol Ther* **21**, 2008 (Nov, 2013).
280. K. Steinbrink *et al.*, Induction of tolerance by IL-10-treated dendritic cells. *J Immunol* **159**, 4772 (Nov 15, 1997).
281. A. S. Yang, E. C. Lattime, Tumor-induced interleukin 10 suppresses the ability of splenic dendritic cells to stimulate CD4 and CD8 T-cell responses. *Cancer Res* **63**, 2150 (May 1, 2003).
282. H. Sauthoff *et al.*, Intratumoral spread of wild-type adenovirus is limited after local injection of human xenograft tumors: virus persists and spreads systemically at late time points. *Hum Gene Ther* **14**, 425 (Mar 20, 2003).
283. M. Ding *et al.*, Newly developed strategies for improving sensitivity to radiation by targeting signal pathways in cancer therapy. *Cancer Sci* **104**, 1401 (Nov, 2013).
284. G. Sulli *et al.*, Crosstalk between chromatin state and DNA damage response in cellular senescence and cancer. *Nat Rev Cancer* **12**, 709 (Oct, 2012).
285. S. J. Advani *et al.*, ReVOLT: radiation-enhanced viral oncolytic therapy. *Int J Radiat Oncol Biol Phys* **66**, 637 (Nov 1, 2006).
286. T. H. Stracker *et al.*, Adenovirus oncoproteins inactivate the Mre11-Rad50-NBS1 DNA repair complex. *Nature* **418**, 348 (Jul 18, 2002).
287. G. J. Williams *et al.*, Mre11-Rad50-Nbs1 conformations and the control of sensing, signaling, and effector responses at DNA double-strand breaks. *DNA Repair (Amst)* **9**, 1299 (Dec 10, 2010).
288. K. A. Karen *et al.*, Temporal regulation of the Mre11-Rad50-Nbs1 complex during adenovirus infection. *J Virol* **83**, 4565 (May, 2009).
289. S. Y. Sohn, P. Hearing, Adenovirus regulates sumoylation of Mre11-Rad50-Nbs1 components through a paralog-specific mechanism. *J Virol* **86**, 9656 (Sep, 2012).

290. J. D. Evans, P. Hearing, Relocalization of the Mre11-Rad50-Nbs1 complex by the adenovirus E4 ORF3 protein is required for viral replication. *J Virol* **79**, 6207 (May, 2005).
291. J. L. Woo, A. J. Berk, Adenovirus ubiquitin-protein ligase stimulates viral late mRNA nuclear export. *J Virol* **81**, 575 (Jan, 2007).
292. Y. Liu *et al.*, Adenovirus exploits the cellular aggresome response to accelerate inactivation of the MRN complex. *J Virol* **79**, 14004 (Nov, 2005).
293. C. T. Carson *et al.*, Mislocalization of the MRN complex prevents ATR signaling during adenovirus infection. *EMBO J* **28**, 652 (Mar 18, 2009).
294. A. N. Blackford *et al.*, Adenovirus 12 E4orf6 inhibits ATR activation by promoting TOPBP1 degradation. *Proc Natl Acad Sci U S A* **107**, 12251 (Jul 6, 2010).
295. C. Y. Cheng *et al.*, The E4orf6/E1B55K E3 ubiquitin ligase complexes of human adenoviruses exhibit heterogeneity in composition and substrate specificity. *J Virol* **85**, 765 (Jan, 2011).
296. N. A. Forrester *et al.*, Serotype-specific inactivation of the cellular DNA damage response during adenovirus infection. *J Virol* **85**, 2201 (Mar, 2011).
297. I. Liikanen *et al.*, Adenoviral E4orf3 and E4orf6 proteins, but not E1B55K, increase killing of cancer cells by radiotherapy in vivo. *Int J Radiat Oncol Biol Phys* **78**, 1201 (Nov 15, 2010).
298. G. J. Nichols *et al.*, Widespread phosphorylation of histone H2AX by species C adenovirus infection requires viral DNA replication. *J Virol* **83**, 5987 (Jun, 2009).
299. M. Stucki, S. P. Jackson, gammaH2AX and MDC1: anchoring the DNA-damage-response machinery to broken chromosomes. *DNA Repair (Amst)* **5**, 534 (May 10, 2006).
300. I. M. Ward *et al.*, Accumulation of checkpoint protein 53BP1 at DNA breaks involves its binding to phosphorylated histone H2AX. *J Biol Chem* **278**, 19579 (May 30, 2003).
301. T. T. Paull *et al.*, A critical role for histone H2AX in recruitment of repair factors to nuclear foci after DNA damage. *Curr Biol* **10**, 886 (Jul 27-Aug 10, 2000).
302. I. M. Ward, J. Chen, Histone H2AX is phosphorylated in an ATR-dependent manner in response to replicational stress. *J Biol Chem* **276**, 47759 (Dec 21, 2001).
303. J. Boyer *et al.*, Adenovirus E4 34k and E4 11k inhibit double strand break repair and are physically associated with the cellular DNA-dependent protein kinase. *Virology* **263**, 307 (Oct 25, 1999).
304. T. Kondo *et al.*, DNA damage sensor MRE11 recognizes cytosolic double-stranded DNA and induces type I interferon by regulating STING trafficking. *Proc Natl Acad Sci U S A* **110**, 2969 (Feb 19, 2013).
305. H. Takahashi *et al.*, Telomerase-specific oncolytic adenovirus: antitumor effects on radiation-resistant head and neck squamous cell carcinoma cells. *Head Neck* **36**, 411 (Mar, 2014).
306. M. L. Lamfers *et al.*, Potential of the conditionally replicative adenovirus Ad5-Delta24RGD in the treatment of malignant gliomas and its enhanced effect with radiotherapy. *Cancer Res* **62**, 5736 (Oct 15, 2002).

307. A. Bieler *et al.*, Impact of radiation therapy on the oncolytic adenovirus dl520: implications on the treatment of glioblastoma. *Radiother Oncol* **86**, 419 (Mar, 2008).
308. G. Portella *et al.*, ONYX-015 enhances radiation-induced death of human anaplastic thyroid carcinoma cells. *J Clin Endocrinol Metab* **88**, 5027 (Oct, 2003).
309. B. Geoerger *et al.*, Potentiation of radiation therapy by the oncolytic adenovirus dl1520 (ONYX-015) in human malignant glioma xenografts. *Br J Cancer* **89**, 577 (Aug 4, 2003).
310. Y. Chen *et al.*, CV706, a prostate cancer-specific adenovirus variant, in combination with radiotherapy produces synergistic antitumor efficacy without increasing toxicity. *Cancer Res* **61**, 5453 (Jul 15, 2001).
311. J. Dilley *et al.*, Oncolytic adenovirus CG7870 in combination with radiation demonstrates synergistic enhancements of antitumor efficacy without loss of specificity. *Cancer Gene Ther* **12**, 715 (Aug, 2005).
312. D. E. Hallahan *et al.*, The interaction between recombinant human tumor necrosis factor and radiation in 13 human tumor cell lines. *Int J Radiat Oncol Biol Phys* **19**, 69 (Jul, 1990).
313. T. Bolling *et al.*, Heterogeneity of radiation- and TNF-alpha-induced programmed cell death in carcinoma, sarcoma and lymphoma cell lines. *Anticancer Res* **30**, 2857 (Jul, 2010).
314. J. Qian *et al.*, Ionizing radiation-induced adenovirus infection is mediated by Dynamin 2. *Cancer Res* **65**, 5493 (Jul 1, 2005).
315. A. N. Blackford *et al.*, A role for E1B-AP5 in ATR signaling pathways during adenovirus infection. *J Virol* **82**, 7640 (Aug, 2008).
316. A. Cuconati *et al.*, DNA damage response and MCL-1 destruction initiate apoptosis in adenovirus-infected cells. *Genes Dev* **17**, 2922 (Dec 1, 2003).
317. G. S. Stewart *et al.*, The DNA double-strand break repair gene hMRE11 is mutated in individuals with an ataxia-telangiectasia-like disorder. *Cell* **99**, 577 (Dec 10, 1999).
318. S. Panier, S. J. Boulton, Double-strand break repair: 53BP1 comes into focus. *Nat Rev Mol Cell Biol* **15**, 7 (Jan, 2014).
319. M. M. Adams, P. B. Carpenter, Tying the loose ends together in DNA double strand break repair with 53BP1. *Cell Div* **1**, 19 (2006).
320. I. Rappold *et al.*, Tumor suppressor p53 binding protein 1 (53BP1) is involved in DNA damage-signaling pathways. *J Cell Biol* **153**, 613 (Apr 30, 2001).
321. J. R. Williams *et al.*, Tumor response to radiotherapy is dependent on genotype-associated mechanisms in vitro and in vivo. *Radiat Oncol* **5**, 71 (2010).
322. K. A. Cimprich, D. Cortez, ATR: an essential regulator of genome integrity. *Nat Rev Mol Cell Biol* **9**, 616 (Aug, 2008).
323. T. Egami *et al.*, Radiation enhances adenoviral gene therapy in pancreatic cancer via activation of cytomegalovirus promoter and increased adenovirus uptake. *Clin Cancer Res* **14**, 1859 (Mar 15, 2008).
324. J. D. Bradley *et al.*, Ionizing radiation improves survival in mice bearing intracranial high-grade gliomas injected with genetically modified herpes simplex virus. *Clin Cancer Res* **5**, 1517 (Jun, 1999).

325. S. V. Blank *et al.*, Replication-selective herpes simplex virus type 1 mutant therapy of cervical cancer is enhanced by low-dose radiation. *Hum Gene Ther* **13**, 627 (Mar 20, 2002).
326. O. Meier, U. F. Greber, Adenovirus endocytosis. *J Gene Med* **6 Suppl 1**, S152 (Feb, 2004).
327. J. M. Tufariello *et al.*, Adenovirus E3 14.7-kilodalton protein, an antagonist of tumor necrosis factor cytolysis, increases the virulence of vaccinia virus in severe combined immunodeficient mice. *Proc Natl Acad Sci U S A* **91**, 10987 (Nov 8, 1994).
328. S. Bortolanza *et al.*, Deletion of the E3-6.7K/gp19K region reduces the persistence of wild-type adenovirus in a permissive tumor model in Syrian hamsters. *Cancer Gene Ther* **16**, 703 (Sep, 2009).
329. J. Altomonte *et al.*, Exponential enhancement of oncolytic vesicular stomatitis virus potency by vector-mediated suppression of inflammatory responses in vivo. *Mol Ther* **16**, 146 (Jan, 2008).
330. S. Bekker-Jensen *et al.*, HERC2 coordinates ubiquitin-dependent assembly of DNA repair factors on damaged chromosomes. *Nat Cell Biol* **12**, 80 (Jan, 2010).
331. C. Doil *et al.*, RNF168 binds and amplifies ubiquitin conjugates on damaged chromosomes to allow accumulation of repair proteins. *Cell* **136**, 435 (Feb 6, 2009).
332. M. F. Lavin, Ataxia-telangiectasia: from a rare disorder to a paradigm for cell signalling and cancer. *Nat Rev Mol Cell Biol* **9**, 759 (Oct, 2008).
333. G. S. Stewart *et al.*, The RIDDLE syndrome protein mediates a ubiquitin-dependent signaling cascade at sites of DNA damage. *Cell* **136**, 420 (Feb 6, 2009).
334. Y. S. Cho *et al.*, Efficacy of CD46-targeting chimeric Ad5/35 adenoviral gene therapy for colorectal cancers. *Oncotarget*, (May 18, 2016).
335. S. T. Beug *et al.*, Smac mimetics and innate immune stimuli synergize to promote tumor death. *Nat Biotechnol* **32**, 182 (Feb, 2014).
336. D. M. Pardoll, The blockade of immune checkpoints in cancer immunotherapy. *Nat Rev Cancer* **12**, 252 (Apr, 2012).